

**Année 2011**

**N° d'ordre : 40667**

**UNIVERSITE LILLE 1 - SCIENCES ET TECHNOLOGIES**

**ECOLE DOCTORALE-SCIENCE DE LA MATIERE, DU  
RAYONNEMENT ET DE L'ENVIRONNEMENT**

**Doctorat**

**Molécules et Matière Condensée**

**Azarmidokht GHOLAMIPOUR-SHIRAZI**

**ORGANIC REACTIVITY: KINETICS STUDIES AND SYNTHESIS  
OPTIMIZATION, USING MICROFLUIDIC DEVICES**

**Soutenue publiquement le 12 décembre 2011**

**Thèse dirigée par Mr. Christian ROLANDO**

**Jury :**

Mr. Didier BARBRY, Co-directeur de thèse, Université Lille 1

Mr. Laurent FALK, Rapporteur, Université de Nancy

Mr. Pierre-Yves RENARD, Rapporteur, Université de Rouen

## Abstract (in French):

Les microsystèmes sont des réacteurs idéaux pour mettre en œuvre des réactions chimiques car ils apportent un rapport de contact entre phases ou entre liquide et catalyseurs un million de fois supérieur à celui rencontré à l'échelle du laboratoire, la possibilité de chauffage et de refroidissement rapide et enfin des réactions sans interaction avec les produits finaux car conduites en flux continu. Les dimensions micro-ou nanométriques de ces réacteurs sont très largement compensées par la possibilité de parallélisation à grande échelle de ces réacteurs qui permet une montée en échelle de la production sans nouveau développement. Nous avons choisi comme réaction-test l'alkylation des acides benzoïques par l'iodure de méthyle en présence d'une éponge à protons (TMGN). Cette réaction a été choisie car elle suit une cinétique parfaitement du second ordre qui peut être modulée sur plusieurs ordres de grandeur en modifiant les substituants de l'acide benzoïque. Nous avons ainsi pu déterminer les cinétiques d'alkylation d'une série d'acides benzoïques substitués ce qui nous a permis de déterminer la valeur de la constante de réaction de Hammett. Nous avons également déterminé les paramètres thermodynamiques d'activation de cette réaction. Pour permettre d'appliquer cette méthodologie à d'autres substrats, une étude comparative de la basicité d'un ensemble de superbases organiques et de leur vitesse de *N*-alkylation par l'iodure de méthyle a été effectuée pour déterminer le rapport entre basicité et nucléophilie de ces bases. Ensuite, le site d'alkylation du TMGN a été déterminé par RMN et il a été montré que cette réaction est en compétition avec l'eau résiduelle. Les constantes de diffusion des différentes espèces chimiques ont été mesurées par RMN DOSY pour mieux comprendre le phénomène de mélange. Enfin nous avons réalisé des expériences préparatives sur des substrats bifonctionnels simples pour mettre en évidence la sélectivité en fonction des conditions de mélange. Ces résultats ont été étendus à l'alkylation à une échelle préparative d'un polyphénol complexe la quercétine et de substrats à haute valeur ajoutée tels que l'acide podocarpique, l'acide clofibrique et le Trolox à l'aide de système microfluidique. Ces réactions conduites à l'échelle de la millimole ont permis une complète caractérisation des produits.

**Mots-clés** Microfluidique, Réacteurs capillaires en flux continu, Mélange et micromélange, Relation de Hammett, Alkylation, Acides benzoïques substitués, Superbases organiques, Synthèse organique en microsystème

## Abstract (in English)

Microsystems are ideal reactors to perform chemical reactions because they provide a high surface area between phases or between liquid and catalyst up to one million fold higher than what is encountered in laboratory scale. Microsystems also provide the possibility of fast cooling and heating and, finally, they run continuously without interaction between the reactant and the final products. The micro- or nanoscale dimensions of these reactors are largely compensated by the possibility of large-scale parallelization of these reactors which allows an increase in production scale without any new development. We have chosen the alkylation reaction of benzoic acids by iodomethane in the presence of a proton sponge (TMGN) as the test reaction as it follows a perfect second-order kinetics, which can be modulated over several orders of magnitudes by modifying the benzoic acid substituents. We were able to determine the kinetics of alkylation for a series of substituted benzoic acids, which allowed us to determine the value of the Hammett reaction constant. We also determined the thermodynamic activation parameters of this reaction. In order to use this methodology on other substrates, a comparative study of the N-alkylation rate of a set of organic superbases by iodomethane was conducted to determine the relationship between basicity and nucleophilicity for these bases. The alkylation site of TMGN was determined by NMR and it was shown that this reaction is in competition with residual water. To better understand micromixing, the diffusion constants of the different chemical species involved were determined by DOSY NMR. Finally, we carried out preparative experiments on simple bifunctional substrates to show the effect of mixing conditions on selectivity. These results were extended to the alkylation of a complex polyphenol quercetin and substrates with high added value such as podocarpic acid, clofibric acid and Trolox using a microfluidic system. These reactions were carried out at millimolar scale allowing us to completely characterize the final products.

**Key words:** Microfluidics, continuous flow capillary reactors, mixing and micromixing, Hammett equation, Alkylation, substituted benzoic acids, organic superbases, organic synthesis in microsystem.

## ACKNOWLEDGMENTS

I am deeply indebted to my thesis supervisor Christian Rolando. Without his steady guidance, wealth of knowledge and kindness, wisdom and bright ideas, generous support and continuous collaboration, limitless patience, warm encouragement and constructive criticism, none of the work presented here would have ever taken off the ground. I owe him an immeasurable debt of gratitude, forever.

Special thanks to French Embassy in Tehran, cultural and consular section, which provide me this opportunity to continue my studies in France.

I wish to acknowledge generous support of Mr. Barbry, MSAP chairman and president of the jury. I appreciate the other jury members, Dr Laurent Falk and Pr Pierre-Yves Renard, whose remarks helped to improve presenting this thesis.

My sincere thanks are also extended to Xavier Trivelli, and Stéphanie Delbaere for doing the NMR based studies (identification of the alkylation site of TMGN and DOSY). Thanks to Maël Penhoat for looking over my shoulder during my first few months in laboratory and his help in interpretation of some NMR spectra

I gratefully acknowledge the excellent MSAP staff, especially Anne-Sophie Lacoste and Geoffrey Vauvy, for providing a supportive environment in which to explore my ideas and to do my experiments.

Finally I would like to thank all my friends in the laboratory for their love and support.



*Once again,*

*In memory of my father, Hassan*

*To the most important person in my life, to my mother, Nassrine*

*To the most beloved and the most precious friend, to my sister, Pourandokht*

## TABLE OF CONTENTS

<b>ACKNOWLEDGMENTS</b>	<b>IV</b>
<b>TABLE OF CONTENTS</b>	<b>VI</b>
<b>1 INTRODUCTION</b>	<b>12</b>
1.1 Esterification in microreactors	13
1.2 Microreactors and Reaction kinetics	17
1.3 Thesis Objectives and Overview	19
<b>2 KINETICS STUDIES</b>	<b>20</b>
2.1 Linear free energy relationships [50-51]	21
2.2 Motivation	23
2.3 Description of Benzoic Acid Alkylation	24
2.3.1 Reaction kinetics Comparison in Batch and in Continuous	25
2.3.2 Effect of Different Reagents Combination	27
2.3.3 Effect of Reaction Temperature	30
2.3.4 Effect of the Alkylating Agent and of the Solvent	33
2.3.5 Substituent Effect	34
<b>3 BASICITY AND NUCLEOPHILICITY</b>	<b>42</b>
3.1 Motivation	42
3.2 Base-Iodomethane stability	43
<b>4 IDENTIFYING SITE OF ALKYLATION IN TMGN</b>	<b>48</b>
4.1 TMGN	53
4.2 TMGN-H <sup>+</sup>	57
4.3 TMGN-Me	59
<b>5 MEASURING DIFFUSION COEFFICIENTS</b>	<b>64</b>
<b>6 PREPARATIVE-SCALE SYNTHESIS</b>	<b>69</b>
6.1 Motivation	69
6.1.1 Quercetin	72

<b>6.2</b>	<b>Syringic acid</b>	<b>76</b>
6.2.1	Reaction kinetics Comparison in Batch and in Continuous	87
6.2.2	Protonation route	89
<b>6.3</b>	<b>Quercetin</b>	<b>93</b>
<b>6.4</b>	<b>Clofibric acid</b>	<b>99</b>
<b>6.5</b>	<b>Trolox</b>	<b>101</b>
<b>6.6</b>	<b>Podocarpic acid</b>	<b>102</b>
<b>7</b>	<b>METHODOLOGY</b>	<b>104</b>
<b>7.1</b>	<b>Micromixers</b>	<b>104</b>
<b>7.2</b>	<b>Kinetics study experiments</b>	<b>107</b>
7.2.1	Analysis method: GC-MS	109
<b>7.3</b>	<b>Base-Mel stability study experiments</b>	<b>109</b>
7.3.1	Analysis method: Mass spectrometry	110
<b>7.4</b>	<b>Preparative-scale experiments</b>	<b>112</b>
7.4.1	Extraction evaluation test	113
7.4.2	Two-Step process	113
7.4.3	Analysis method: NMR	115
7.4.4	Analysis method: LC-MS	115
<b>8</b>	<b>CONCLUSION</b>	<b>116</b>
<b>9</b>	<b>APPENDICES</b>	<b>118</b>
<b>9.1</b>	<b>Appendix A</b>	<b>118</b>
<b>9.2</b>	<b>Appendix B</b>	<b>120</b>
<b>9.3</b>	<b>Appendix C</b>	<b>123</b>
<b>9.4</b>	<b>Appendix D</b>	<b>125</b>
<b>9.5</b>	<b>Appendix E</b>	<b>126</b>
<b>10</b>	<b>EXTENDED ABSTRACT (IN FRENCH)</b>	<b>130</b>
<b>11</b>	<b>EXTRACTED PAPERS</b>	<b>135</b>
<b>12</b>	<b>BIBLIOGRAPHY</b>	<b>150</b>

## LIST OF TABLES

TABLE 1-1 ESTERIFICATION REACTIONS PERFORMED IN MICROREACTORS. ....	15
TABLE 2-1 KINETICS COMPARISON IN BATCH AND IN CONTINUOUS.....	27
TABLE 2-2 THE EFFECT OF THE REAGENT COMBINATION. CONCENTRATIONS OF 1, 16 AND 6 ARE ~26MM. 27	
TABLE 2-3 EFFECT OF TEMPERATURE. 16:1 AND 6:1 MOLAR RATIOS: 1.0. REAGENTS COMBINATION :[( 1, 16), 6].....	31
TABLE 2-4 EFFECT OF THE ALKYLATING AGENT. CONCENTRATIONS OF BENZOIC ACID, 1, TMGN, 16 AND ALKYLATING AGENT ARE ~26MM. REAGENT COMBINATION IS [(1, 16), ALKYLATING AGENT]. ....	33
TABLE 2-5 EFFECT OF THE SOLVENT. CONCENTRATIONS OF BENZOIC ACID, 1, TMGN, 16 AND IODOMETHANE, 6 ARE ~26MM. REAGENT COMBINATION IS [(1, 16), 6]. ....	34
TABLE 2-6 SUBSTITUENT EFFECT. CONCENTRATIONS OF SUBSTITUTED BENZOIC ACID, TMGN, 16 AND IODOMETHANE, 6: ~26MM. [(SUBSTITUTED BENZOIC ACID, 16), 6].....	35
TABLE 3-1 BASE ALKYLATION KINETICS RESULTS .....	44
TABLE 4-1 <sup>1</sup> H, <sup>13</sup> C AND <sup>15</sup> N CHEMICAL SHIFT ASSIGNMENT OF TMGN IN DMSO-D <sub>6</sub> AT 300K .....	50
TABLE 4-2 <sup>1</sup> H, <sup>13</sup> C AND <sup>15</sup> N CHEMICAL SHIFT ASSIGNMENT OF TMGN-H <sup>+</sup> IN DMSO-D <sub>6</sub> AT 300K .....	51
TABLE 4-3 <sup>1</sup> H, <sup>13</sup> C AND <sup>15</sup> N CHEMICAL SHIFT ASSIGNMENT OF TMGN-ME IN DMSO-D <sub>6</sub> AT 300K.....	51
TABLE 4-4 <sup>15</sup> N CHEMICAL SHIFTS OF TMGN, TMGN-H <sup>+</sup> AND TMGN-ME .....	62
TABLE 5-1 NMR EXPERIMENTAL PARAMETERS FOR DOSY EXPERIMENTS .....	65
TABLE 5-2 DIFFUSION AND STOKES RADIUS DATA FOR MODEL COMPONENTS.....	66
TABLE 6-1 BATCH EXPERIMENTS <sup>†</sup> .....	80
TABLE 6-2 EFFECT OF THE ALKYLATING AGENT AND BASE QUANTITY <sup>†</sup> . MICROMIXER:NANOMIXER <sup>®</sup> ; TOTAL FLOWRATE: 20 μL MIN <sup>-1</sup> . REAGENTS COMBINATION: [(2, 6), BASE]). ....	81
TABLE 6-3 EFFECT OF THE REAGENTS COMBINATION <sup>†</sup> . MICROMIXER: NANOMIXER <sup>®</sup> ; TOTAL FLOWRATE: 20 μL MIN <sup>-1</sup> .....	82
TABLE 6-4 EFFECT OF REAGENTS COMBINATION <sup>†</sup> . MICROMIXER: NANOMIXER <sup>®</sup> ; TOTAL FLOWRATE: 20 μL MIN <sup>-1</sup> .....	83
TABLE 6-5 EFFECT OF MICROMIXER <sup>†</sup> . TOTAL FLOWRATE: 20 μL MIN <sup>-1</sup> ; REAGENTS COMBINATION: [(2, 6), BASE]). ....	84
TABLE 6-6 EFFECT OF THE RESIDENCE TIME <sup>†</sup> ; MICROMIXER: NANOMIXER <sup>®</sup> .REAGENTS COMBINATION: [(2, 6), 21])......	85
TABLE 6-7 EFFECT OF THE RESIDENCE TIME <sup>†</sup> ; MICROMIXER: NANOMIXER <sup>®</sup> . REAGENTS COMBINATION: [(2, 6), 16])......	86
TABLE 6-8 RATE CONSTANTS OF THE REACTION OF SYRINGIC ACID, 2, AND IODOMETHANE, 6 AT THE PRESENCE OF AN ORGANIC BASE (TMGN, 16 AND DBU, 21) AT VARIOUS REAGENTS COMBINATION .	87
TABLE 6-9 RATE CONSTANTS OF THE REACTION OF METHYL SYRINGATE, 2A, AND IODOMETHANE, 6 AT THE PRESENCE OF AN ORGANIC BASE (TMGN, 16 AND DBU, 21). ....	87
TABLE 6-10 CALCULATED VALUES OF THE AQUEOUS PKA AND BDE FOR THE DIFFERENT OH POSITIONS IN QUERCETIN .....	93
TABLE 6-11 BATCH MODE EXPERIMENTS <sup>†</sup> , CONCENTRATION OF 25: 0.11 MMOL L <sup>-1</sup> , MOLAR RATIO OF BASE: 25=: 1.26 AND OF 6:25 = 1.26 <sup>A</sup> .....	96
TABLE 6-12 CONTINUOUS MODE EXPERIMENTS <sup>†</sup> ; CONCENTRATION OF 25: 0.11 MMOL L <sup>-1</sup> , MOLAR RATIO OF 16: 25= 1.27 AND OF 6:25 = 1.26; MICROMIXER: NANOMIXER .....	97
TABLE 6-13 CONTINUOUS MODE EXPERIMENTS <sup>†</sup> ; CONCENTRATION OF 25: 0.11 MMOL L <sup>-1</sup> , MOLAR RATIO OF 21: 25= 1.27 AND OF 6:25 = 1.26; MICROMIXER: NANOMIXER .....	98
TABLE 6-14 ALKYLATION OF CLOFIBRIC ACID <sup>†</sup> , MICROMIXER: NANOMIXER <sup>®</sup> . REAGENTS COMBINATION: [(3,16),6]). ....	99
TABLE 6-15 ALKYLATION OF TROLOX <sup>®†</sup> , MICROMIXER: NANOMIXER <sup>®</sup> . REAGENTS COMBINATION: [(5, 16), 6])......	101

TABLE 6-16 ALKYLATION OF PODOCARPIC ACID <sup>†</sup> , MICROMIXER: NANOMIXER <sup>®</sup> . REAGENTS COMBINATION: [(4, 16), 6]. .....	102
TABLE 7-1 MIXING TIME MEASUREMENT FOR DIFFERENT APPLIED MICROMIXERS .....	106
TABLE 7-2 FLOWRATES USED IN KINETICS STUDIES AND THEIR CORRESPONDING RESIDENCE TIMES .....	108
TABLE 7-3 FLOWRATES USED IN BASE-MEI STABILITY STUDY EXPERIMENTS AND THEIR CORRESPONDING RESIDENCE TIMES .....	110
TABLE 7-4 FLOWRATES USED IN PREPARATIVE-SCALE EXPERIMENTS AND THEIR CORRESPONDING RESIDENCE TIMES .....	112
TABLE 7-5 FLOWRATES USED IN PREPARATIVE-SCALE EXPERIMENTS (QUERCETIN) AND THEIR CORRESPONDING RESIDENCE TIMES.....	114
TABLE 9-1 CALCULATED LÖWDIN CHARGES FOR PARA SUBSTITUTED BENZOIC ACIDS [92].....	119
TABLE 9-2 THE RELATIVE $V_{\text{MIN}}$ VALUES OF DIFFERENT SUBSTITUTED BENZOIC ACIDS [94] .....	119
TABLE 9-3 DIFFUSION COEFFICIENT OF DIFFERENT COMPOUNDS IN DMF BY <sup>1</sup> H NMR.....	123
TABLE 9-4 MEASURING DIFFUSION COEFFICIENT OF DMF BY <sup>1</sup> H DOSY NMR.....	123
TABLE 9-5 MEASURING DIFFUSION COEFFICIENT OF WATER BY <sup>1</sup> H DOSY NMR.....	124
TABLE 9-6 PEAK AREA DATA FOR A TYPICAL EXPERIMENT.....	125
TABLE 9-7 STATISTICAL ANALYSIS FOR THE TYPICAL EXPERIMENT .....	125

## LIST OF FIGURES

FIGURE 1-1. SCHEMATIC DIAGRAM OF CONTINUOUS FLOW KINETIC SYSTEM[39].....	17
FIGURE 2-1 SECOND-ORDER KINETICS PLOT IN BATCH EXPERIMENT.....	26
FIGURE 2-2 SECOND-ORDER KINETICS PLOT IN CONTINUOUS MODE.....	26
FIGURE 2-3 THE EFFECT OF PROTONATION OF 16. REAGENT COMBINATION IS [(6, 16), 1].....	29
FIGURE 2-4 THE EFFECT OF HYDROLYSIS OF 6. REAGENT COMBINATION: [(1, 16), 6].....	30
FIGURE 2-5 ARRHENIUS PLOT.....	32
FIGURE 2-6 HAMMETT PLOT.....	36
FIGURE 2-7 HAMMETT PLOT USING $\sigma^-$ VALUES.....	37
FIGURE 2-8 RATE CONSTANT VERSUS THE ELECTROSTATIC POTENTIAL MINIMUM ( $V_{MIN}$ ).....	38
FIGURE 2-9 RESONANCE IN PHENOXIDE ION.....	40
FIGURE 2-10 HAMMETT PLOT BASED ON THE IONIZATION CONSTANTS OF DIFFERENT SUBSTITUTED BENZOIC ACIDS.....	40
FIGURE 3-1 PLOT OF LOG K AND PKA FOR BASES 14-24.....	45
FIGURE 3-2 BEMP-TMGN KINETICS COMPARISON ON BENZOIC ACID ALKYLATION BY MEI.....	46
FIGURE 4-1 QUANTIFICATION OF TMGN- $H^+$ AND TMGN-ME FOR A SOLUTION OF 25MM TAKEN FROM 800 MHZ $^1H$ NMR SPECTRUM OF TMGN- $H^+$ AND TMGN-ME.....	52
FIGURE 4-2 QUANTIFICATION OF TMGN- $H^+$ AND TMGN-ME FOR A SOLUTION OF 25MM TAKEN FROM 400 MHZ $^1H$ NMR SPECTRUM OF TMGN- $H^+$ AND TMGN-ME.....	53
FIGURE 4-3 800 MHZ SPECTRUM OF TMGN, THE TRIPLET OF H13/19 AND THE DOUBLETS OF DOUBLETS OF H14/20.....	54
FIGURE 4-4 800 MHZ SPECTRUM OF TMGN, THE DOUBLETS OF DOUBLETS OF H12/18.....	54
FIGURE 4-5 400MHZ NMR 2D-HMBC (BLUE) AND 2D-HSQC (RED) OF TMGN.....	56
FIGURE 4-6 400MHZ 2D NMR $^1H$ - $^{15}N$ HMBC OF TMGN.....	56
FIGURE 4-7 800MHZ 1HNMR (ABOVE) AND 400 MHZ 1HNMR (BELOW) OF TMGN-ME, AROMATIC RANGE.....	59
FIGURE 4-8 400MHZ $^1H$ NMR OF TMGN-ME, METHYL RANGE.....	61
FIGURE 5-1 THE PGSE PULSE SEQUENCE (LEFT). G IS THE AMPLITUDE OF THE PULSED GRADIENT, $\Delta$ ITS DURATION AND $\Delta$ THE SEPARATION BETWEEN THE LEADING EDGES OF THE PULSED GRADIENTS[132]. THE STE SEQUENCE (CENTER) [134].BIPOLEAR PULSE PAIR-LONGITUDINAL EDDY CURRENT DELAY(RIGHT)[135].....	65
FIGURE 5-2 RELATIONSHIP BETWEEN STOKE'S RADIUS AND VAN DER WAALS RADIUS.....	67
FIGURE 6-1 SYRINGIC ACID ALKYLATION BY IODOMETHANE.....	76
FIGURE 6-2 PERCENTAGE OF PROTONATION OF DMAN,17 IN 1:1 SALT [194].....	91
FIGURE 6-3 CLOFIBRIC ACID ALKYLATION BY IODOMETHANE.....	99
FIGURE 6-4 TROLOX ALKYLATION BY IODOMETHANE.....	101
FIGURE 6-5 PODOCARPIC ACID ALKYLATION BY IODOMETHANE.....	102
FIGURE 7-1. EXPERIMENTAL SET-UP AND LAYOUT OF NANOMIXER®.....	107
FIGURE 7-2. SCHEMATIC DIAGRAM OF THE EXPERIMENTAL SET-UP. IT COMPRISES OF A MICROMIXER AND A FUSED SILICA-BASED CAPILLARY TUBULAR REACTOR. THE TWO SYRINGES, CONTAINING REAGENTS ARE CONNECTED VIA 30CM CAPILLARIES (ID: 50 $\mu$ M) TO THE MICROMIXER. THE MICROMIXER IS FOLLOWED TO A 300CM FUSED SILICA-BASED CAPILLARY TUBULAR REACTOR (ID: 75 $\mu$ M). THE CAPILLARY REACTOR IS KEPT AT 20°C IN A WATER BATH. ....	107
FIGURE 7-3 SCHEMATIC DIAGRAM OF THE EXPERIMENTAL TWO STEP SET-UP. IT COMPRISES OF TWO MICROMIXERS AND A FUSED SILICA-BASED CAPILLARY TUBULAR REACTOR. THE THREE SYRINGES, CONTAINING REAGENTS ARE CONNECTED VIA 30CM CAPILLARIES (ID: 50 $\mu$ M) TO THE MICROMIXER. MICROMIXER1 IS FOLLOWED TO A 25 CM FUSED SILICA-BASED CAPILLARY TUBULAR REACTOR (ID: 50 $\mu$ M) AND THEN TO MICROMIXER 2. THE CAPILLARY REACTOR (3M, 75 $\mu$ M) IS KEPT AT 20°C IN A WATER BATH.....	113

FIGURE 9-1 SECOND ORDER KINETICS PLOT OF BENZOIC ACID ALKYLATION BY IODOMETHANE IN THE PRESENCE OF TMGN AND IN DMF AT 4 °C .....	118
FIGURE 9-2 SECOND ORDER KINETICS PLOT OF BENZOIC ACID ALKYLATION BY IODOMETHANE IN THE PRESENCE OF TMGN AND IN DMF AT 70 °C .....	118
FIGURE 9-3 $^1\text{H}$ NMR OF TMGN- $\text{H}^+$ AND THE SIGNAL OF LABILE HYDROGEN NUCLEUS.....	120
FIGURE 9-4 800MHZ 2D NMR $^1\text{H}$ - $^{15}\text{N}$ HMBC OF TMGN-ME, METHYL GROUPS OF C7/8/9/10.....	120
FIGURE 9-5 400MHZ 2D NMR $^1\text{H}$ - $^{15}\text{N}$ HMBC OF TMGN-ME .....	121
FIGURE 9-6 $^{13}\text{C}$ -DECOUPLED $^1\text{H}$ NMR SPECTRUM OF TMGN-ME AND THREE PEAKS FOR $^{13}\text{C}$ -LABELED METHYL GROUPS .....	121
FIGURE 9-7 400MHZ 2D NMR $^1\text{H}$ - $^{15}\text{N}$ HMBC OF TMGN-ME, METHYL GROUPS OF C7/8/9/10 .....	122

## 1 INTRODUCTION

“Faster, cleaner, safer” [1] these three words are enough used to reflect the benefits of microfluidics in chemistry . A simple search for “microfluidics” in the Chemical Abstracts Service (CAS) database of chemical and bibliographic information, turned up beyond 27000 hits in english and french language documents excluding patents. Chemistry in continuous flow microreactors has received considerable attention over the past decade [1-8]. In microreactors, potentially explosive and hazardous reactions can be safely conducted, [9-11] short-lived intermediates can be trapped to increase chemical yield [12], a cascade of reactions can be carried out without the necessity of isolating intermediates, and alternatively it is possible to use high pressure and/or temperature conditions [13]. Continuous flow microreactor have found broad applications in multi-step organic synthesis [14] and in the synthesis of complex natural products.

Reactors, mixers, pumps, valves,... there is a wide variety of microfluidics devices for many different purposes, using various fabrication methods. They have been widely reviewed, for example [15-20]. Among them microreactors and micro structured reactors<sup>1</sup> offer the attractive feature of continuous flow. In fact, despite many advances in synthetic chemistry over the years, organic synthesis is still being carried out using the batch methodologies (“flask”). However a continuous process based mainly on microreactor technology (“flow”) can bring many advantages to a synthetic chemist [1, 6-8, 14, 21-24]. Despite predicting a long-term future of flow reactors, a debate has been launched around obtaining more efficient results from microflow reactors than flasks for homogeneous catalytic reactions [25]. Nevertheless, because of their lower solvent usage, they have

---

1 . Microstructured reactors are compact units with small scale channels within, while microreactors are small size reactor with microchannel within.



lower carbon footprint and regarding the climate change regulations around the world, this benefit becomes increasingly important [26-27].

Microreactors have been already used for a broad range of reactions [5, 28-29] but in the framework of the objectives of this thesis, the present discussion is confined to the survey of the literature pertaining to the use of microreactors in esterification as well as in collecting reaction kinetics data.

## **1.1 Esterification in microreactors**

Esterification reactions give relatively high yields in batch mode, but they require also long reaction times. By using microreactors, it is possible to take advantage of high concentrations, reduced waste and increased reaction rate [23]. Table 1-1 lists those esterification reactions conducted in micro reactors.

Acid-catalyzed esterification reaction, entry 1 in the table, has been reported using a set-up composed of a commercial micromixer followed by two consecutive capillary segments (ID.600 $\mu$ m and 1200 $\mu$ m). The first segment is heating while the second one is cooling to quench the reaction. The residence time has been 5 min but it has had no obvious effect on conversion. The highest oleic acid conversion of 99.5% has been obtained at the catalyst concentration of 3 wt% and the methanol to oleic acid molar ratio of 40 [30].

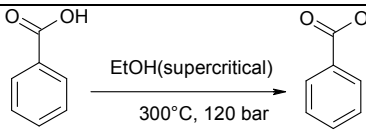
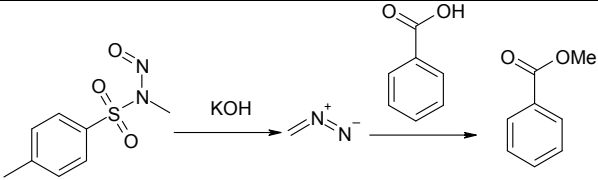
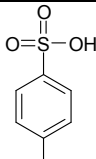
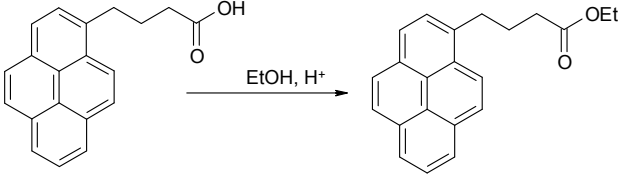

In another study, the synthesis of ethyl benzoate from benzoic acid, entry 2 in the table, within a microreactor has been demonstrated [13]. This reaction has been carried out at 300 °C and 120 bar. Due to its high ionic product of ethanol in supercritical conditions, it plays the role of the solvent as well as the catalyst. The initial concentration of the benzoic acid and ethanol was 0.33 M. The utilized set-up again consists of a commercial

micromixer and a capillary reactor (ID.1000 $\mu$ m) but micromixer type has not been mentioned.

Alongside those examples, Stark et al. [9, 31] utilized in situ generation of diazomethane and its use in the synthesis of methyl benzoate (entry 3 in the table). Diazomethane was generated from a commercial precursor, Diazald<sup>®</sup>, and was consumed on-site by reaction with benzoic acid to benzoic acid methyl ester at a yield of up to 75 % at temperatures of 0 and 50 °C. This two step process has been done in a set-up comprised of two commercial micromixers and two capillary segments. In the first step, Diazald<sup>®</sup> and KOH are mixed together in a micromixer and the reaction undergoes in a first capillary segment (residence time 5-15s) another micromixer is connected to the end of the first capillary and it is there that benzoic acid is introduced and reacts with diazomethane through the second capillary segment ( $10 < \text{residence time} < 70\text{s}$ ). All continuous experiments were carried out using at a ratio of Diazald<sup>®</sup>: KOH: benzoic acid = 1.0: 1.5: 4.0. They have demonstrated that this second residence time has not a major effect on the yield of benzoic acid methyl ester. A constant yield higher than 65% has been obtained in the temperature range of 0-50°C.

Kulkarni *et al.* [32] carried out the homogeneous and heterogeneous acid-catalyzed esterification of acetic acid with butanol (entries 4 and 5 in the Table 1-1). In case of homogeneous esterification, a set-up comprising of a commercial micromixer followed by an isothermal tubular reactor (ID. 1.3mm) was used. Sulfuric acid was used as the catalyst, residence time was in the range of 100-8300 s and the maximum temperature was 80°C. In these conditions and with a quantity of 0.005–4.5% w/w of the homogeneous catalyst (H<sub>2</sub>SO<sub>4</sub>), they have reported a conversion of 85%. The heterogeneous reaction was conducted in a system of commercial micromixer connected to a custom-built miniaturized fixed-reactor. The catalyst was Amberlyst-15 and the residence time was in the range of 100-4000 s. The reaction underwent at a temperature of 80°C with a conversion of 74%.

Table 1-1 Esterification reactions performed in microreactors.

Entry	Reaction	Residence time	Conversion (%)	Ref
1	$\text{RCOOH} + \text{CH}_3\text{OH} \xrightarrow{\text{H}_2\text{SO}_4} \text{RCOOCH}_3 + \text{H}_2\text{O}$ (Oleic acid)	5min	99.5	[30]
2	 $\text{C}_6\text{H}_5\text{COOH} \xrightarrow[300^\circ\text{C}, 120\text{ bar}]{\text{EtOH (supercritical)}} \text{C}_6\text{H}_5\text{COOEt}$	12 min	87	[13]
3		< 3 min	>65	[9]
4	$\text{CH}_3\text{COOH} + \text{ROH} \xrightarrow{\text{H}_2\text{SO}_4} \text{CH}_3\text{COOR} + \text{H}_2\text{O}$ R is $-(\text{CH}_2)_3\text{CH}_3$	100-8300s	85	[32]
5	$\text{CH}_3\text{COOH} + \text{ROH} \xrightarrow{\text{Amberlyst-15}} \text{CH}_3\text{COOR} + \text{H}_2\text{O}$ R is $-(\text{CH}_2)_3\text{CH}_3$	100-4000s	74	[32]
6	 $\text{CH}_3\text{COOH} + \text{ROH} \xrightarrow{\text{Catalyst}} \text{CH}_3\text{COOR} + \text{H}_2\text{O}$ R: $-\text{CH}_3$ $-\text{CH}_2\text{CH}_3$ , $-(\text{CH}_2)_2\text{CH}_3$ $-(\text{CH}_2)_3\text{CH}_3$	14.7 min	74.0 70.1 97.2 92.2	[33]
7		40min	83	[34]
8		20 min	100	[35]

In all the above studies, “elements” of a micro device are one or two micromixers and tubular reactors. However, there are other possibilities. The simplest one is to mix all the reagents together before introducing them into the microreactor. In such a case, a capillary tube plays the role of the microreactor. Using this, esterification of acetic acid with short chain alcohols in the presence of p-toluene sulfonic acid as catalyst (entry 6 in the table) has been reported [33]. Under identical conditions, the batch reactor only went to 94.1% yield in 40 min.

An alternative method is to have both of micromixer and microreactor on a single chip. Brivio *et al.* [34] investigated the acid-catalyzed esterification of 9-pyrenbutyric acid with ethanol (entry 7 of the table) in a “home-made” glass microreactor. Mixtures of 9-pyrenbutyric and sulfuric acid as well as ethanol and sulfuric acid were used as the reagents and the experiments were carried out at 50 °C. In these conditions they could achieve a conversion of 83 % during 40 min. In these conditions the batch reaction leads to only 15 % conversion. To simulate the glass walls of the microreactor, silica gel had been applied in the batch reactor experiments. The authors concluded that the excess of SiOH groups present in the glass microreactor assist in ethanol activation [23]. Usually the reagents/solvents are introduced into the microreactor by external pumps (syringe pumps or microfabricated pumps). This has been applied in all aforementioned examples. An alternative method to drive the liquid inside the glass microreactors and to generate precise plug flow is electroosmotic flow (EOF). EOF is fluid motion driven by electric field acting on the net fluid charge produced by charge separation at a fluid-solid interface [36]. But it is typically only applicable for aqueous systems, low flow rates, and small channel dimensions [37]. Wiles *et al.*[35] demonstrated catalytic esterification of benzoic acid and nitrobenzoic acid within an EOF-based, borosilicate glass microreactor. Their reaction

scheme (only for benzoic acid) is presented as entry 8 of the Table 1-1. They achieved 100% conversion over a period of 20 min.

## 1.2 Microreactors and Reaction kinetics

Kinetics can be determined by various methods; flow method, competition method, relaxation method,...[38]. In flow studies of fast reactions streams of two reactant solutions are forced under pressure to meet in a mixing chamber from which the mixed solution passes to an observation chamber [39]. These methods function in the time range of (approximately) 1 ms to 10 s [39]. Among flow methods, continuous flow method is generally used to study the kinetics of fast reactions, in liquid and gas phases. The basis of this technique, as illustrated in Figure 1-1, involves the injection of two reactants A and B in a mixing chamber, whose design contributes to rapid mixing, followed by an observation tube where the determination of their concentrations or that of the products takes place at a certain distance from the mixing chamber. With continuing injection of reactant solutions a steady state is set up in the observation tube, the concentration at any point being independent of time [38-39].

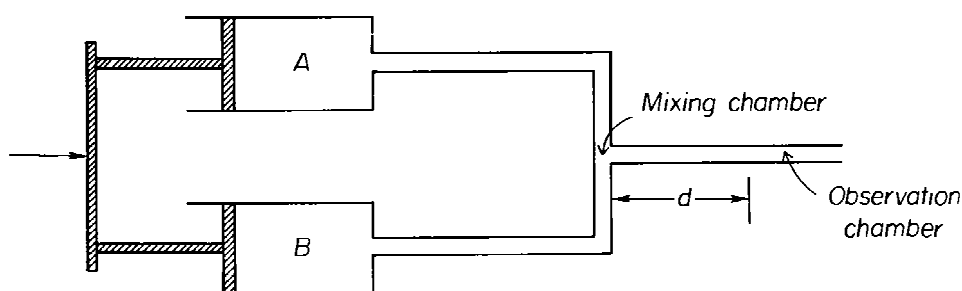


Figure 1-1. Schematic diagram of continuous flow kinetic system[39]

In this method mixing is essentially complete in a tiny fraction of second. The concentrations are at steady state and analytical method is not needed to be fast response. The major drawback of this method is to maintain the steady-state conditions throughout

the experiments; this technique requires the use of large quantities of reactants. This disadvantage however can largely be compensated by using microreactors. Besides this, microreactors are appropriate for determining the kinetics of extremely fast reactions, reactions that involve an unstable intermediate or a highly toxic compound and reactions that show improved operations at high temperature and pressures. Furthermore, it is possible to combine continuous flow microreactors with in line analysis [40].

### 1.3 Thesis Objectives and Overview

Here, we develop a set-up comprised of a commercial micromixer and a capillary reactor to study the reaction kinetics. Benzoic acid esterification by iodomethane in the presence of an organic superbases was chosen as model reaction. The effect of several parameters, such as temperature, alkylating agent and solvent were investigated. Further the microreactor was used to study the substituent effect and Hammett equation. Chapter 2 describes this parameter optimization process and a comprehensive discussion about several structure-reactivity correlations.

The second class of chemistries, as described in Chapter 3, to be explored by microreactor was a group of organic superbases. In this chapter the kinetics of superbases *N*-alkylation by iodomethane is studied. Using different bases for different chemical synthesis is quite usual. However there is not enough information about the rate of their *N*-alkylation.

Chapters 4 and 5 are two NMR based studies to identify the alkylation site in TMGN molecule and to determine the diffusion coefficients of some key components in this study.

Chapter 6 describes the optimization of natural carboxylic acids, phenol-acids and polyphenols *O*-alkylation. This study is an example of that the same reactor system that was used for the kinetic studies could also generate production scale quantities of material. Finally, in Chapters 7 and 8 the experimental procedures in detail and a conclusion to this thesis are brought.

## 2 KINETICS STUDIES

In the chemical industry and fine chemistry, the process of designing a new molecule and bringing it to market is a complex multistep [41]. To accommodate market fluctuations and reducing the overall time to market, it is essential to have a rapid process development. One solution is to improve the initial steps of physical and chemical data acquisition, especially chemical kinetics data and transport phenomena parameters. Even routine operation of a plant is safer if the fundamental kinetics of its chemistry is fully understood [42]. The measurement and the acquisition of massive amounts of rate data must be carried out at steady state and at isothermal conditions [43]. Also, rapid mixing of reagents and low consumption of sample are the two other desired features of a system for making high temporal resolution kinetic measurements of samples [44].

Microfluidic systems are attractive for performing measurements using minute amounts of reagents. Optimized reaction conditions and rapid experimentation as well as shortening product development life cycles are some of their advantages [17]. In recent years, an increased interest and considerable progress have been seen in the use of miniaturized systems for the study of chemical reactions. Several micro-devices, among them [44-48], have been developed to investigate physical and chemical phenomena as well as fast acquisition of chemical kinetic data and crucial transport phenomena parameters. Continuous flow microfluidic reactors provide a platform for reaction kinetics studies [2, 45-49]. Microfluidic systems operate at low *Reynolds* Number ( $Re < 100$ ) and therefore it is possible to highly limit reagents consumption. Moreover, they provide a small diffusive mixing time and hence a rapid diffusion mixing, due to their small diameter (diffusive mixing time is directly proportional to the square of striation thickness) [44].



## 2.1 Linear free energy relationships [50-51]

An understanding of the dependence of reactivity upon the many reaction variables, particularly substrate structure, reagent structure and reaction medium, is one of the primary aims of chemistry. During the past century the steady accumulation of rate and equilibrium data has led to the formulation of a number of empirical correlations.

The general form of these correlations is a linear relationship between the logarithms of the rate or equilibrium constants for one reaction (A) and those for a second reaction (B) subjected to the same variations of reactant structure or reaction conditions.

A free energy relationship is defined by following equation where the parameter  $a$  is called the *similarity* coefficient.

$$\Delta G = a\Delta G_s + b \quad (1-1)$$

The term  $\Delta G$  is the free energy of a process such as a rate or equilibrium and  $\Delta G_s$  is the free energy of a standard process, often equilibrium, which could be the process under investigation or some other standard reaction.

Linear free energy relationships are divided into two classes: Class **I** free energy relationships compare a rate constant with the equilibrium constant of the same process and Class **II** where the rate or equilibrium constant is related to the rate or equilibrium constant of an unconnected but (often) similar process.

Class **II** free energy relationships are in general more common than those of Class **I** because equilibrium constants are more difficult to measure than rate constants (except in certain cases such as dissociation constants). The Hammett equation is the best-known Class **II** free energy relationship.

It was proposed in 1937 as an empirical correlation:

$$\log k - \log k_0 = \rho\sigma \quad (1-2)$$

where  $k$  and  $k_0$  are rate or equilibrium constants for reactions of  $m$ - and  $p$ -substituted and unsubstituted benzene derivatives, respectively,  $\sigma$  is a parameter dependent only on the substituent and its position and  $\rho$  is a parameter dependent only upon the nature of the derivative, the reaction and conditions under which it takes place.

The  $\rho$  value for a reaction measures its susceptibility to change in substituent and a positive  $\rho$  value registers that electron withdrawing substituents increase the rate or equilibrium constant consistent with an increase in negative charge at the reaction centre. The  $\rho$  value is therefore a measure of the change in charge in the system *relative* to that in the dissociation of benzoic acids where  $\rho$  is defined as 1.0 and change in charge in the carboxyl group is -1.0.

The Hammett relationship only applies to systems where substituents are attached to the reaction centre *via* aromatic rings and are situated *meta* or *para*; *ortho* substituents are *not* included in the Hammett equation owing to steric and through-space interactions. It is not also applicable to aliphatic compounds.

## 2.2 Motivation

Transformation of carboxylic acids into the corresponding methyl esters is a fundamental process in organic synthesis and many methods have been developed for it [52]. Chlorobenzyl Merrifield resins (Chloromethylated polystyrene-1% divinylbenzene) were efficiently alkylated by cesium salts of amino acids without quaternization of their protected amine group and using *N,N'*-dimethylformamide (DMF) as solvent [53-54]. The scope of this reaction has been extended to the alkylation of crowded carboxylic acids using hexamethylphosphoramide (HMPA) as solvent [55] and been used in several synthesis [56-57] including the synthesis of short-lived  $^{11}\text{C}$  propyl and butyl esters [58]. Kondo *et al.* [59-61] demonstrated that the reaction of tetraalkylammonium benzoate salts with alkyl halides in acetonitrile follows a second order kinetics. There are several reports on esterification of carboxylic acids in basic mediums [54-55, 62-65]. This alternative method appears to be milder compared to classical esterification procedures (Fischer esterification, for example). Ono *et al.* [64] used 1,8-diazabicyclo [5.4.0]-undec-7-ene (DBU) as the base to efficiently deprotonate benzoic acid. They reported a yield of 95% after 1.5 h for the alkylation of benzoic acid in benzene by iodomethane at room temperature. The concentration of the starting materials was  $2 \text{ mol L}^{-1}$ . However in these conditions the obtained  $\text{DBUH}^+\text{T}^-$  salt is insoluble and the resulting white slurry precludes its use in a microsystem. Mal *et al.* [65] employed the same procedure to the *O*-methylation of various carboxylic acids in acetone and acetonitrile as solvents. One of the most serious side reactions in these syntheses is the alkylation of DBU by iodomethane. Barton *et al.* [66-67] reported that their hindered guanidine bases are much more stable toward alkylation and therefore enable alkylating crowded carboxylic acid like adamantane-1-carboxylic acid even with secondary alkyl halide, isopropyl iodide [62]. This reaction has been used during the total synthesis of salinomycin [68].

In the first part of this chapter, we have examined in detail the kinetics of benzoic acid alkylation, deprotonated by TMGN in a microfluidic device. The comparison of the reagents (TMGN, benzoic acid and iodomethane) mixing strategies, the temperature dependence of reaction rate and finally different linear free energy relationships for this reaction have been investigated. We used DMF as solvent, because its high polarity avoids the formation of aggregates or strong ion pairs which complicate the kinetics of the reaction [69-70]. Here, we have chosen 1,8-bis(tetramethylguanidino)naphthalene (TMGN) as base. Our development was guided by preliminary results obtained from monitoring reaction, using different bases, by  $^1\text{H}$  NMR spectroscopy.

### 2.3 Description of Benzoic Acid Alkylation

Benzoic acids  $\text{pK}_a$  in DMF is in the range of 10.6 (for 4-nitrobenzoic acid) to 13.0 (for 3,4-dimethylbenzoic acid) [71]. The ionization constant ( $\text{pK}_{\text{BH}^+}$ ) of TMGN in acetonitrile is 25.1 [72]. By using either of the two linear correlations [73] between the equilibrium acidities in DMF versus those determined in acetonitrile,  $\text{pK}_{\text{BH}^+}$  of TMGN in DMF is estimated to be 16.4 or 17.5. Therefore TMGN is able to effectively remove benzoic acid's acidic hydrogen.

The reaction of substituted benzoate with iodomethane is a well-known  $\text{S}_{\text{N}}2$  reaction, and hence follows a second order kinetics. If reaction conversion is shown by  $f$ , the values of  $k$  are determined graphically by plotting the function  $1/(1-f)$ , against time( $t$ ) which results in a straight line with a slope equal to  $k[\text{YC}_7\text{H}_5\text{O}_2^-]_0$ , where  $[\text{YC}_7\text{H}_5\text{O}_2^-]_0$  is the initial concentration of benzoic acid. Here, conversion,  $f$ , was calculated by the peak area ratio based on GC-MS data:

$$f = \frac{\text{peak area of benzoic acid methyl ester}}{(\text{peak area of benzoic acid methyl ester} + \text{peak area of benzoic acid silyl ester})} \quad (1-3)$$

In continuous mode, the flow rates were varied to give different residence times. The backmixing can be described by Taylor-Aris model, where the molecular diffusion coefficient is replaced by an effective axial diffusion coefficient  $D_{ax}$  and expressed by the dimensionless Bodenstein number[74]:

$$D_{ax} = D + \frac{\bar{w}^2 d_h^2}{192 D} \quad (1-4)$$

$$Bo = \frac{\bar{w}L}{D_{ax}} \quad (1-5)$$

In these equations,  $D$  is diffusion coefficient;  $L$  and  $d_h$  are length (here, 3m) and hydrodynamic radius (here, 75 $\mu$ m).  $\bar{w}$  is the average velocity that can be calculated by dividing flowrate to cross-sectional area. The flow rate range employed in continuous mode corresponds to a Bodenstein number  $Bo$  range of 90-1810. For these large  $Bo$  numbers, no dispersion occurs and plug flow is assumed in the capillary tubular reactor [74].

### 2.3.1 Reaction kinetics Comparison in Batch and in Continuous

The kinetics of benzoic acid, **1**, alkylation by iodomethane, **6**, in the presence of TMGN, **16** was investigated in batch and in continuous. The straight line relationship (batch:  $R^2=0.983$  and continuous:  $R^2=0.999$ ) which we observed in every case, substantiated our assumption of second-order kinetics. Figure 2-1 and 2-2 show second-order kinetic plot for the reaction in batch and in microfluidic device.

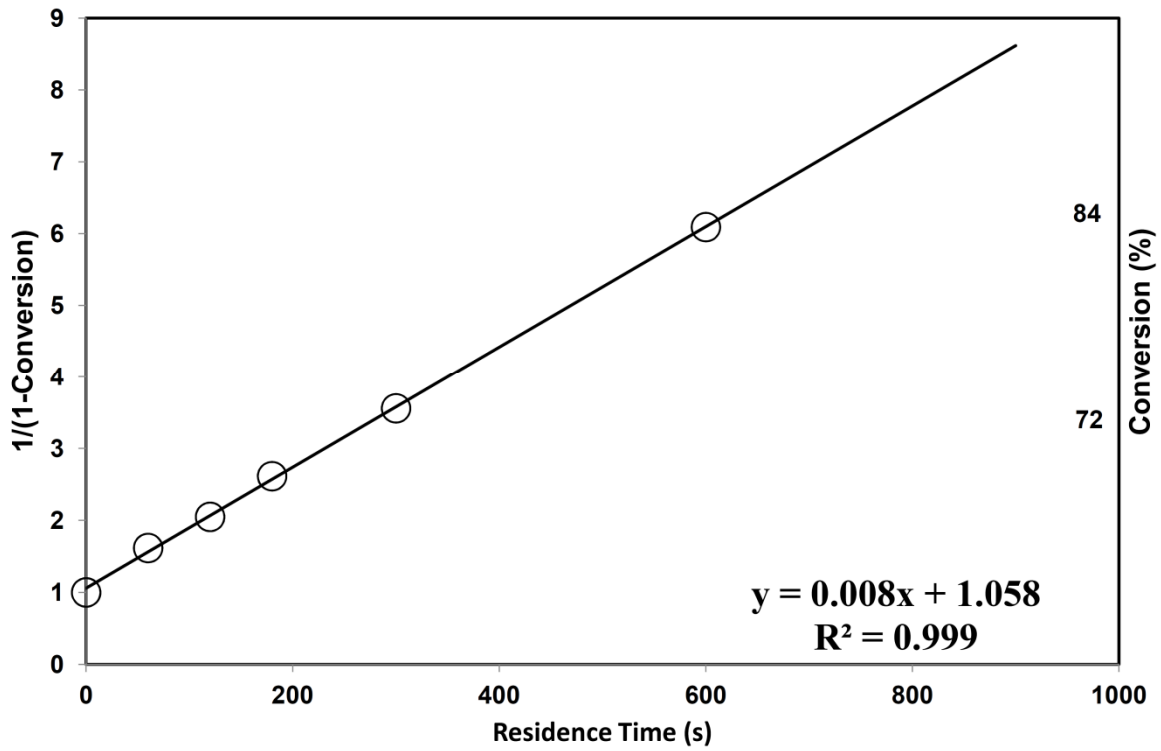


Figure 2-1 Second-order kinetics plot in batch experiment

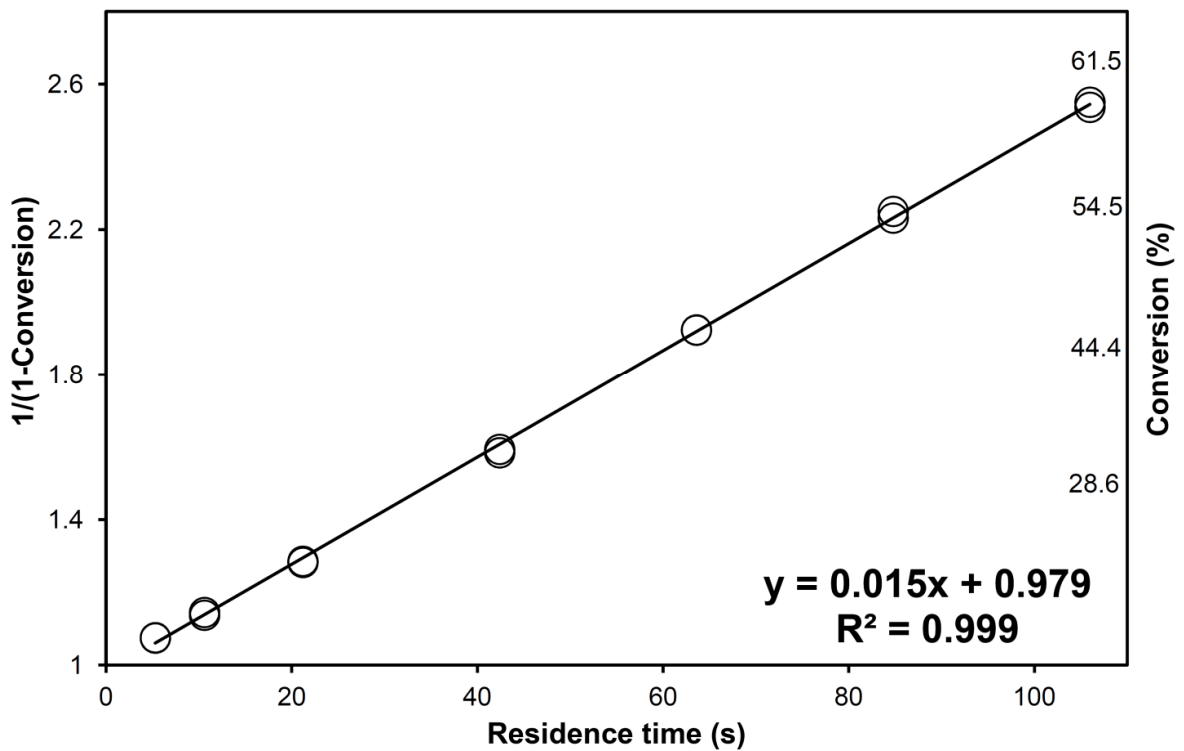


Figure 2-2 Second-order kinetics plot in continuous mode.

Table 2-1 lists the obtained  $k$  values for these experiments. The obtained reaction rate constant in batch is  $0.5948 \text{ mol}^{-1} \cdot \text{L} \cdot \text{s}^{-1}$ , which is slightly higher than that of the continuous.

**Table 2-1 Kinetics comparison in batch and in continuous**

Entry	Process Type	Concentration of <b>1</b> (mmol L <sup>-1</sup> )	<b>16:1</b> molar ratio	<b>6:1</b> molar ratio	$k$ (mol <sup>-1</sup> L s <sup>-1</sup> )
1	Batch	14.4	1.0	1.0	0.636±0.0578
2	Continuous	26.7	1.0	1.1	0.571±0.0216

In batch experiments no temperature control was applied and this slightly higher kinetics can be attributed to the higher ambient temperature on the day of experiment.

### 2.3.2 Effect of Different Reagents Combination

Since in our microfluidics system there are only two inlet flows, but three main reactants; it is possible to have three possible combinations for introducing the reagents into the micromixer. Hence, the effect of reagent combinations on the esterification of benzoic acid, **1**, with iodomethane, **6**, in the presence of TMGN, **16**, was also studied. A summary of these experiments and their obtained  $k$  values are presented in Table 2-2.

**Table 2-2 The effect of the reagent combination. Concentrations of **1**, **16** and **6** are ~26mM**

First syringe	<b>1,16</b>	<b>1,6</b>	<b>1</b>
Second syringe	<b>6</b>	<b>16</b>	<b>6,16</b>
$k$ (mol <sup>-1</sup> .L.s <sup>-1</sup> )	0.571±0.0216	0.536±0.0652	0.227

The slight difference in reaction rate constant value between the first two combinations (first and second entries in Table 2-2) is negligible. The reported reaction rate constant for the last reagents combination belongs to the residence time up to 60 s. After this the reaction no more follows a second order kinetics. Moreover the  $f-t$  graph is curved downward. Some side reactions seem to occur (it will be discussed later). Hereinafter to

refer a reagent combination, it is shown as [(A, B), C], which means that compounds A and B are pre-mixed together in one syringe and compound C is in another syringe.

### **2.3.2.1 Side Reactions**

One side reaction is alkylation of TMGN, **16**, by iodomethane, **6**. Our studies (Section 3.2) show that this reaction proceeds at very slow rates. DMF is hygroscopic and even when it is “anhydrous”, the trace amounts of water can be considered a significant contaminant with respect to the reactants concentrations [75]. In a separate study of ours (Chapter4), studying alkylation of TMGN, **16** by NMR technique also illustrates that using dry solvent is critical. Hence, another possible side reaction is protonation of TMGN, **16** by residual water in solvent. It means that TMGN, **16** reacts with the residual water to give  $\text{OH}^-$  (as an ion pair  $\text{TMGNH}^+\text{OH}^-$ ). This competitive reaction is faster than the main reaction with the free base. Better results were obtained when this experiment was carried out using DMF dried over molecular sieve (UOP type 3A) and also an amount of 2-3 gr of molecular sieve was added in each syringe. The graph below, Figure 2-3, clearly illustrates the difference between the two experiments. This finding shows that the addition of molecular sieves improves the reaction rate ( $k = 0.320 \text{ mol}^{-1} \cdot \text{L} \cdot \text{s}^{-1}$  up to 60s) but the reaction still does not follow the second-order kinetics after 60 s, which is due to the alkylation of TMGN, **16**, by iodomethane, **6**.



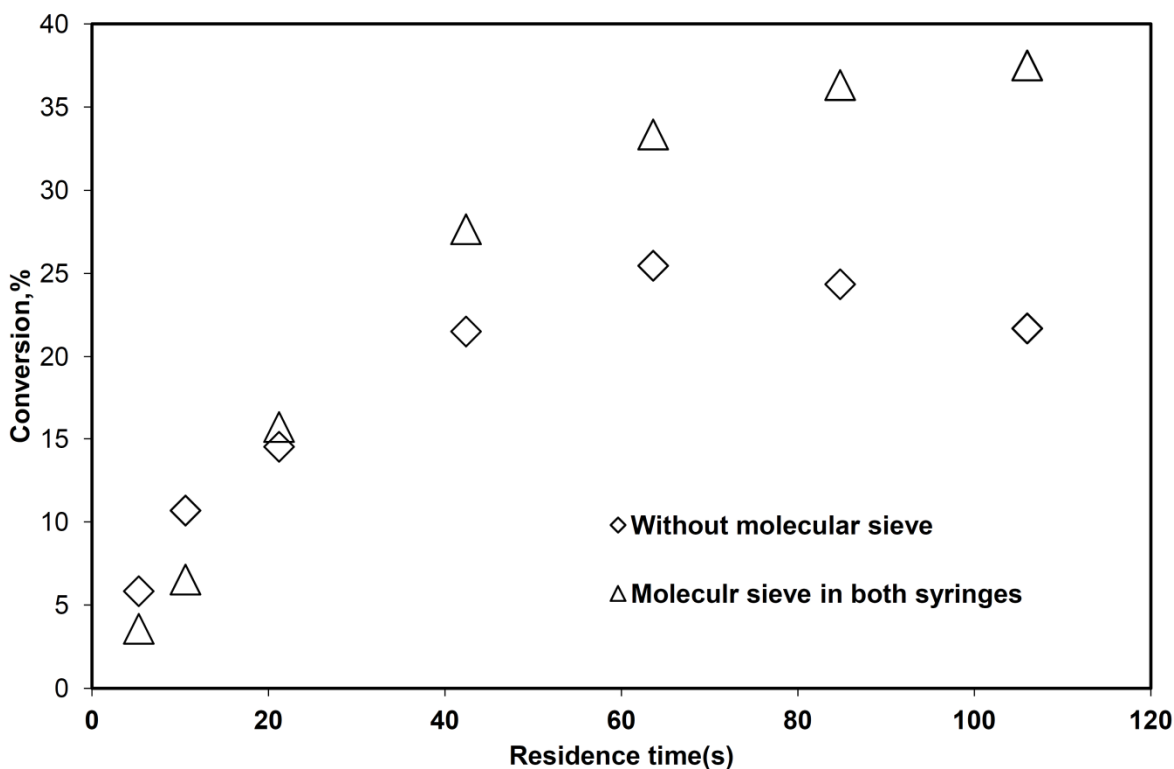


Figure 2-3 The effect of Protonation of **16**. Reagent combination is [(**6**, **16**), **1**]

Partial hydrolysis of iodomethane, **6**, due to the residual water is another possible side-reaction. The hydrolysis of iodomethane, **6**, in pure water is kinetically first order with respect to iodomethane, **6** [76]. It is extremely slow (reaction half life of 103 days) at ambient temperature (25°C) but is accelerated in an alkaline medium (reaction half life of 3h) [77]. Due to its low molecular weight, methanol can hardly be detected by mass spectroscopy. To check if this reaction happens, the kinetic experiments were conducted in pseudo first order conditions with a large excess (10 equivalents) of iodomethane, **6**. The kinetics run was carried out in this condition and the obtained  $f-t$  graph is curved downward. To check if it is due to the reaction and not the mixing, we repeated this experiment using other micromixers, MicroTee and Y connector and every time the result was the same.

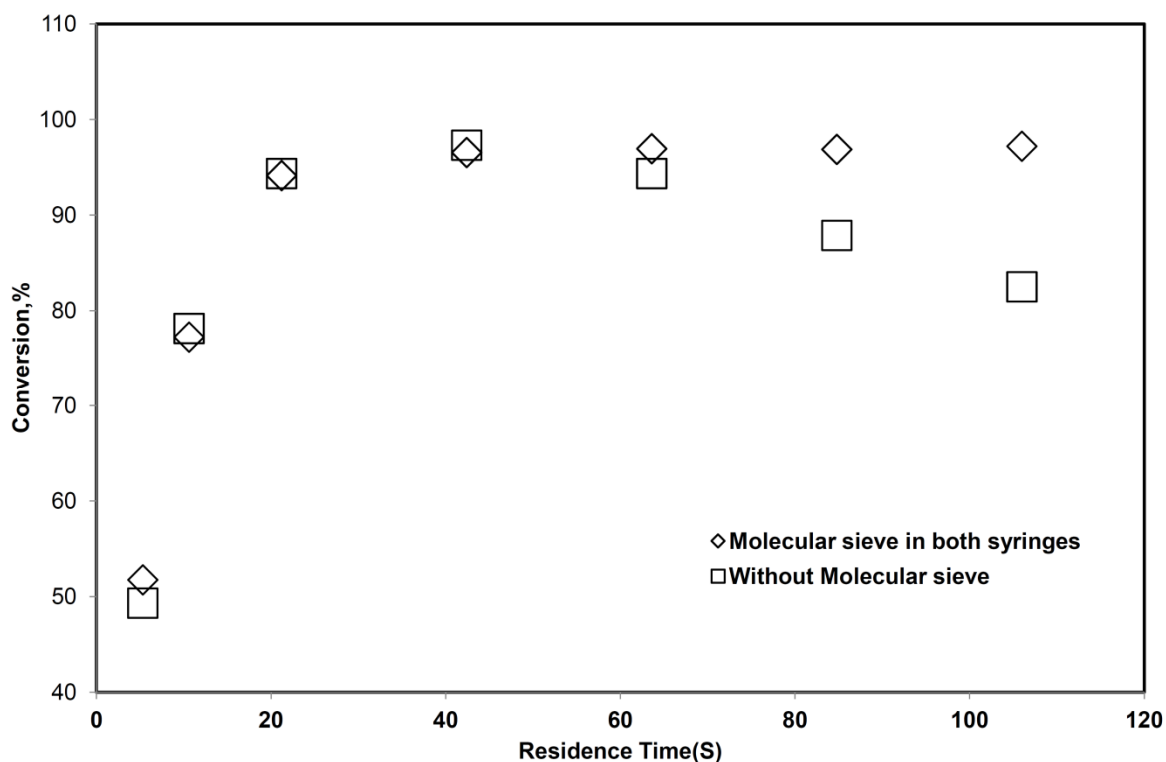


Figure 2-4 The effect of hydrolysis of **6**. Reagent combination: [(**1**, **16**), **6**].

This experiment was also carried out using DMF dried over molecular sieve (UOP type 3A) and also an amount of 2-3 gr of molecular sieve was added in each syringe. Figure 2-4 depicts the difference between the results of these two experimental conditions. As it is observed, a slow hydrolysis of iodomethane is undergoing.

### 2.3.3 Effect of Reaction Temperature

The effect of the reaction temperature in the range of 4-70 °C on the alkylation of benzoic acid, **1**, by iodomethane, **6**, in the presence of TMGN, **16**, was then investigated (Table 2-3). Kinetics for each temperature even the highest show no deviation at shortest residence time which proves that the thermal equilibrium is rapidly achieved in microreactor (Appendix A). Otherwise the kinetics would have been slower at short residence time.

**Table 2-3 Effect of Temperature. 16:1 and 6:1 molar ratios: 1.0. Reagents combination :[( 1, 16), 6].**

T(°C)	70	50	40	30	4
Concentration of benzoic acid,1 (mmol L <sup>-1</sup> )	26.0	26.1	25.9	25.9	26.3
Experimental <i>k</i> (mol <sup>-1</sup> .L.s <sup>-1</sup> )	8.8465, 9.0181	3.6134, 2.8245	1.7784, 1.7476	0.9343, 0.9885	0.2770,0.2104
<i>k</i> <sub>avg</sub> (mol <sup>-1</sup> .L.s <sup>-1</sup> )	8.932±0.1213	2.767±0.8771	1.763±0.0217	0.961±0.0383	0.244±0.0471

The obtained rate constants were used to construct Arrhenius plot (Figure 2-5). The Arrhenius plot is linear ( $R^2 = 0.992$ ) in the applied temperature range (4 to 70°C) and gives a value of 43.27 kJ.mol<sup>-1</sup> for the activation energy. The Eyring-Polanyi equation for a second order reaction is written as:

$$kC_0 = \frac{k_B T}{h} \exp\left(\frac{\Delta S^\ddagger}{R}\right) \left(-\frac{\Delta H^\ddagger}{RT}\right) \quad (1-6)$$

In this equation:

*k*: Reaction rate constant

*C*<sub>0</sub>: Initial concentration of limiting reagent

*k*<sub>B</sub>: Boltzmann constant, 1.380 × 10<sup>-23</sup> J. K<sup>-1</sup>

T: Absolute temperature

*h*: Planck's constant, 6.626 × 10<sup>-34</sup> J.s

$\Delta S^\ddagger$  and  $\Delta H^\ddagger$  are the entropy and enthalpy of activation and R is the gas constant (8.314 J.K<sup>-1</sup>.mol<sup>-1</sup>)

After linearizing this equation, it turns out to

$$\ln\left(\frac{kC_0}{T} \times \frac{h}{k_B}\right) = -\frac{\Delta H^\ddagger}{R} \cdot \frac{1}{T} + \frac{\Delta S^\ddagger}{R} \quad (1-7)$$

It means that if  $\ln\left(\frac{kC_0}{T} \times \frac{h}{k_B}\right)$  is plotted against  $\frac{1}{T}$ , the activation parameters can be derived from its slope and its intercept. From these data the enthalpy and the entropy of activation are estimated as  $\Delta H^\ddagger = 40.3 \text{ kJ mol}^{-1}$  and  $\Delta S^\ddagger = -142.4 \text{ J.K}^{-1} \text{ mol}^{-1}$ . There are few reports for the activation parameters for the alkylation of benzoic acid. Kondo *et al* [59] found  $\Delta H^\ddagger = 66.6 \text{ kJ.mol}^{-1}$  and  $\Delta S^\ddagger = -51.0 \text{ J.K}^{-1}.\text{mol}^{-1}$  for the alkylation of 4-nitrobenzoate by iodomethane in acetonitrile and  $\Delta H^\ddagger = 61.9 \text{ kJ.mol}^{-1}$  and  $\Delta S^\ddagger = -66.0 \text{ J.K}^{-1} \text{ mol}^{-1}$  for the alkylation of benzoate by iodoethane also in acetonitrile [78].

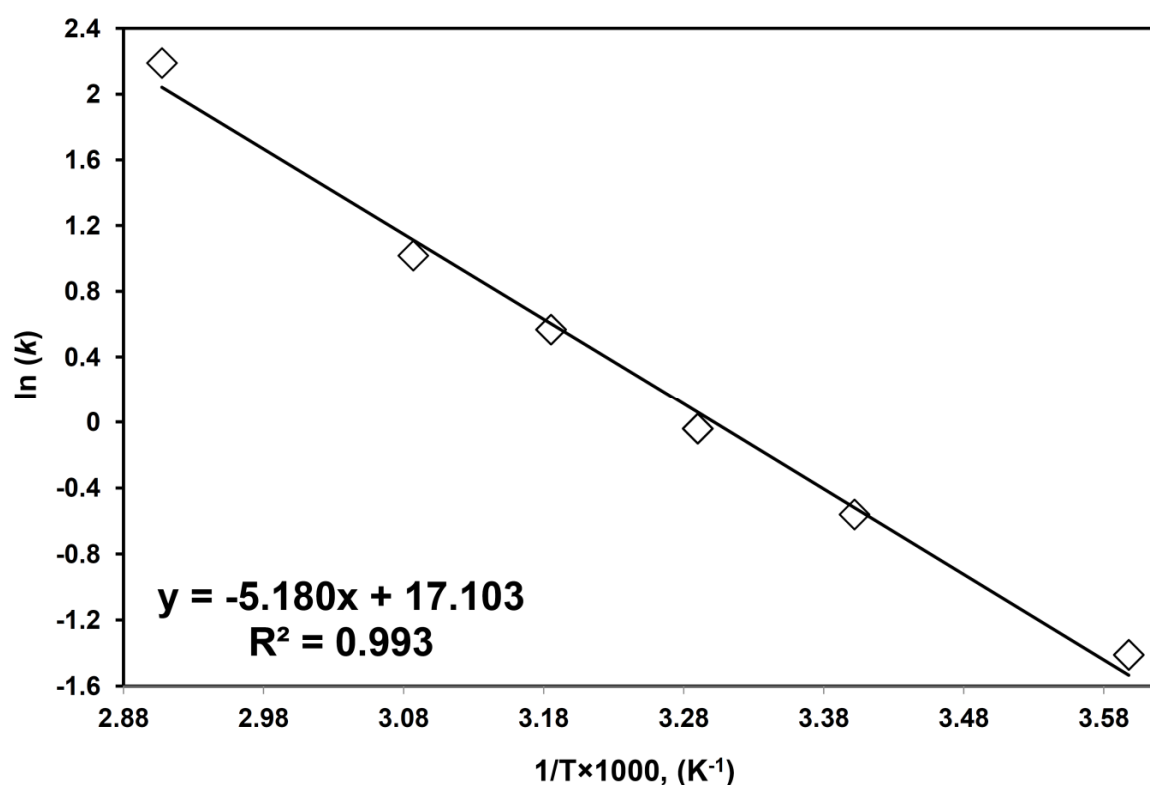


Figure 2-5 Arrhenius plot

### 2.3.4 Effect of the Alkylating Agent and of the Solvent

The nature of the alkylating agent affects the rate of the reaction. The effect of the alkylating agents iodomethane, **6**, iodoethane, **7**, benzylbromide, **8**, 1,2-diiodoethane, **9**, 2-iodopropane, **10**, chloromethyl methyl ether, **11**, *tert*-butyl bromoacetate, **12** and 2-iodo-2-methylpropane, **13** (Appendix E) was investigated and the reaction rate constants are brought in Table 2-4. The reaction rate order observed for iodomethane **6**, iodoethane, **7** and 2-iodopropane, **10**, is connected to the inherent reactivity of this class (methyl, primary and secondary alkyl halides) of compounds in a S<sub>N</sub>2 reaction. Roberts *et al.* [79] have reported that the reactivity of *tert*-butyl bromoacetate, **12**, is 2.2 times higher than that of benzyl bromide, **8**. Here their reactivity ratio is 2.7. 2-iodo-2-methylpropane, **13**, is a tertiary alkyl halides and 1,2-diiodoethane, **9**, decomposes readily, even at moderate temperatures and in the absence of oxygen, into ethylene and iodine [80-81]. That is the reason that no reaction was observed for them. For chloromethyl methyl ether, **11**, conversion is decreasing with time. It is due to the silylation that we do to prepare the samples for gas chromatography. It has been shown that trimethylsilyl bromide is an effective reagent for the deprotection of methoxymethyl ethers [82].

**Table 2-4 Effect of the alkylating agent. Concentrations of benzoic acid, **1**, TMGN, **16** and alkylating agent are ~26mM. Reagent combination is [(**1**, **16**), alkylating agent].**

Alkylating agent	<b>7</b>	<b>8</b>	<b>9</b>	<b>10<sup>a</sup></b>	<b>11</b>	<b>12</b>	<b>13</b>
$k$ (mol <sup>-1</sup> .L.s <sup>-1</sup> )	0.0589, 0.0679	0.3130, 0.2392		0.0395, 0.0387		0.7545, 0.7178	
$k_{avg}$ (mol <sup>-1</sup> .L.s <sup>-1</sup> )	0.063±0.0064	0.276±0.0522	No rxn	0.039±0.0005	b	0.736±0.0259	No rxn

a. At 50°C

b. No reaction rate constant can be defined.

The effect of the solvent was also investigated and the reaction rate constants as well as solvent properties are listed in Table 2-5. As it is illustrated in this table, toluene is a non-

polar solvent and it is not surprising that no reaction undergoes in toluene. Regarding their dielectric constant and dipole moment, acetonitrile and DMF both are dipolar aprotic solvents. But as it is observed the reaction in acetonitrile is much slower than in DMF. Alexander *et al* [69] have shown that solvation of polar reactants (e.g. CH<sub>3</sub>I) and uncharged transition states decreases slightly and roughly in the order of solvent: DMF > CH<sub>3</sub>CN.

**Table 2-5 Effect of the solvent. Concentrations of benzoic acid, 1, TMGN, 16 and iodomethane, 6 are ~26mM. Reagent combination is [(1, 16), 6].**

Solvent	Toluene	Acetonitrile	DMF
Dielectric constant [39]	2.38	36.2	36.7
Dipole moment [39]	0.36	3.92	3.86
$k$ (mol <sup>-1</sup> .L.s <sup>-1</sup> )	No rxn	0.0740±0.0105	0.571±0.0216

### 2.3.5 Substituent Effect

To evaluate the effect of the substituent, we did several experiments using different substituted benzoic acids and each time the value of  $\log\left(\frac{k_Y}{k_0}\right)$  was determined by measuring the formation of products. A summary of the results is presented in Table 2-6.

**Table 2-6 Substituent Effect. Concentrations of substituted benzoic acid, TMGN, 16 and iodomethane, 6: ~26mM. [(substituted benzoic acid, 16), 6].**

Entry	Substituent	$\sigma$	pK <sub>a</sub> in DMF	$k$ (mol <sup>-1</sup> .L.s <sup>-1</sup> )
1	4-NO <sub>2</sub>	0.778[83]	10.6[71]	0.175±0.004
2	4-CN	0.628[83]	11.02[84]	0.249±0.002
3	4-I	0.276[83]	11.65[85]	0.723±0.035
4	3,5-(OCH <sub>3</sub> ) <sub>2</sub>	0.24[86]	11.84 <sup>a</sup>	0.533±0.050
5	4-Br	0.232[83]	11.6[71]	0.647±0.102
6	4-Cl	0.227[83]	11.5[71]	0.456±0.069
7	4-F	0.062[83]	11.84[87]	0.563±0.014
8	4-H	0.00	12.3[71]	0.571±0.022
9	2,3-(OCH <sub>3</sub> ) <sub>2</sub>	-0.054 <sup>b,c</sup>	12.01 <sup>a</sup>	1.950±0.354
10	3,4-(OCH <sub>3</sub> ) <sub>2</sub>	-0.15[86]	12.50 <sup>a</sup>	0.751±0.0343
11	4-CH <sub>3</sub>	-0.170[83]	12.6[71]	0.472±0.046
12	3,4-(CH <sub>3</sub> ) <sub>2</sub>	-0.24[86]	13.0[71]	0.447±0.039
13	4-OCH <sub>3</sub>	-0.268[83]	12.78[87]	0.900±0.063
14	4-OH	-0.357[83]	13.25[87]	0.315±0.042
15	2,4-(OCH <sub>3</sub> ) <sub>2</sub>	-0.442 <sup>b,c</sup>	12.58 <sup>a</sup>	1.181±0.097
16	4-NH <sub>2</sub>	-0.660[83]	13.96[71]	0.313±0.016

- a. Values of pK<sub>a</sub> calculated using pK<sub>a</sub> values in DMSO[88] and the pK<sub>a</sub>(DMF)-pK<sub>a</sub>(DMSO) correlation [71]
- b. Sum of the corresponding *ortho*-, *meta*- and *para* [89]
- c.  $\sigma_{ortho} = 0.65 \sigma_{para}$  [90]

In order to provide a quantitative correlation to calculate the impact of substituent, a Hammett plot was constructed to determine the value of  $\rho$  (Figure 2-6).

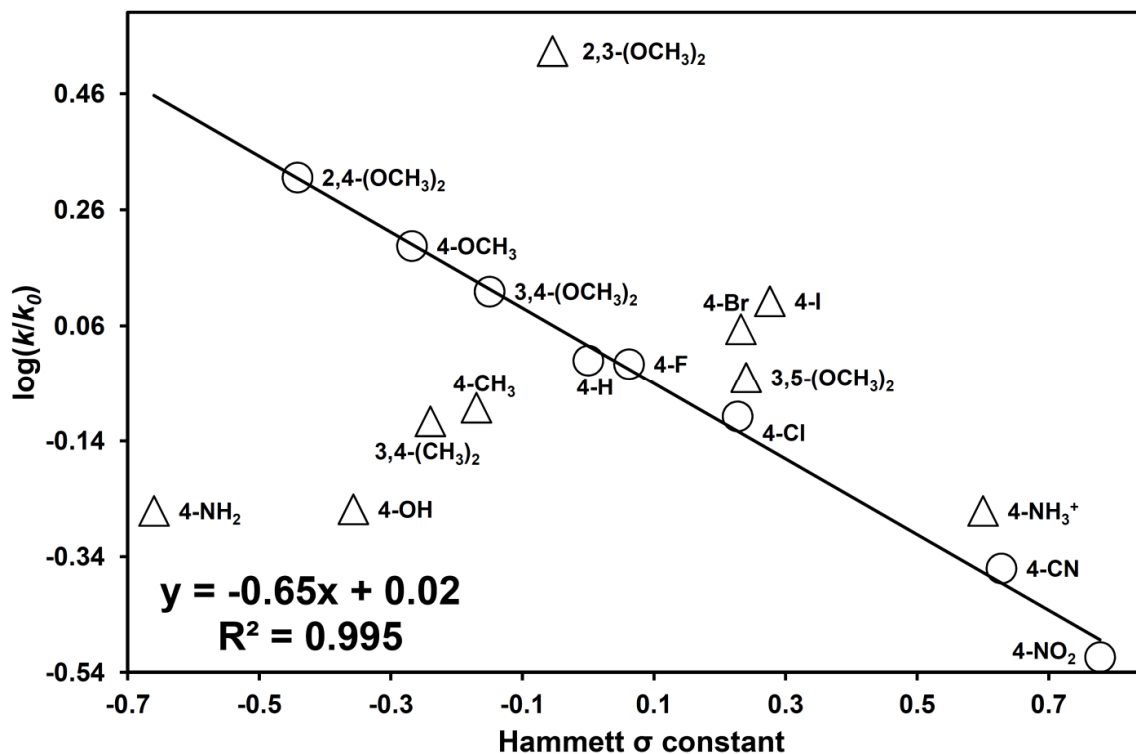


Figure 2-6 Hammett plot

As it is illustrated, most of the points fall on a straight line but also there are some outliers. The obtained  $\rho$  value for the points marked with  $\circ$  symbols is  $-0.65$  ( $n = 8$ ,  $R^2 = 0.995$ ). Since a negative charge is created over the reaction center,  $\sigma^-$  values were chosen to construct another Hammett plot. But, the non-linearity is much more pronounced in the plot of  $\log\left(\frac{k_Y}{k_0}\right)$  vs.  $\sigma^-$  (Figure 2-7). Values of  $\sigma^-$  were obtained from [91].

An attempt was also made to correlate reaction rate constants with quantum calculated descriptors but they did not yield the better (linear) correlations.

Hollingsworth *et al* [92] have demonstrated that calculated Löwdin charges are effective parameters for the correlation of benzoic acid  $pK_a$  values in water. Thus we tried to use



calculated Löwdin charges (Appendix A). Here again, 4-OH and 4-CH<sub>3</sub> substituted benzoic acids do not fall on the straight line. Equations 1-8 to 1-11 show the obtained correlations (n=6). These correlations show that by increasing the positive charge in the acid functional group, the reactivity is decreased.

$$\log \frac{k_Y}{k_0} = -16.20 Q_L(\text{COOH}) - 0.8636, R^2 = 0.9836 \quad (1-8)$$

$$\log \frac{k_Y}{k_0} = -96.096 Q_L(\text{H}) + 10.994, R^2 = 0.9555 \quad (1-9)$$

$$\log \frac{k_Y}{k_0} = -33.7560 Q_L(\text{O}^-) - 12.3523, R^2 = 0.9697 \quad (1-10)$$

$$\log \frac{k_Y}{k_0} = -17.892 Q_L(\text{COO}^-) - 14.272, R^2 = 0.9672 \quad (1-11)$$

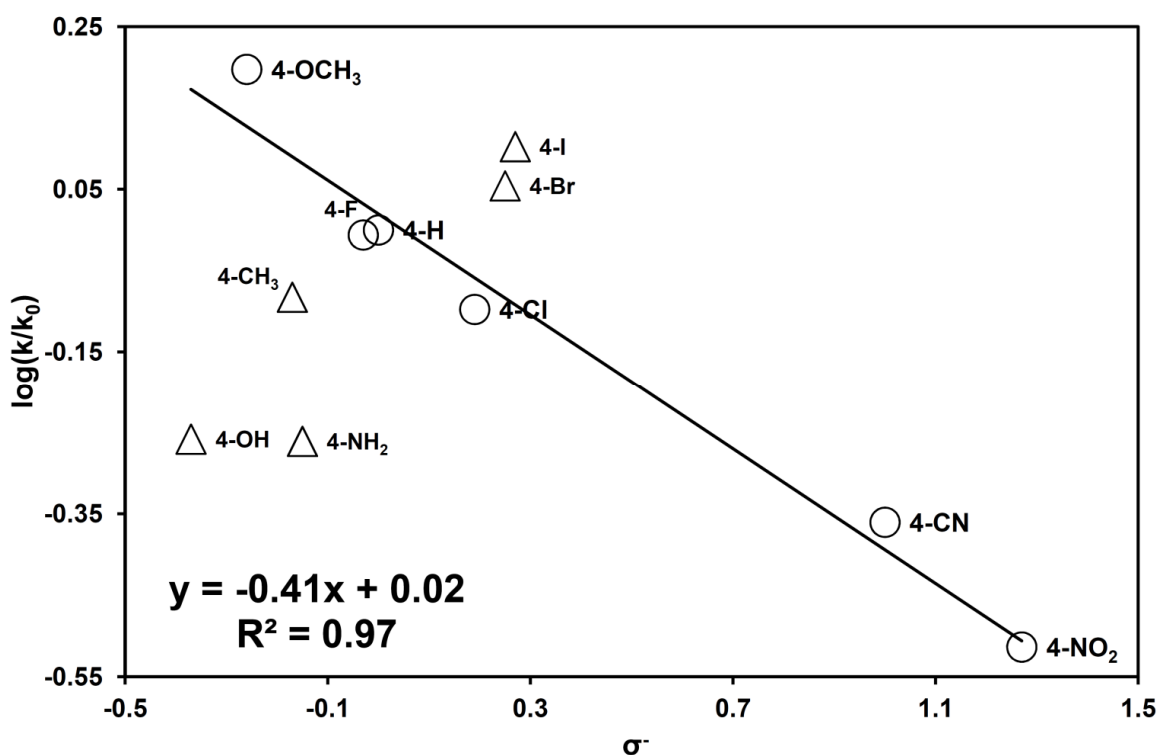


Figure 2-7 Hammett plot using  $\sigma^-$  values

Another descriptor that has already been used to quantify substituent effects for benzene [93] and benzoic acids [94] is the molecular electrostatic potential minimum ( $V_{\min}$ ).

Molecular electrostatic potential (MESP) is a degree to which a negative/positive charge is attracted/repelled to a molecule and has been widely used to quantify molecular reactivity and substituent effects [95]. The relative  $V_{\min}$  values for different substituted benzoic acids have been presented in Appendix A. For the series of disubstituted benzoic acids (except of 3,4-(CH<sub>3</sub>)<sub>2</sub> that the value is taken from reference [94]), the  $V_{\min}$  values were considered to be sum of the corresponding *ortho*-, *meta*- and *para* values. However if the values of  $V_{\min}$  are plotted against  $\sigma$  constants, except of 2,4-dimethoxybenzoic acid, other dimethoxybenzoic acids do not fall on the fitted regression line ( $R^2=0.9734$ ). Therefore, they have been excluded from the following discussion. Figure 2-8 presents the relative reaction rate constants against  $V_{\min}$  values. Here, again, it is observed that *mono*- and dimethyl substituted benzoic acids, *para*- bromobenzoic acid, as well as *para*-hydroxyl and aminobenzoic acids do not follow the fitted regression line.

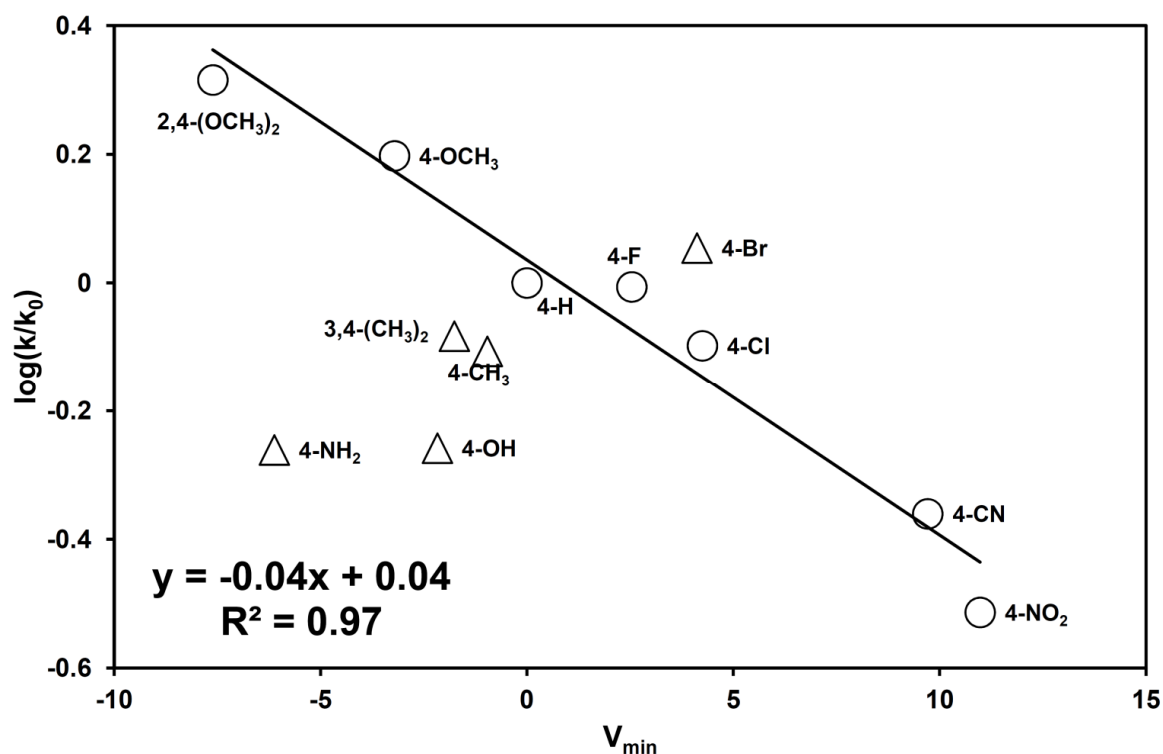


Figure 2-8 Rate constant versus the electrostatic potential minimum ( $V_{\min}$ )

The study of these figures shows that outliers can be divided in three groups: bulky halogens (4-I and 4-Br), alkyl substituents (4-Me and 3, 4-Me<sub>2</sub>) and two active sites carboxylic acids (4-NH<sub>2</sub> and 4-OH). Miron and Hercules [96] attribute deviation of 4-methylbenzoic acid in nitro solvents to  $\pi$ -electron complexation of the acid and solvent. Nagarajan *et al.* [97] have concluded that in case of a stabilized transition state, due to polarizability effects, the deviation from Bronsted (or Hammett) equation for *ortho* halo benzoate, should be increased by increasing the group size, *i.e.* I > Br > Cl > F. It can also explain the significant deviation, which we observe here.

The study of Figures 2-6 to 2-8, shows that bulky halogens (4-I, 4-Br) are more reactive than expected and alkyl substituents (4-Me, 3, 4-Me<sub>2</sub>) are less reactive than expected. This led us to suspect that it might be due to solvation effects. In fact, halogen series have a higher solvatochromic parameter ( $\pi^*$ , a measure of solute dipolarity/polarizability) than unsubstituted benzene ( $\pi^* = 0.59$ ), arranged in ascending order from fluorine to iodine ( $\pi^*_F = 0.62$ ,  $\pi^*_{Cl} = 0.71$ ,  $\pi^*_{Br} = 0.79$ ,  $\pi^*_I = 0.81$ ) but alkyl substituents have  $\pi^*$  values lower than that of unsubstituted benzene ( $\pi^*_{Me} = 0.55$ ) [98].

Deviation of *para*-amino- and hydroxybenzoic acids from Hammett 'normal' behavior has already been reported [99]. These are groups that would be especially affected by hydrogen bonding in aqueous solutions [99]. *para*-Aminobenzoic acid exists as a zwitterion in solution and when we use  $\sigma_{NH_3^+}$  (instead of  $\sigma_{NH_2}$ ) the point displaces much closer to the fitted straight line (Figure 2-6). Also no alkylation on amino group was detected by GC-MS. McMahon and Kebarle [100] have shown that in the gas phase the lowest energy anion derived from *p*-hydroxybenzoic acid appears to be *p*-carboxyphenoxide ion rather than *p*-hydroxybenzoate ion because phenoxide ion receives the resonance stabilization (Figure 2-9) while no equivalent stabilization by the OH group is available to the *p*-hydroxybenzoate anion. No methoxy benzoic acid was detected by GC-MS, but the

existence of this *p*-carboxyphenoxide ion conjugated form is in agreement with lower reactivity than expected from Hammett correlation of *p*-hydroxybenzoic acid

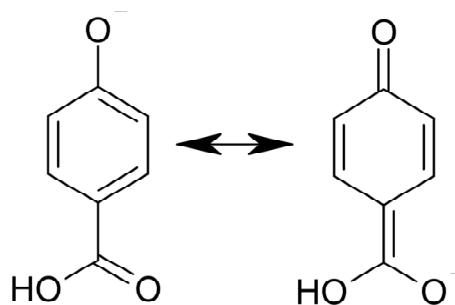


Figure 2-9 Resonance in phenoxide ion

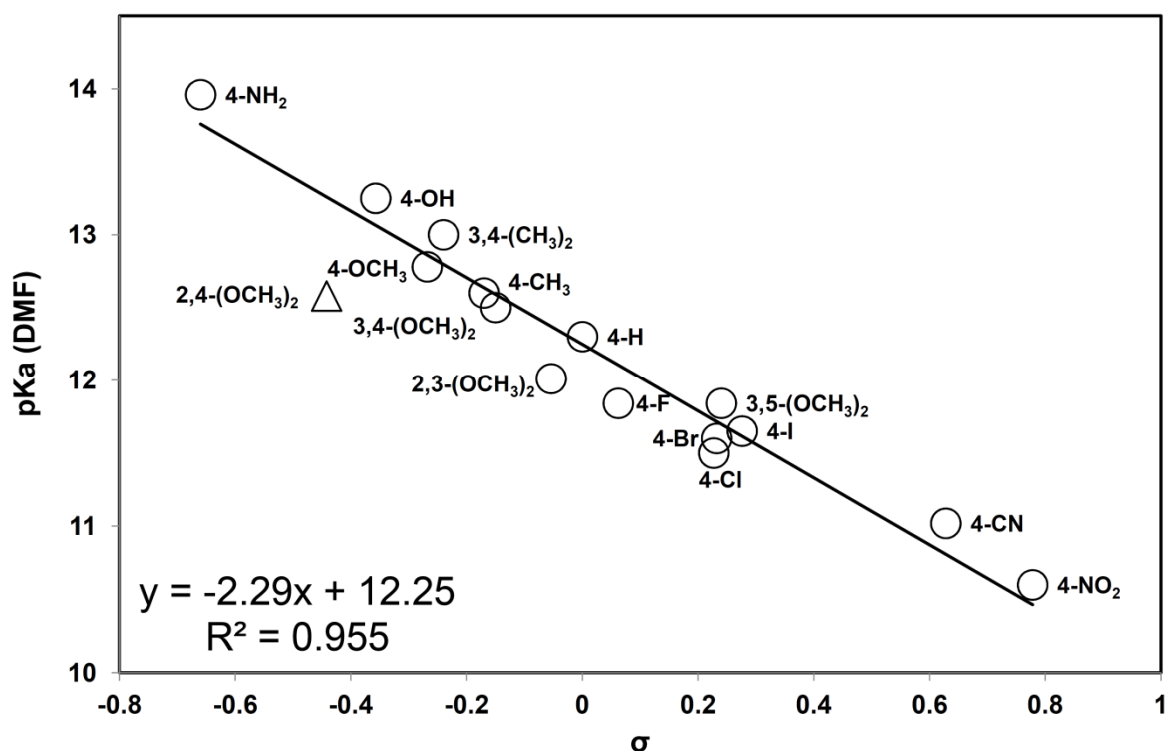


Figure 2-10 Hammett plot based on the ionization constants of different substituted benzoic acids.

A  $\rho$  value of -0.92 for alkylation of substituted tetra-methylammonium benzoate with iodomethane in acetonitrile have already been reported by Kondo *et al* [59] ( $n=4$ ,  $R^2=0.9895$ ). Our higher Hammett reaction constant value can be attributed to the solvent effect. The solvent basicity parameter for DMF and acetonitrile are 0.69 and 0.37 respectively [85]. Bartnicka *et al.*[85] have demonstrated that for the ionization of

substituted benzoic acids the greater the basicity of the solvent, the greater are the proton solvation and the  $\rho$  value.

The reported  $\rho$  values for a Hammett plot of  $\text{pK}_a$  (in DMF) vs sigma constants, are -2.36 (n=8) [101] and -2.49 (n=13) [85]. The obtained  $\rho$  value in this work is -2.29 (Figure 2-10). Values of  $\text{pK}_a$  (in DMF) for *dimethoxy*-substituents were obtained from  $\text{pK}_a$  values in DMSO by Exner *et al.*[88], using an equation proposed by Maran *et al.*[71] Comparing these  $\rho$  values to those obtained using alkylation reaction rate constants; shows that the kinetic substituent effect on the equilibrium of ion pair formation is larger than that of on benzoate reaction.

### 3 Basicity and Nucleophilicity

According to the IUPAC definition, nucleophilicity is the ability of an attacking group, to furnish nucleophilic displacement in a  $S_N2$  reaction [102]. A nucleophile is a Lewis base that uses an available electron pair to form a bond to its reaction partner (an electrophile) [103]. Chemical quantities of nucleophilicity and basicity are different, but they are closely related [102]. However, there is no unanimous agreement about the relationship between basicity and nucleophilicity [104-105]. It is generally accepted that basicity is a thermodynamic concept and nucleophilicity a kinetic one [103]. Basicity is determined chiefly by the original distribution of charge and to a lesser degree by the redistribution of charge caused by proton [106]. Various factors affect basicity; among them electron donating ability, accessibility of the protonation site (steric factor), thermodynamic/kinetics stability of the protonated base and solvent effects play important roles [107-108]. The important factors governing the nucleophilic ability are the solvation energy of the nucleophile, the strength of the bond being formed, the size of the nucleophile, the electronegativity and the polarizability of the attacking atom [103].

#### 3.1 Motivation

In conventional methods [109] for direct alkylation of carboxylic acids, usually strong inorganic acids are used which lead to the harsh reaction conditions, undesirable side reactions and consequently low yields. In a new method [64-65] an organic base, that is readily protonated and is a weak nucleophile, serves as the proton acceptor. Among some general conditions such as solubility, (1) this base must have a larger  $pK_a$  than the reacting carboxylic acids and (2) its alkylation rate must be significantly lower than that of the carboxylic acids. In order to satisfy these two contradictory requirements, it is necessary to examine the relationship between basicity and nucleophilicity [102-103, 110-111]. The

goal of this investigation is to quantify the nucleophilicity of organic superbases **14-24** (Appendix E). For this purpose we have conducted kinetics studies for the reaction between the base and iodomethane in DMF using our microfluidic device.

The organic superbases, **14-24**, can be classified as guanidine-type (TMG, **14** and Barton's base, **15**), proton sponge (TMGN, **16** and DMAN, **17**), bicyclic guanidine (TBD, **18** and MTBD, **19**), amidines (DBN, **20** and DBU, **21**), DABCO, **22** and phosphazenes (BEMP, **23** and P2Et, **24**). Amidines and guanidines are very important agents in the deprotonation of weak O-H, N-H and C-H acids [112]. Phosphazenes are also non-ionic, strong organic bases with low nucleophilicity and high  $pK_a$  and they have been already used in several organic synthesis [113]. The strong Bronsted basicity of **14-24** makes them attractive for carboxylic acids alkylation.

### 3.2 Base-Iodomethane stability

The rate of reaction of iodomethane with a variety of nucleophiles follows second-order kinetics [77]. Rates of the reactions of organic bases with iodomethane were determined by monitoring the relative concentrations of the organic base and its methylated product. If reaction conversion is shown by  $f$ , the values of  $k$  were determined graphically by plotting the function  $1/(1-f)$ , against residence time ( $t$ ) which resulted in a straight line with a slope equal to  $k[B]_0$ , where  $[B]_0$  is the initial concentration of organic base. The straight line relationship which we observed in every case substantiated our assumption of second-order kinetics. Several hindered organic bases were studied and their alkylation rates constant as well as their  $pK_a$  values are listed in Table 3-1.

**Table 3-1 Base alkylation kinetics results**

Base	Initial concentration (mM)	pK <sub>BH</sub> <sup>+</sup> in acetonitrile	pK <sub>BH</sub> <sup>+</sup> in DMF, calculated [73]	k <sub>obs</sub> (mol <sup>-1</sup> L s <sup>-1</sup> )
TMG, <b>14</b>	45.8	23.3 [113]	14.7-15.8	6.6(±1.4)×10 <sup>-2</sup>
Barton's base, <b>15</b>	47.9	23.56 [114]	14.9-16.0	1.8(±0.3)×10 <sup>-2</sup>
TMGN, <b>16</b>	46.6	25.10 [72]	16.4-17.5	1.2 (±0.01)×10 <sup>-4</sup>
DMAN, <b>17</b>	46.1	18.18 [113]	9.9-10.8	No reaction
TBD, <b>18</b>	46.0	25.98 [107]	17.2-18.4	3.8×10 <sup>-1</sup>
MTBD, <b>19</b>	47.0	24.70 [107]	16.0-17.1	5.6(±0.89)×10 <sup>-2</sup>
DBN, <b>20</b>	46.0	23.79 [107, 113]	15.2-16.3	5.5(±1.2)×10 <sup>-1</sup>
DBU, <b>21</b>	46.8	24.33 [107, 113]	15.7-16.8	2.5 (±0.11)×10 <sup>-1</sup>
DABCO, <b>22</b>	46.3	18.29 [115]	10.0-10.9	8.3(±1.0)
BEMP, <b>23</b>	46.3	27.63 [107]	18.8-20.0	9.6×10 <sup>-4</sup>
P2Et, <b>24</b>	4.6	32.8 [116]	23.6-25.0	72±12

But, the interaction of a sterically hindered organic base with a proton is different than its interaction with an alkylating agent. Due to its small size and its electron deficiency, a proton is able to approach the protonation site of the base, while the alkylating agent attack is blocked [117]. Hence, there is a relationship between nucleophilicity and basicity but they are not directly proportional [103]. As it is observed in Figure 3-1 a general pattern is observed between the basicity and nucleophilicity.

In guanidine type bases, studied here, Barton's base **15** has lower methylation reactivity than TMG **14** due to its steric hinderance [67]. Alkylation of a 0.5 mol L<sup>-1</sup> solution of **15** in CDCl<sub>3</sub> by three equivalents of iodomethane at room temperature, using NMR techniques, has given a reaction half-life less than 5 minutes [67]. In this work, using only one equivalent of iodomethane reaction half life is 19.3 min.

DMAN, **17** has not at all nucleophilic reactivity. In order to validate this result, this experiment was repeated using CD<sub>3</sub>Cl; however again no reaction occurred. This low nucleophilicity is directly proportional with its basicity, which is also low. However, the guanidine proton sponge, TMGN, **16**, has high Bronsted basicity and low nucleophilicity, which make it a very good candidate for using in alkylation reactions. TMGN nucleophilicity has been reported much lower than that of MTBD, **19** [72].



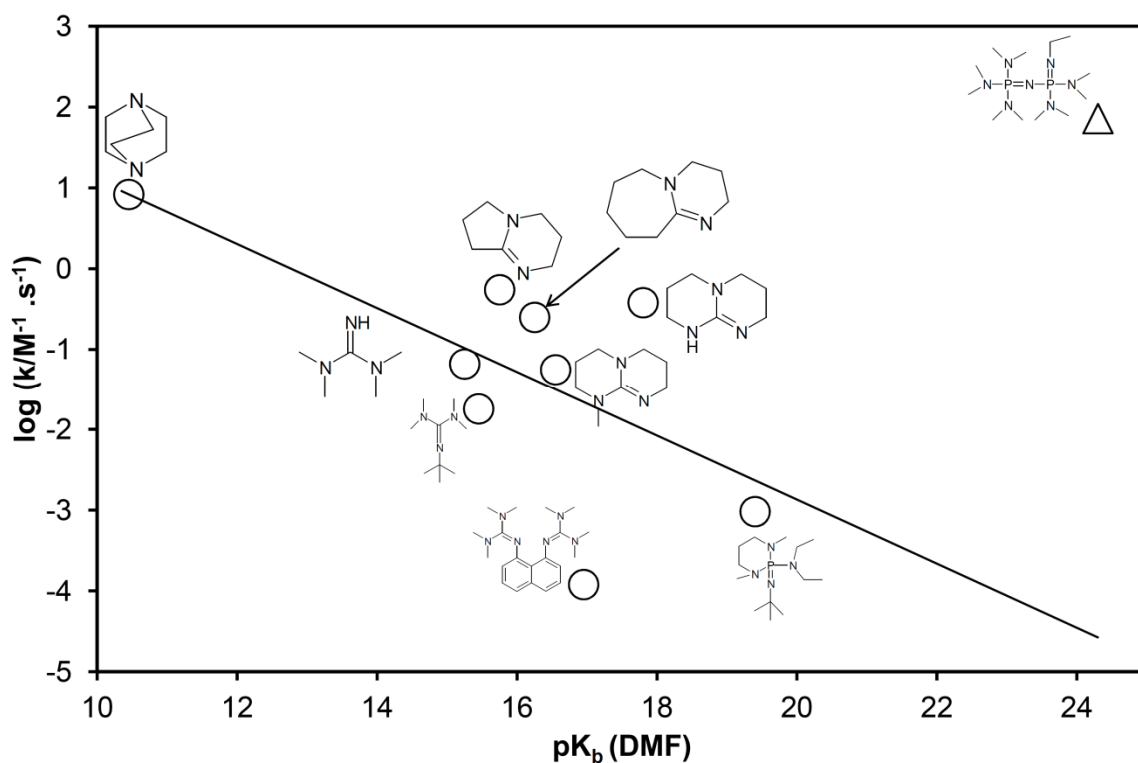


Figure 3-1 plot of log k and pKa for bases 14-24

Between bicyclic guanidines, MTBD, **19**, is less nucleophile than TBD, **18**, probably due to its non planar structure and steric reasons [118]. Rabb *et al* [72] have evaluated the nucleophilicity of MTBD **19**, by following its alkylation of a 1.0 M solution by 2.5 equivalents of iodoethane in  $\text{CD}_2\text{Cl}_2$  at 25°C by means of  $^1\text{H}$  NMR and have reported a reaction half-life of 15 min. In this work, using only one equivalent of iodomethane reaction half life is 6.33 min.

DBN, **20** and DBU, **21** have frequently been described in the literature as nonnucleophilic bases [119]. Baidya and Mayr [120] have investigated the nucleophilicity of several amidines and DABCO, **22**, and they have found that nucleophilicity increases in the series as **21** < **20** < **22**. The same trend can also be seen in our experiments with their methylation rates. This is probably due to differences in ring strain in these molecules and the effects of ring strain upon kinetic reactivity [121-122]. For comparison, alkylation of a  $0.5 \text{ mol L}^{-1}$

solution of DBN **20** in  $\text{CDCl}_3$  by three equivalents of iodomethane at room temperature, using NMR techniques, has given a reaction half-life less than 2 minutes [67].

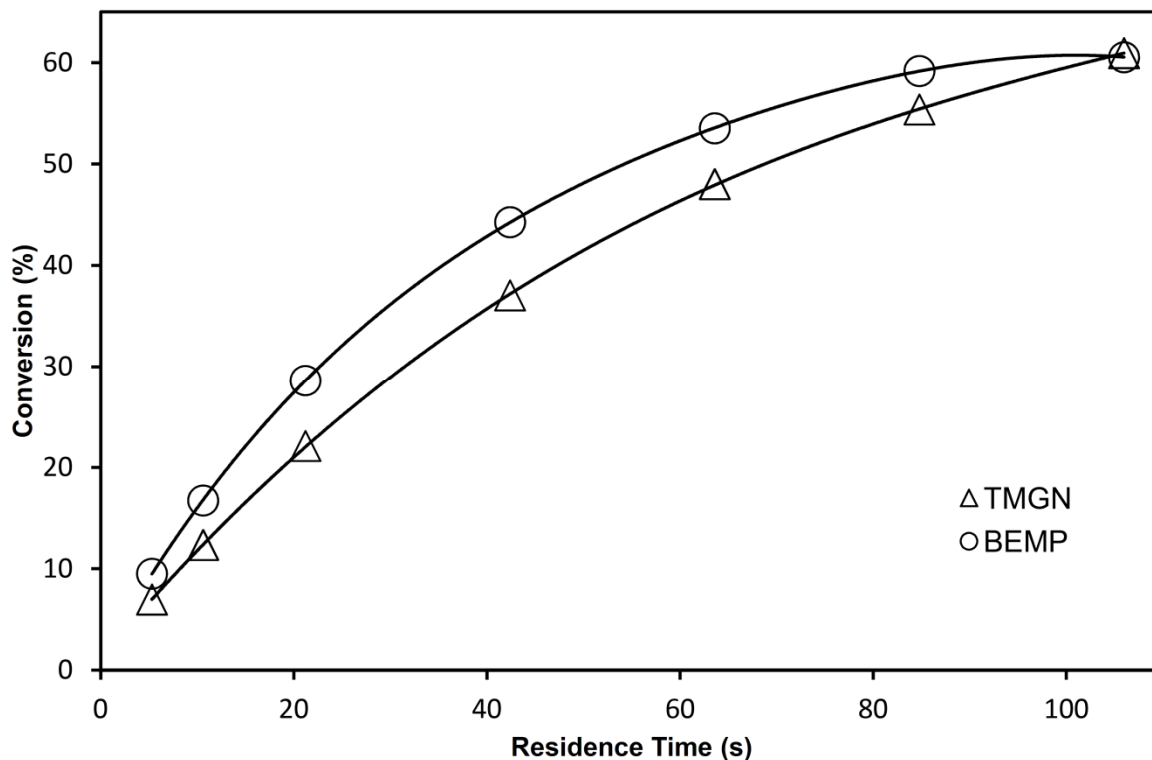


Figure 3-2 BEMP-TMGN kinetics comparison on benzoic acid alkylation by MeI

In the group of phosphazenes, BEMP, **23**, is much less nucleophilic than  $\text{P}_2\text{Et}$ , **24**. The steric hindrance shown by BEMP, **23** is so significant that it is practically inert to iodomethane [123]. This low nucleophilicity along with its high Bronsted basicity make it another good candidate for alkylation reactions at the presence of the base. To compare how the addition of either of the two candidate bases affects benzoic acid alkylation by iodomethane, two kinetics study experiments were carried out using our microfluidic device. The conversion vs. residence time plot is shown in Figure 3-2.

As it is observed, the reaction catalyzed by BEMP, **23**, is faster than by TMGN, **16**. But due to higher alkylation rate of BEMP, **23** by iodomethane, the reaction rate slows down in longer residence times and finally the conversion is nearly the same for both bases.

## 4 IDENTIFYING SITE OF ALKYLATION IN TMGN

All the bases studied here, **14-24** (Appendix E) contain one or several nitrogen lone pairs, which serve as protonation sites as well as alkylation sites. The goal of this part is to identify the alkylation site for TMGN by NMR techniques.

The term “superbases” applies to bases resulting from a mixing of two (or more) bases leading to new basic species possessing inherent new properties. It does not mean a base is thermodynamically and/or kinetically stronger than another, instead it means that a basic reagent is created by combining the characteristics of several different bases [113].

Classically, proton sponges are organic diamines with unusually high basicity. The name proton sponge is given because of the high thermodynamic basicity combined with a kinetic inactivity to deprotonation that resembles the affinity of a sponge for water. The general feature of all proton sponges is the presence of two basic nitrogen centres in the molecule, which have an orientation that allows the uptake of one proton to yield a stabilized intramolecular hydrogen bond (IMHB). The trend that proton sponges with high thermodynamic basicity typically have a low kinetic basicity (kinetic activity in proton exchange reactions) is a serious limitation of proton sponges: the captured proton does not usually take part in rapid proton exchange reactions, which would allow such neutral superbases to serve as catalysts in base-catalysed reactions. Their further limitations are moderate solubility in aprotic nonpolar solvents and stability towards auto-oxidation[113].

By combining the proton sponge skeleton, with highly basic guanidine, a superbasic TMGN was obtained by Raab[72]. It represents the one of most basic guanidines experimentally determined, with  $pK_a$  (MeCN)=25.1,  $P_A$  (MP2)=257.5. The basicity of this bisguanidines is the combined result of the unfavourable nonbonded repulsions in the

initial base, the large PA of guanidine group and strong IMHB present in the protonated species[113]. Its structure as well as the structure of its mono-protonated and di-protonated derivatives has been studied and reported by  $^1\text{H}$  NMR [72]. Its proton accepting properties has been studied extensively by  $^{13}\text{C}$  NMR, FT-IR and ESI MS spectroscopy [124]. Also, its transition metal complex has already been synthesized and its structure has comprehensively been studied by  $^1\text{H}$ NMR [125].

Several samples were prepared for NMR studies:

- a) Four samples of 25-28 mM TMGN in DMSO-*d*6
- b) Two samples of 24-25 mM TMGN and 27mM of iodomethane in DMSO-*d*6 (stirring and gently heating overnight before analysis)
- c) Two samples of 24-25 mM TMGN and 27 mM  $^{13}\text{CH}_3\text{I}$  in DMSO-*d*6 (stirring and gently heating overnight before analysis)
- d) Two control samples of 27 mM  $^{13}\text{CH}_3\text{I}$  in DMSO-*d*6
- e) One control sample of 1.0 M TMGN and 1.2 M iodomethane in DMSO-*d*6 (stirring and gently heating overnight before analysis)

Unless otherwise necessary only one sample of each group was analyzed.  $^1\text{H}$ ,  $^{13}\text{C}$  and  $^{15}\text{N}$  NMR spectra were recorded with either a Bruker Avance 400 equipped with a 5 mm broad-band inverse or direct probe with a z-gradient or a Bruker Avance III 800 equipped with a 5 mm TXI probe with xyz-gradients (Bruker, Wissembourg, France).  $^1\text{H}$  and  $^{13}\text{C}$  chemical shifts were referenced against internal tetramethylsilane at 0.00 ppm while  $^{15}\text{N}$  chemical shifts were referenced indirectly [126]. Classical 2D NMR techniques were used: COSY  $90^\circ$  (COrrrelation SpectroscopY), NOESY (Nuclear Overhauser Effect SpectroscopY) with 200 ms mixing time, HSQC (Heteronuclear Single-Quantum Correlation), HSQC-TOCSY (HSQC-TOTAL Correlation SpectroscopY) with 40 ms mixing time, HMBC (Heteronuclear Multi-Bond Correlation) with an 8 Hz long-range coupling

constant. Scalar connections and spatial proximities between protons were observed in COSY and NOESY spectra, respectively. HSQC and HMBC gave scalar connections between  $^1\text{H}$  and  $^{13}\text{C}$  (or  $^{15}\text{N}$ ) through one and (two-) three (-four) bonds, respectively.

Experiments were mainly run at 300 K or 313 K in order to get some weak hetero-nuclear correlations. All spectra were processed with Bruker Topspin 1.3 and  $^1\text{H}$ ,  $^{13}\text{C}$  and  $^{15}\text{N}$  peak assignments are listed in Tables 4-1 to 4-3 (Chemical shift (ppm), multiplicity (s=singlet, d=doublet, t=triplet, and br=broad)). The assignments are based on the results obtained in the 2D spectra. The chemical-shift differences and the relative peak intensities are in good agreement with the results obtained using conventional high-resolution NMR spectrometers [72, 124].

Table 4-1  $^1\text{H}$ ,  $^{13}\text{C}$  and  $^{15}\text{N}$  chemical shift assignment of TMGN in DMSO-d<sub>6</sub> at 300K

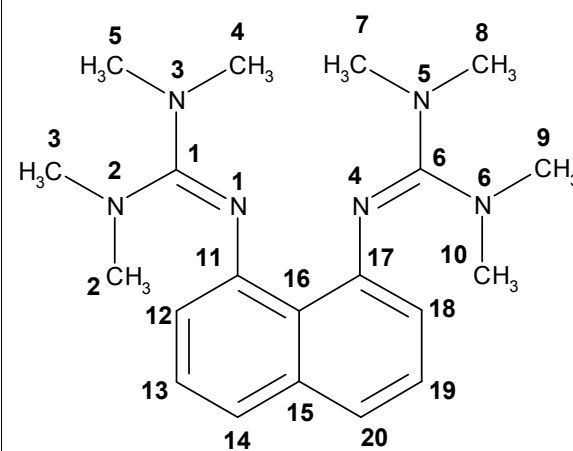
	Position	$^1\text{H}$ (ppm)(multiplicity)	$^{13}\text{C}$ (ppm)
		1/6	/
	2/3/4/5/7/8/9/10	2.63 (s)	39.6
	11/17	/	149.6
	12/18	6.16 (d)	114.7
	13/19	7.12 (t)	125.4
	14/20	7.15 (d)	119.1
	15	/	136.2
	16	/	122.3
	N1/N4	/	215.9 ( $^{15}\text{N}$ )
	N2/N3/N5/N6	/	53.7 ( $^{15}\text{N}$ )

Table 4-2  $^1\text{H}$ ,  $^{13}\text{C}$  and  $^{15}\text{N}$  chemical shift assignment of TMGN- $\text{H}^+$  in  $\text{DMSO-}d_6$  at 300K

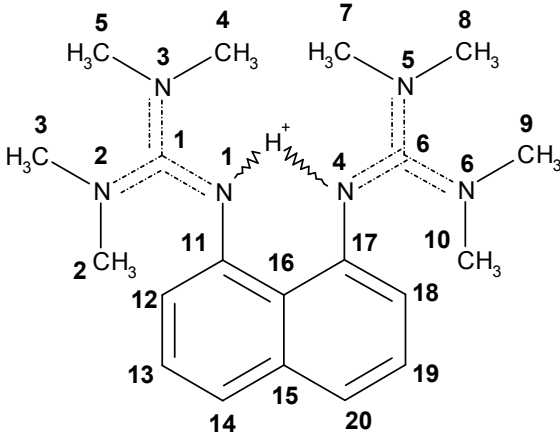
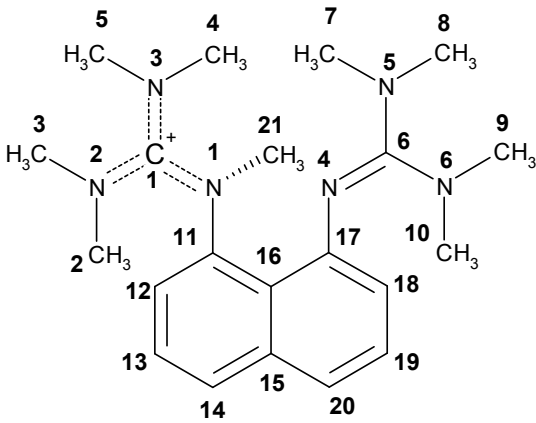
	Position	$^1\text{H}(\text{ppm})(\text{multiplicity})$	$^{13}\text{C}$ (ppm)
		1/6	/
	2/3/4/5/7/8/9/10	2.88 (s)	39.8
	11/17	/	141.8
	12/18	6.50 (d)	113.5
	13/19	7.33 (t)	126.2
	14/20	7.38 (d)	121.2
	15	/	135.9
	16	/	117.4
	N1/N4	14.19 (br)	144.9 ( $^{15}\text{N}$ )
	N2/N3/N5/N6	/	73.1 ( $^{15}\text{N}$ )

Table 4-3  $^1\text{H}$ ,  $^{13}\text{C}$  and  $^{15}\text{N}$  chemical shift assignment of TMGN-Me in  $\text{DMSO-}d_6$  at 300K

	Position	$^1\text{H}$ (ppm)(multiplicity)	$^{13}\text{C}$ (ppm)
		1	/
	6	/	159.2
	-	3.08 (s) <sup>a</sup>	40.1
	7/8/9/10	2.59 (s) <sup>a</sup>	39.4
	-	2.57 (br) <sup>a</sup>	~39.4
	11	/	138.4
	12	7.33 (d)	124.6
	13	7.40 (t)	125.0
	14	7.82 (d)	129.0
	15	/	136.7
	16	/	122.7
	17	/	146.3
	18	6.38 (d)	117.7
	19	7.35 (t)	126.8
	20	7.42 (d)	120.4
	21	3.35 (s)	43.1
	N1	/	105.9 ( $^{15}\text{N}$ )(313K)
	N2/N3	/	75.2 ( $^{15}\text{N}$ ) (313K)
	N4	/	197.5 ( $^{15}\text{N}$ )
	N5/N6	/	60.6 ( $^{15}\text{N}$ )

- a. These are three peaks, integrated for 2, 4 and 2 methyl group from top to bottom respectively; but an unambiguous numerical locator cannot be directly assigned to each.

In a preliminary inspection of the spectra, two products (TMGN-H<sup>+</sup> and TMGN-Me) were observed. TMGN-H<sup>+</sup> to TMGN-Me molar quantitative ratio is 85 % to 15 %, for 25mM solution, and 32% to 68%, for 1M solution (Figures 4-1 and 2). Quantification was made by integration of <sup>1</sup>H NMR signals at 6.50 ppm and 6.38 ppm corresponding to the proton H18 of TMGN-H<sup>+</sup> and TMGN-Me respectively. TMGN is protonated by water molecule present in NMR solvent (DMSO-*d*<sub>6</sub>) and the –OH group, belonging to the water molecule, attacks iodomethane to give methanol. This reaction is considered as a side reaction and can be avoided in anhydrous conditions.

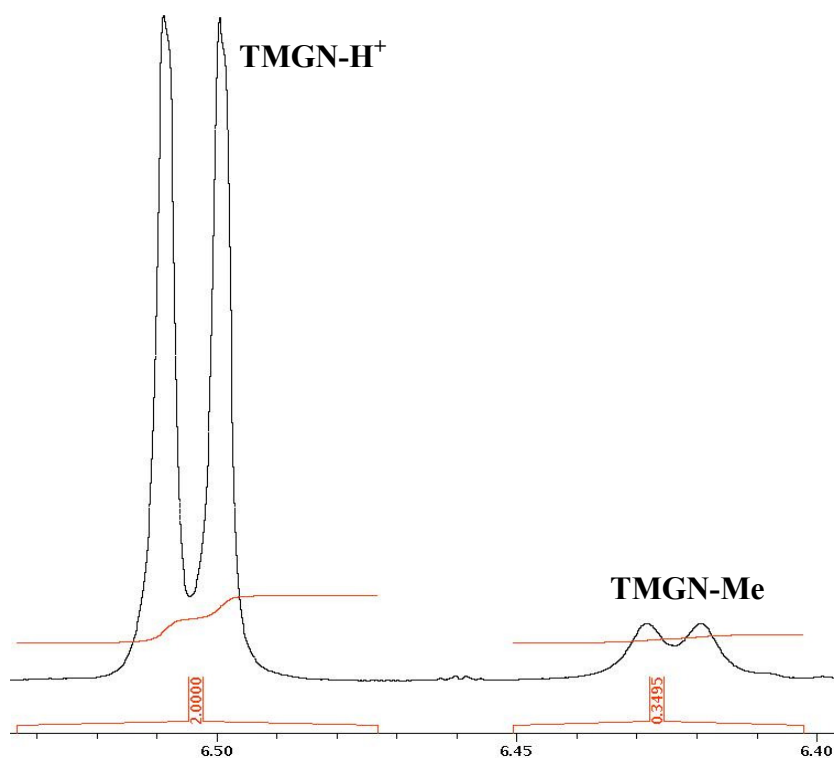


Figure 4-1 Quantification of TMGN-H<sup>+</sup> and TMGN-Me for a solution of 25mM taken from 800 MHz <sup>1</sup>H NMR spectrum of TMGN-H<sup>+</sup> and TMGN-Me



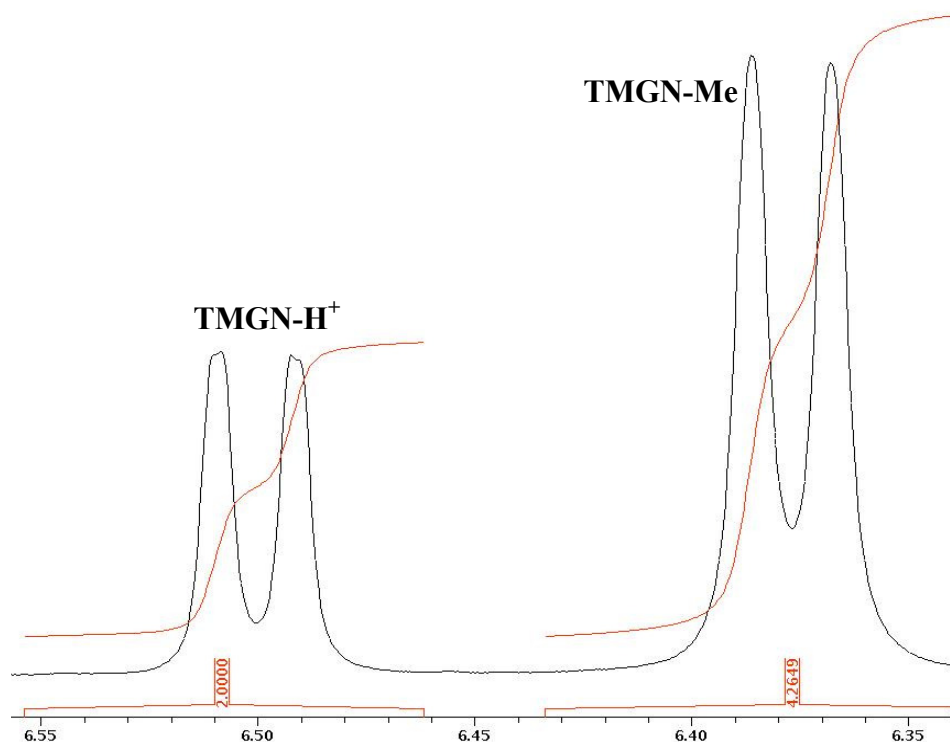


Figure 4-2 Quantification of TMGN-H<sup>+</sup> and TMGN-Me for a solution of 25mM taken from 400 MHz <sup>1</sup>H NMR spectrum of TMGN-H<sup>+</sup> and TMGN-Me

## 4.1 TMGN

The <sup>1</sup>H spectrum of TMGN consists of three aromatic peaks therefore, molecule has a symmetry axis along the C15-C16, but only one peak for the eight methyl groups (at 2.63 ppm). Kovacevic and Maksic [127] have shown that in TMGN molecule, the naphthalene frame is only slightly nonplanar, the imine nitrogen nuclei are not in the plane of the molecule, amine nitrogen nuclei are pyramidalized and the guanidine subunits are planar but one of them is above and the other is below the molecular plane.

Vicinal proton coupling constants (~7Hz) and the number of nearby neighbors, allow complete assignment of aromatic proton signals. The protons 13 /19 appear as a triplet at 7.12 ppm (Figure 4-3), while the doublets at 6.16 and 7.15 ppm are from protons 12/18 and 14/20. However, four bond scalar coupling (1.3 Hz) between H12 and H14 indicates that

these doublets are actually doublets of doublets; as later confirmed by NMR 800MHz studies (Figures 4-3 and 4).

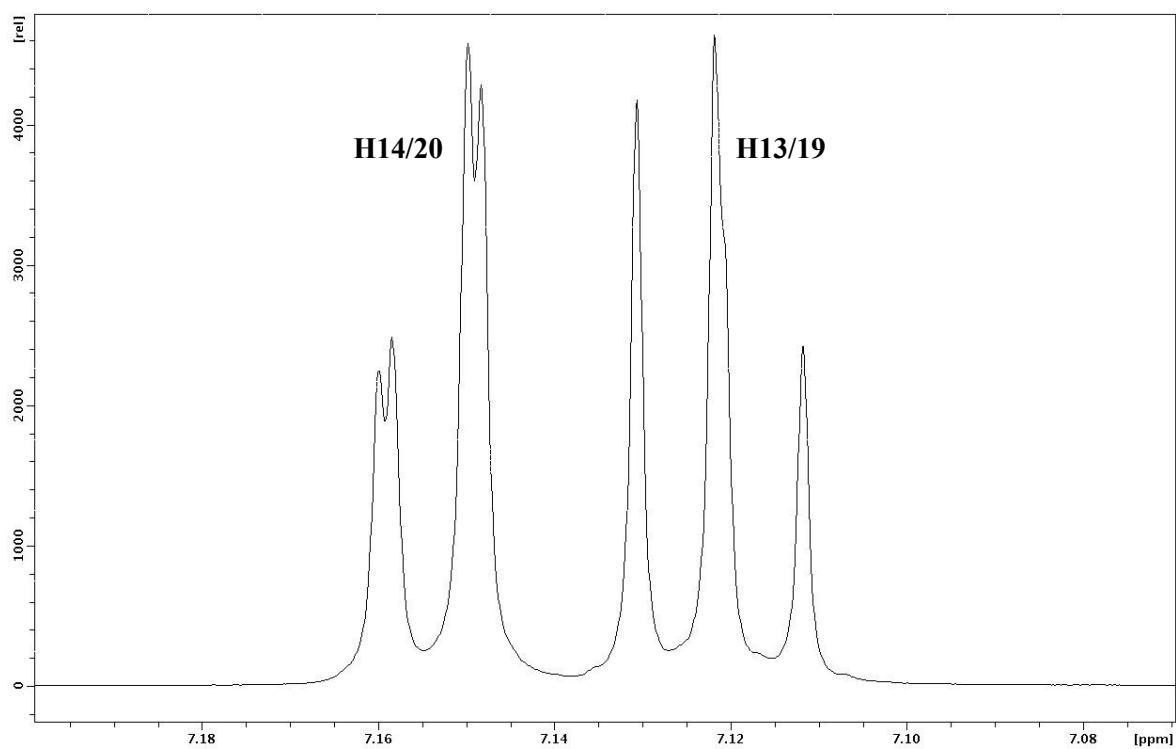


Figure 4-3 800 MHz spectrum of TMGN, the triplet of H13/19 and the doublets of doublets of H14/20

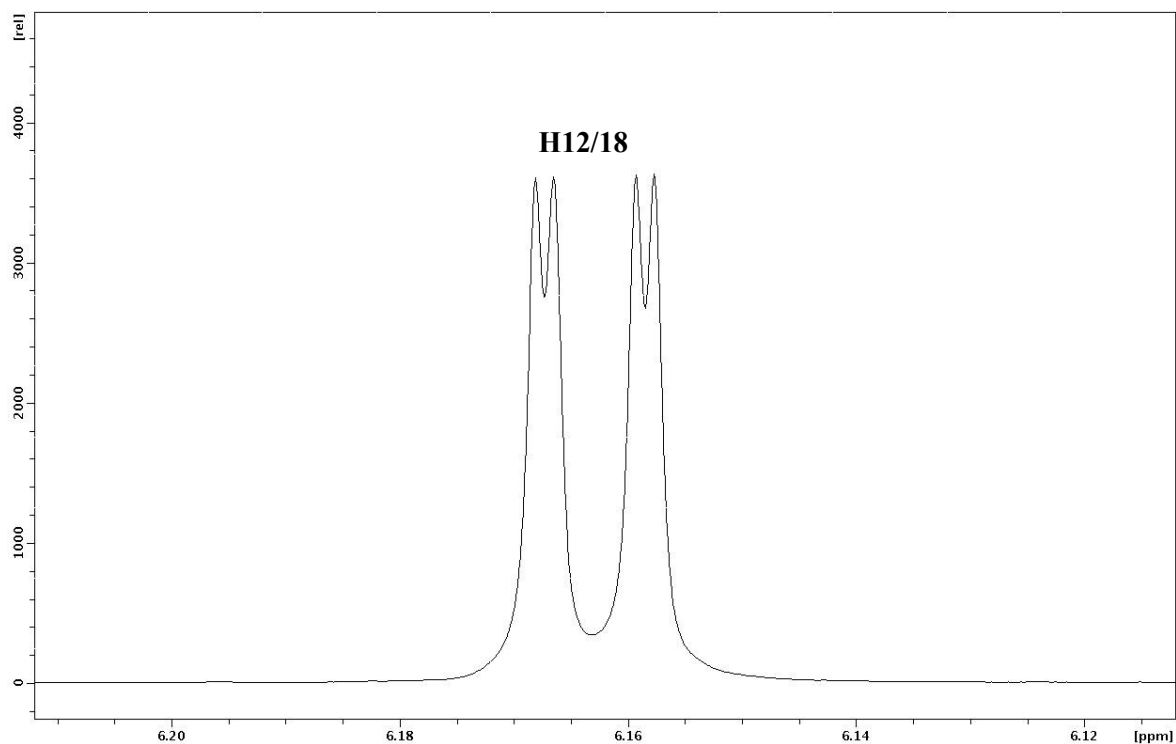


Figure 4-4 800 MHz spectrum of TMGN, the doublets of doublets of H12/18

The connectivity through space with the protons of the dimethyl amino group allows the identification of the protons 12/18. Therefore, analysis methyl protons in NOESY spectrum provides the assignment of protons 12/18 directly (at 6.16 ppm) and that of 14/20 protons (at 7.15 ppm) indirectly.  $^{13}\text{C}$  assignments for C2/3/4/5/7/8/9/10, C12/18, C13/19 and C14/20 were directly obtained from the  $^1\text{H}$ - $^{13}\text{C}$  HSQC and C1/6, C11/17, C15 and C16 (quaternary carbons) were assigned from  $^1\text{H}$ - $^{13}\text{C}$  HMBC (Figure 4-5).

The methyl proton signal at 2.63 ppm is correlated with the  $^{13}\text{C}$  signal of C1/C6 at 153.6 ppm. The signal at 149.6 ppm (C11/17) is twice as intense as the signal at 136.2 ppm (C15) and the one at 122.3 ppm (C16). Finally, the proton signal at 6.16 ppm (H12/18) is correlated with the  $^{13}\text{C}$  signal at 122.3 ppm which is for C16. The remaining  $^{13}\text{C}$  signal is assigned to C15.

Two different kind of  $^{15}\text{N}$  are found in  $^1\text{H}$ - $^{15}\text{N}$ -HMBC experiment (Figure 4-6). It is known that the amino nitrogen nucleus should be more shielded than the imino one by about 100 ppm [128]. So the first nitrogen nucleus, at 215.9 ppm that shows a correlation with protons H12/18, is assigned to an imino nitrogen nucleus (N1/N4). However, the other one, at 53.7 ppm, that correlates with the methyl protons (H2/3/4/5/7/8/9/10) is assigned to an amino one (N2/3/5/6).

Only one signal is observed for protons and carbon nuclei 2/3/4/5/7/8/9/10 (at 2.63 ppm and at 39.6 ppm) and at 53.7 ppm for nitrogen nuclei 2/3/5/6 which proves that the chemical exchange of the methyl groups bonded to one nitrogen nuclei and of the methyl groups in different dimethylamino groups should be very fast.

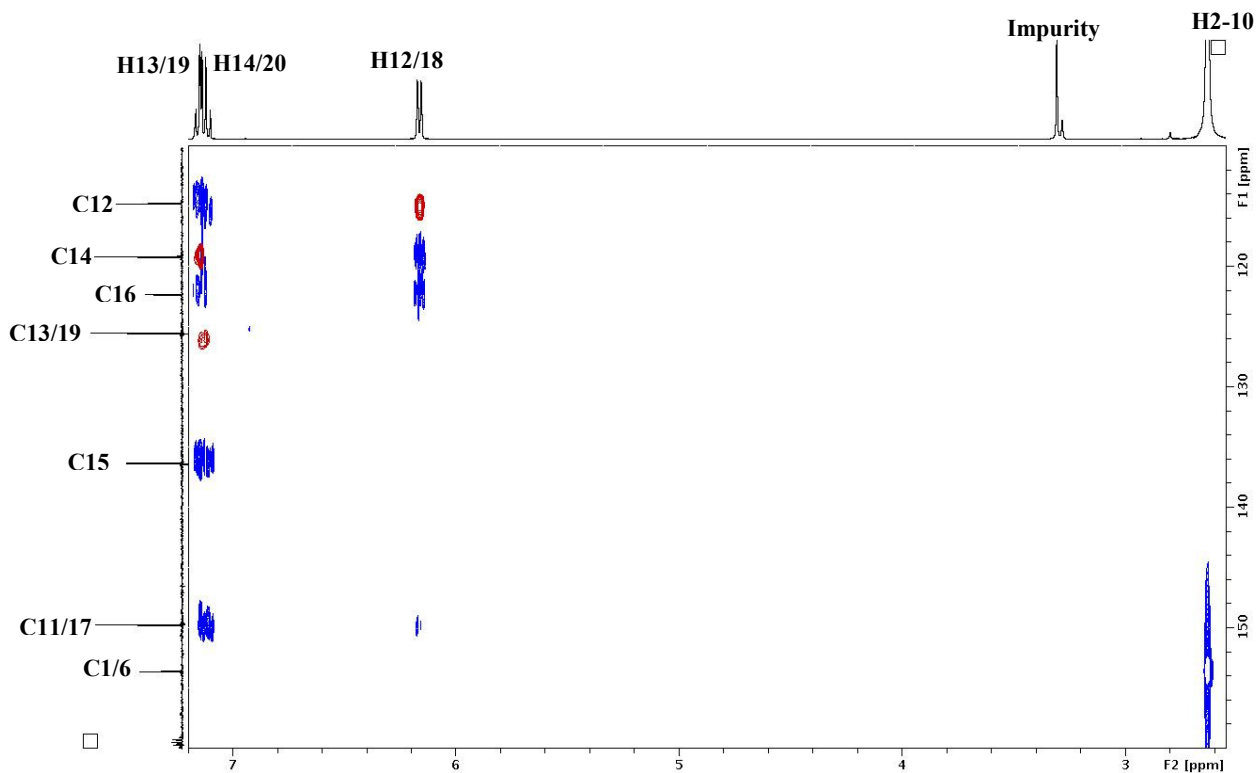


Figure 4-5 400MHz NMR 2D-HMBC (blue) and 2D-HSQC (red) of TMGN

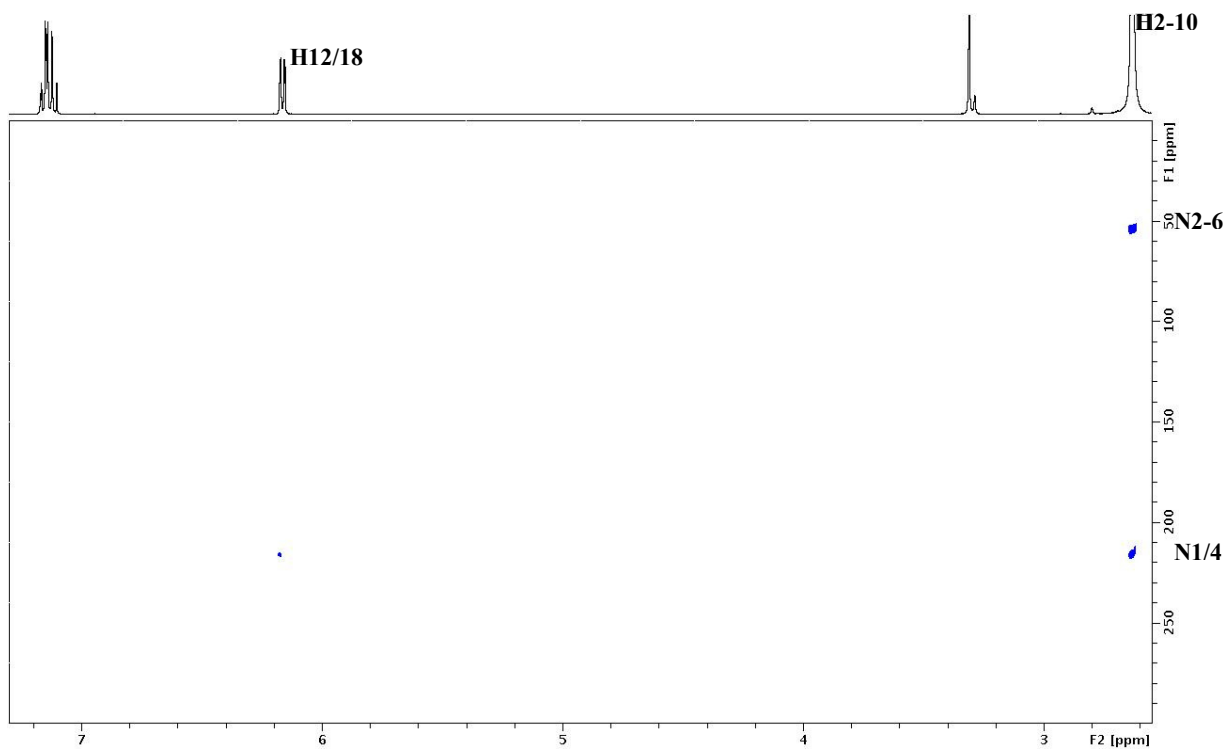


Figure 4-6 400MHz 2D NMR  $^1\text{H}$ - $^{15}\text{N}$ HMBC of TMGN

## 4.2 TMGN-H<sup>+</sup>

TMGN protonation is a side reaction due to the presence of residual water in deuterated solvent and can be avoided in anhydrous conditions. The <sup>1</sup>H NMR spectra of <sup>13</sup>CH<sub>3</sub>I in DMSO-*d*<sub>6</sub> consists of an intense water peak, without any methanol peak. However, methanol peak is observed in the presence of TMGN. It means that TMGN plays its role of base for the hydrolysis of iodomethane.

TMGN is protonated on either N1 or N4 [72]. The <sup>1</sup>H spectrum of TMGN-H<sup>+</sup> consists of a strongly deshielded proton signal at 14.19 ppm that might unambiguously be assigned to labile hydrogen nucleus. It can be seen that this signal correlates with a signal at 145.6 ppm in <sup>1</sup>H-<sup>15</sup>N-HQSC spectrum and with the dimethylamino groups in the NOESY spectrum (<sup>1</sup>H at 2.88 ppm, <sup>13</sup>C at 39.8 ppm and <sup>15</sup>N at 73.1 ppm). These also correlate with an aromatic proton signal at 6.50 ppm in the NOESY spectrum. The proton signals at 6.50 and at 14.19 ppm have an integrated ratio of 2:1. Considering all <sup>1</sup>H and <sup>13</sup>C chemical shifts, these signals belong to a molecule with a very close structure to TMGN, but with a strongly deshielded proton signal. Therefore this molecule is protonated TMGN (TMGN-H<sup>+</sup>).

Here again, only one signal is observed for protons and carbon nuclei 2/3/4/5/7/8/9/10 (at 2.88 ppm and at 39.8 ppm) and at 72.9 ppm for nitrogen nuclei 2/3/5/6. A comparison of the chemical shifts of the signals observed in the <sup>1</sup>H NMR spectra demonstrates that with the protonation of TMGN, the signals of the naphthalene ring protons (except 12/18) and of the methyl groups are displaced around 0.2 ppm. The chemical shifts of protons 12/18 are shifted around 0.3 ppm. It is a sign of intramolecular hydrogen bond and shows that its deshielding effect on protons 12/18 is slightly higher. It has already been shown that intramolecular hydrogen bonding triggers an appreciable resonance effect in the

neighboring guanidine fragment in the protonated species and the introduced positive charge causes substantial polarization and redistribution of the electron density [127]. Protonation of TMGN has a much pronounced effect on the chemical shifts of almost all naphthalene ring carbon nuclei. The signals of all carbon nuclei (except C13/19 and C14/20) shift toward lower ppm values, a sign of increasing electron density at these nuclei. However, The C13/19 and C14/20 signals shift toward higher ppm values that indicate decreasing electron density around them.

The protonation in one guanidine group is accompanied by the substantial charge relocation on the other. The spatial proximity of the N1 and N4 (their distance is 271.7 pm [72]) allows rapid exchange of labile proton, which extends the redistribution of the electron density over two guanidine/guanidinium groups. Therefore, the effect of TMGN protonation on the chemical shifts of nitrogen nuclei is remarkable. In TMGN molecule, the large  $^{15}\text{N}$  chemical shift of N1/4 is due to the N1-C1 and N4-C6 double bonds. But their  $^{15}\text{N}$  chemical shifts moves (about 70 ppm) to lower frequency on protonation showing a loss in double bond character. Also, the  $^{15}\text{N}$  signal for N2/3/5/6 shows an increase in deshielding in passing from the free base to the salt of about 20 ppm, indicating more double bond character [129]. This reflects that those double bonds that are not attached to these nitrogen nuclei are largely involved in redistribution of the electron density. This result requires that naphthyl, guanidine and guanidinium groups become more coplanar. It has already been reported that after protonation, the naphthalene frame is planar with the captured proton located between the imine nitrogen nuclei in the same plane [72]. Also as a result of the cationic resonance effect within the guanidine subunits, amino groups also become planar [127].

### 4.3 TMGN-Me

If TMGN was alkylated on N2/3/5/6, it was expected to find one singlet which integrates for 9H. However, such a signal was not observed and therefore, either N1 or N4 is the site of alkylation.

The 400 MHz  $^1\text{H}$  NMR spectrum of TMGN and iodomethane reaction product is very complex. Many peaks were observed in high field (methyl range) as well as low field (aromatic range), which means more than one compound, is present in the reaction medium. The remaining signals (those that are not already assigned to TMGN- $\text{H}^+$ ) belong to a molecule that has a more complex structure.

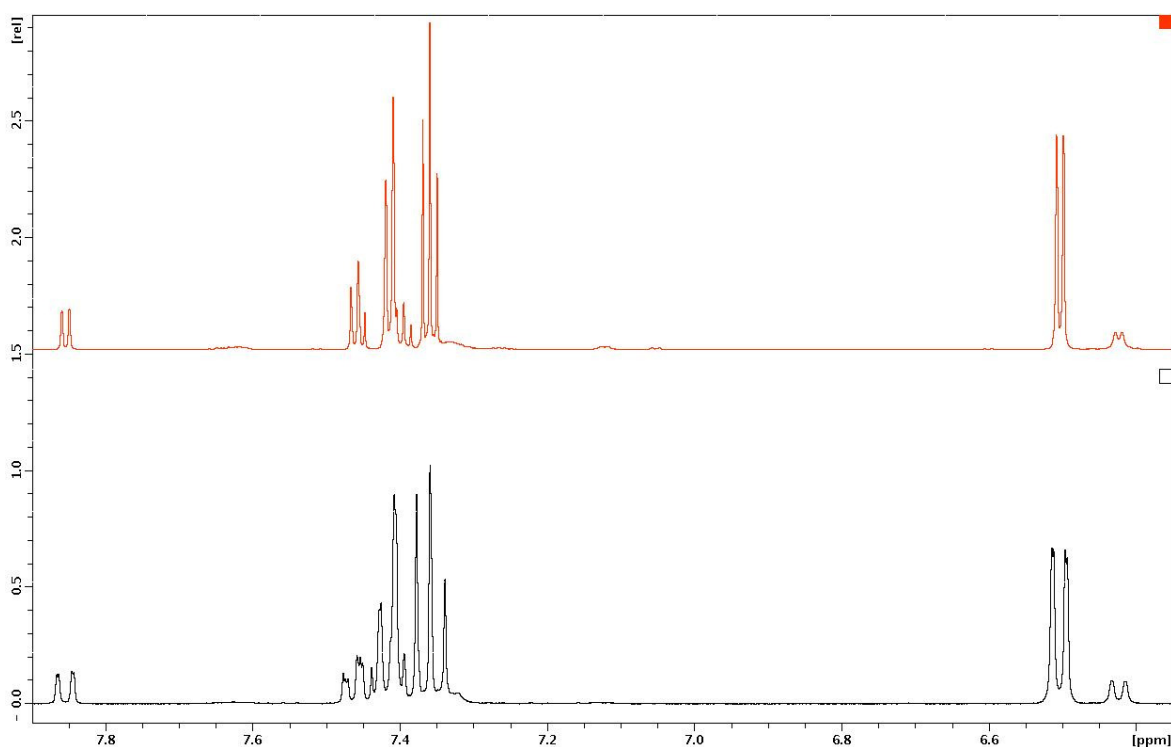


Figure 4-7 800MHz  $^1\text{H}$ NMR (above) and 400 MHz  $^1\text{H}$ NMR (below) of TMGN-Me, aromatic range

For this molecule, six signals are observed in the aromatic region and four signals are found in the methyl region. This indicates a loss of symmetry, *i.e.* right and left parts of the

molecule are not equivalent anymore and therefore, give different NMR signals. Far better resolution in low field (aromatic range), was achieved by re-running spectrum on the 800MHz NMR spectrometer and thereby aid the assignment of aromatic protons. Scalar-coupled protons H13 and H19 appear as triplet, while the signals of other four aromatic protons are doublets (Figure 4-7).

For six signals of aromatic protons, COSY, TOCSY and  $^{13}\text{C}$ -HSQC-TOCSY spectra identified two different spin systems corresponding to system A, the signals at 6.38, 7.35 and 7.42 ppm and to system B, the signals 7.33, 7.40 and 7.82 ppm. The values of chemical shifts of the former are very similar to those of TMGN / TMGN-H, whereas those of the latter are different. On  $^1\text{H}$ - $^{15}\text{N}$  HMBC spectrum, it can be seen that the most shielded proton signal of system A (6.38 ppm) correlates with a  $^{15}\text{N}$  nucleus at 197.5 ppm, while the second (7.33 ppm) which is very large, shows correlation with a  $^{15}\text{N}$  nucleus at 105.9 ppm. Therefore, system A is assigned to H18/19/20 and system B to H12/13/14.

In order to determine, in high field (methyl range), which peaks come from the alkylating agent and thus verify if there is at least one *N*-alkylation product,  $^{13}\text{CH}_3\text{I}$  was used as the source of label. The labeled sample was analyzed through its  $^{13}\text{C}$ -decoupled  $^1\text{H}$  NMR spectrum and three peaks for  $^{13}\text{C}$ -labeled methyl groups were observed at 2.18 (assigned to unreacted  $^{13}\text{CH}_3\text{I}$ ), 3.16 (assigned to  $^{13}\text{CH}_3\text{OH}$ ) and 3.35 (unknown) ppm. For the first two peaks, the assignment was confirmed by  $^1\text{H}$ - $^{13}\text{C}$ -HSQC. These two peaks show correlations at -22.6 and 48.5 ppm respectively. The unknown peak correlates with a  $^{13}\text{C}$  at 43.1 ppm.

On NOESY spectrum, it can be observed that the proton signal at 6.38 ppm correlates with a relatively broad signal (width at half-height, 7 Hz) of a dimethylamino group at 2.63 ppm. The integration ratio of these two peaks is 1 to 11 (almost four methyl groups), then



this broad signal can be assigned to methyl groups C7/8/9/10. It can be seen that, on  $^1\text{H}$ - $^{15}\text{N}$  HMBC spectrum, it is correlated with a nitrogen nucleus at 60.6 ppm. As in TMGN and in  $\text{TMGN-H}^+$ , the chemical exchange of these methyl groups is very fast.

The two methyl signals at 3.08 and 2.58 ppm are more shielded. They integrate for six protons each, but they do not look like the same; the more shielded one (width at half-height, 2.2 Hz) is rather sharp, however, the other one is very broad (width at half-height, 19 Hz) and extends over 2.63 ppm (Figure 4-8).

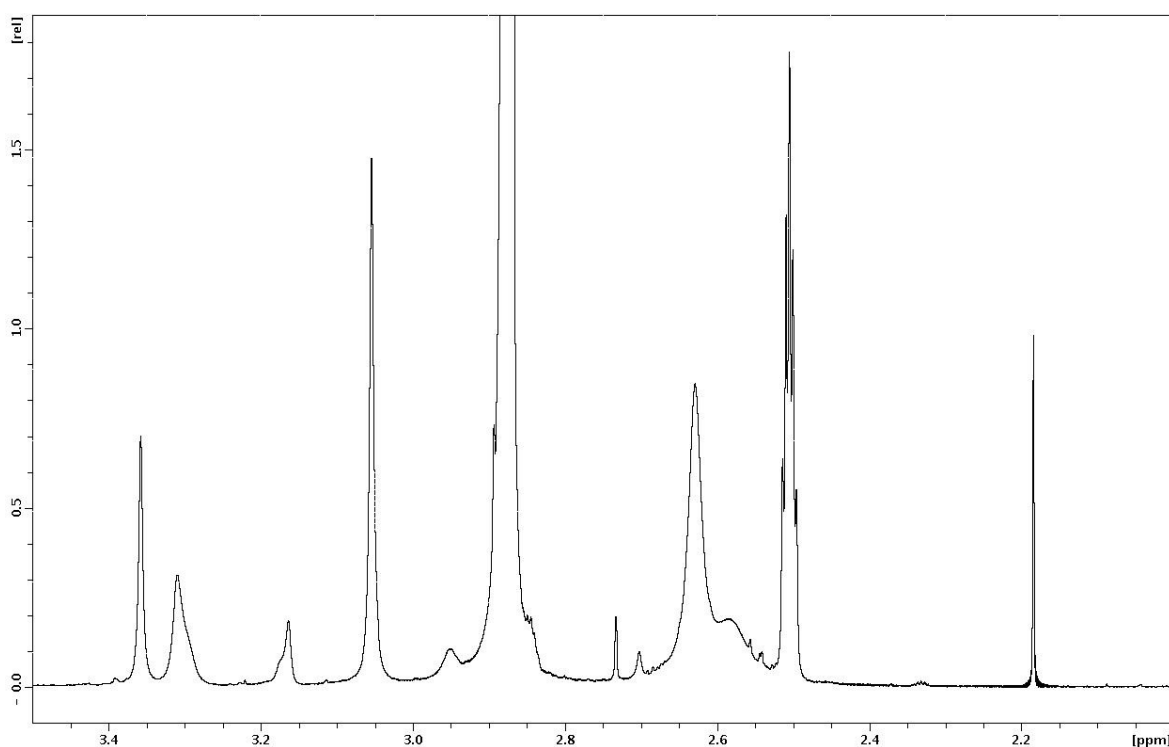


Figure 4-8 400MHz  $^1\text{H}$  NMR of TMGN-Me, methyl range

Both of these signals display connectivity to C12 (at 7.33 ppm) in NOESY spectrum. This identifies them as methyl groups C2/3/4/5 who are in slow exchange on the NMR time-scale without being possible to unambiguously assign them to specific sites. It is only the methyl group signal at 3.08 ppm that shows a correlation with a  $^{15}\text{N}$  nucleus at 75.5 ppm on  $^1\text{H}$ - $^{15}\text{N}$  HMBC spectrum. The labeled singlet at 3.35 ppm, integrates for 3H and hence

belongs to the remaining methyl group. Through examining  $^1\text{H}$ - $^{15}\text{N}$  HMBC, it is found that it, as well as H12, correlates with a  $^{15}\text{N}$  nucleus at 105.9 ppm and can safely be assigned to methyl group C21. The NOESY spectrum indicates that protons of this methyl group, as well as those of methyl groups C2/3/4/5, and C12 must be in close spatial proximity.

It is important to have a clue on the structure of TMGN-Me and thus it is required to have a closer look at the chemical shifts of nitrogen nuclei. For this purpose the chemical shifts of nitrogen nuclei for TMGN, TMGN- $\text{H}^+$  and TMGN-Me are listed again in Table 4-4.

**Table 4-4  $^{15}\text{N}$  chemical shifts of TMGN, TMGN- $\text{H}^+$  and TMGN-Me**

	Bond	TMGN	TMGN- $\text{H}^+$	TMGN-Me
N1	N1-C1	215.9	144.9	105.9
N2/3	N2-C1/ N3-C1	53.7	73.1	75.5
N4	N4-C6	215.9	144.9	197.5
N5/6	N5-C6/N6-C6	53.7	73.1	60.6

It has already been reported that for TMGN, there is no conjugation between the  $\pi$ -systems of the naphthalene ring and the guanidine moiety [127] or the degree of their conjugation is marginal [72] and for TMGN- $\text{H}^+$ , due to spatial configuration conjugation is only possible with only one of the guanidine groups [72]. This is not corroborated by our observations here that show a N1/4-naphthalene conjugation for TMGN and N4-naphthalene conjugation for TMGN-Me. However, we cannot quantify the degree of conjugation. As illustrated in Table 4-4, on alkylation, N4 nucleus is shielded by about 20 ppm (215.9 to 197.5 ppm) while N5 and N6 are slightly (7 ppm) deshielded (53.7 to 60.6 ppm). Increased  $^{15}\text{N}$  shielding signifies a decrease in the double bond character [129]. When the double bond character decreases for the central nitrogen (N1 or N4), it increases for the terminal nitrogen (N2/N3 or N5/N6), and vice versa. This reflects the contributions

of the mesomeric forms. Sibi and Lichter [130] have demonstrated that for different methylated N, N-dimethylaniline, nitrogen resonance position move upfield as nitrogen lone-pair  $\pi$  delocalization is inhibited and it is consistent with an increase in electron density as well as a decrease in the C-N  $\pi$  bond character. In TMGN-Me, pentamethylguanidinium, N1 lone-pair delocalization is influenced by the electronic interaction of guanidine group and therefore is sterically inhibited from conjugation.

$^{15}\text{N}$  chemical shifts of N2/N3 for TMGN-Me (75.5 ppm) are very close to those observed for TMGN- $\text{H}^+$  (73.1 ppm). However, N1 is 39 ppm more shielded in TMGN-Me than in TMGN- $\text{H}^+$ . The shielding effect of methyl groups on the nitrogen nuclei in urea has already been demonstrated and has been explained in terms of a decrease in the lone pair delocalization upon substitution [131].

$^{15}\text{N}$  chemical shifts of N4 and N5/N6 indicate that in TMGN-Me, the degree of guanidine-naphthalene conjugation is not as much as that of in TMGN and therefore they are not coplanar.

Moreover,  $^1\text{H}$  and  $^{13}\text{C}$  chemical shifts of C12/14 are not similar to those of TMGN and of TMGN- $\text{H}^+$  and to C18/20 of TMGN-Me. It is, therefore, another reason to conclude that pentamethylguanidinium group in TMGN-Me is not coplanar with naphthalene. There are also other reasons to rationalize it; such as the observed correlation between methyl group C21 and proton H12, steric hinderence of methyl group C21 and N4, some observed broad proton signals (H12, methyl group C2/3 and C4/5).

## 5 Measuring Diffusion Coefficients

Diffusion is the term used to describe random, Brownian (translational) motion of a solute in solution. This motion is characterized by the coefficient of lateral diffusion, which is critically dependent on sample temperature, solvent viscosity, molecular shape, and molecular size.

NMR has been used to study diffusion for many years [132]. It can be used to measure self-diffusion constants with an accuracy approaching 1% for objects in solution from the size of molecules to micelles. DOSY is an example of a pulsed field gradient stimulated echo experiment. Such experiments incorporate a series of magnetic pulses of varying intensity and duration. In DOSY experiment, the NMR signal is attenuated by increasing the gradient strength. In other words, the gradient strength increases, the NMR signal diminishes. A plot is made of intensity of one or several selected peaks against gradient strength. Stejskal et Tanner[133] have shown that the intensity of the signals in diffusion experiments is described by the following equation:

$$\frac{I}{I_0} = \exp \left[ -\gamma^2 \delta^2 G^2 \left( \Delta - \frac{1}{3} \delta \right) D \right] \quad (5-1)$$

where:

$I$  = intensity or integral of the peak at a given  $G$

$I_0$  = intensity or integral of the peak at  $G = 0$

$g$  = magnetogyric constant of the nucleus (for  $^1\text{H}$ ,  $g = 2.675 \times 10^8 \text{ T}^{-1} \text{ s}^{-1}$ )

$\delta$  = diffusion gradient length (set to 1ms)

$\Delta$  = diffusion delay

$G$  = gradient field strength

$D$  = diffusion coefficient

The diffusion coefficient  $D$  is generally determined as the slope of the linear plot of  $\ln(I/I_0)$  versus  $k$ , where  $k$  is equal to  $-\gamma^2 \delta^2 G^2 \left( \Delta - \frac{1}{3} \delta \right)$ .

Here, diffusion ordered nuclear magnetic resonance spectroscopy (DOSY-NMR) was applied to measure the self diffusion coefficients of benzoic acid, **1**, syringic acid, **2**, TMGN, **16**, DBU, **21**, iodomethane, **6**, and methyl syringate and syringic acid methyl ether (**2a** and **2b**) in DMF- $d_7$ .

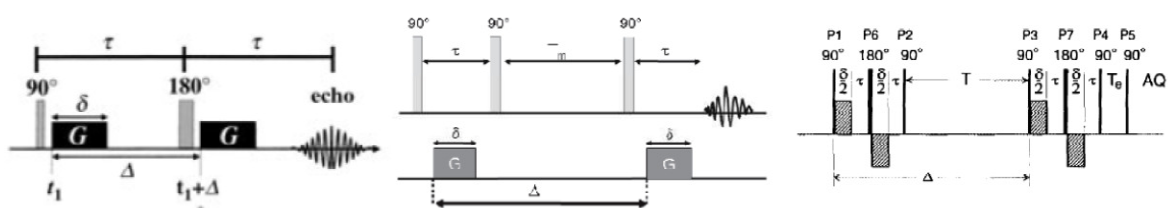


Figure 5-1 The PGSE pulse sequence (left).  $G$  is the amplitude of the pulsed gradient,  $\delta$  its duration and  $\Delta$  the separation between the leading edges of the pulsed gradients[132]. The STE sequence (center) [134]. Bipolar pulse pair-longitudinal eddy current delay(right)[135].

Table 5-1 NMR experimental parameters for DOSY experiments

Diffusion time ( $\Delta$ )	60 ms
Length of the diffusion gradient ( $\delta$ )	3 ms (2 ms for <b>6</b> )
Number of steps (TD)	2048
Relaxation delay	5s
Number of scans	16
Number of points	32
Gradient level	5-95%
Maximum intensity of gradient	32 G cm <sup>-1</sup>
Experimental time	11h

The concentration of the prepared solutions was approximately 0.01 mol L<sup>-1</sup>. <sup>1</sup>H DOSY NMR spectra were recorded on a Bruker Avance 300 MHz spectrometer using a Quattro Nucleus Probe (QNP) probe. Pulsed Gradient Spin Echo (PGSE) experiments were measured using the STE sequence, modified with bipolar pulses and longitudinal eddy current delay (BPP-STE-LED). The PGSE sequence and BPP-LED are shown in Figure 5-1. The experimental parameters used in the NMR measurements are summarized in Table 5-1.

**Table 5-2 Diffusion and Stokes radius data for model components**

Sample	D (m <sup>2</sup> s <sup>-1</sup> ) × 10 <sup>9</sup>		r <sub>H</sub> (Å)		r <sub>vaw</sub> (Å)
	This work	Literature value	This work	Literature value	This work
Benzoic acid, <b>1</b>	0.8783	1.78 [136] <sup>a</sup> 0.91 [137] <sup>b</sup>	3.29	3.7 [138]	3.43
Syringic acid, <b>2</b>	0.6127		4.72		3.89
Methyl syringate, <b>2a</b>	0.7104		4.07		4.10
Syringic acid methyl ether, <b>2b</b>	0.6749		4.28		4.10
Iodomethane, <b>6</b>	1.806	1.70±0.4 [139] <sup>c</sup>	1.60	1.8 [140]	2.94
TMGN, <b>16</b>	0.6678		4.33		5.15
DBU, <b>21</b>	1.033		2.80		3.78
<b>1, 16</b>	0.5786				
<b>1, 21</b>	0.7590				
DMF (solvent)	1.48		1.95		3.20

a. In CH<sub>2</sub>Cl<sub>2</sub>,

b. In water,

c. In a solution of 0.3M tetrabutylammonium perchlorate/DMF

Table 5-2 lists the obtained diffusion coefficient values and the calculated Stokes radius. Appendix C offers the detailed raw results of these experiments.

Through the Stokes-Einstein equation (equation 5-2), it is possible to correlate the diffusion coefficient (D) with the hydrodynamic radius ( $r_H$ ):

$$r_H = \frac{k_B T}{6\pi\eta D} \quad (5-2)$$

where  $k_B$  is the Boltzmann constant ( $1.3806503 \times 10^{-23} \text{ m}^2 \text{ kg s}^{-2} \text{ K}^{-1}$ ), T is the temperature expressed in Kelvin (here 293 K) and  $\eta$  is the dynamic viscosity of solution. For DMF-*d*7,  $\eta=7.550 \times 10^{-4} \text{ Pa.s}$  [141]. As it is seen in this table, molecules that are not much bigger than those of the solvent diffuse faster. However, large non-spherical molecules diffuse slower.

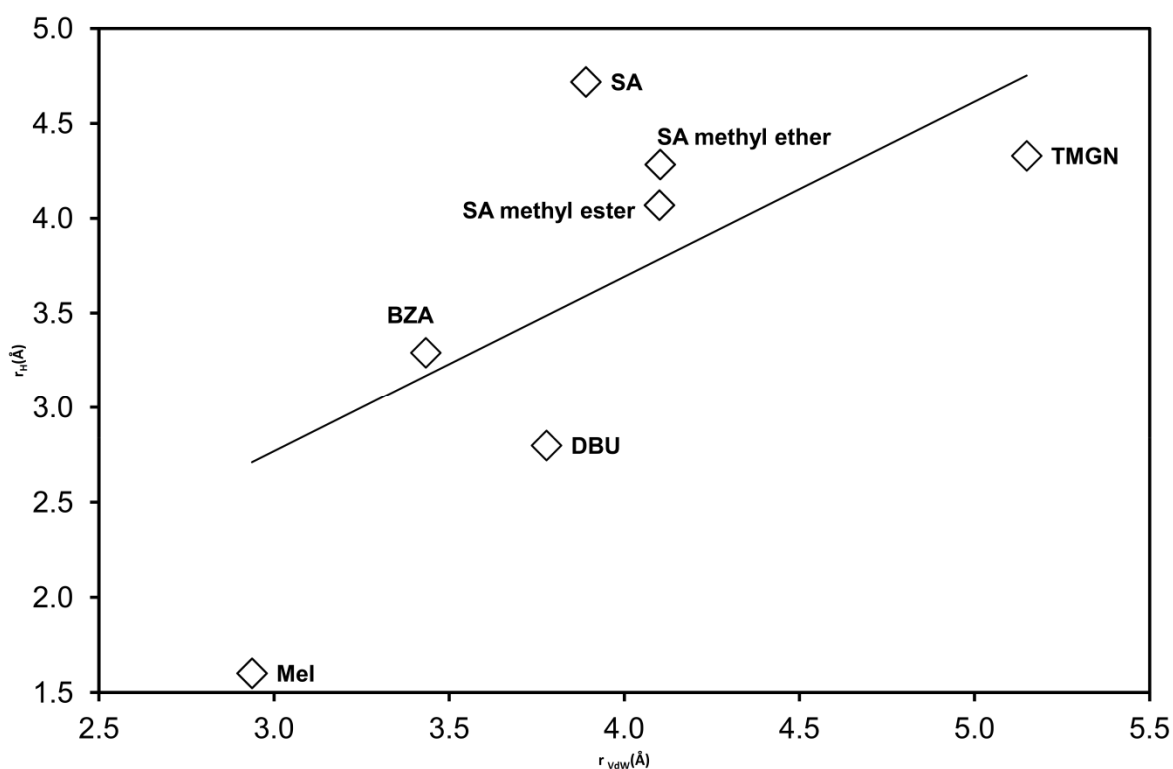


Figure 5-2 Relationship between Stoke's radius and van der Waals radius

In this table, finally van der Waals radius ( $r_{vdw}$ ) was calculated through the following equation:

$$r_{vdw} = \left[ \frac{3 MW}{4 \pi N \rho} \right]^{1/3} \quad (5-3)$$

In this equation MW, and  $\rho$  are the molecular weight and the density of the compound (their values were taken from CAS data bank) and N is the Avogadro constant.

Figure 5-2 shows the correspondence between the van der Waals and Stokes radius. Their relation however is very poor. It is clear that the hydrodynamic radii are different from the van der Waals ones and this fact can be associated with formation of ion-pairs and neutral aggregates mainly due to Coulombic interactions between ions and the equilibrium between these species[142].



## 6 Preparative-scale synthesis

Despite many technological improvements, it is still the traditional “round-bottomed flask” concept that is widely used for most chemical reactions. However, because of excellent potential for the integration of a high level of automation and for the incorporation of on-demand reaction analysis, continuous flow technology can be a better alternative [3].

In recent years, an increased interest and considerable progress have been seen in the use of miniaturized systems for the study of chemical reactions. Several micro-devices, among them [44-49], have been developed to investigate physical and chemical phenomena as well as fast acquisition of chemical kinetic data and crucial transport phenomena parameters. Microfluidic technologies have, also, emerged as viable tools for carrying out the chemical reactions in continuous flow processes, among them [143-145]. The many advantages and efficiency gains, such as reduced reaction times, better mass and heat transfer, the enhanced safety, reduced solvent usage and lower waste generation, combined with the easier scale-up and reproducibility due to the precise control over reaction conditions in these devices, adds considerable value to the concept [3-4, 145-146].

### 6.1 Motivation

Phenolic compounds, “phenolics”, constitute a large group of secondary plant products with an aromatic ring bearing one or more hydroxyl substituents [147-148]. Phenolic acids and flavonoids are examples. In plants foods, flavonoids account for approximately two-thirds of the dietary phenols, however, phenolic acids account for almost all of the remaining third [148]

There are two classes of phenolic acids; hydroxybenzoic acids and hydroxycinnamic acids [149]. Both occur frequently in foods. Phenolic acids are mainly protective antioxidants. But beyond this other biological activities of phenolic acids have been reported. For example, syringic acid (studied here), exhibits *in vitro* antibacterial [150], antimicrobial activity and fungitoxicity [151].

Many of cinnamic and benzoic acid derivatives exist in all plant and plant-derived foods (e.g., fruits, vegetables, and grains). But only a minor fraction exists in the free acid form and the major fraction is linked through ester, ether, or acetal bonds to cellulose, proteins, lignin, flavonoids, glucose, terpenes, etc [152]. Then, the extraction of bioactive compounds from plant materials is the first step in synthesis of phenolic acids derivatives. But it is not a straight-forward process [153-154]. Then chemical or bio-synthesis methods can appear very helpful.

A brief research overview of the literature on the single step alkylation of syringic acid, **2**, shows that mainly four methods have been employed; the first method involves benzyl bromide to synthesis either di-alkylated product or its mixture with the ester.

Catel *et al.* [155] have synthesized benzyl 3,5-dimethoxy-4-benzyloxybenzoate with a yield of 76% by adding potassium carbonate ( 3.0 equiv) and benzyl bromide (3.0 equiv) to a solution of syringic acid (0.257 M) in dry DMF under an argon blanket. After stirring the mixture for 15 h, the reaction medium has been transferred into distilled water. The final product has been extracted with diethyl ether and distilled water. Another route to esterification of syringic acid, **2**, is Fischer esterification. Methyl 4-hydroxy-3,5-dimethoxybenzoate with a yield of 96% has been obtained by adding 0.015 mol H<sub>2</sub>SO<sub>4</sub>(98%) to a 0.3M solution of syringic acid in methanol. The reaction is carried out by heating under reflux for 3 h. The final product obtains after cooling the system, adding water and saturating by sodium chloride and extracting five times by dichloromethane

[156]. In another report, using a more concentrated solution of syringic acid in methanol (0.6M) and a higher amount of H<sub>2</sub>SO<sub>4</sub> (0.037 mol) and a reflux time of 10h a yield of 95% has been achieved. In this report the residue has been dissolved in ethyl acetate and been washed with a saturated solution of NaHCO<sub>3</sub> [157]. Lipase-catalyzed esterification of syringic acid with hexanol has been also investigated in selected diethyl ether with a yield of only 2% [158]. Buisman *et al.* [158], reported that the reactivity of the carboxylic function of syringic acid are affected by the electron donating substituents (methoxy groups) in its aromatic rings, hence limiting the nucleophilic attack of the alcohol. Syringic acid ethers may also be prepared by the alkylating esterification of syringic acid with alkyl halides. It is usually done in the presence of a base. As part of the synthesis of 3,5-dimethoxy-4-hydroxy-benzoic acid 4-(*N,N'*-Boc-guanidino)-butyl ester, Liu *et al* [159] have synthesized 4-(acetyloxy)-3,5-dimethoxy- benzoic acid by using triethylamine as base and dichloromethane as the solvent. This reaction has been done at room temperature and it has taken two hours.

Clofibric acid, **3**, is a pharmaceutical drug and a structural isomer of the phenoxyalkanoic acid herbicide 2-[4-chloro-2-methylphenoxy] propionic acid (MCPD). It is a high volume chemical with an estimated annual production in the low kiloton range [160]. It is mainly used in the form of the ethyl ester (clofibrate) in human medical care as a blood lipid regulator [161]. Clofibrate has been prepared by using the Ph<sub>3</sub>P-CCl<sub>3</sub>CN with a yield of 78%. The total reaction time was 5h and THF was employed as the solvent [162]. In another report [163] and using distannoxane ([Cl(C<sub>6</sub>F<sub>13</sub>C<sub>2</sub>H<sub>4</sub>)<sub>2</sub>SnOSn(C<sub>2</sub>H<sub>4</sub>C<sub>6</sub>F<sub>13</sub>)<sub>2</sub>Cl]<sub>2</sub>) as catalyst, benzyl alcohol as alkylating agent and toluene as solvent, phenylmethyl ester of clofibric acid has been obtained with a yield of 98%. The reaction time and temperature are 16h and 150°C respectively.

Podocarpic acid, **4**, is an abietic-type resin phenol -acid obtained from rimu resin [164] has been considered as an attractive starting material for the synthesis of biologically important compounds [165]. Methyl-O-methyl podocarpate (**4c**) exhibits antiviral activity [166].

Podocarpic acid esters were synthesized by acid chloride activation( using  $\text{SOCl}_2$ ), followed by reaction with appropriate alkyl halides [167]. In this way a large number of podocarpic esters were generated. Dimethylated podocarpic acid derivative was synthesized by using caustic soda and  $\text{Me}_2\text{SO}_4$  [167].

Trolox, **5**, is a water-soluble analogue of vitamin E and a stronger antioxidant than vitamin E [168]. It is used as a standard for measuring antioxidant activity [169].

In one report, trolox has been perbenzylated (benzyl bromide,  $\text{K}_2\text{CO}_3$ , DMF) at room temperature to give dialkylated trolox. The reflux time was 15h [155]. The obtained yield has not been precised but the utilized method suggests a yield around 91-92% [170]. Muller *et al* [171] when the reflux time is increased to 40h, obtained a yield of 95%. In their experiments DMF has been replaced by acetone and for one equivalent of trolox, 9 equivalents of potassium carbonate and three equivalents of benzylbromide have been used.

### 6.1.1 Quercetin

Flavonoids belong to a group of natural substances with variable phenolic structure and are found in the fruits, vegetables, grains, bark, roots, stem, flowers, tea and wine [172]. Flavonoids have multiple biological activities including potent anti-allergic, anti-inflammatory, and antiviral actions, which may result, at least in part, from their antioxidant and free radical-scavenging abilities [173].

The flavonoid, quercetin, **25**, (flavonol subclass) is one of the most extensively studied polyphenols. It serves as a good example here because of its overwhelming presence in

foods and because its metabolism in humans is well understood, and many conjugates have been identified [174-175].

Quercetin could especially be effective in preventing atherosclerosis and thrombosis by protecting low density lipoproteins (LDL) against oxidation, as well as by lowering the cytotoxicity of oxidized LDL and platelet aggregation [176-177]. Furthermore, quercetin exhibits antitumor effects *in vitro* and inhibits the development of experimental cancers in animal models [176]. Most of the knowledge about quercetin has originated from *in vitro* studies while *in vivo* data that take into consideration the complex interplay of diverse processes like uptake, metabolism and organ and tissue interactions within a whole animal are more limited [178]. As its adverse health effects, quercetin appears to stimulate the proliferation of estrogen receptor-positive cells *in vitro* at concentrations physiologically relevant *in vivo*. Moreover, quercetin is genotoxic in various *in vitro* systems. Furthermore, evidence for covalent binding of quercetin to cellular protein and DNA has been reported [177].

Methylation to isorhamnetin (3'-*O*-Methylquercetin) or tamarixetin (4'-*O*-Methylquercetin) seems to be an important conjugation process in quercetin metabolism [178]. Conjugated metabolites are likely to possess different biological properties than parent compounds do. A decrease in the *in vitro* antioxidant activity of quercetin following methylation of the hydroxyl groups was found in different studies [179]. Despite this, 3-*O*-Methylquercetin presents pronounced antiviral activity and moderate anti-inflammatory and antioxidant properties [180]. Isorhamnetin, which is found in sea-buckthorn, has recently been reported to have antioxidant activity, the ability to increase the resistance of human low-density lipoprotein to oxidation induced by  $\text{Cu}^{2+}$ , scavenger radical activity, and antitumor activity [181]. 7-*O*-Methylquercetin (rhamnetin) (as well as isorhamnetin

and quercetin) reduces serum cholesterol in the rats fed with cholesterol-enriched diet[182].

Quercetin, isorhamnetin and tamarixetin increase the resistance of worms against thermal and oxidative stress and are also able to prolong their lifespan [178]. Azaleatin 3 $\beta$ -glucoside, a derivative of azaleatin (5-*O*-Methylquercetin) has a very high antioxidant activity [183]

Flavanoids are usually obtained in pure forms by extraction/purification from their natural sources. However, chemical synthesis or biotechnological approaches clearly play an important role in accessing polyphenols in pure forms [172, 184].

The general strategy for the synthesis of quercetin alkyl derivatives involves the selective protection of hydroxyls, selective *O*-alkylation to introduce an alkyl group and unblocking (deprotection) of hydroxyls. As an example for a single-step quercetin *O*-alkylation, 3', 7-Di-*O*-benzylquercetin was synthesized at room temperature over 24h by mixing quercetin (3.315 mmol), borax (9.966 mmol), benzyltriethylammonium chloride (0.483 mmol), benzyl chloride (13.29 mmol) and potassium carbonate (9.957 mmol). The reported yield, after extraction and purification is 52%. It shows that borax-type protection of adjacent hydroxyl groups could be effective in inducing selective alkylation [184].

*O*-methylation is a reaction characterized by the transfer of a methyl group from a donor, to an oxygen atom [185]. This transformation can even be detected in bacteria. *O*-Methyltransferase (OMT), *SaOMT-2*, isolated from *Streptomyces avermilitis*, and expressed in *E. Coli* transfers a methyl group to the C-7 hydroxyl of Quercetin. The reported relative conversion is even higher than 100% for a reaction time of 12 h at 30°C [186].

Matsuda *et al.* [187] were treated a solution of quercetin in methanol by ethereal diazomethane (1 h , room temperature) to produce a mixture of mono-, di- and

tetramethylated quercetin. The product distribution is as following; 7 and 4' monomethyl (22% and 2%), 3,7-dimethyl (13%), 4',7-dimethyl (16%), 3,4',7 trimethyl (32%) and 3,3',4',7-tetramethyl (14%).

As illustrated in the aforementioned examples for phenol-acids and quercetin, the process of acid-phenols esterification and quercetin methylation usually involves harsh reagents and conditions and the reaction time is long. Therefore, it is important to develop approaches that would insure regioselectivity with relative simplicity and high yields. Here, we disclose our findings regarding using our microfluidic device to synthesize esters and ethers in a single step process. The synthesized products as well as their reactants are listed in Appendix E.

## 6.2 Syringic acid

The purpose of this work is to use syringic acid, **2**, as a model compound to study the selectivity in the microfluidic device. Mechanism of its alkylation to produce methyl ester, **2a**, is similar to that of benzoic acid. Ionization constants for syringic acid, **2**, in water are  $pK_{a1}=4.46$  for carboxyl group and  $pK_{a2}=9.33$  for phenolic one [188]. Using the equation proposed by Gonzalez and Herrador [189] to correlate the aqueous  $pK_a$  to that of in DMF,  $pK_a$  values in DMF for syringic acid are roughly estimated to be  $pK_{a1}=7.69$  and  $pK_{a2}=12.56$ . Recalling  $pK_a$  of TMGN, **16**, in DMF is in the range of 16.5-17.5, therefore TMGN is able to effectively remove both syringic acid acidic and phenolic hydrogen. Guided by previous researches done in our laboratory [190], DBU, **21**, was chosen as the alternative base. Its  $pK_a$  in acetonitrile is 24.33 [107] and in DMF is estimated to be 16-17 [73].

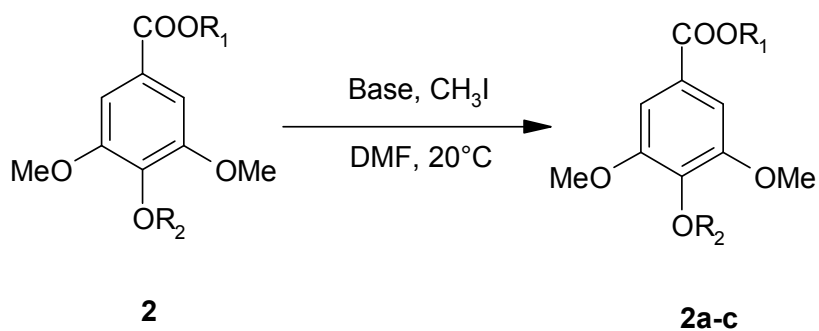


Figure 6-1 Syringic acid alkylation by iodomethane

Syringic acid, **2**, alkylation by iodomethane, **6**, in the presence of an organic base (TMGN, **16**, or DBU, **21**) in preparative scale experiments were carried out in batch as well as in continuous mode and the effect of several parameters was investigated. Figure 6-1 presents the reaction scheme. The results are presented in Tables 6-1 to 6-7. In these tables,  $F_{2a}$ ,  $F_{2b}$  and  $F_{2c}$  are weight percents of methyl syringate, **2a**, syringic acid methyl ether, **2b**



and dialkylated syringic acid **2c** in the pure product and  $F_2$  is the weight percent of syringic acid **2** in the residue.

Through these tables the following points have been emerged:

- i) The NMR (300 MHz) results are in good agreement with gas chromatographic (GC) analyses
- ii) In general, conversion is lower in the presence of DBU **21** than in the presence of TMGN**16**.
- iii) Regardless of the reaction conditions employed, syringic acid methyl ether **2b** is not produced while using TMGN **16** as base (which will be discussed later)
- iv) By increasing reaction time,  $F_{2a}$  is decreased in favor of  $F_{2c}$  (entries 1, 2 and 3 or 4, 5 and 6 in Table 6-1).
- v) The conversion and the selectivity toward methyl syringate **2a** are higher in continuous mode than in batch mode for both bases TMGN **16** ( entry 4 in Table 6-1 and entries 1,2 in Table 6-7) and DBU **21**(entry 1 in Table 6-1 and entries 1,2 in Table 6-6)
- vi) In the presence of DBU **21**, when DBU **21** and iodomethane **6** to syringic acid **2** molar ratios are 1.0, by doubling concentration of syringic acid **2**, conversion is decreased around 13% ( entries 1and 2 in Table 6-2). However, when DBU **21** and iodomethane **6** to syringic acid **2** molar ratios are 1.6 by doubling concentration of syringic acid **2**, conversion is increased by 2% or 15%( entries 3, 4 and 5 in Table 6-2)
- vii) In the presence of DBU **21**, by doubling base concentration, conversion and  $F_{2a}$  are decreased around 14% and 6 % ( entries 1and 6 in Table 6-2).
- viii) In the presence of DBU **21**, maximum conversion has obtained when DBU **21** and iodomethane **6** to syringic acid **2** molar ratios are 1.6 (entries 3 and 5 in

Table 6-2) and the reagents combination is [(**2**, **6**), **21**] (entry 2 in Table 6-3). Because of the alkylation of DBU **21** by iodomethane **6** (section 3.2), the third combination of [**2**, (**6**, **21**)] does not work.

- ix) In the presence of TMGN **16**, by doubling concentration of syringic acid **2**, conversion is increased around 13% (entries 7 and 8 in Table 6-2).
- x) In the presence of TMGN **16**, by doubling base concentration, conversion is increased around 15% without noticeable change in  $F_{2a}$  and  $F_{2c}$  (entries 8 and 10 in Table 6-2).
- xi) In the presence of TMGN **16**, maximum conversion has again obtained when TMGN **16** and iodomethane **6** to syringic acid **2** molar ratios are 1.6 (entry 9 in Table 6-2)
- xii) In the presence of TMGN **16**, maximum conversion has obtained when reagents combinations are [(**2**, **6**), **16**] (entry 2 in Table 6-4) and [(**2**, **16**), **6**] (entry 6 in Table 6-4). However  $F_{2a}$  is slightly higher in the former than in the latter.
- xiii) In the presence of DBU **21**, the reaction is not affected by changing micromixer from Nanomixer® to Y-Microreactor. Because despite a less efficient mixing in Y-microreactor, because of its volume (13 $\mu$ L), the reaction residence time is 39 s longer than usual. However, reaction conversion is decreased by 18% when using MicroTee. Nevertheless, the products distribution remains almost unchanged (entries 1, 3 and 5 in Table 6-5).
- xiv) In the presence of TMGN **16**, the reaction conversion is not again affected by changing micromixer from Nanomixer® to Y-Microreactor but slightly affected (2%) by using Microtee (entries 2, 4 and 6 in Table 6-5).
- xv) Both for TMGN **16** and DBU **21** by increasing flowrate (decreasing residence time), reaction conversion is decreased. But it is decreased more dramatically

with DBU **21** than with TMGN **16**. At the same time by increasing flowrate,  $F_{2c}$  is decreased. But it is decreased more dramatically with TMGN **16** than with DBU **21**. However,  $F_{2a}$  remains nearly constant and  $F_{2b}$  does not follow any particular trend (Tables 6-6 and 6-7).

**Table 6-1 Batch experiments†**

Base	Entry	Concentration of <b>2</b> (mmol L <sup>-1</sup> )	Base: <b>2</b> molar ratio	<b>6</b> : <b>2</b> molar ratio	Recovered mass (%)	NMR			GC			
						F <sub>2a</sub>	F <sub>2c</sub>	F <sub>2</sub>	F <sub>2a</sub>	F <sub>2b</sub>	F <sub>2c</sub>	F <sub>2</sub>
DBU, <b>21</b>	1 <sup>a</sup>	168.0	1.7	1.7	85.1	79.1	21.0	6.5	82.5	1.6	15.8	6.7
	2	168.4	1.7	1.7	88.7	76.3	23.7	0	83.0	0.2	16.8	1.5
	3	167.7	1.7	1.7	84.5	74.0	26.0	0	81.1	0.4	18.4	1.4
TMGN, <b>16</b>	4 <sup>a</sup>	96.4	1.7	1.7	93.6	72.2	27.8	0	78.4	0	21.6	0
	5	97.3	1.7	1.7	60.4	56.0	44.0	0	64.0	0	36.0	0.3
	6	98.0	1.7	1.6	67.2	62.0	38.0	0	73.5	0	26.5	0

a. Reaction time for entries 1 and 4 is 9 min and for other entries is 1 h

† syringic acid, **2**, methyl syringate, **2a**, syringic acid methyl ether, **2b**, dialkylated syringic acid, **2c**, iodomethane, **6**.

**Table 6-2 Effect of the alkylating agent and base quantity†. Micromixer: NanoMixer®; Total flowrate: 20  $\mu\text{L min}^{-1}$ . Reagents combination: [(**2**, **6**), Base]).**

Base	Entry	Concentration of <b>2</b> ( $\text{mmol L}^{-1}$ )	Base: <b>2</b> molar ratio	<b>6</b> : <b>2</b> molar ratio	Recovered mass (%)	NMR	GC				
						$F_2^a$	$F_{2a}$	$F_{2b}$	$F_{2c}$	$F_2$	
DBU, <b>21</b>	1	96.4	1.0	1.0	48.2	50.3	99.1	0.0	0.9	52.2	
	2	168.3	1.0	1.0	42.6	67.0	97.5	1.9	0.6	65.1	
	3	97.6	1.6	1.6	56.3	32.6	91.8	3.0	5.2	34.3	
	4	97.4	1.6	1.6	43.4	56.3	95.3	4.3	0.4	53.5	
	5	168.5	1.7	1.7	43.9	39.4	89.9	5.0	5.1	38.6	
	6	96.4	2.0	1.0	40.8	56.3	93.5	4.4	2.1	53.3	
TMGN, <b>16</b>	7	47.3	1.0	1.0	84.5	41.8	99.6	0	0.4	39.8	
	8	95.3	1.1	1.1	67.1	22.3	98.9	0	1.1	26.5	
	9	96.5	1.6	1.7	62.5	0.0	97.2	0	2.8	6.0	
	10	96.9	2.0	1.0	58.5	12.7	97.1	0	2.9	11.0	

a.  $F_{2a}$ ,  $F_{2c}$  by NMR analysis are 100 and 0% respectively

† syringic acid, **2**, methyl syringate, **2a**, syringic acid methyl ether, **2b**, dialkylated syringic acid, **2c**, iodomethane, **6**.

Table 6-3 Effect of the reagents combination†. Micromixer: Nanomixer®; Total flowrate: 20  $\mu\text{L min}^{-1}$

	Entry	Concentration of <b>2</b> ( $\text{mmol L}^{-1}$ )	<b>21:2</b> molar ratio	<b>6:2</b> molar ratio	Recovered mass (%)	NMR	GC			
						F <sub>2</sub> <sup>a</sup>	F <sub>2a</sub>	F <sub>2b</sub>	F <sub>2c</sub>	F <sub>2</sub>
[( <b>2,6</b> ), <b>21</b> ]	1	96.4	1.0	1.0	48.2	50.3	99.1	0.0	0.9	52.2
	2	97.6	1.6	1.6	56.3	32.6	91.8	3.0	5.2	34.3
	3	96.4	2.0	1.0	40.8	56.3	93.5	4.4	2.1	53.3
[( <b>2, 21</b> ), <b>6</b> ]	4	96.3	1.0	1.0	45.6	57.1	99.1	0.0	0.9	56.6
	5	93.0	1.7	1.6	54.3	45.6	93.8	3.6	2.6	46.1
	6	96.4	2.0	1.0	37.8	53.6	92.7	4.8	2.5	55.4

a. F<sub>2a</sub>, F<sub>2c</sub> by NMR analysis are 100 and 0% respectively

† syringic acid, **2**, methyl syringate, **2a**, syringic acid methyl ether, **2b**, dialkylated syringic acid, **2c**, iodomethane, **6**.

Table 6-4 Effect of reagents combination†. Micromixer: Nanomixer®; Total flowrate: 20  $\mu\text{L min}^{-1}$

	Entry	Concentration of <b>2</b> (mmol L <sup>-1</sup> )	<b>16:2</b> molar ratio	<b>6:2</b> molar ratio	Recovered mass (%)	NMR	GC				
						F <sub>2</sub> <sup>a</sup>	F <sub>2a</sub>	F <sub>2b</sub>	F <sub>2c</sub>	F <sub>2</sub>	
[( <b>2,6</b> ), <b>16</b> ]	1	95.3	1.1	1.1	67.1	22.6	98.9	0.0	1.1	26.5	
	2	96.5	1.6	1.7	62.5	0.0	97.2	0.0	2.8	6.0	
	3	96.9	2.0	1.0	58.5	12.7	97.1	0.0	2.9	11.0	
[( <b>2,16</b> ), <b>6</b> ]	4	95.5	1.0	1.1	60.8	19.5	99.3	0.0	0.7	15.1	
	5	190.2	1.1	1.1	41.2	21.9	98.9	0.0	1.1	18.5	
	6	90.1	1.8	1.7	66.8	4.0	96.3	0.0	3.7	6.4	
	7	96.6	2.0	1.0	64.4	18.1	96.7	0.0	3.3	18.8	
[ <b>2</b> , ( <b>6,16</b> )]	8	96.1	1.0	1.0	45.0	40.2	99.4	0.0	0.6	43.9	
	9	96.4	1.6	1.7	62.4	31.0	98.7	0.0	1.3	30.1	
	10	96.5	2.0	1.0	44.7	51.4	99.0	0.0	1.0	48.2	

a. F<sub>2a</sub>, F<sub>2c</sub> by NMR analysis are 100 and 0% respectively

† syringic acid, **2**, methyl syringate, **2a**, syringic acid methyl ether, **2b**, dialkylated syringic acid, **2c**, iodomethane, **6**, TMGN, **16**, iodomethane, **6**.

Table 6-5 Effect of micromixer†. Total flowrate: 20  $\mu\text{L min}^{-1}$ ; Reagents combination: [(2, 6), Base].

	Entry	Base	Concentration of <b>2</b> ( $\text{mmol L}^{-1}$ )	Base: <b>2</b> molar ratio	<b>6</b> : <b>2</b> molar ratio	Recovered mass (%)	NMR	GC				
							F <sub>2</sub> <sup>a</sup>	F <sub>2a</sub>	F <sub>2b</sub>	F <sub>2c</sub>	F <sub>2</sub>	
Nanomixer®	1	<b>21</b>	97.6	1.6	1.6	56.3	32.6	91.8	3.0	5.2	34.3	
	2	<b>16</b>	96.5	1.6	1.7	62.5	0.0	97.2	0.0	2.8	6.0	
Y-microreactor	3	<b>21</b>	98.4	1.6	1.6	62.6	35.4	92.4	2.3	5.3	33.8	
	4	<b>16</b>	96.4	1.7	1.7	82.4	8.3	96.4	0.0	3.6	6.3	
MicroTee	5	<b>21</b>	96.1	1.7	1.7	44.5	53.6	93.7	3.5	2.8	52.0	
	6	<b>16</b>	96.9	1.7	1.7	79.7	6.5	96.6	0.0	3.4	8.6	

a. F<sub>2a</sub>, F<sub>2c</sub> by NMR analysis are 100 and 0% respectively, except for entry 6 where F<sub>2a</sub> and F<sub>2c</sub> are 97.0 and 3.0%

† syringic acid, **2**, methyl syringate, **2a**, syringic acid methyl ether, **2b**, dialkylated syringic acid, **2c**, iodomethane, **6**, TMGN, **16**, DBU, **21**, iodomethane, **6**.



Table 6-6 Effect of the residence time†; Micromixer: NanoMixer®. Reagents combination: [(2, 6), 21]).

Entry	Residence time (s), Flowrate ( $\mu\text{L min}^{-1}$ )	Concentration of <b>2</b> ( $\text{mmol L}^{-1}$ )	<b>21:2</b> molar ratio	<b>6:2</b> molar ratio	Recovered mass (%)	NMR			GC			
						F <sub>2a</sub>	F <sub>2c</sub>	F <sub>2</sub>	F <sub>2a</sub>	F <sub>2b</sub>	F <sub>2c</sub>	F <sub>2</sub>
1	530, 1.5	168.8	1.7	1.7	-	88.3	11.7	5.9	93.1	0.1	6.8	10.6
2	530, 1.5	168.5	1.7	1.7	-	87.2	12.8	9.0	92.8	0.0	7.2	7.9
3	79, 10	168.8	1.6	1.6	49.5	96.4	3.6	35.4	90.9	3.5	5.6	34.0
4	79, 10	168.7	1.1	1.0	50.1	100	0	45.3	98.0	0.0	1.9	46.6
5	40, 20	168.5	1.7	1.7	43.9	100	0	39.4	89.9	5.0	5.1	38.6
6	40, 20	97.4	1.6	1.6	43.4	100	0	56.3	95.3	4.3	0.4	53.5
7	40, 20	168.3	1.0	1.0	42.6	100	0	67.0	97.5	1.9	0.6	65.1
8	20, 40	168.9	1.7	1.7	41.4	100	0	52.8	90.5	5.9	3.5	46.7
9	20, 40	168.5	1.7	1.7	44.8	100	0	56.9	88.5	8.8	2.7	53.9
10	20, 40	168.4	1.7	1.7	37.7	100	0	47.3	91.7	5.0	3.3	49.0
11	8, 100	168.4	1.7	1.7	35.7	100	0	62.4	92.4	5.7	1.9	59.9
12	8, 100	168.9	1.7	1.7	-	100	0	68.5	92.6	5.2	2.2	65.7

† syringic acid, **2**, methyl syringate, **2a**, syringic acid methyl ether, **2b**, dialkylated syringic acid, **2c**, iodomethane, **6**, DBU, **21**, iodomethane, **6**.

Table 6-7 Effect of the residence time†; Micromixer: NanoMixer®. Reagents combination: [(2, 6), 16]).

Entry	Residence time (s), Flowrate ( $\mu\text{L min}^{-1}$ )	Concentration of <b>2</b> ( $\text{mmol L}^{-1}$ )	<b>16:2</b> molar ratio	<b>6:2</b> molar ratio	Recovered mass (%)	NMR			GC			
						F <sub>2a</sub>	F <sub>2c</sub>	F <sub>2</sub> <sup>a</sup>	F <sub>2a</sub>	F <sub>2b</sub>	F <sub>2c</sub>	F <sub>2</sub>
1	530, 1.5	97.3	1.7	1.7	70.9	85	15	0.0	91.2	0	8.8	1.2
2	530, 1.5	97.6	1.7	1.6	70.9	95.5	4.6	0.0	92.6	0	7.4	1.2
3	79, 10	96.6	1.1	1.1	-	100	0	25.2	98.9	0	1.1	25.9
4	79, 10	94.7	1.6	1.6	-	100	0	0.0	95.6	0	4.4	0.4
5	40, 20	47.3	1.0	1.0	84.5	100	0	41.8	99.6	0	0.4	39.8
6	40, 20	96.5	1.6	1.7	62.5	100	0	0.0	97.2	0	2.8	6.0
7	20, 40	90.7	1.7	1.7	69.3	100	0	18.3	100	0	0.0	20.9
8	8, 100	91.0	1.7	1.7	-	100	0	38.8	98.9	0	1.1	32.4

†syringic acid, **2**, methyl syringate, **2a**, syringic acid methyl ether, **2b**, dialkylated syringic acid, **2c**, iodomethane, **6**, TMGN, **16**, iodomethane, **6**.

### 6.2.1 Reaction kinetics Comparison in Batch and in Continuous

In order to explain our results in the previous section we have to open parenthesis in to the kinetics of syringic acid, **2**, alkylation in the presence of TMGN, **16**, or DBU, **21** by iodomethane, **6**. The kinetics studies were carried out in batch and in continuous mode. Both reactions follow second order kinetics and the main product is the ester and no ether was detected with none of the bases. Table 6-8 summarizes results for these experiments.

**Table 6-8 Rate constants of the reaction of syringic acid, **2**, and iodomethane, **6** at the presence of an organic base (TMGN, **16** and DBU, **21**) at various reagents combination**

Entry	Reagents Combination	Base	Concentration of <b>2</b> (mM)	Base: <b>2</b>	<b>6</b> : <b>2</b>	k/mol <sup>-1</sup> .L.s <sup>-1</sup>
1	[( <b>2</b> , base), <b>6</b> ]	<b>16</b>	21.6	1.1	1.0	1.49±0.6142
		<b>21</b>	21.5	1.0	1.0	0.2±0.0181
2	[( <b>2</b> , <b>6</b> ), base]	<b>16</b>	20.7	1.0	1.1	1.07±0.2437
		<b>21</b>	19.8	1.0	1.0	0.14±0.0289
3	batch	<b>16</b>	11.7	1.0	1.0	1.05±0.0278
		<b>21</b>	11.6	1.0	1.0	0.17±0.0178

It is observed in this table, with DBU, **21**, the reaction goes much slower than with TMGN, **16**. It was seen (section 3.2) that the rate of alkylation of DBU, **21** by iodomethane, **6** is roughly 2000 times greater than that of TMGN **16**. Here it is observed again that reagents combination and reaction mode (batch or continuous) have no major effect on the reaction rate. However, the reaction rate constant is slightly higher for the first reagents combination (entry 1) which is due to this point that diffusion coefficient of bases are less than that of iodomethane.

**Table 6-9 Rate constants of the reaction of methyl syringate, **2a**, and iodomethane, **6** at the presence of an organic base (TMGN, **16** and DBU, **21**).**

Reagents Combination	Base	Concentration of <b>2a</b> (mM)	Base: <b>2</b>	<b>6</b> : <b>2</b>	k/mol <sup>-1</sup> .L.s <sup>-1</sup>
[( <b>2a</b> , base), <b>6</b> ]	<b>16</b>	21.6	1.1	1.0	0.0457±0.0057
	<b>21</b>	21.5	1.0	1.0	0.0400±0.0096

In order to study chemical kinetics of the phenolic function of syringic acid, the kinetics studies were carried out on authentic methyl syringate, **2a**, in continuous mode in the presence of TMGN, **16** and DBU, **21**. Here again both reactions follow second order kinetics Table 6-9 summarizes results for these experiments. As it is seen in this table, the reaction rate constant ratio is surprisingly 1.0.

### 6.2.2 Protonation route

To answer to the question of why no ether is produced when TMGN, **16** is used as base; we have to look to its protonation by phenols. A simple search shows that this subject has not been extensively studied except [124].

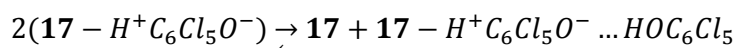
However, protonation of DMAN, **17** has been investigated comprehensively and it can be considered as a model for the proton sponges. Basicity of DMAN, **17** is due to sterically favorable arrangement of two basic centers so that an attached proton can be shared between the two nitrogen atoms, forming strong  $\text{NHN}^+$  hydrogen bridges [191]. This intramolecular hydrogen bond is also observed in our studies about protonation of TMGN, **16** by NMR method (Chapter 4). The high basicity of 'proton sponges' is combined with low rates of their protonation - deprotonation. The deprotonation rate constant for DMAN **17** in DMSO- $\text{H}_2\text{O}$  (v: v 3:7) is  $6.1 \times 10^5 \text{ mol}^{-1} \text{ L s}^{-1}$ . The low rates of cation deprotonation are mainly caused by the necessity of cleavage of the strong intramolecular hydrogen bond [192]. Another consequence of the strong hydrogen bond and rigid structure<sup>1</sup> of the monoprotonated ion of DMAN **17** is that diprotonation is exceptionally difficult. The second protonation of DMAN **17** is only half complete in 86% sulfuric acid and it is clear that the dication must be badly strained [193]. The second protonation of DBU **21** is possible in its complex with two equivalents of TFA [128].

Usually IR and NMR methods have been used to investigate the interaction of **17** with phenols. An unexpected finding is that phenol ( $\text{pK}_a=9.99$ ) hardly protonates "proton sponge", although its basicity exceeds that of the phenolate anion by more than two orders of magnitude. Distinct protonation is observed only with phenols having  $\text{pK}_a < 8.4$  [192]. This reaction gives two types of salts having composition of 1:1 and 1:2, the latter being

---

<sup>1</sup> The effect of the protonation on the structure of TMGN **16** has been discussed in chapter 4

much more stable [192]. The formation constant for 2:1 complexes is one order of magnitude higher than that for 1:1 complexes [194]. The protonation of DMAN **17** by phenols in polar solvents proceeds mainly with the participation of two phenol molecules [194] and the formation of homoconjugated anions, ArOH...<sup>-</sup>OAr [192]. In fact, DMAN **17** interacts with phenol derivatives to give the protonated base and homoconjugated (OHO)<sup>-</sup> anions and in several cases, complexes of higher stoichiometry are formed [195]. There is a competition between molecules of DMAN **17** and phenolate anions as proton acceptors. Even in the case of such a strong proton donor as pentachlorophenol both in acetonitrile and in 1, 2-dichloroethane the protonation takes place only to a limited extent if no excess of phenol is used for binding the phenolate anion into a homoconjugated species [194]. The salt of DMAN **17** with pentachlorophenol (1:1) disproportionate in acetonitrile to give a 1:2 salt and a non-protonated “proton sponge” [192]



These homoconjugated (OHO)<sup>-</sup> anions have been also observed in the case of TMGN, **16**, complex with pentachlorophenol. Przybylski, P., *et al.* [124] have found that in this case, an intramolecular hydrogen bond [N-H...N]<sup>+</sup> as well as intermolecular hydrogen bond [O...H...O]<sup>-</sup> are formed.

Brzezinski and Zundel [196] have studied the formation of hydrogen-bonded chains between a bicyclic guanidine base, MTBD **19** and phenols in acetonitrile. N<sup>+</sup>H...O<sup>-</sup> hydrogen bonds were observed for a mixture of MTBD **19** and *para*-cyanophenol (pK<sub>a</sub>=7.95) (1:1). These homoconjugated hydrogen bonds show large proton polarizability and with increasing the acidity of the phenols, these hydrogen bonds become more asymmetrical and these bonds dissociate more and more. The experimental results show

that there is a rough correlation between the degree of protonation and the  $pK_a$  of the proton donor [191, 194]. Toppet *et al* [191] have shown that percentage protonation of DMAN **17** by 3,5-dichlorophenol ( aqueous  $pK_a=8.04$  [197]) in dichloromethane is around 10% when molar ratio of phenol to base is 0.6. Huyskens *et al* [198] have demonstrated that using identical phenol-base molar ratio, in acetonitrile none of the molecules of 3,5-dichlorophenol are perturbed by one molecule of DMAN **17**.

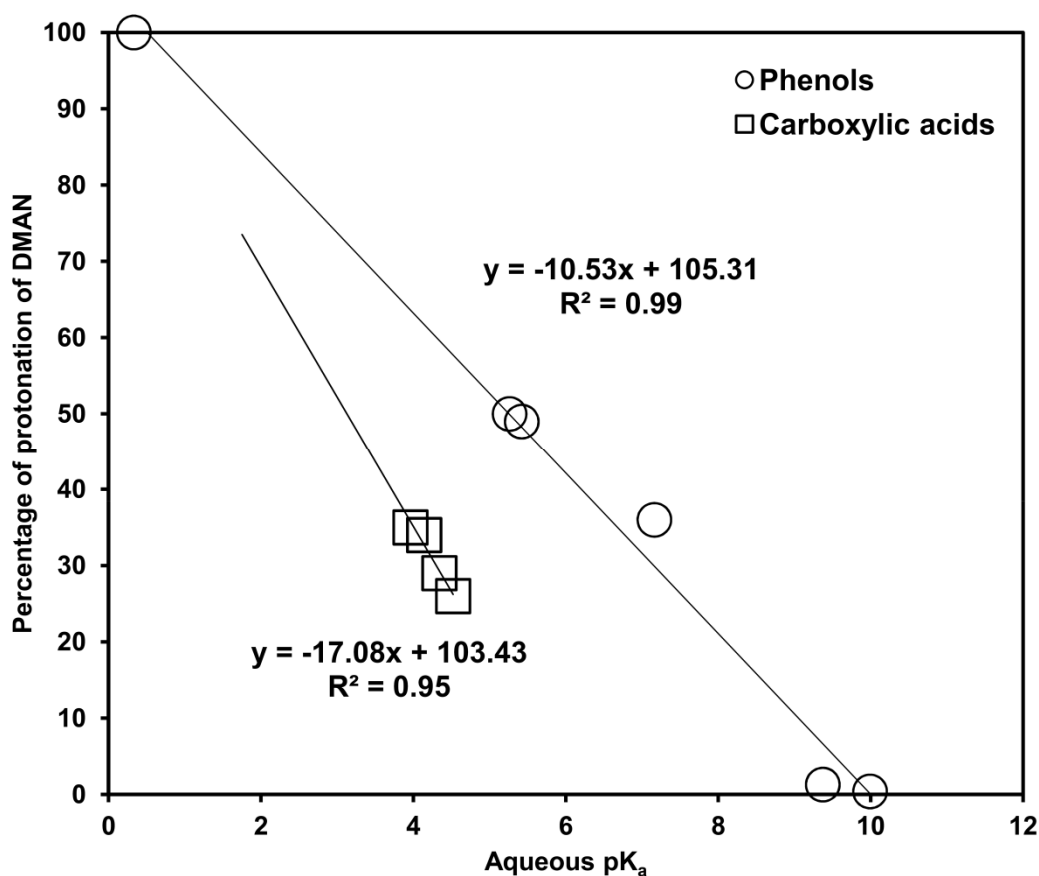


Figure 6-2 Percentage of protonation of DMAN,17 in 1:1 salt [194]

Brzezinski *et al* [194] have shown that by increasing  $pK_a$  of phenol and carboxylic acids, the percentage of protonation of DMAN **17** in 1:1 salt is decreased dramatically (Figure 6-2) Assuming that these figures hold also for TMGN **16**, we try now to estimate the protonation percentage in our experiments. Ionization constants for syringic acid **2** in

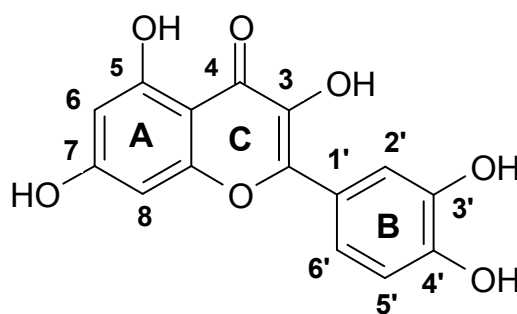
water are  $pK_{a1}=4.46$  for carboxyl group and  $pK_{a2}=9.33$  for phenolic one [188]. Therefore protonation of TMGN **16** will be less than 0.4 % by phenolic group and less than 29% by carboxyl group in 1:1 salt. Moreover aqueous  $pK_a$  of methyl syringate **2a** is 8.38 [199] and in this case again around 17% protonation of TMGN **16** will be expected in 1:1 salt. However, in these experiments the molar ratio of phenol to base is 0.6.



### 6.3 Quercetin

The structure of quercetin contains five hydroxyl functional groups that have the potential to be conjugated and that differ in their inherent chemical reactivities [174], with the following decreasing reactivity: OH-C(7)>OH-C(4') ~ OH-C(3)>OH-C(3')>>OH-C(5) [200]. The following bond dissociation enthalpy (BDE) sequence for quercetin OH groups has been reported [201]: OH-C(4') < OH-C(3') < OH-C(3) < OH-C(7) < OH-C(5). The values of aqueous macroscopic pKa as well as the values of individual BDE have been brought in Table 4-11. This clearly confirms that H-transfer from the B-ring (4'-OH and 3'-OH groups) is easier than from the A-ring (7-OH and 5-OH groups) [201]. However, the methylation rates of 7- and 4'-OH groups and 3- and 4'-OH groups do not differ sufficiently for a satisfactory selective methylation[202].

Table 6-10 Calculated values of the aqueous pKa and BDE for the different OH positions in quercetin



Hydroxyl group	Macroscopic aqueous pK <sub>a</sub> [203]	BDE (kcal mol <sup>-1</sup> )[201]
7-OH	7.04	88.6
4'-OH	8.55	74.6
5-OH	11.26	99.3
3-OH	13.06	83.7
3'-OH	-	77.0

Quercetin, **25**, alkylation by iodomethane, **6**, in the presence of an organic base in preparative scale experiments were carried out in batch and in continuous mode. The results are summarized in Tables 6-11 to 6-13. In these tables, F<sub>25</sub> is the weight percent of

quercetin **25** in the residue;  $W_{25a-c}$ ,  $W_{25d-f}$ ,  $W_{25g}$  and  $W_{25h}$  are weight percents of mono-, di-, tri- and tetramethyl quercetin in the residue;  $F_{25a}$ ,  $F_{25b}$  and  $F_{25c}$  are weight percents of 3-methyl quercetin **25a**, 4'-methyl quercetin **25b** and 7-methyl quercetin **25c** in monomethyl quercetins and  $F_{25d}$ ,  $F_{25e}$  and  $F_{25f}$  are weight percents of 3,4'-dimethyl quercetin **25d**, 3,7-dimethyl quercetin **25e** and 4',7-dimethyl quercetin **25f** in dimethyl quercetins.

Through these tables the following points have been emerged:

- i) Maximum conversion in batch mode has been obtained while using TMG **14** as base (entry 6, Table 6-11).
- ii) While using TMGN **16** as base, by increasing reaction time, conversion is increased by 12% majorly in favor of producing trimethyl quercetin **25g**, dimethyl quercetin **25d-f** and tetramethyl quercetin **25h** at the expense of monomethyl quercetin **25a-c** (entry 1 and 3 in Table 6-11). This demonstrates that during the reaction time monomethyl quercetins are converted to di- and polymethyl quercetins. However, by using a threefold excess of iodomethane, conversion is increased by 3% in slightly favor of only trimethyl quercetin **25g** and tetramethyl quercetin **25h** at the slight expense of dimethyl quercetin **25d-f** and of monomethyl quercetin **25a-c** (entry 1,2 in Table 6-11). During all of these changes, the mono- and dimethyl product distributions remain nearly constant.
- iii) The best selectivity of 3-methyl quercetin **25a** is seen while using DBU **21** as base.
- iv) With TMGN **16** as base in batch and continuous mode, selectivity is observed for 3,7-dimethyl quercetin **25e**.
- v) In continuous mode, while using TMGN **16** as base, minimum conversion has been obtained while mixing TMGN **16** and iodomethane **6** together in one syringe,

due to the alkylation of TMGN **16** by iodomethane **6**. However, mixing these two in a two-step process increases the conversion dramatically (entries 4 and 5 in Table 6-12). Moving to a two-step process has also a positive effect while the reagent combination is [(**25**, **6**), **16**] (entries 3 and 6 in Table 6-12).

- vi) Unlike the already reported [190], because of the alkylation of DBU **21** by iodomethane **6** (section 3.2), the third combination of [**2**, (**6**, **21**)] did not work. Moving to the two-step process, while keeping the same mixing strategy, was not at all selective either as already reported.
- vii) Here again, by using a threefold excess of iodomethane, conversion is increased by 15% in favor of trimethyl quercetin **25g**, dimethyl quercetin **25d-f** and tetramethyl quercetin **25h** at the expense of monomethyl quercetin **25a-c** (entry 1,2 in Table 6-12).
- viii) Comparing different mixing strategies, maximum conversion has obtained while the reagent combination of [(**25**, **16**), **6**]. Nevertheless, by increasing flowrate (decreasing residence time), conversion is decreased (entries 3 and 7 in Table 6-12).
- ix) Changing reagents molar ratio, number of steps and even reagents combination (except [(**25**, (**6**, **16**))]) do not have a major effect of the individual mono- and dimethyl quercetins.
- x) With DBU **21** as base, with up to eight times more of flowrate, conversion is decreased only by 20% (entries 1-6 in Table 6-13). However by changing the mixing strategy to [(**25**, **21**), **6**] conversion is increased up to 30% (entries 5, 7). Moving to a two-step process has a positive effect on conversion (entries 5, 8) but it has a negative effect on selectivity.

- xi) Experiments by two-pumps are not reproducible, probably due to the high difference between the powers of the two pumps which gives a back mixing toward the third syringe (entries 9, 10 in Table 6-13).
- xii) In two-step process by increasing the flowrate (decreasing the residence time) conversion is decreased which is not surprising (entries 11 and 13 in Table 6-13). Also by increasing the amount of iodomethane **6** conversion is decreased which is due to the high alkylation rate of DBU **21** by iodomethane **6** (entries 11 and 12 in Table 6-13).
- xiii) As illustrated in Table 6-13, changing the aforementioned parameters, does not have a significant effect on mono- and dimethyl quercetin individual distribution.

**Table 6-11** Batch mode experiments†, Concentration of **25**: 0.11 mmol L<sup>-1</sup>, Molar ratio of base: **25**=: 1.26 and of **6**:**25** = 1.26<sup>a</sup>

Entry	Base	Rxn time	F <sub>25</sub>	W <sub>25a-c</sub> (F <sub>25a</sub> , F <sub>25b</sub> , F <sub>25c</sub> )	W <sub>25d-f</sub> (F <sub>25d</sub> , F <sub>25e</sub> , F <sub>25f</sub> )	W <sub>25g</sub>	W <sub>25h</sub>
1	TMGN, <b>16</b>	4-5 h	6.3	22.1 (43.1,24.1,32.8)	36.6 (29.9,50.3,19.8)	33.4	1.7
2	TMGN, <b>16</b>	4-5 h	3.7	17.2 (43.5,24.2,32.3)	35.9 (30.3,50.4,19.2)	40.0	3.3
3	TMGN, <b>16</b>	9 min	18.8	39.2 (44.3,26.1,29.5)	30.6 (27.5,56.7,15.7)	11.2	0.4
4	DBU, <b>21</b>	9 min	23.1	48.4 (62.9,18.5,18.6)	24.3 (37.6,52.9,9.5)	4.2	0.0
5	DMAN, <b>17</b>	9 min	97.5	2.5 (48.9,18.2,32.9)	0	0	0
6	TMG, <b>14</b>	9 min	17.1	42.0 (53.5,22.9,23.6)	31.2 (31.9,53.8,14.3)	9.3	0.3

a. These ratios for entry 2 are 1.4 and 3.42 respectively.

† Quercetin, **25**, 3-monomethyl quercetin, **25a**, 4'-monomethyl quercetin, **25b**, 7-monomethyl quercetin, **25c**, 3,4'-dimethyl quercetin, **25d**, 3,7-dimethyl quercetin, **25e**, 4',7-dimethyl quercetin, **25f**, 3,4',7-trimethyl quercetin, **25g** and 3,3',4',7-tetramethyl quercetin, **25h**.

**Table 6-12 Continuous mode experiments†; Concentration of 25: 0.11 mmol L<sup>-1</sup>, Molar ratio of 16: 25= 1.27 and of 6:25 = 1.26; Micromixer: Nanomixer**

Entry	Flowrate (μL min <sup>-1</sup> )	Reagents combination	F <sub>25</sub>	W <sub>25a-c</sub> (F <sub>25a</sub> , F <sub>25b</sub> , F <sub>25c</sub> )	W <sub>25d-f</sub> (F <sub>25d</sub> , F <sub>25e</sub> , F <sub>25f</sub> )	W <sub>25g</sub>	W <sub>25h</sub>
1	1.5	[(25,16),6] <sup>a</sup>	11.4	30.8 (45.3,25.1,29.6)	35.6 (29.4,54.4,16.2)	21.3	0.9
2	1.5	[(25,16),6]	27.5	39.9 (46.1,24.1,29.9)	24.4 (27.7,57.3,15.0)	7.9	0.2
3	1.5	[(25,6),16]	34.9	37.2 (48.0,24.9,27.1)	20.3 (26.4,60.0,13.6)	7.4	0.2
4	1.5	[25,(6,16)]	72.5	6.8 (63.6,17.7,18.7)	5.2 (28.5,62.9,8.6)	10.2	5.3
5	2.25	[25,(6,16)] <sup>b</sup>	46.0	31.3 (41.0,25.7,33.3)	15.5 (25.4,60.1,14.5)	6.6	0.5
6	2.25	[(25,6),16] <sup>b</sup>	31.1	31.7 (44.7,24.9,30.4)	18.8 (25.5,61.2,13.4)	15.8	2.6
7	5	[(25,16),6]	55.6	31.1 (48.8,23.3, 28.0)	9.7 (27.6,57.2,15.2)	3.6	0.0

a. 16:25 molar ratio=1.39, 6:25 molar ratio=3.42

b. Two- step

† Quercetin, **25**, 3-monomethyl quercetin, **25a**, 4'-monomethyl quercetin, **25b**, 7-monomethyl quercetin, **25c**, 3,4'-dimethyl quercetin, **25d**, 3,7-dimethyl quercetin, **25e**, 4',7-dimethyl quercetin, **25f**, 3,4',7-trimethyl quercetin, **25g** and 3,3',4',7-tetramethyl quercetin, **25h**.

**Table 6-13 Continuous mode experiments†; Concentration of 25: 0.11 mmol L<sup>-1</sup>, Molar ratio of 21: 25= 1.27 and of 6:25 = 1.26; Micromixer: Nanomixer**

Entry	Flowrate ( $\mu\text{L min}^{-1}$ )	Reagents combination	F <sub>25</sub>	W <sub>25a-c</sub> (F <sub>25a</sub> , F <sub>25b</sub> , F <sub>25c</sub> )	W <sub>25d-f</sub> (F <sub>25d</sub> , F <sub>25e</sub> , F <sub>25f</sub> )	W <sub>25g</sub>	W <sub>25h</sub>
1	8.5	[(25,6),21]	68.5	28.6 (67.0,17.6,15.3)	2.9 (41.9,58.1,0.0)	0.0	0.0
2	5	[(25,6),21]	60.4	34.2 (66.4,17.2,16.3)	5.0 (36.7,52.3,11.0)	0.4	0.0
3	3	[(25,6),21]	58.3	34.5 (69.4,15.3,15.3)	6.5 (38.5,48.5,12.9)	0.7	0.0
4	2	[(25,6),21]	51.0	39.0 (65.8,16.1,18.0)	9.1 (37.4,53.0,9.6)	0.9	0.0
5	1.5	[(25,6),21]	50.1	38.6 (67.1,16.4,16.6)	10.2 (40.4,50.5,9.1)	1.2	0.0
6	1	[(25,6),21]	48.8	37.9 (62.5,17.2,20.4)	11.7 (34.5,51.6,13.8)	1.6	0.0
7	1.5	[(25,21),6]	20.2	48.8 (52.6,23.2,24.2)	25.9 (34.6,49.8,15.6)	4.9	0.1
8	2.25	[(25,6),21] <sup>a,b</sup>	41.5	37.3 (67.5,16.2,16.3)	16.1 (45.3,46.5,8.3)	4.6	0.5
9	2.25	[(21,6),25] <sup>a,b</sup>	78.3	13.8 (68.3,15.9,15.8)	5.7 (46.4,46.2,7.4)	1.9	0.3
10	2.25	[(21,6),25] <sup>a,b</sup>	64.6	27.9 (63.4,18.2,18.4)	6.0 (38.4,49.1,12.5)	1.4	0.0
11	2.25	[(21,6),25] <sup>a</sup>	55.1	37.6 (60.0,18.2,21.7)	5.8 (38.1,50.8,11.1)	1.3	0.2
12	2.25	[(21,6),25] <sup>a,c</sup>	80.6	16.6 (55.4,18.5,26.1)	2.0 (34.9,49.1,16.0)	0.8	0.0
13	7.5	[(21,6),25] <sup>a</sup>	70.8	26.3 (63.6,17.6,18.8)	2.6 (34.3,55.0,10.7)	0.2	0.0

a. Two- step

b. using two pumps

c. 6:25 molar ratio=2.52

† Quercetin, **25**, 3-monomethyl quercetin, **25a**, 4'-monomethyl quercetin, **25b**, 7-monomethyl quercetin, **25c**, 3,4'-dimethyl quercetin, **25d**, 3,7-dimethyl quercetin, **25e**, 4',7-dimethyl quercetin, **25f**, 3,4',7-trimethyl quercetin, **25g** and 3,3',4',7-tetramethyl quercetin, **25h**.

## 6.4 Clofibric acid

Clofibric acid alkylation by iodomethane in the presence of TMGN, **16**, in preparative scale experiments were carried out in continuous mode. Figure 6-3 presents the reaction scheme

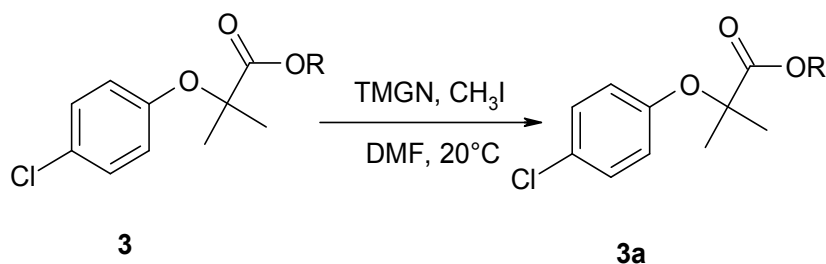


Figure 6-3 Clofibric acid alkylation by iodomethane

Table 6-14 Alkylation of clofibric acid<sup>†</sup>, Micromixer: NanoMixer<sup>®</sup>. Reagents combination: [(3,16),6].

Entry	Flowrate ( $\mu\text{L min}^{-1}$ )	Concentration of <b>3</b> ( $\text{mmol L}^{-1}$ )	<b>16:3</b> molar ratio	<b>6:3</b> molar ratio	Recovered mass (%)	F <sub>3a</sub>
1	5	115.1	1.3	1.3	18.9 <sup>a</sup>	100
2	5	115.1	1.3	1.3	10.1	88-100
3	5	114.5	1.3	1.3	26.3	100
4	10	109.3	1.0	1.0	-	70
5	10	101.8	1.0	1.0	-	56

a. After washing filtrate of the first extraction with diethyl ether ( $3 \times 30 \text{ cm}^3$ ) and adding the obtained mass to the previous one, the total recovered mass was increased to 89.8%. However the NMR analysis shows that the obtained mass is totally comprised of **3**

<sup>†</sup> Clofibric acid methyl ester, **3a**, iodomethane, **6**, TMGN, **16**.

The results are presented in Table 6-14. The value of  $\text{pK}_a$  for clofibric acid in acetonitrile using the equation proposed by Canbay *et al* [204] is 7.0. Therefore TMGN can strip away the acid proton totally. Despite it, the conversion and the yield are low. The most important feature of clofibric resistance to deprotonation can be due to steric hindrance from two

methyl groups adjacent to carboxylic acid function. The presence of these two methyl groups even makes it resistant to microbial degradation [205].

While obtaining a pure product, the recovered mass is low. The value of Log P for clofibric acid is 2.57 [206]. This value is relatively low. Zhang *et al* [206] have shown that 1-octanol is a better solvent for clofibric acid extraction from water.



## 6.5 Trolox

Trolox alkylation by iodomethane in the presence of TMGN, **16**, in preparative scale experiments were carried out in continuous mode. Figure 6-4 presents the reaction scheme and the results are summarized in Table 6-15.

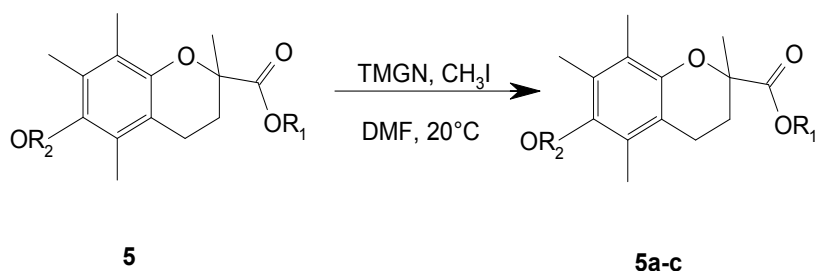


Figure 6-4 Trolox alkylation by iodomethane

The obtained product is trolox methyl ester **5a** and other expectable products are absent here. The aqueous acidic and phenolic pK<sub>a</sub> values of Trolox are 4.4 and 11.9 respectively [207]. Using the equation proposed by Chmurzyński [208] the value of phenolic pK<sub>a</sub> in DMF is estimated to be around 19.0, which is far beyond the pK<sub>a</sub> value of TMGN in DMF. As it is observed, changing the temperature or quenching medium does not have a significant effect on F<sub>5a</sub>.

Table 6-15 Alkylation of Trolox<sup>†</sup>, Micromixer: NanoMixer<sup>®</sup>. Reagents combination: [(5, 16), 6].

Entry	Flowrate (μL min <sup>-1</sup> )	Concentration of <b>5</b> (mmol L <sup>-1</sup> )	<b>16:5</b> molar ratio	<b>6:5</b> molar ratio	Recovered mass (%)	F <sub>5a</sub>
1	10	110.4	1.0	1.0	-	100
2	10	111.0	1.0	1.1	75	90 <sup>a</sup>
3	10	113.2	1.1	1.1	74	93 <sup>a,b</sup>
4	10	113.3	1.3	1.3	-	90
5	5	113.7	1.3	1.3	81.5	100

a. Temperature: 30°C,

b. Quenched in a solution of methanol and formic acid (v/v, 10:1)

† Trolox<sup>®</sup> methyl ester, **5a**, iodomethane, **6**, TMGN, **16**

## 6.6 Podocarpic acid

Podocarpic acid alkylation by iodomethane in the presence of TMGN, **16**, in preparative scale experiments were carried out in continuous mode. Podocarpic acid ionization constant for its carboxylic acid function was estimated to be in the range of the  $pK_a$  of dimethylpropanoic acid (aqueous  $pK_a = 5.03$ [209]) and for its phenolic function was approximated by the  $pK_a$  of 3,4-dimethyl phenol ( aqueous  $pK_a = 10.36$ [210]). Using the equation proposed by [208] to correlate the aqueous  $pK_a$  to that of in DMF,  $pK_a$  values in DMF for podocarpic acid are roughly estimated to be  $pK_{a1} = 8.6$  and  $pK_{a2} = 16.9$ . Recalling  $pK_a$  of TMGN, **16**, in DMF is in the range of 16.5-17.5, therefore TMGN is able to effectively remove podocarpic acid acidic hydrogen but not its phenolic hydrogen.

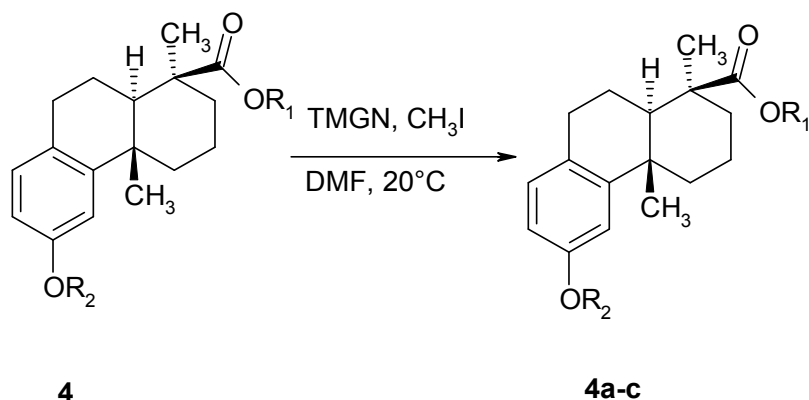


Figure 6-5 Podocarpic acid alkylation by iodomethane

Table 6-16 Alkylation of podocarpic acid<sup>†</sup>, Micromixer: NanoMixer<sup>®</sup>. Reagents combination: [(**4**), **16**], **6**].

Entry	Flowrate ( $\mu\text{L min}^{-1}$ )	Concentration of <b>4</b> ( $\text{mmol L}^{-1}$ )	<b>16:4</b> molar ratio	<b>6:4</b> molar ratio	Recovered mass (%)	$F_{4a}$
1	10	114.1	1.1	1.1	-	74
2	5	114.5	1.1	1.1	71.2	88
3	Batch (1 hr)	114.3	1.1	1.1	87.1	100

<sup>†</sup> Podocarpic acid methyl ester, **4a**, iodomethane, **6**, TMGN, **16**.

Figure 6-5 presents the reaction scheme and the results are summarized in Table 6-16. The obtained product is only **4a** and other expectable products are absent here. Shaw and Kunerth [55] reported a quantitative yield of **4c** for the reaction of podocarpic acid, **4**, with sodium hydroxide and methyl iodide in HMPA. The deprotonation and alkylation time were 0.5 h and 7 h. Therefore, an experiment in batch with the reaction time of one hour was carried out but again **4b** and **4c** were not observed.

## 7 METHODOLOGY

### 7.1 Micromixers

Mixing is a transport process for species, temperature and phases to reduce inhomogeneity. Mixing leads to secondary effects such as reaction and change in properties [20]. There are three established terminology for mixing in conventional macroscale mixing techniques; Macromixing is concerned with mixing on a macroscopic scale [211]. It is governed by mechanical stirring [211] and refers to the overall mixing performance in a reactor [212]. Micromixing is concerned with contact and mixing on a molecular scale [211]. It comprises the viscous-convective deformation of fluid elements, followed and dominated by molecular diffusion [211-212]. Mesomixing is in the scale between macromixing and micromixing [20]. Micromixing is normally the much slower process [213]. The process of mixing is classified as: Passive mixing, where the interfaces between the substances being mixed follow the flow and have no back effect on it [214]. In active mixing processes, the interfaces between the substances being mixed interact with the flow and modify it [214]. Therefore, mixing devices are classified as: Passive (static, in-line) mixers; they have no moving parts and achieve mixing by virtue of their topology alone. Mixing in passive micromixers is induced by lamination, injection, chaotic advection or droplet. In case of lamination; it can be achieved in two ways, parallel lamination and serial (sequential) lamination. In parallel lamination, the inlet streams are split into several substreams, and then are joined altogether into one stream [215]. Sequential (serial) lamination segregates the joined stream into two channels, and rejoins them in the next transformation stage. Injection-based micromixers, split only one flow into many streams and inject them into the solvent flow [215]. In droplet-type of micromixers, for reducing the mixing path, the droplets of mixed liquids is formed.

Active mixers, they have either moving parts (rotor-stator) or they use externally applied forcing functions such as pressure or electromagnetic fields. Lack of moving parts, makes passive mixers free of additional friction and wear effects. But their complicated topology is often hard to fabricate. Also they cannot be controlled externally [214].

As micromixer we used four passive micromixers; a multilaminating distributive micromixer chip (NanoMixer®, Upchurch), a Y configuration microreactor (Micronit), a MicroTee junction (Upchurch) and a Y connector (Upchurch).

The NanoMixer® consists of two inlets (A and B), the microchannel cascades, and one outlet, which operate in co-current flow mode. The layout of the micromixer is based on the principle of distributive mixing. The microchip is made up from a glass/silicon/glass sandwich. On the silicon wafer, the inlet channel of liquid A is split into 16 partial flows. This is achieved by repeated splitting of the channels in such a way that an array of symmetrical elements results. On the backside of the silicon wafer (layer 2), liquid B is split into the same number of partial flows by an identical arrangement. In order to bring the two liquids together, liquid B is introduced to layer 1 via a number of wafer-through nozzles. Coming out of a nozzle, liquid B is allowed to develop into the full vertical height of the channel before it enters a channel with liquid A. Sequentially combining two neighboring channels into one is repeated until all partial flows are united in one broad outlet channel.

Y configuration microreactor (Micronit) has two inlets and one outlet. Two fluids can be injected separately and will mix by diffusion, without turbulence. It is made of borosilicate glass and has a volume of 13 $\mu$ L.

MicroTee and Y connector are made of chemically compatible PEEK® polymer and have very low swept volumes.

Mixing time ( $t_m$ ) of these micromixers was calculated by measuring the pressure drop ( $\Delta P$ ) in them and calculating the energy dissipation ( $\varepsilon$ ):

$$\varepsilon = \frac{Q \Delta P}{\rho V} \quad (7-1)$$

$$t_m = 0.15\varepsilon^{-0.45} \quad (7-2)$$

In these equations Q, V and  $\rho$  are flow rate, micro mixer volume and fluid density respectively. Pressure drop was measured using a Knauer Smartline pump 100, equipped with a pressure sensor. The results have been listed in Table 7-1.

**Table 7-1 mixing time measurement for different applied micromixers**

Micromixer	V (nL)	Q (ml.min <sup>-1</sup> )	$\Delta P$ (Mpa)	$\varepsilon \times 10^{-4}$ (W.kg <sup>-1</sup> )	$t_m \times 10^4$ (s)
Y Connector	17	0.3	4.6	135	2.61
		0.2	3.5	68.6	3.55
		0.1	1.7	16.7	6.70
MicroTee	29	0.3	4.4	75.9	3.39
		0.2	2.9	33.3	4.91
		0.1	1.5	8.62	9.02
Nanomixer	60	0.05	4.5	6.25	10.4

## 7.2 Kinetics study experiments

We used a set-up (Figs.7-1 and 7-2) composed of two streams of reagents solution in DMF simultaneously delivered, by a high pressure syringe pump, to a micromixer followed by a fused silica-based capillary tubular reactor. As micromixer, we utilized a multilaminating distributive micromixer chip (NanoMixer®, Upchurch).

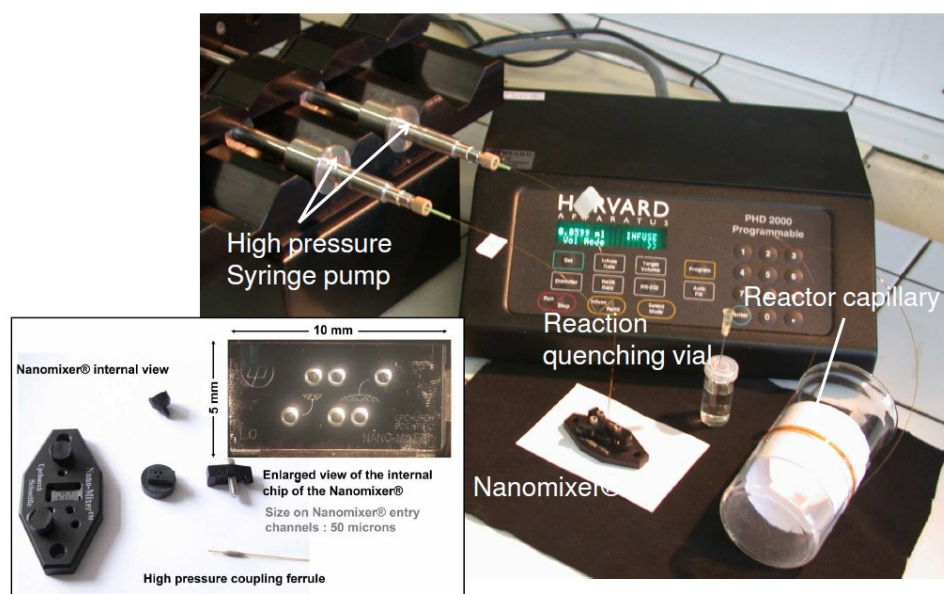


Figure 7-1. Experimental set-up and layout of NanoMixer®

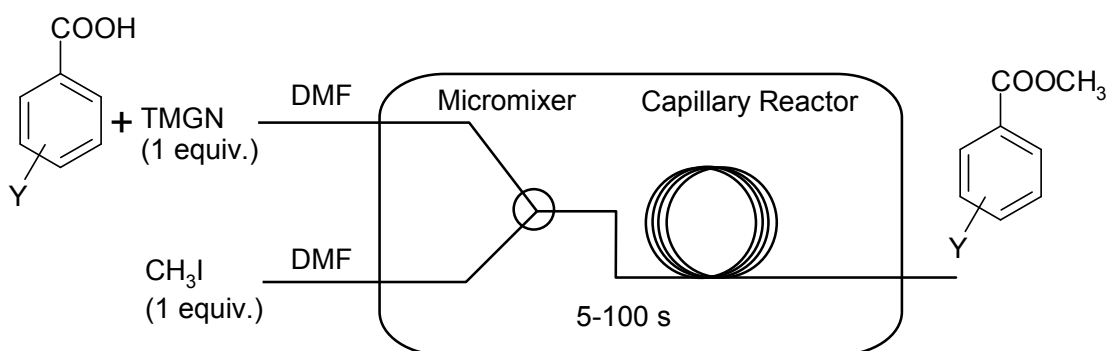


Figure 7-2. Schematic diagram of the experimental set-up. It comprises of a micromixer and a fused silica-based capillary tubular reactor. The two syringes, containing reagents are connected via 30cm capillaries (ID: 50µm) to the micromixer. The micromixer is followed to a 300cm fused silica-based capillary tubular reactor (ID: 75µm). The capillary reactor is kept at 20°C in a water bath.

The high pressure syringe pump (PHD 22/2000 Hpsi) was a product of Harvard Apparatus (Les Ulis, France). Capillary tubes were purchased from Polymicro Technologies. Capillary reactor internal diameter and length were 75  $\mu\text{m}$  and 300 cm respectively. Capillaries with the internal diameter of 50  $\mu\text{m}$  were employed as inlets to stop backward flow. In order to provide heating (70°C) or cooling (4°C) the capillary tubular reactor was immersed in a water bath equipped by thermostat or an ice/water bath.

To control the system performance, two internal standards, 1,3,5-trimethoxybenzene(TMB) and 1,4-dimethoxybenzene (DMB), were dissolved in reagents inlet streams. 4-Iodoanisole is another internal standard which was added to the samples, just before being analyzed by GC.

Table 7-2 displays different flow rates and their corresponding residence time and Tables 9-6 and 9-7 (Appendix D) display the results as well as the statistical analysis for a typical experiment.

For different flow rates, 240  $\mu\text{L}$  sample of reaction medium was collected at the outlet of the tubular reactor and quenched in a mixture of 400  $\mu\text{L}$  of dichloromethane and 50  $\mu\text{L}$  of formic acid. For each flow rate, two samples were taken directly and analyzed independently. A volume of 30  $\mu\text{L}$  of the taken sample was diluted by 400  $\mu\text{L}$  of iodoanisole in dichloromethane solution. This sample, was later derivatized by 50  $\mu\text{L}$  of BSTFA and 20  $\mu\text{L}$  of pyridine and was kept overnight for GC-MS analysis.

**Table 7-2 Flowrates used in kinetics studies and their corresponding residence times**

Flowrate ( $\mu\text{L}\cdot\text{min}^{-1}$ )	150	75	37.5	18.75	12.5	9.375	7.5
Residence time (s)	5.3	10.6	21.2	42.4	63.6	84.8	106



Batch kinetics studies were conducted in a 10ml vial or a beaker containing a certain volume solution comprised of acid and base in DMF. To begin the reaction, a stoichiometric volume of alkylating agent was injected as rapidly as possible. During the experiments samples of 240  $\mu\text{L}$  volume, were withdrawn at different times and were quenched. Quenching medium, dilution and derivatization, as well as the analysis method, are exactly those that were applied in continuous method.

### **7.2.1 Analysis method: GC-MS**

All samples were analyzed on a Thermo Finnigan® TRACE GC Ultra gas chromatograph equipped with a split/splitless injector, a Thermo Finnigan® AS3000 Variable-volume autosampler and a Thermo Finnigan® PolarisQ mass spectrometer. Thermo Finnigan® Xcalibur® software was used to control the instrument and analyze data. Separations were accomplished using a 60 m, 0.25mm i.d., 0.50 $\mu\text{m}$  film thickness Rxi®-5ms column (Crossbond® 5% diphenyl/95% dimethyl polysiloxane; Restek). Liquid injections of 1 $\mu\text{L}$  were introduced into a 250 °C injector with a 50:1 split ratio and a mobile phase (Helium) flow rate of 1 mL/min. Unless otherwise noted, all separations were performed using the a linear temperature program 50 °C, 10 °C/min to 250 °C, 250 °C for 10 min. The mass selective detector was scanned from 40 to 400 (m/z).

### **7.3 Base-MeI stability study experiments**

The principal of operation and set-up is similar to that of the previous experiment (described in section 7.2). The only difference was that here, we did not used the internal standards. We ran several preliminary tests for each compound to find the best micromixer, capillary size and residence time range. Table 7-3 displays different flow rates and their corresponding residence time for different bases. As micromixer, for all bases except TMGN **16** and BEMP **23**, we utilized a multilaminating distributive micromixer chip

(NanoMixer®, Upchurch) and capillary reactor internal diameter and length were 75  $\mu\text{m}$  and 300 cm respectively. To do the kinetics studies for TMGN **16** and BEMP **23** we used a MicroTee and we employed a capillary reactor size of 200  $\mu\text{m}$  and 400 cm.

For different flow rates, 40  $\mu\text{L}$  (10  $\mu\text{L}$  for TMGN, **16**, DMAN, **17**, and BEMP, **23**, 100  $\mu\text{L}$  for DABCO, **22**, and P2Et, **24**) sample of reaction medium was collected at the outlet of the tubular reactor and quenched in 1000  $\mu\text{L}$  methanol:water:trifluoroacetic acid (50:50:0.1, v/v/v). A volume of 20  $\mu\text{L}$  (100  $\mu\text{L}$  for DABCO, **22**, and P2Et, **24**) of the taken sample was diluted again to 1000  $\mu\text{L}$  (500  $\mu\text{L}$  for TMGN, **16**, and BEMP, **23**) of methanol:water:trifluoroacetic acid (50:50:0.1, v/v/v). This sample was later analyzed by mass spectrometry.

**Table 7-3 Flowrates used in base-Mel stability study experiments and their corresponding residence times**

Capillary size 75 $\mu\text{m}$ and 300 cm,		Capillary size 75 $\mu\text{m}$ and 300 cm, for <b>22</b> and <b>24</b>		Capillary size 200 $\mu\text{m}$ and 400 cm, for <b>16</b> and <b>23</b>	
Flowrate ( $\mu\text{L. min}^{-1}$ )	Time(s)	Flowrate ( $\mu\text{L. min}^{-1}$ )	Time (s)	Flowrate ( $\mu\text{L. min}^{-1}$ )	Time(s)
7.948	100	79.48	10	1.047	7200
8.832	90	88.32	9	1.142	6600
9.936	80	99.36	8	1.26	6000
11.35	70	113.5	7	1.396	5400
13.25	60	132.5	6	1.571	4800
15.90	50	159.0	5	1.795	4200
19.87	40	198.7	4	2.094	3600
26.50	30	265.0	3	2.513	3000
39.74	20	397.4	2	3.142	2400
79.48	10			4.188	1800
				6.283	1200
				12.566	600
				75.398	100

### 7.3.1 Analysis method: Mass spectrometry

The electrospray and tandem mass spectra were recorded on a Micromass Quattro II triple quadrupole mass spectrometer (Micromass, France) equipped with an ESI source. Nitrogen was used as the nebulizing and drying gas at flow rates of 10-15 and 250-300  $\text{L h}^{-1}$

respectively. The samples were infused into the ESI source by using a Harvard apparatus Biomedical Dispensing system syringe pump at the flow rate of 0.5 mL hr<sup>-1</sup>. The ESI source potentials were: Capillary 3.5 kV and cone at 25 V. The mass spectrometer scan time was fixed at 4.00 seconds and mass scan range was set depending to the component mass. Data acquisition and processing were carried out using Mass Lynx 4.0 software supplied with the instrument. Data acquisition was conducted in the multichannel analyzer (MCA) mode and the spectra were accumulated over ten scans.

## 7.4 Preparative-scale experiments

The same set-up and the same procedure as the continuous kinetics experiments were followed. But the flow rate was kept constant all over the experiment. Table 7-4 displays different flow rates and their corresponding residence time.

Table 7-4 Flowrates used in preparative-scale experiments and their corresponding residence times

Flowrate ( $\mu\text{L}\cdot\text{min}^{-1}$ )	100	40	20	10	5	1.5
Residence time (s)	8	20	40	79	159	530

The reactor output was entirely collected in a quenching medium containing 100 ml of dionized water and 10 ml of formic acid. At the end of the reaction(except for **25**), the aqueous solution was washed with dichloromethane ( $3 \times 30 \text{ cm}^3$ ), acidified and extracted with hydrochloric acid  $1 \text{ mol L}^{-1}$  ( $3 \times 30 \text{ cm}^3$ ). The extract was dried over  $\text{MgSO}_4$ , filtered through Whatman No. 1 filter paper, evaporated *in vacuo* and kept overnight at 60-70 °C. The total amount of the residue was dissolved in NMR solvent ( $\text{DMSO-}d_6$ ) and was analyzed through its  $^{13}\text{C}$  NMR spectra.

To do further investigation, for syringic acid, **2**, 30  $\mu\text{L}$  of this NMR sample was diluted to 400  $\mu\text{L}$  of dichloromethane and silylated and analyzed by GC/MS as described before (Section 7.2.1). Batch kinetics studies were conducted in a 10ml vial or a beaker containing a certain volume solution comprised of acid and base in DMF. To begin the reaction, a stoichiometric volume of alkylating agent was injected as rapidly as possible and at the end of the reaction all the compounds were transferred to a flask containing quenching medium. Quenching medium, extraction procedure, as well as the analysis method, are exactly those that were applied in continuous method.

#### 7.4.1 Extraction evaluation test

Using authentic compounds, the extraction procedure was evaluated. For this, 0.2002 gr of syringic acid, **2**, was mixed with 0.2138 gr of methyl syringate, **2a**, and 0.2121 gr of syringic acid methyl ether, **2b**. This mixture was entirely dissolved in the quenching medium containing 100 ml of dionized water and 10 ml of formic acid and further extracted with dichloromethane ( $3 \times 30 \text{ cm}^3$ ), and with water ( $3 \times 10 \text{ cm}^3$ ). The extract was dried over  $\text{MgSO}_4$ , filtered through Whatman No. 1 filter paper, evaporated *in vacuo* and kept overnight at 60-70 °C. The total amount of the recovered mass was 93% of the initial mass.

#### 7.4.2 Two-Step process

For Quercetin, **25**, some experiments were carried out in a two-step process, using two pumps or one pump (Figure 7-3). The inlets of the first micromixer are connected to the first syringe pump which is high pressure syringe pump (multiple syringe, PHD 22/2000 Hpsi, Harvard Apparatus, Les Ulis, France).

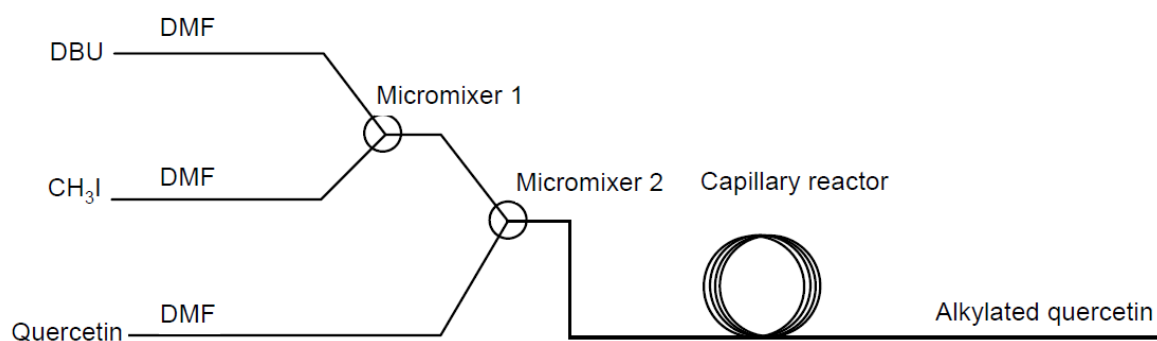


Figure 7-3 Schematic diagram of the experimental two step set-up. It comprises of two micromixers and a fused silica-based capillary tubular reactor. The three syringes, containing reagents are connected via 30cm capillaries (ID: 50µm) to the micromixer. Micromixer1 is followed to a 25 cm fused silica-based capillary tubular reactor (ID: 50µm) and then to Micromixer 2. The capillary reactor (3m, 75µm) is kept at 20°C in a water bath

The first inlet of the second micromixer is fed from the first stage outlet. The third reagent is delivered to the second inlet of the second micromixer either by a second syringe pump (double syringe, PHD 22/2000 Advance Syringe Pump, Harvard Apparatus, Les Ulis, France) or by using another syringe drive of the first syringe pump. Micromixer 1 and 2 were Nanomixer® and MicroTee respectively. Table 7-5 displays different flow rates and their corresponding residence time in quercetin experiments (one step and two-step).

**Table 7-5 Flowrates used in preparative-scale experiments (Quercetin) and their corresponding residence times**

Flowrate ( $\mu\text{L}\cdot\text{min}^{-1}$ )	1	1.5	2	2.25	3	5	7.5	8.5
Residence time (s)	795	530	397	353	265	159	106	94

The reactor output was entirely collected in a quenching medium containing 100 ml of dionized water and 10 ml of formic acid. At the end of the reaction, the aqueous solution was washed with ethyl acetate until no further color was detectable visually. The organic layer was then acidified and extracted with hydrochloric acid  $1\text{ mol L}^{-1}$  ( $1 \times 30\text{ cm}^3$ ). The extract was dried over  $\text{MgSO}_4$ , filtered through Whatman No. 1 filter paper, evaporated *in vacuo* and kept overnight at 60-70 °C. The total amount of the residue was dissolved in NMR solvent ( $\text{DMSO-}d_6$ ) and was analyzed through its  $^{13}\text{C}$  NMR spectrum. For some experiments the step of drying over  $\text{MgSO}_4$  was skipped.

To prepare a sample for a LC-MS analysis, 25  $\mu\text{L}$  of NMR sample was diluted in 1ml acetonitrile/0.1 % (v/v) formic acid in water (50:50). 10  $\mu\text{L}$  of this sample was then further diluted to 500  $\mu\text{L}$  acetonitrile/0.1 % (v/v) formic acid in water (50:50) to make a suitable concentration for LC-MS analysis.

#### 7.4.3 Analysis method: NMR

All NMR spectroscopy was conducted at 7 Tesla, using a Bruker Avance 300 spectrometer (Wissembourg, France) with TOPSPIN software (version 2.1) for data acquisition and processing.  $^{13}\text{C}$  NMR spectra were recorded in DMSO-*d*<sub>6</sub> at 25°C, with the sample spinning at 20 Hz for one-dimensional experiments. Both  $^1\text{H}$  and  $^{13}\text{C}$  chemical shifts were referenced to internal tetramethylsilane (TMS), chemical shifts are given in  $\delta$  (ppm) and coupling constants in Hz.

#### 7.4.4 Analysis method: LC-MS

Samples were analyzed by LC-MS using a Hewlett Packard Model 1100 liquid chromatography (Palo Alto, USA) coupled to a Quattro II tandem quadrupole mass spectrometer (Micromass, Manchester, UK) fitted with an electrospray ionization source (ESI) and equipped with a Micromass MassLynx data system. Separation were achieved on a C18 HPLC column (250  $\times$  20 mm, 5  $\mu\text{m}$ ) (Intechim, Montluçon, France) with a QS-guard C18 guard column (10  $\times$  20 mm) (Interchim) at 25°C. The mobile phase consisted of (A) 0.5 % formic acid in water and (B) 0.5% formic acid in acetonitrile at a flowrate of 150  $\mu\text{L min}^{-1}$ . The percentage of solvent B was increased linearly from 10 to 50% in 30 min and then from 50 to 90% in 10 min. The injected volume was 10  $\mu\text{L}$ . The column was re-equilibrated following each injection by 10% solvent B for 13 min.

The column eluent was first directed to a UV detector set at 280 nm and then without splitting to a pneumatically assisted ESI interface operating with a capillary voltage of 3.17 kV and temperature at 120°C. The cone voltage was maintained at 30V. Nitrogen was used as nebulization and drying gas at flowrates of 10-15 and 250-300 L  $\text{hr}^{-1}$  respectively. The mass spectrum was acquired from  $m/z$  200 to 400 with scan duration of 1.5 s.

## 8 CONCLUSION

A microchemical device was developed to study the kinetics of the reaction in continuous flow mode and the results were compared to that of batch mode. The model reaction was base catalyzed benzoic acid alkylation by iodomethane. An organic superbases, TMGN was used as the base.

This reaction follows a second order kinetics. Additionally it was determined that the reagents combination as long as mixing iodomethane and TMGN is avoided, does not have a remarkable effect on reaction kinetics. The set-up enabled also the study of the effect of temperature on this reaction. The large negative entropy of activation indicates that the transition state in DMF has a relatively specific structure and is more strongly solvated than the initial neutral state. The values of the enthalpy of activation indicate that the process is endothermic. The rate constants were determined for the reaction between some different alkylating agents and benzoic acid and also in different solvents. To investigate the origin of substituent effects on the reactivity of benzoic acids, the alkylation kinetics of a series of *para*-substituted benzoic acids was also studied. Their reactivities are correlated with a slope of -0.65 (Hammett reaction constant). This indicates a decrease in electron density at the reaction site. With this system, the kinetics of syringic acid alkylation in the identical conditions was also studied. Syringic acid is a phenol acid but the reaction proceeds quantitatively to ester product.

Guided by the observed side reaction in the first section (TMGN alkylation by iodomethane), the microreactor system was used to investigate the kinetics of several organic superbases alkylation by iodomethane. These organic superbases are of guanidine-type, of proton sponges, of bicyclic guanidines, of amidines and of phosphazenes and their strong Bronsted basicity makes them attractive for many chemical syntheses. As the result, it is found that TMGN has the lowest alkylation rate.



In order to find the alkylation site on TMGN, this compound was extensively studied by different NMR techniques and the central nitrogen was identified as the *N*-alkylation site. It was also found that in methylated TMGN molecule, the naphthalene and the pentamethylguanidinium group are perpendicular.

To explain our results by the <sup>1</sup>H NMR DOSY technique, diffusivity coefficients of several compounds were measured.

The microreactor as a chemical tool shows great promise, particularly in the areas of determining optimum reaction conditions. The ability to rapidly scan a wide range of reaction conditions in addition to the flexibility to test multiple reagents can greatly accelerate chemical research. With the reduced reagent consumption and increased speed of data collection, the microreactor system enabled small scale synthesis of several natural compounds. An extensive study of determining the effect of the reaction conditions on the selectivity and yield was done for syringic acid alkylation. In these studies, better results were obtained with TMGN than with DBU. Reagents combination and micromixer type have no remarkable effect on the selectivity and yield but the flowrate of 10 μL min<sup>-1</sup> was determined as the optimum flowrate. In methylquercetin synthesis, DBU was more selective toward monomethyl quercetins, however with TMGN, a wide product distribution was observed. For trolox and clofibric acid, the reaction proceeded quantitatively, however for podocarpic acid, the obtained yield is fairly good.

## 9 APPENDICES

### 9.1 Appendix A

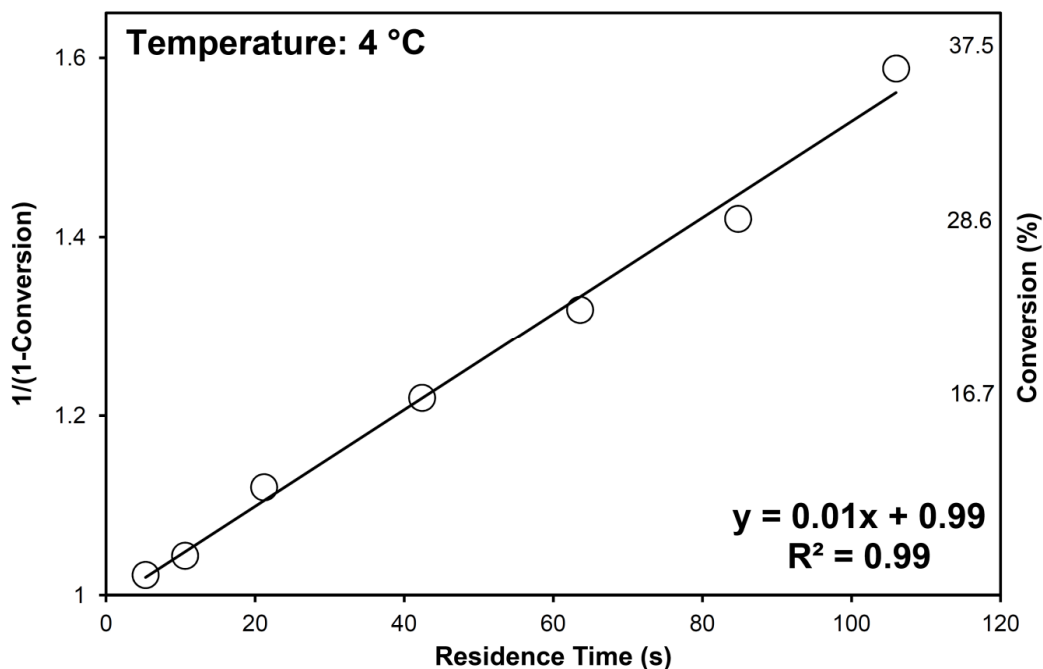


Figure 9-1 Second order kinetics plot of benzoic acid alkylation by iodomethane in the presence of TMGN and in DMF at 4 °C

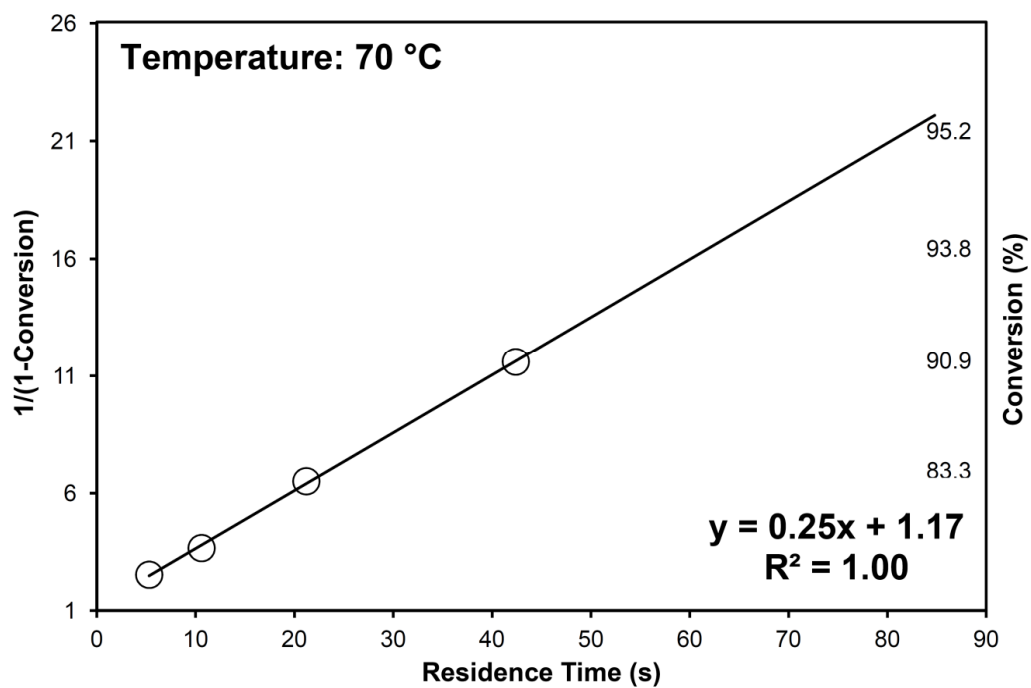


Figure 9-2 Second order kinetics plot of benzoic acid alkylation by iodomethane in the presence of TMGN and in DMF at 70 °C

**Table 9-1 Calculated Löwdin charges for para substituted benzoic acids [92]**

Substituent	QL(H)	QL(O <sup>-</sup> )	QL(COO <sup>-</sup> )	QL(COOH)
-NO <sub>2</sub>	0.1191	-0.3540	-0.7719	-0.0254
-CN	0.1182	-0.3567	-0.7768	-0.0312
-Cl	0.1156	-0.3645	-0.7907	-0.0459
-F	0.1149	-0.3688	-0.7986	-0.0526
-H	0.1135	-0.3699	-0.8018	-0.0533
-CH <sub>3</sub>	0.1126	-0.3713	-0.8046	-0.0597
-OCH <sub>3</sub>	0.1123	-0.3729	-0.8076	-0.0688
-OH	0.1150	-0.3637	-0.7956	-0.0471

**Table 9-2 The relative V<sub>min</sub> values of different substituted benzoic acids [94]**

Substituent	V <sub>ortho</sub>	V <sub>meta</sub>	V <sub>para</sub>
-NO <sub>2</sub>	1.53	10.67	10.98
-CN	8.88	8.79	9.71
-Br	3.85	4.21	4.12
-Cl	1.49	4.47	4.25
-F	1.89	3.11	2.54
-H	0.00	0.00	0.00
-CH <sub>3</sub>	-0.72	-1.30	-1.76
-OCH <sub>3</sub>	-4.40	-1.02	-3.21
-OH	5.03	0.02	-2.17
-NH <sub>2</sub>	-3.16	-3.76	-6.12

## 9.2 Appendix B

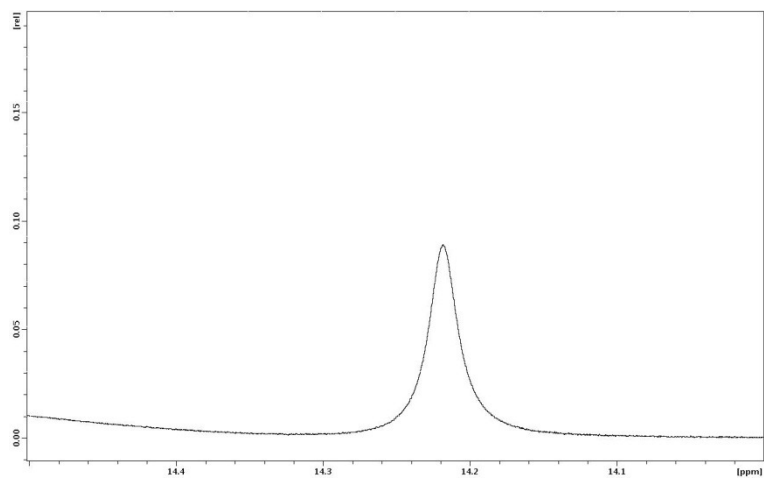


Figure 9-3  $^1\text{H}$  NMR of  $\text{TMGN-H}^+$  and the signal of labile hydrogen nucleus

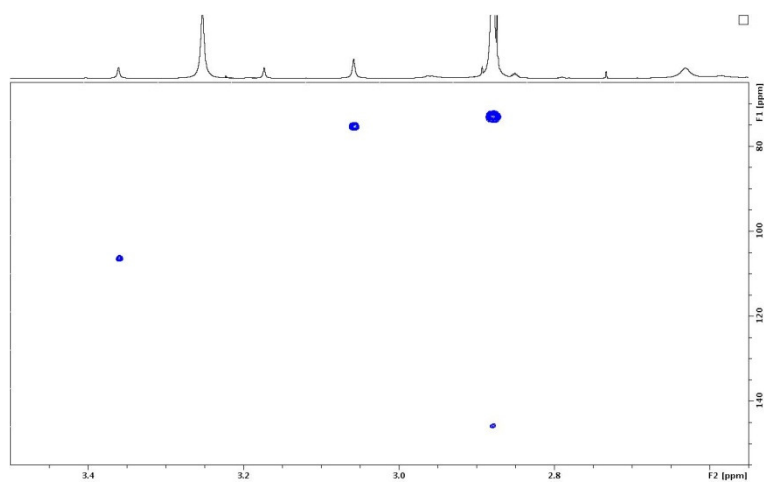


Figure 9-4 800MHz 2D NMR  $^1\text{H}$ - $^{15}\text{N}$ HMBC of  $\text{TMGN-Me}$ , methyl groups of C7/8/9/10

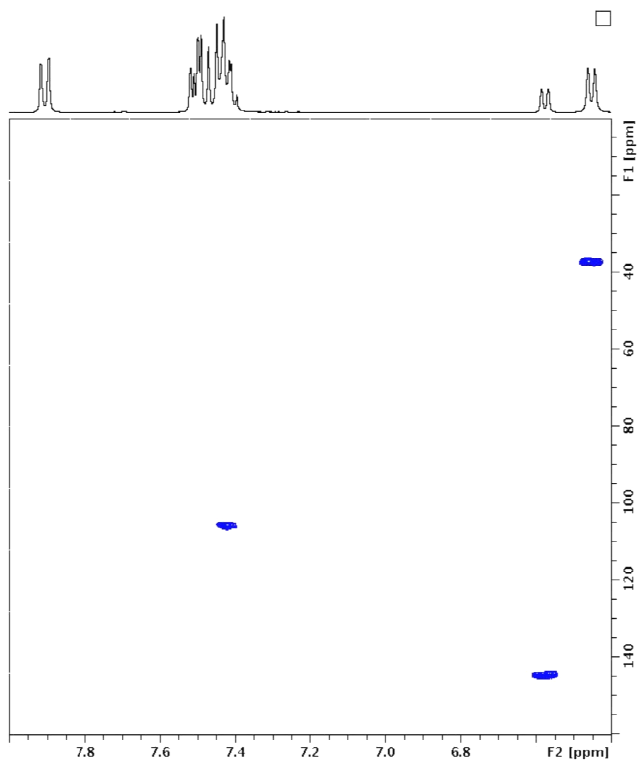


Figure 9-5 400MHz 2D NMR  $^1\text{H}$ - $^{15}\text{N}$ HMBC of TMGN-Me

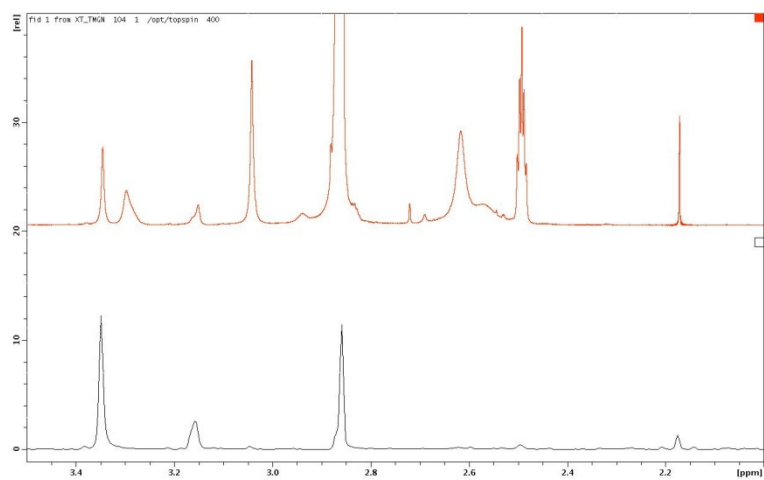


Figure 9-6  $^{13}\text{C}$ -decoupled  $^1\text{H}$  NMR spectrum of TMGN-Me and three peaks for  $^{13}\text{C}$ -labeled methyl groups

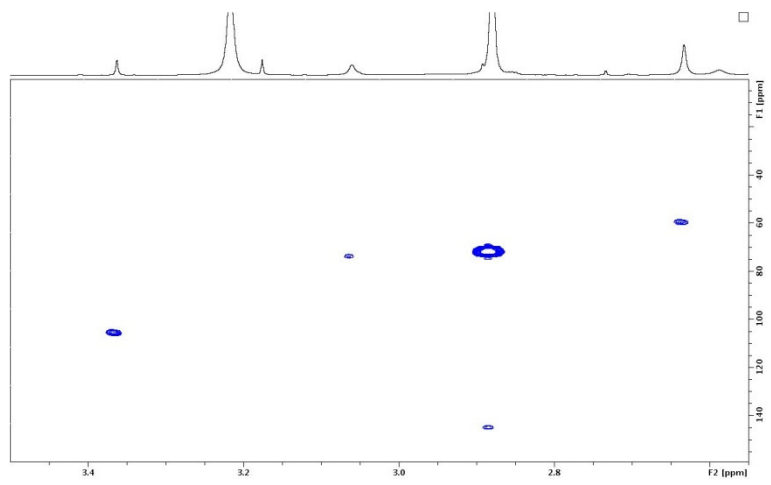


Figure 9-7 400MHz 2D NMR  $^1\text{H}$ - $^{15}\text{N}$ HMBC of TMGN-Me, methyl groups of C7/8/9/10

### 9.3 Appendix C

**Table 9-3 Diffusion coefficient of different compounds in DMF by <sup>1</sup>H NMR**

Sample	Signals	D (m <sup>2</sup> s <sup>-1</sup> )×10 <sup>9</sup>	D <sub>avg</sub> (m <sup>2</sup> s <sup>-1</sup> ) ×10 <sup>9</sup>
<b>1</b>	Aromatic (7.73 ppm)	0.8783	0.8783
<b>2</b>	OCH <sub>3</sub> , Aromatic	0.6131, 0.6123	0.6127
<b>2a</b>	CH <sub>3</sub> (3.91 ppm), CH <sub>3</sub> (3.88 ppm), Aromatic (7.32 ppm)	0.7086, 0.7136, 0.7091	0.7104
<b>2b</b>	CH <sub>3</sub> (4.01 ppm), CH <sub>3</sub> (3.99 ppm), Aromatic (7.53 ppm)	0.6730, 0.6770, 0.6746	0.6749
<b>6</b>	CH <sub>3</sub>	1.806	1.806
<b>16</b>	CH <sub>3</sub> , Aromatic (7.39 ppm), Aromatic (6.42 ppm)	0.6713, 0.6651, 0.6669	0.6678
<b>21</b>	Aliphatic (3.35 ppm), Aliphatic (2.5 ppm), Aliphatic (1.8 ppm),	1.033, 1.033, 1.032	1.033
<b>1, 16</b>	<b>1, 16</b> (6.8 ppm), <b>16</b> (3.16 ppm)	a, 0.5716, 0.5856	0.5786
<b>1, 21</b>	<b>1, 21</b>	0.70260, 0.76370, 0.76250, 0.75860, 0.76300, 0.74700	0.7590

a. Not measurable(superimposed with DMF)

**Table 9-4 Measuring diffusion coefficient of DMF by <sup>1</sup>H DOSY NMR**

	D (CH <sub>3</sub> ) ×10 <sup>9</sup> (m <sup>2</sup> s <sup>-1</sup> )	D (COH) ×10 <sup>9</sup> (m <sup>2</sup> s <sup>-1</sup> )	D <sub>avg</sub> (m <sup>2</sup> s <sup>-1</sup> ) ×10 <sup>9</sup>
DMF( <b>1</b> )	1.485	a	1.485
DMF( <b>2</b> )	1.468	1.472	1.470
DMF( <b>2a</b> )	1.478	1.484	1.481
DMF( <b>2b</b> )	1.484	1.484	1.484
DMF ( <b>6</b> )	1.488	1.490	1.489
DMF( <b>16</b> )	1.453	1.481	1.467
DMF( <b>1,16</b> )	1.451	a	1.451
DMF( <b>21</b> )	1.484	1.487	1.486
DMF( <b>1, 21</b> )	1.466	1.455	1.461

a. Not measurable (superimposed with sample)

**Table 9-5 Measuring diffusion coefficient of Water by  $^1\text{H}$  DOSY NMR**

	$D (\text{m}^2 \text{s}^{-1}) \times 10^9$
Water in <b>1</b>	1.624
Water in <b>2</b>	1.567
Water in <b>2a</b>	1.662
Water in <b>2b</b>	1.602
Water in <b>6</b>	1.700
Water in <b>16</b>	1.692
Water in <b>21</b>	1.673
Water in ( <b>21, 1</b> )	a
Water in ( <b>16,1</b> )	a

a. Not measurable (very large signal)



## 9.4 Appendix D

Table 9-6 Peak area data for a typical experiment

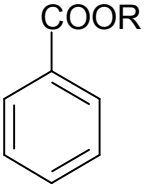
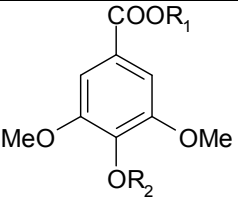
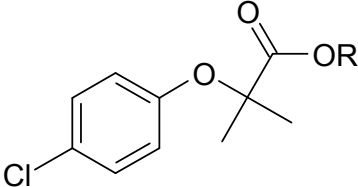
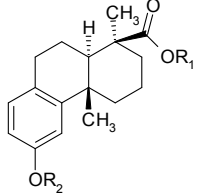
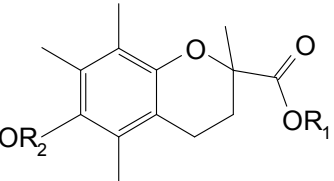
Flowrate ( $\mu\text{L. min}^{-1}$ )	TMB peak area	DMB peak area	Iodoanisole peak area
150	1011733	895986	943854
150	1058023	912141	984773
75	984080	919312	951730
75	1028007	925414	958760
37.5	1007530	918272	944272
37.5	1005388	926264	964276
18.75	1050252	946008	988435
18.75	1059301	936870	988676
12.5	1008086	918933	972378
12.5	1040201	929565	994153
9.375	1023249	926211	980643
9.375	1019407	926312	982046
7.5	1026044	923791	992671
7.5	1039291	922644	972631
7.5	858977	756139	824274

Table 9-7 Statistical analysis for the typical experiment

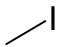
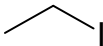
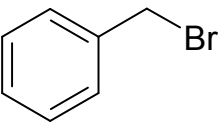
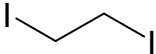
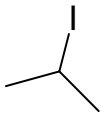
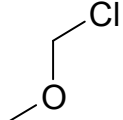
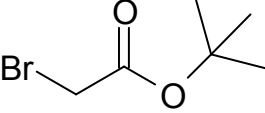

	TMB	DMB	Iodoanisole	$\frac{\text{TMB}}{\text{TMB} + \text{DMB}}$	$\frac{\text{DMB}}{\text{TMB} + \text{DMB}}$
Average Peak area	1014638	912257	962904	0.5	0.5
Standard Deviation	47931	44573	41913	0.5	0.5
Standard Deviation to Average ratio (%)	4.72	4.89	4.35	0.5	0.5

## 9.5 Appendix E

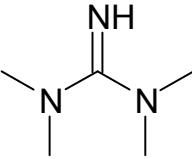
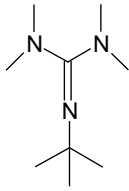
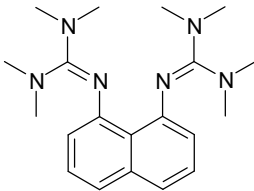
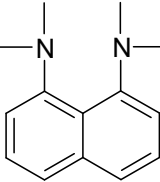
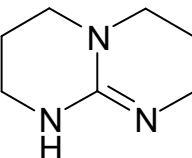
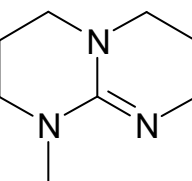
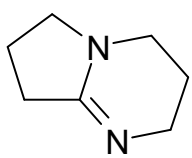
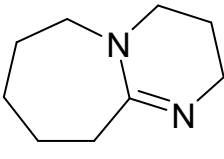
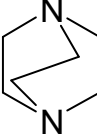
### Carboxylic acids and acid-phenols

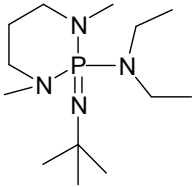
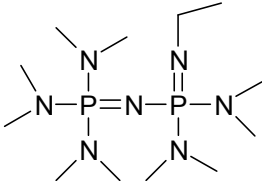
<p><b>1, 1a</b></p>		<p><b>1</b> R:H <b>1a</b> R:CH<sub>3</sub></p>
<p><b>2, 2a-c</b></p>		<p><b>2</b> R<sub>1</sub>=R<sub>2</sub>:H <b>2a</b> R<sub>1</sub>:CH<sub>3</sub>, R<sub>2</sub>:H <b>2b</b> R<sub>1</sub>:H, R<sub>2</sub>:CH<sub>3</sub> <b>2c</b> R<sub>1</sub>:CH<sub>3</sub>, R<sub>2</sub>:CH<sub>3</sub></p> <p><b>2:</b> <sup>13</sup>C NMR (DMSO-<i>d</i><sup>6</sup>, 300MHz): δ (ppm) 166.27, 147.42, 140.16, 120.35, 106.79, 55.96, 51.90. <b>2a:</b> <sup>13</sup>C NMR (DMSO-<i>d</i><sup>6</sup>, 300MHz): δ (ppm) 166.12, 147.54, 140.60, 119.17, 106.65, 56.019, 51.90. <b>2b:</b> <sup>13</sup>C NMR (DMSO-<i>d</i><sup>6</sup>, 300MHz): δ (ppm) 166.96, 152.66, 141.33, 125.93, 106.51, 60.12, 55.92.</p>
<p><b>3, 3a</b></p>		<p><b>3</b> R:H <b>3a</b> R:CH<sub>3</sub></p> <p><b>3:</b> <sup>13</sup>C NMR (DMSO-<i>d</i><sup>6</sup>, 300MHz): δ (ppm) 174.69, 154.15, 129.00, 125.35, 120.05, 78.74, 25.14</p>
<p><b>4, 4a-c</b></p>		<p><b>4</b> R<sub>1</sub>=R<sub>2</sub>:H <b>4a</b> R<sub>1</sub>:CH<sub>3</sub>, R<sub>2</sub>:H <b>4b</b> R<sub>1</sub>:H, R<sub>2</sub>:CH<sub>3</sub> <b>4c</b> R<sub>1</sub>:CH<sub>3</sub>, R<sub>2</sub>:CH<sub>3</sub></p> <p><b>4:</b> <sup>13</sup>C NMR (DMSO-<i>d</i><sup>6</sup>, 300MHz): δ (ppm) 178.54, 155.10, 148.82, 129.49, 125.02, 112.96, 111.51, 51.88, 42.98, 39.03, 38.05, 37.07, 30.64, 28.33, 23.01, 20.93, 19.69. <b>4c:</b> <sup>13</sup>C NMR (DMSO-<i>d</i><sup>6</sup>, 300MHz): δ (ppm) 176.97, 157.35, 148.73, 129.59, 126.81, 111.38, 110.62, 54.81, 51.93, 51.15, 43.33, 38.70, 38.10, 36.89, 30.58, 27.95, 22.52, 20.73, 19.55</p>
<p><b>5, 5a-c</b></p>		<p><b>5</b> R<sub>1</sub>=R<sub>2</sub>:H <b>5a</b> R<sub>1</sub>:CH<sub>3</sub>, R<sub>2</sub>:H <b>5b</b> R<sub>1</sub>:H, R<sub>2</sub>:CH<sub>3</sub> <b>5c</b> R<sub>1</sub>:CH<sub>3</sub>, R<sub>2</sub>:CH<sub>3</sub></p> <p><b>5:</b> <sup>13</sup>C NMR (DMSO-<i>d</i><sup>6</sup>, 300MHz): δ (ppm) 174.71, 145.54, 144.94, 122.52, 120.82, 120.07, 116.40, 76.05, 30.10, 25.15, 20.56, 12.69, 11.82, 11.72 <b>5b:</b> <sup>13</sup>C NMR (DMSO-<i>d</i><sup>6</sup>, 300MHz): δ (ppm) 174.45, 149.35, 147.51, 126.97, 125.13, 121.64, 117.16, 76.37, 59.78, 29.83, 25.14, 20.39, 12.30, 11.76, 11.39</p>

### Alkylating agents

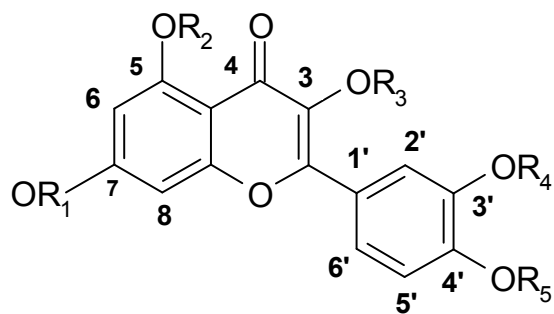
6		Iodomethane(MeI)
7		Iodoethane(EtI)
8		Benzyl bromide
9		1,2-Diiodoethane
10		2-Iodopropane
11		Chloromethyl methyl ether
12		<i>tert</i> -Butyl bromoacetate
13		2-Iodo-2-methylpropane

Bases

14		TMG
15		Barton's base
16		TMGN
17		DMAN
18		TBD
19		MTBD
20		DBN
21		DBU
22		DABCO

23		BEMP
24		P2Et

### Polyphenols



25, 25a-h

Compound	R <sub>1</sub> (7A)	R <sub>2</sub> (5B)	R <sub>3</sub> (3C)	R <sub>4</sub> (3'D)	R <sub>5</sub> (4'E)
<b>25</b>	H	H	H	H	H
<b>25a</b>	H	H	CH <sub>3</sub>	H	H
<b>25b</b>	H	H	H	H	CH <sub>3</sub>
<b>25c</b>	CH <sub>3</sub>	H	H	H	H
<b>25d</b>	H	H	CH <sub>3</sub>	H	CH <sub>3</sub>
<b>25e</b>	CH <sub>3</sub>	H	CH <sub>3</sub>	H	H
<b>25f</b>	CH <sub>3</sub>	H	H	H	CH <sub>3</sub>
<b>25g</b>	CH <sub>3</sub>	H	CH <sub>3</sub>	H	CH <sub>3</sub>
<b>25h</b>	CH <sub>3</sub>	H	CH <sub>3</sub>	CH <sub>3</sub>	CH <sub>3</sub>

## 10 Extended Abstract (In French)

### REACTIVITE ORGANIQUE: ETUDES CINETIQUES ET OPTIMISATION DE SYNTHES EN SYSTEMES MICROFLUIDIQUES

*Azarmidokht GHOLAMIPOUR-SHIRAZI*

**Résumé:** Les microsystèmes sont des réacteurs extraordinaires pour mettre en œuvre des réactions chimiques car ils apportent : un rapport de contact entre phases ou entre liquide et catalyseurs un million de fois supérieur à celui rencontré à l'échelle du laboratoire, la possibilité d'hypertrempe thermique tant au chauffage qu'au refroidissement et enfin des réactions sans interactions avec les produits finaux car conduites en flux continu. Les dimensions micro-ou nanométriques de ces réacteurs sont très largement compensées par la possibilité de parallélisme à grande échelle de ces réacteurs qui permet une montée en échelle de la production sans nouveau développement. Nous avons choisi comme réaction test l'alkylation des acides benzoïques par l'iodure de méthyle en présence d'une éponge à proton (TMGN). Cette réaction a été choisie car c'est une réaction qui suit une cinétique parfaitement du second ordre. Nous avons ainsi pu déterminer la relation de Hammett pour une série d'acides benzoïques substitués et réaliser des expériences préparatives sur des substrats bifonctionnels simples et de mettre en évidence la sélectivité. Une étude comparative de la basicité des superbases organiques comparée à leur vitesse d'alkylation par l'iodure de méthyle a été effectuée pour mieux cerner le rapport basicité, nucléophilie de ces bases qui est peu étudiée. Parallèlement l'alkylation d'un polyphénol complexe la quercétine et de substrats à haute valeur ajoutée tels l'acide podocarpique, l'acide clofibrique et le Trolox à l'aide de système microfluidique ont été étudiés à l'échelle de la millimole.

**Mots-clés:** corrélation de Hammett, cinétique, microfluidique, *N*-alkylation, *O*-alkylation, phénol-acide, polyphénols, superbase organique, éponge à proton, TMGN

#### **Introduction:**

La transformation des acides carboxyliques en leurs esters méthyliques est une réaction fondamentale en synthèse organique pour laquelle de nombreuses méthodes ont été développées [52]. L'estérification des acides carboxyliques par alkylation après déprotonation par une base a fait l'objet de nombreuses études [54-55, 62-65]. La chimie en microréacteurs à flux continu a reçu une attention considérable au cours des dix dernières années [1-8]. Dans un microréacteur, les réactions potentiellement explosives et dangereuses peuvent être effectuées sans danger [9-11], les intermédiaires à courte durée de vie peuvent être piégés afin d'augmenter le rendement chimique [12], une cascade de réactions peut être réalisée sans la nécessité d'isoler les intermédiaires et, enfin il est possible d'utiliser des conditions de pression et / ou température élevées [13]. Les microréacteurs ont trouvé de nombreuses applications dans plusieurs étapes de la synthèse organique [14] et dans la synthèse de produits naturels complexes. Différents microréacteurs, par exemple [44-48], ont été développés pour étudier des phénomènes physiques et chimiques ainsi que l'acquisition rapide de données cinétiques et les paramètres cruciaux liés aux phénomènes de transport. Pour ces études un mélange rapide des réactifs et une faible

consommation de l'échantillon, sont les deux caractéristiques souhaitées, ainsi que la comptabilité avec l'analyse en ligne. Les réacteurs microfluidiques remplissent parfaitement ces conditions [44] et fournissent ainsi une plateforme pour les études cinétiques de réaction [45-48].

Dans cette thèse, nous avons développé un montage expérimental composé d'un micromélangeur commercial, suivi d'un réacteur capillaire pour étudier la cinétique de la réaction d'*O*-alkylation des acides carboxyliques en présence d'une superbase organique (TMGN), la cinétique de *N*-alkylation des superbases organiques, et enfin l'optimisation de l'*O*-alkylation des acides carboxyliques, de phénol-acides et de polyphénols naturels.

Ce même montage a été utilisé pour étudier l'effet de substituant sur la réactivité des acides benzoïques. Cette réaction suit la relation de Hammett. La précision des mesures nous a permis de discuter précisément les points mal corrélés. Nous avons pu montrer que la solvation joue un rôle fondamental dans ces écarts. Des études de RMN ont été conduites afin d'identifier le site d'alkylation de la molécule de TMGN (site amine ou imine). Les coefficients de diffusion de produits clés de cette étude sont aussi déterminés par la technique DOSY afin de préparer des simulations numériques.

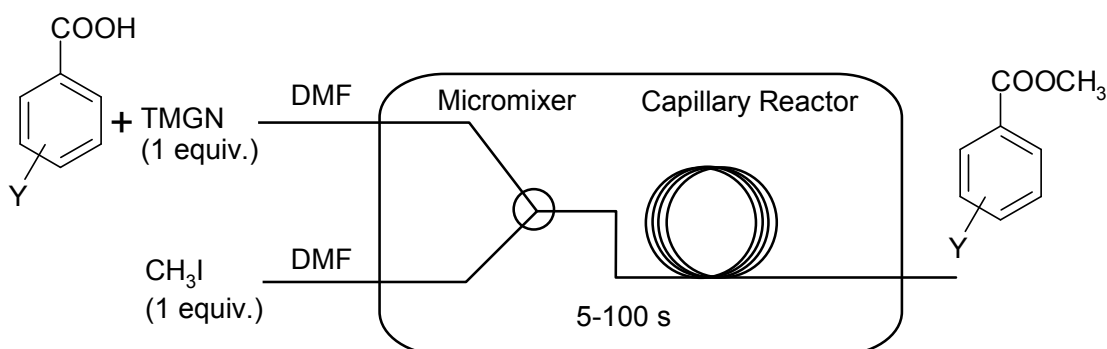


*Figure 1.* Schéma du montage expérimental. Il comprend un micromélangeur et un capillaire en silice fondue qui sert de réacteur tubulaire. Les deux seringues qui contiennent les réactifs sont connectées au micromélangeur par des capillaires de 30 cm de long et de 50 microns de diamètre interne. Le micromélangeur est suivi par un capillaire en silice fondue de 300 cm de long et de diamètre interne 75 microns. Le réacteur capillaire est maintenu à 20°C par un bain d'eau thermostaté.

### Matériel et Méthodes:

Nous avons utilisé un montage (Figure 1) composée de deux flux d'une solution de réactifs dans le DMF délivrés simultanément par une pompe seringue à haute pression, à un micromélangeur suivie d'une capillaire qui sert de microréacteur. Nous avons utilisé un micromélangeur (NanoMixer®, Upchurch) basé sur une technique de multi-lamination distribuée. Pour les études cinétiques à

différents débits, un échantillon de milieu réactionnel a été collecté à la sortie du réacteur pour chaque débit. La réaction est arrêtée immédiatement à la sortie par dilution dans une solution acide. Le mélange réactionnel est ensuite analysé par GC-MS en utilisant l'ionisation par impact électronique ou en LC-MS en utilisant l'électronébulisation. Pour les expériences préparatives, le débit a été maintenu constant tout au cours de l'expérience. La sortie du réacteur a été entièrement collectée dans un milieu acidifié, stoppant ainsi la réaction. A la fin de la réaction, et après plusieurs étapes d'extraction et de séchage, la totalité du résidu a été dissout dans le solvant deutéré (en général le DMSO-*d*6). L'échantillon a ensuite été analysé en RMN <sup>13</sup>C. Pour la quercétine, certaines expériences ont été réalisées en utilisant un montage à deux étages, en utilisant deux micromélangeurs en série. Les échantillons ont été analysés par LC-MS.

## Résultats et discussion

Les réactions dont les cinétiques ont été étudiées dans cette thèse, sont :

### 1-Alkylation de l'acide benzoïque par l'iodométhane en la présence de TMGN

Cette réaction suit une cinétique de second ordre. Les différentes combinaisons des réactifs (1 : acide benzoïque, TMGN ; MeI. 2 : acide benzoïque, MeI ; TMGN. 3 : acide benzoïque ; MeI, TMGN ) n'a pas d'effet sur la cinétique de la réaction tant que le mélange d'iodométhane et de TMGN est évité. Dans ce dernier cas la réaction parasite est due à l'hydrolyse de l'iodure de méthyle par l'anion hydroxyde généré par la réaction du TMGN avec l'eau résiduelle. Le dispositif expérimental a également permis l'étude de l'effet de la température sur cette réaction. L'entropie négative importante de l'activation indique que l'état de transition dans le DMF a une structure relativement spécifique et est plus fortement solvaté que l'état initial neutre. Les valeurs de l'enthalpie d'activation indiquent que le processus est endothermique. Les constantes de vitesse ont été déterminées pour la réaction entre différents agents alkylants, et une série acide benzoïque substitués et aussi dans différents solvants.

### 2-Alkylation d'une série d'acides benzoïques para-substitués

Cette étude a été conduite pour déterminer l'effet des substituants sur la réactivité des acides benzoïques. Toutes ces réactions suivent une cinétique de second ordre. Leurs réactivités sont corrélées avec une pente de -0,66 (Figure 2, log(k) versus constante  $\sigma$  de Hammett). Ceci indique qu'une augmentation de la densité électronique sur le groupe acide carboxylique accélère la réaction. La précision des mesures a permis d'interpréter les points mal corrélés. Ces écarts sont dus à de fortes différences de solvation entre l'état initial (avec charge localisée) et l'état de transition (avec charge répartie)



#### 4- N-alkylation des superbases organiques par iodomethane.

Ces superbases organiques sont des guanidines, des éponges à proton, des guanidines bicycliques, des amidines et des phosphazènes. Leur basicité de Brønsted est très forte et ceci les rend attrayantes en synthèses chimiques. Toutes ces réactions suivent une cinétique de second ordre. Globalement, on observe comme attendu une corrélation entre basicité et nucléophilie. Les bases TMGN et BEMP sont en dehors de cette corrélation et ont le meilleur rapport basicité/nucléophilie (Figure 3).

#### 4-Alkylation de l'acide syringique par l'iodométhane en présence de TMGN ou de DBU

L'acide syringique est un acide phénol. Cette réaction suit pour les deux bases une cinétique du second ordre. Le produit principal est l'ester et aucunes traces d'éther n'ont été détectées avec aucunes des bases dans les conditions analytiques. Une vaste étude de détermination de l'effet des conditions de réaction sur la sélectivité et le rendement a été conduite. De meilleurs résultats ont été obtenus avec le TMGN qu'avec le DBU. En effet en présence de DBU, la réaction va beaucoup plus lentement qu'avec TMGN car la réaction parasite d'alkylation du DBU par l'iodométhane est environ 2000 fois supérieure à celle de l'alkylation du TMGN. En augmentant la concentration des réactifs la formation d'éther a pu être observée. La quantité d'éther est inversement proportionnelle au temps de réaction ce qui montre clairement un effet lié au mélange.

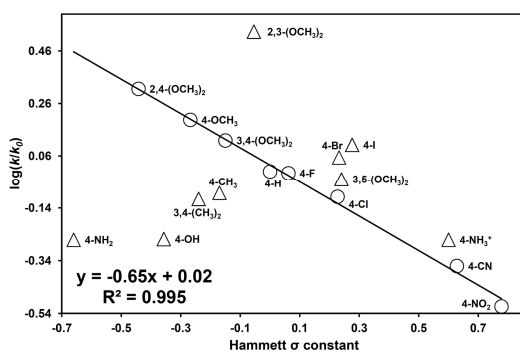


Figure 2 Hammett plot

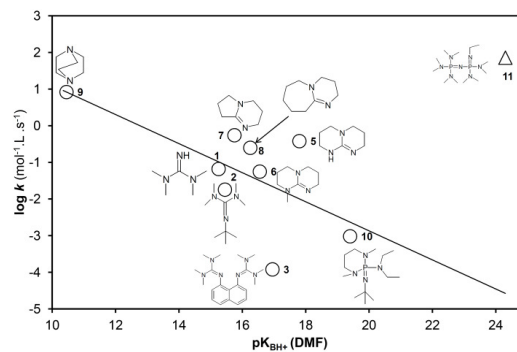


Figure 3 Plot of log k and pK<sub>a</sub> for bases

#### 5-Alkylation sélective de produits naturels par l'iodométhane en présence de TMGN

Les conditions opératoires ont été optimisées pour le Trolox, l'acide clofibrique, l'acide podocarpique et le quercétine. Les produits ont été isolés et analysés par RMN <sup>1</sup>H et <sup>13</sup>C et par spectrométrie de masse. La réaction est quantitative pour le Trolox, ainsi que pour l'acide clofibrique, et sélective pour la formation de l'ester de l'acide podocarpique qui possède une fonction hydroxyle avec de plus un assez bon rendement obtenu. Le DBU s'est montré le plus sélective pour l'obtention d'un monoéther à partir de la quercétine qui est un polyphénol

comprenant cinq fonctions hydroxyles différentes. Avec le TMGN, une large distribution de produits a par contre été observée.

### **Conclusion**

Un dispositif microfluidique de type microréacteur capillaire a été développé afin d'étudier les cinétique de réaction puis d'effectuer ces mêmes réactions en mode continu Les cinétiques de plus d'une trentaine de réactions ont été étudiées et des conditions optimales ont été obtenues pour l'alkylation préparative des acides carboxyliques et des polyphénols avec un rendement quantitatif. Les microréacteurs apparaissent donc comme un outil très prometteur, en particulier pour la détermination des conditions optimales de réaction. La capacité d'étudier quantitativement et rapidement un large éventail de conditions de réaction, la flexibilité de tester des réactifs multiples permettent d'accélérer grandement l'obtention de conditions optimales. Avec une consommation de réactif réduite et une vitesse accrue de collecte de données, le microsystème développé a permis la synthèse à l'échelle de plusieurs millimoles de composés naturels à forte valeur ajoutée.

## 11 Extracted Papers

---

**Gholamipour-Shirazi, A.** and C. Rolando, *N-alkylation of organic superbases kinetics screening using a continuous flow microfluidic device: basicity versus nucleophilicity*, Journal of organic and biomolecular chemistry, accepted pending revision.

---

**Gholamipour-Shirazi, A.** and C. Rolando, *Alkylation of Substituted Benzoic acids in a Continuous Flow Microfluidic device: Kinetics and Linear Free Energy Relationships*, *Org. Process Res. Dev.*, 2012, 16 (5), pp 811–818

---

**Gholamipour-Shirazi, A.**, Trivelli, X, and C. Rolando, *Identification of the Methylation Site of 1,8-Bis(Tetramethylguanidino)Naphthalene (TMGN) by Multinuclear <sup>1</sup>H, <sup>13</sup>C, <sup>15</sup>N Magnetic Resonance Spectroscopy*, Manuscript in preparation to be submitted to the European journal of organic chemistry

---

**Gholamipour-Shirazi, A. and C. Rolando**, *Regioselective esterification of small organic molecules with drug-like properties by using a microfluidics device*, Manuscript in preparation

---

## Alkylation of Substituted Benzoic Acids in a Continuous Flow Microfluidic Microreactor: Kinetics and Linear Free Energy Relationships

Azarmidokht Gholamipour-Shirazi and Christian Rolando\*

USR CNRS 3290, Miniaturisation pour la Synthèse, l'Analyse et la Protéomique and FR CNRS 2638 Institut Michel-Eugène Chevreul, Université de Lille 1, Sciences et Technologies, 59655 Villeneuve d'Ascq, France

**S** Supporting Information

**ABSTRACT:** Alkylation of para-substituted benzoic acids by iodomethane using an organic superbases, 1,8-bis-(tetramethylguanidino)naphthalene (TMGN) in DMF was chosen as a model reaction to test the quality of the control of experimental parameters in a continuous flow microfluidic reactor as it is expected to follow a perfect second order kinetics with a large dynamics by varying the substituents. These conditions may be directly used for the synthesis of natural product esters. Because TMGN reacts slowly with iodomethane, the three different mixing strategies between substrate, base and alkylating reagent were compared. The rate constants were determined for the reaction with a set of alkylating agents and in different solvents. In order to test the quality of the obtained data, temperature effect and free energy relationships, which are expected to follow predictable laws, were investigated. The kinetics vary over 6 orders of magnitude and follows a perfect Arrhenius law, allowing the determination of the energies, enthalpies, and entropies of activation. Finally, we established a Hammett linear relationship for a series of 16 substituted benzoic acids, leading to a reaction constant  $\rho$  of  $-0.65$  for this reaction. The quality of the obtained kinetics allowed us to discuss the outliers. All kinetics were obtained with less than 0.5 mmol of substrate.

### INTRODUCTION

Chemistry in continuous flow microreactors has received considerable attention over the past decade.<sup>1</sup> In microreactors, potentially explosive and hazardous reactions can be safely conducted,<sup>2a–c</sup> short-lived intermediates can be trapped to increase chemical yield,<sup>2d</sup> a cascade of reactions can be carried out without the necessity of isolating intermediates, and alternatively it is possible to use high-pressure and/or temperature conditions.<sup>2e</sup> Continuous flow microreactors have found broad applications in multistep organic synthesis<sup>3a</sup> and in the synthesis of complex natural products.<sup>3b–d</sup> One more advantage of microreactors is that they provide an opportunity for greener chemistry and faster process development.<sup>3e–g</sup> Scale-up of microreactors can be easily achieved by using multiple microreactors in parallel.<sup>4</sup> The efficiency of a given reaction in a microreactor compared to that in batch relies critically on the mixing process of the reagents.<sup>5a–e</sup> Most of the mixing evaluation reactions are based on highly nonlinear reactions such as Bourne's reactions,<sup>5b–d</sup> and the iodine-iodate Villermaux–Dushman reaction, which leads to complicated kinetics valid only in a limited range of concentrations.<sup>5e</sup> Furthermore, these conventional methods are based on spectrophotometric determination of the products rather than using the isolated product yield.<sup>6</sup> We were interested, therefore, to find and to study in a continuous flow microreactor, a second-order reaction with isolable products and variable rates by varying the substrate without changing the reaction kinetics. The reaction of substituted benzoate with iodomethane, which is a well-known S<sub>N</sub>2 reaction, seems to fulfill these criteria. Chlorobenzyl Merrifield resins (chloromethylated polystyrene–1% divinylbenzene) were efficiently alkylated by cesium salts of amino

acids without quaternization of their protected amine group and using *N,N'*-dimethylformamide (DMF) as solvent.<sup>7a,b</sup> The scope of this reaction has been extended to the alkylation of crowded carboxylic acids using hexamethylphosphoramide (HMPA) as solvent<sup>7c</sup> and has been used in several syntheses<sup>7d,e</sup> including the synthesis of short-lived <sup>11</sup>C propyl and butyl esters.<sup>7f</sup> Kondo et al. demonstrated that the reaction of tetramethylammonium benzoate salts with alkyl halides in acetonitrile follows a second-order kinetics.<sup>8</sup> Instead of using cesium or tetraalkylammonium salts, Ono et al. used 1,8-diazabicyclo[5.4.0]-undec-7-ene (DBU) as the base to efficiently deprotonate benzoic acid in toluene at room temperature.<sup>9a</sup> However, in these conditions the obtained DBUH<sup>+</sup>T<sup>−</sup> salt is insoluble, and the resulting white slurry precludes its use in a microsystem. In another study, Mal et al. employed the same procedure for the *O*-methylation of various carboxylic acids in acetone and in acetonitrile as solvent.<sup>9b</sup> However, one of the most serious side reactions in these syntheses is the alkylation of DBU by iodomethane. Barton et al. reported that the hindered guanidine bases they synthesized were much more stable toward alkylation.<sup>10a,b</sup> Barton's bases enable the alkylation of crowded carboxylic acid such as adamantane-1-carboxylic acid even with a secondary alkyl halide such as isopropyl iodide.<sup>10c</sup> This reaction has been used during the total synthesis of salinomycin.<sup>10d</sup> In order to apply the results of this work to the synthesis of more complex molecules such as phenol acids we used DMF as solvent, which was a good solvent in carboxylate cesium or sodium salt alkylation.<sup>11</sup> Furthermore, the high polarity of DMF avoids the

Received: March 31, 2012

Published: April 17, 2012

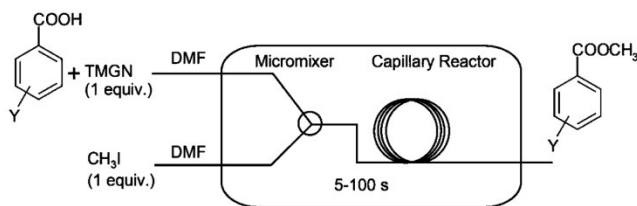


Figure 1. Experimental setup. It comprises a commercially available micromixer (NanoMixer) and a fused silica-based capillary tubular reactor.

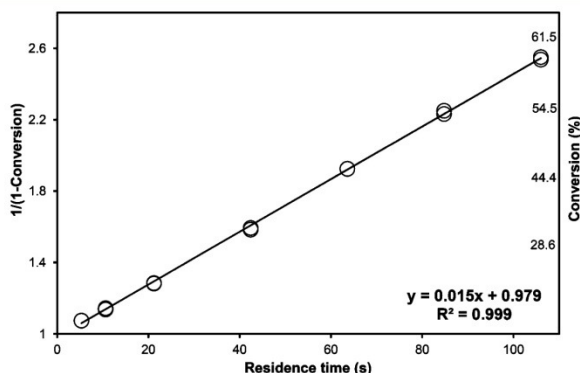


Figure 2. Second-order kinetics plot of benzoic acid alkylation by iodomethane in the presence of TMGN and in DMF at 20 °C.

formation of aggregates or strong ion pairs which complicate the kinetics of the reaction.<sup>12</sup> We chose 1,8-bis-(tetramethylguanidino)naphthalene (*N,N''''*-1,8-naphthalenediyl-bis[*N,N,N',N'*-tetramethyl]-guanidine, TMGN) as a base as it is even less reactive than Barton's bases toward alkylation.<sup>13a</sup> Its backbone is the well-known 'proton sponge' 1,8-bis(dimethylamino)naphthalene (DMAN) which does not react with methyl iodide but which, unfortunately, is not basic enough.<sup>13b,c</sup> The ionization constant ( $pK_{\text{BH}}^+$ ) of TMGN in acetonitrile (25.1) is higher than that of DBU (24.33).<sup>14a-c</sup> By using the linear correlations between acidities in DMF and in acetonitrile,  $pK_{\text{BH}}^+$  of TMGN in DMF is estimated to range from 16.4 to 17.5.<sup>14d</sup>  $pK_a$ 's of benzoic acids in DMF are in the range of 10.6 for 4-nitrobenzoic acid to 13.0 for 3,4-dimethylbenzoic acid.<sup>14e</sup> Therefore, TMGN is able to fully remove acidic hydrogen of all benzoic acids. Furthermore, in those conditions either for DBU or TMGN the salt of the protonated base cation with iodide remains soluble in DMF, which is a requirement for experimental studies in microreactors.

While several groups have developed their own continuous flow microreactors dedicated to organic synthesis,<sup>15</sup> the setup we used in this study has the advantage of being based on commercially available devices and thus can be reproduced easily. We present here results obtained with this setup on the kinetics of alkylation of substituted benzoic acid deprotonated by TMGN, which is focused on the comparison of three mixing strategies of the three reagents, TMGN, benzoic acid, and iodomethane, which may be mixed in any combination, the influence on the rate of the alkylating agents and of the solvent,

the temperature dependence of reaction rate, and finally the linear free energy relationships for this reaction. The linear correlation obtained shows that continuous flow microreactors may be used in physical chemistry experiments with the consumption of very small amounts of reagents.

## RESULTS AND DISCUSSION

Fused glass capillary tubes with inherent microscale internal dimensions provide modular and inexpensive building blocks for the on-demand assembly of microfluidic reactors.<sup>16</sup> All the microfluidic experiments were carried out in a setup (Figure 1) composed of two streams of reagent solutions in DMF simultaneously delivered by a high-pressure syringe pump to a micromixer followed by a fused silica-based capillary tubular reactor which are all readily available commercial devices. The two syringes containing the reagents are connected via 0.30 m capillaries (i.d. 50  $\mu\text{m}$ ) to the micromixer. Because of the high pressure drop along these inlet tubes, the liquid flows only in one direction, and no backmixing occurs. The micromixer is followed by a 3.0 m fused silica-based capillary (i.d. 75  $\mu\text{m}$ ) which is the tubular reactor.<sup>17</sup> The capillary tubular reactor is kept at the desired temperature in a water bath. For the micromixer, we utilized a commercially available multilaminating distributive micromixer chip.<sup>17a</sup> This mixer has been used previously for time-resolved studies of protein conformation by NMR.<sup>17b</sup> A similar PDMS device has also been used for the controlled polymerization of *N*-carboxy anhydrides.<sup>17c</sup> It is one of the more efficient mixing devices in this flow range.<sup>17d</sup> In our case, slightly worse results were obtained with a simple MicroTee filled with porous material.



The flow rates were varied from  $5 \mu\text{L}\cdot\text{min}^{-1}$  to  $150 \mu\text{L}\cdot\text{min}^{-1}$  to give residence times of 5 to 105 s (SI Table S1). This flow rate range corresponds to a Bodenstein number  $Bo$  varying from 90 to 1810. For these large  $Bo$  numbers, no dispersion occurs, and plug flow is assumed in the capillary tubular reactor.<sup>18</sup> The concentrations of the remaining benzoic acid and methyl benzoate were determined by GC/MS with electron ionization (EI) after silylating the quenched reaction mixture. To ensure the quality and integrity of the data generated, we added three internal standards, one in each syringe and another one in the collected sample. The absolute average and the relative average deviation were 3% and less than 0.5%, respectively (SI Tables S2 and S3). The conversion,  $f$ , used in kinetics analysis, was calculated from the integrated areas of benzoic acid methyl ester and silyl ester peak ( $f = (\text{peak area of methyl ester})/(\text{peak area of methyl ester} + \text{peak area of silyl ester})$ ) since it is more reliable than the absolute area of remaining benzoic acid or of produced methyl ester alone. The kinetics constants  $k$  were determined graphically by plotting the function  $1/(1-f)$ , against residence time ( $t$ ) which resulted in a straight line with a slope equal to  $k \times [\text{C}_7\text{H}_5\text{O}_2^-]_0$ , where  $[\text{C}_7\text{H}_5\text{O}_2^-]_0$  is the initial concentration of the substituted benzoic acid. In all the experiments, unless otherwise mentioned, the solution of benzoic acid and base (TMGN) in DMF was in one syringe, whereas the solution of the alkylating reagent, MeI, also in DMF, was kept alone in the second syringe.

Figure 2 shows the results obtained for an initial concentration of benzoic acid of 26.7 mM and molar ratios of TMGN and iodomethane to benzoic acid of 1.0 and 1.1, respectively. These concentrations have been applied for all the experiments described in this paper. The straight line relationship ( $n = 7$ ;  $R^2 = 0.999$ ) which we observed up to a conversion of 60% shows that the second-order kinetics not only is observed at the initial stage of the reaction but also remains verified up to a nearly preparative yield.

There are two other combinations for introducing the three reagents (benzoic acid, the base TMGN, and iodomethane) into the micromixer. Since it might lead to different selectivity in case of complex molecules, their kinetics were also recorded. The two combinations in which reagents cannot react irreversibly (i.e., benzoic acid and TMGN in one syringe and iodomethane in another syringe or benzoic acid and iodomethane in one syringe and TMGN in another syringe) gave quite similar rate constants  $0.57$  and  $0.55 \text{ mol}^{-1}\cdot\text{L}\cdot\text{s}^{-1}$ , respectively (Table 1, entries a, b) close to the value obtained in batch which is  $0.64 \text{ mol}^{-1}\cdot\text{L}\cdot\text{s}^{-1}$ . These three experiments

**Table 1. Effect of reagent combination on the reaction rate constant of the alkylation of TMGN deprotonated benzoic acid by iodomethane in DMF at 20 °C<sup>a</sup>**

entry	syringe A	syringe B	$k$ ( $\text{mol}^{-1}\cdot\text{L}\cdot\text{s}^{-1}$ )
a	benzoic acid, TMGN	iodomethane	$0.57 \pm 0.02^{b,c}$
b	benzoic acid, iodomethane	TMGN	$0.55 \pm 0.07^{b,d}$
c	benzoic acid	iodomethane, TMGN	$0.24^b$
d	benzoic acid	iodomethane, TMGN	$0.32^e$

<sup>a</sup>Conditions: benzoic acid 26.7 mM and molar ratios of TMGN and iodomethane to benzoic acid of 1.0 and 1.1, respectively. <sup>b</sup>HPLC grade DMF used as received. <sup>c</sup>Average and standard deviation from three independent studies. <sup>d</sup>Average and standard deviation from three independent studies. <sup>e</sup>DMF dried overnight on molecular sieves, with a small amount of molecular sieves added in each syringe.

were repeated several times using different capillaries and micromixer units and at different periods. From these data the dispersion of results may be estimated to be around 4%. However, the last combination (benzoic acid in one syringe, TMGN and iodomethane in another syringe) does not follow a clean second-order kinetics for residence times beyond 60 s and gives a lower reaction constant nearly half of the previous value (Table 1, entry c). Investigation by mass spectrometry and NMR techniques show that the side reaction is the hydrolysis of MeI as well as TMGN protonation by residual water. Improved results were obtained using DMF dried overnight over molecular sieves and using a small amount of molecular sieve in each syringe (Table 1, entry d).

**Effect of the Alkylating Reagent and Solvent.** We next investigated a set of alkylating reagents. For all alkylating agents the reaction remained cleanly second order. The observed reaction rate constants are displayed in Table 2. The  $k$  value

**Table 2. Effect of alkylating reagent and solvent on the reaction rate constant of benzoic acid alkylation in the presence of TMGN<sup>a</sup>**

entry	solvent	alkylating reagent	temperature (°C)	$k$ ( $\text{mol}^{-1}\cdot\text{L}\cdot\text{s}^{-1}$ ) <sup>b</sup>
a	DMF	iodomethane	20	$0.57 \pm 0.02^b$
b	DMF	iodoethane	20	$0.063 \pm 0.006$
c	DMF	2-iodopropane	50	$0.039 \pm 0.001$
d	DMF	benzyl bromide	20	$0.28 \pm 0.05$
e	DMF	<i>tert</i> -butyl bromoacetate	20	$0.74 \pm 0.03$
f	acetonitrile	iodomethane	20	$0.074 \pm 0.01$
g	toluene	iodomethane	20	—

<sup>a</sup>Conditions: benzoic acid 26.7 mM and molar ratios of TMGN and iodomethane to benzoic acid of 1.0 and 1.1, respectively, in HPLC grade solvents used as received. <sup>b</sup>Average and standard deviation from two or three independent measurements.

order observed for iodomethane, iodoethane and 2-iodopropane, respectively  $0.57$ ,  $0.063$ ,  $0.039 \text{ mol}^{-1}\cdot\text{L}\cdot\text{s}^{-1}$  (Table 2, entries a, b, and c), follows the expected trend for methyl, primary, and secondary alkyl halides in  $S_N2$  reactions.

No reaction was observed for 2-iodo-2-methylpropane suggesting that elimination to 2-methylpropene is the main reaction. Benzyl bromide and *tert*-butyl bromoacetate were very reactive with  $k$  values of  $0.28$  and  $0.74 \text{ mol}^{-1}\cdot\text{L}\cdot\text{s}^{-1}$ , respectively (Table 2, entries d and e). Roberts et al. reported that the reactivity of *tert*-butyl bromoacetate was 2.2 times higher than that of benzyl bromide in the alkylation of the cysteine thiol of glutathione in water/DMSO (between 10 and 20%).<sup>19</sup> Here the observed ratio in DMF is 2.7. The effect of the solvent on the reaction rate constants was also investigated and as expected the reaction in acetonitrile is much slower than in DMF with  $k$  values of  $0.074$  and  $0.57 \text{ mol}^{-1}\cdot\text{L}\cdot\text{s}^{-1}$  respectively (Table 2 entries a, f). The rate observed in acetonitrile is one-third the value ( $0.26 \text{ mol}^{-1}\cdot\text{L}\cdot\text{s}^{-1}$ ) which can be obtained using the Hammett equation given by Kondo et al.<sup>8d</sup> using the preformed ion with tetramethylammonium as counterion. No trace of the expected ester was observed by GC/MS when the reaction was conducted in toluene at 20 °C (Table 2, entry g). This result is at first glance surprising since Ono et al.<sup>2a</sup> described the alkylation of benzoic acid by iodoethane using DBU as base in toluene at room temperature. These conditions (DBU, toluene) cannot be tested in our microdevice because by reproducing the experiment in batch we observed that white

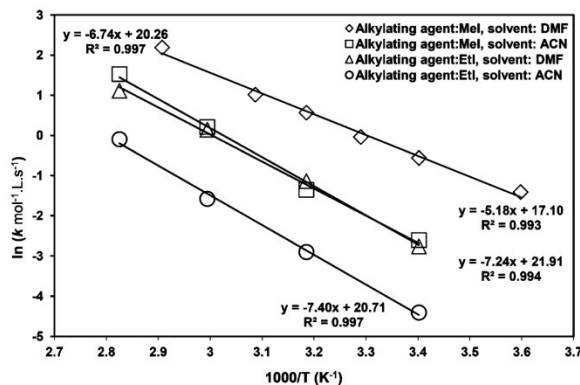


Figure 3. Arrhenius plot for the alkylation of benzoic acid deprotonated by TMGN in acetonitrile or DMF by iodomethane or iodoethane.

Table 3. Effect of alkylating agents and solvents on activation parameters of benzoic acid alkylation in the presence of TMGN<sup>a</sup>

entry	solvent	alkylating agent	$\Delta H^{\ddagger}$ (kJ·mol <sup>-1</sup> )	$\Delta S^{\ddagger b}$ (J·mol <sup>-1</sup> ·K <sup>-1</sup> )	$\Delta G^{\ddagger b}$ (kJ·mol <sup>-1</sup> )	$E_a$ (kJ·mol <sup>-1</sup> )
a	DMF	iodomethane	40.3	-112.2	73.3	43.1
b	DMF	iodoethane	53.1	-86.4	78.6	56.1
c	acetonitrile	iodomethane	57.2	-72.7	78.2	60.2
d	acetonitrile	iodoethane	58.5	-82.7	82.6	61.5

<sup>a</sup>Conditions: benzoic acid 26.7 mM and molar ratios of TMGN and iodomethane to benzoic acid of 1.0 and 1.1, respectively, in HPLC grade solvents used as received. <sup>b</sup>Standard conditions:  $T = 20$  °C, reagent concentrations = 1 mol·L<sup>-1</sup>.

slurry appears rapidly in the toluene solution. Furthermore, the estimated half-life of the reaction from batch study at dilution level of this work is higher than 10 h which precludes observing it in a microfluidic device. In summary, the continuous flow microfluidic reactor allowed us to screen rapidly and quantitatively the reactivity of different substrates using less than 0.5 mmol and to investigate various solvents.

**Temperature Effect.** The effect of the temperature for the alkylation of benzoic acid itself by iodomethane in DMF was then investigated in the range of 4–70 °C (SI, Table S4). Kinetics for each temperature, even the highest (SI Figures S3–S7), show no deviation for short residence time, which proves that the thermal equilibrium is quickly achieved in the tubular reactor. Otherwise, the kinetics would be slower at short residence time for temperature above ambient temperature and faster at temperature below ambient temperature.

The rate constants were used to construct an Arrhenius plot (Figure 3) which is linear ( $R^2 = 0.993$ ) in the studied temperature range (4–70 °C) and gives a value of 43.1 kJ·mol<sup>-1</sup> for the activation energy. From these data the enthalpy and the entropy of activation are estimated to be  $\Delta H^{\ddagger} = 40.3$  kJ·mol<sup>-1</sup> and  $\Delta S^{\ddagger} = -112.2$  J·K<sup>-1</sup>·mol<sup>-1</sup> leading to a standard free energy of activation  $\Delta G^{\ddagger} = 73.3$  kJ·mol<sup>-1</sup> at 293 K in standard conditions ( $c_0 = 1$  mol·L<sup>-1</sup>) (Table 3, entry a). Kondo et al. found  $\Delta H^{\ddagger} = 61.9$  kJ·mol<sup>-1</sup> and  $\Delta S^{\ddagger} = -66.0$  J·K<sup>-1</sup>·mol<sup>-1</sup> for the alkylation of tetramethyl ammonium benzoate salt by iodoethane in acetonitrile.<sup>8c</sup>

In order to be able to compare our data with Kondo's results we conducted three experiments by changing the solvent-alkylating agent pairs: (i) DMF, iodoethane; (ii) acetonitrile, iodomethane, and (iii) acetonitrile, iodoethane (Table 3, entries b, c, d, respectively). For the alkylation of benzoic

acid by iodoethane in acetonitrile our results  $\Delta H^{\ddagger} = 58.5$  kJ·mol<sup>-1</sup> and  $\Delta S^{\ddagger} = -82.7$  J·K<sup>-1</sup>·mol<sup>-1</sup> (Table 3, entry d) are in agreement with Kondo's data quoted above. The slightly lower enthalpy of activation (3.5 kJ·mol<sup>-1</sup>) may be due to a looser ion pair as the charge is more hidden in protonated TMGN. As expected, the enthalpy of activation is always smaller for the same reaction in DMF than in acetonitrile (Table 3 entries a and c for alkylation by MeI, and b and d for alkylation by EtI). The behavior of iodomethane in DMF is singular with a much lower enthalpy of activation  $\Delta H^{\ddagger} = 40.3$  kJ·mol<sup>-1</sup> and a more negative entropy of activation  $\Delta S^{\ddagger} = -112.2$  J·K<sup>-1</sup>·mol<sup>-1</sup> (Table 3, entry a). These results show that continuous flow microfluidic devices enable us to determine activation parameters based on a very broad range of rate constants covering 6 orders of magnitude using a very small amount of substrates as only less than 0.5 mmol of benzoic acid were used here per temperature.

**Substituent Effect.** We then used our setup to determine the reaction rate of substituted benzoic acids over a wide range of Hammett  $\sigma$  constant values (-0.66 to 0.78). A summary of the results is presented in Table 4. Most of the benzoic acids used were para-substituted, but some more functionalized benzoic acids were also studied including meta,para- and ortho,meta-disubstituted benzoic acids.<sup>14e,20</sup> Hammett  $\sigma$  values for para-substituted benzoic acid were obtained from the classical Jaffe's or Hansch's tables,<sup>20a,b</sup> Hammett  $\sigma$  values for ortho-substituents were obtained by multiplying those of *para* values with 0.65.<sup>20c</sup> For 2,3- and 2,4-dimethoxy benzoic acids,  $\sigma$  constants were obtained by summing the corresponding ortho,meta and ortho,para values.<sup>20d</sup> Values of  $pK_a$  in DMF for dimethoxy substituents were obtained from  $pK_a$  values in DMSO by Exner et al.<sup>20e</sup> using the equation proposed by

**Table 4.** Reaction rate constants for the alkylation of substituted benzoic acids by iodomethane in the presence of TMGN and in DMF at 20 °C

entry	substituent	$\sigma$	$pK_a$ in DMF	$k$ (mol <sup>-1</sup> ·L·s <sup>-1</sup> ) <sup>k</sup>
a	4-NO <sub>2</sub>	0.778 <sup>a</sup>	10.6 <sup>f</sup>	0.175 ± 0.004
b	4-CN	0.628 <sup>a</sup>	11.02 <sup>g</sup>	0.249 ± 0.002
c	4-I	0.276 <sup>a</sup>	11.65 <sup>h</sup>	0.72 ± 0.04
d	3,5-(OCH <sub>3</sub> ) <sub>2</sub>	0.24 <sup>a</sup>	11.84 <sup>f</sup>	0.53 ± 0.05
e	4-Br	0.232 <sup>a</sup>	11.6 <sup>f</sup>	0.65 ± 0.10 <sup>i</sup>
f	4-Cl	0.227 <sup>a</sup>	11.5 <sup>f</sup>	0.46 ± 0.07 <sup>i</sup>
g	4-F	0.062 <sup>a</sup>	11.84 <sup>f</sup>	0.56 ± 0.01
h	4-H	0.00	12.3 <sup>f</sup>	0.57 ± 0.02 <sup>i</sup>
i	2,3-(OCH <sub>3</sub> ) <sub>2</sub>	-0.054 <sup>c,d</sup>	12.01 <sup>f</sup>	1.95 ± 0.35
j	3,4-(OCH <sub>3</sub> ) <sub>2</sub>	-0.15 <sup>b</sup>	12.50 <sup>f</sup>	0.75 ± 0.03
k	4-CH <sub>3</sub>	-0.170 <sup>a</sup>	12.6 <sup>f</sup>	0.47 ± 0.05
l	3,4-(CH <sub>3</sub> ) <sub>2</sub>	-0.24 <sup>b</sup>	13.0 <sup>f</sup>	0.45 ± 0.04
m	4-OCH <sub>3</sub>	-0.268 <sup>a</sup>	12.78 <sup>f</sup>	0.90 ± 0.06
n	4-OH	-0.357 <sup>a</sup>	13.25 <sup>f</sup>	0.32 ± 0.04
o	2,4-(OCH <sub>3</sub> ) <sub>2</sub>	-0.442 <sup>c,d</sup>	12.58 <sup>f</sup>	1.18 ± 0.10
p	4-NH <sub>2</sub>	-0.660 <sup>a</sup>	13.96 <sup>f</sup>	0.31 ± 0.02
q	(4-NH <sub>3</sub> <sup>+</sup> )	0.600 <sup>e</sup>		0.31 ± 0.02

<sup>a</sup>From references 20a and b. <sup>b</sup>From reference 20h. <sup>c</sup>Calculated using  $\sigma_{ortho} = 0.65 \times \sigma_{para}$  based on reference 20c. <sup>d</sup>Sum of the corresponding ortho-, meta- and para constants based on reference 20d. <sup>e</sup>From reference 20b. <sup>f</sup>From reference 14e. <sup>g</sup>From reference 20i. <sup>h</sup>From reference 20g. <sup>i</sup>From reference 20j. <sup>j</sup>Calculated using  $pK_a$  values in DMSO from reference 20e and  $pK_a$ (DMSO) to  $pK_a$ (DMF) correlation from reference 14e. <sup>k</sup>Average and standard deviation from 2 or better independent measurements. <sup>l</sup>From 3 independent measurements.

Maran et al.<sup>14e</sup> The reported  $\rho$  values for the Hammett plot of  $pK_a$  of benzoic acid in DMF vs  $\sigma$  constants are -2.36 ( $n = 8$ ) and -2.49 ( $n = 13$ ) from Kolthoff et al. and Bartnicka et al. respectively.<sup>20i,g</sup> In this work we obtained a  $\rho$  value of -2.29 for 16 substituents from a compilation of literature data.

The Hammett plot of  $\log(k_i/k_0)$  versus  $\sigma$  constant, displayed in Figure 4, shows that there is a good correlation between the logarithm of relative rate constants of the substituted benzoic

acids alkylation and the values of  $\sigma$  for most para-substituted benzoic acids. The obtained  $\rho$  Hammett constant reaction value for the data marked with the  $\circ$  symbol is -0.65 ( $n = 8$ ,  $R^2 = 0.995$ ). A  $\rho$  value of -0.92 for alkylation of substituted tetramethylammonium benzoate with iodomethane in acetonitrile has already been reported by Kondo et al. ( $n = 4$ ,  $R^2 = 0.9895$ ).<sup>8d</sup> In DMF as in acetonitrile, the Hammett alkylation constant  $\rho$  is much smaller ( $\rho_{alkylation}^{DMF} = -0.65$ ,  $\rho_{alkylation}^{ACN} = -0.92$ ) than the Hammett ionization constant  $\rho$  ( $\rho_{ionization}^{DMF} = -2.29$ ;  $\rho_{ionization}^{ACN} = -2.49$ ) showing that compensation of solvation effects is taking place during the alkylation. Indeed, during ionization the system is going from neutral to charged benzoate, whereas during alkylation the system is going from localized charge on benzoate anion to delocalized charges in the transition step which leads to a smaller difference in the transition states. The Hammett alkylation constant  $\rho$  is smaller in DMF than in acetonitrile as expected due to the higher reactivity in DMF than in acetonitrile (Table 2).

The quality of the kinetics data pushed us to find a correlation including more substituted benzoic acids. Our first trial was based on using Hammett substituent constant  $\sigma^-$  values<sup>20b</sup> but we found that the nonlinearity was much more pronounced (SI Table S5 and Figure S1). Several correlations based on quantum-calculated descriptors were also investigated and proved to be unsuccessful. Hollingsworth et al.<sup>21a</sup> demonstrated that calculated Löwdin charges are effective parameters for the description of benzoic acids  $pK_a$  values in water. Thus, we tried to use them (SI Table S6) to correlate reaction rate constants using the six substituents included in our set, but they did not yield better linear correlations. Molecular electrostatic potential minimum  $V_{min}$  is another descriptor used to quantify substituent effects in benzene<sup>21b</sup> and benzoic acids.<sup>21c</sup> Again, we observed that some benzoic acids fail to give a well-fitting regression line (SI, Table S7 and Figure S2).

If we look back to the data, Figure 4 shows that outliers can be divided into three groups: bulky halogens (4-I and 4-Br), alkyl substituents (4-Me and 3,4-Me<sub>2</sub>), and benzoic acids bearing two reactive sites (4-NH<sub>2</sub> and 4-OH). Deviation of  $p$ -

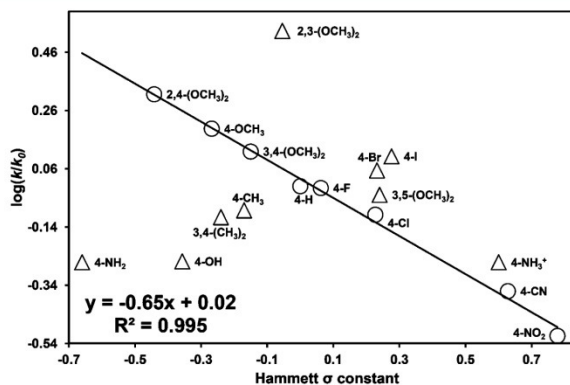


**Figure 4.** Log<sub>10</sub> of the rate constant for the alkylation of benzoic acids by iodomethane versus Hammett substituent constant,  $\sigma$ , in the presence of TMGN and in DMF at 20 °C. Data represented with  $\circ$  symbols are taken into account in the Hammett linear free energy correlation, and  $\Delta$  symbols refer to the outliers.



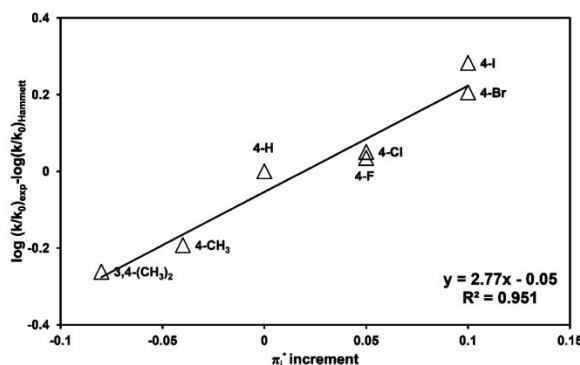


Figure 5. Difference between observed  $\log(k/k_0)$  and predicted  $\log(k/k_0)$  for Hammett correlation outliers versus the Kamlet–Taft  $\pi^*$  parameter substituent incremental values for aromatic compounds.

amino- and hydroxybenzoic acids from normal Hammett behavior has already been reported in the literature. *p*-Aminobenzoic acid may exist as a zwitterion in the solution leading to protonation of the amino site.<sup>22a</sup> When we use  $\sigma_{\text{NH}_3^+}$  instead of  $\sigma_{\text{NH}_2}$ , the point displaces much closer to the fitted straight line (Figure 4). McMahon and Kebarle have shown that in the gas phase the lowest-energy anion derived from *p*-hydroxybenzoic acid appears to be *p*-carboxyphenoxide ion rather than *p*-hydroxybenzoate, because phenoxide ion receives resonance stabilization while no equivalent stabilization by the OH group is available to the *p*-hydroxybenzoate anion.<sup>22b</sup> No methoxy benzoic acid or its methyl ester was detected by GC/MS, but the existence of this *p*-carboxyphenoxide ion in conjugated form is in agreement with the reactivity which is lower than expected from Hammett's correlation of *p*-hydroxybenzoic acid.

A brief survey of the data shows that bulky halogens (4-I, 4-Br) are more reactive and alkyl substituents (4-Me, 3,4-Me<sub>2</sub>) are less reactive than expected. Several authors, such as Herbst and Jacox,<sup>23a</sup> Kochai and Hammond,<sup>23b</sup> Kloosterziel and Backer,<sup>23c</sup> Miron and Hercules,<sup>23d</sup> have already described the abnormal behavior for *p*-methyl-substituted benzene in different reactions that they attribute to the strong sensitivity of the hyperconjugation effect to the solvent. Nagarajan et al. studied the rate of deprotonation of the 2-methyl group in 1,2,3-trimethylpyrazinium ion by benzoates in D<sub>2</sub>O.<sup>23e</sup> They observed a deviation from Bronsted's equation for *o*-halobenzoate which is increasing with the group size, i.e. I > Br > Cl > F. This led us to suspect that these variations may be due to the solvation effects. Bartnicka et al.<sup>20g</sup> showed that the Hammett acidity reaction constant for benzoic acid ionization is well correlated by Kamlet and Taft solvatochromic parameters for the solvent,<sup>24a</sup> with a good confidence for 10 very different solvents:

$$\rho_{\text{ionization}}^{\text{Solvent}} = -(0.898 \pm 0.198)\alpha^{\text{Solvent}} + (0.916 \pm 0.427)\beta^{\text{Solvent}} + (1.790 \pm 0.241)$$

where  $\alpha^{\text{Solvent}}$  and  $\beta^{\text{Solvent}}$  are the Kamlet–Taft parameters which describe respectively the ability of a solvent to donate a proton in a solvent-to-solute hydrogen bond and a measure of

the solvent ability to accept a proton (donate an electron pair) in a solute-to-solvent hydrogen bond.

This equation does not depend on  $\pi^*$  solvent dipolarity/polarizability parameter which measures the ability of the solvent to stabilize a charge or a dipole by virtue of its dielectric effect. The halogen-substituted benzene series have a higher  $\pi^*$  than unsubstituted benzene ( $\pi^* = 0.59$ ), arranged in ascending order of size from fluorine to iodine ( $\pi^*_\text{F} = 0.62$ ,  $\pi^*_\text{Cl} = 0.71$ ,  $\pi^*_\text{Br} = 0.79$ ,  $\pi^*_\text{I} = 0.81$ ), but the  $\pi^*$  values of alkyl substituents are lower than that of unsubstituted benzene ( $\pi^*_\text{Me} = 0.55$ ), whereas their  $\alpha$  and  $\beta$  parameters are nearly constant.<sup>24a</sup> A less complete list of values is available for para-substituted benzoic acid but follows the same trends:  $\pi^*_\text{H} = 0.74$ ,  $\pi^*_\text{Cl} = 0.74$ ,  $\pi^*_\text{Br} = 0.79$ , and  $\pi^*_\text{Me} = 0.70$ .<sup>24a</sup> This variation clearly is in line with our observation that bulky halogens (4-I, 4-Br) are more reactive, and that alkyl substituents (4-Me, 3,4-Me) are less reactive than expected. Figure 5 shows the good correlation obtained for the difference between the observed  $\log(k/k_0)$  and the value  $\log(k/k_0)$  predicted by the Hammett equation using the  $\rho = 0.65$  value we found based on the  $\pi^*$  incremental values calculated according to Hickey et al. tabulated values.<sup>24b</sup> It must be pointed out that between  $\sigma = -0.3$  to  $\sigma = 0.3$ , where the outliers are located, the  $\pi^*$  additive values are correlated to  $\sigma$ , whereas  $V_i/100$ ,  $\alpha$  and  $\beta$  increment are independent (see SI, Figures 8–11). Unfortunately, the Kamlet–Taft parameter substituent incremental values for aromatic compounds are not precise enough; for example, they do not include substituent position, which precludes a quantitative treatment. Such a stabilization of the ground state versus the transition state has been proposed for interpreting the curved Hammett relationship during the reaction of various nucleophiles with substituted aryl benzoates.<sup>25</sup> Clearly the influence of  $\pi^*$  solvent dipolarity/polarizability parameter on the reactivity of benzoic acids reactivity in DMF deserves further studies.

## CONCLUSION

A microfluidic setup based on commercially available devices was developed to study the kinetics of reactions in continuous flow mode, and the results were compared to the results obtained in batch mode. We chose as the model reaction, benzoic acid alkylation by iodomethane in DMF using an organic superbase TMGN for deprotonation because this

reaction is synthetically useful and is a good candidate for physical chemistry correlations. As expected, this reaction follows a very clean second-order kinetics which is preserved up to complete conversion in the continuous flow microreactor. The use of an organic superbase allowed us to try the three possible reagent combinations: (i) benzoic acid + MeI, TMGN; (ii) benzoic acid + TMGN, MeI; but also (iii) TMGN + MeI, benzoic acid, as the proton sponge base is only slowly alkylated in our conditions. The first two combinations exhibited nearly the same kinetics as the batch values, whereas the last one was shown to be very sensitive to residual water. The rate constants for the reaction between different alkylating agents and benzoic acid and in different solvents were also determined. This setup enabled us to study the effect of temperature on this reaction during which the variations of rate constant cover 6 orders of magnitude. The plot of the conversion versus flow rate was found to be linear at all temperatures, which proves that the thermal equilibrium is rapidly established. From this data, energy, enthalpy, and entropy of activation of benzoic acid alkylation by MeI in DMF are estimated to be  $43.1 \text{ kJ}\cdot\text{mol}^{-1}$ ,  $40.2 \text{ kJ}\cdot\text{mol}^{-1}$ , and  $-112.2 \text{ J}\cdot\text{K}^{-1}\cdot\text{mol}^{-1}$ , respectively. The activation parameters obtained in acetonitrile are in agreement with previously published values. Finally, the alkylation kinetics of a series of para-substituted benzoic acids was studied. Their reactivities are well correlated with Hammett reaction constant of  $-0.65$ . The quality of the data allowed us to ascertain the origin of the deviations which were explained using the Kamlet and Taft solvatochromic parameters. It must be pointed out that reaction rates were measured consuming less than  $0.5 \text{ mmol}$  of substrate per condition. The very good correlations obtained for Arrhenius plot and Hammett free energy relationships demonstrate that capillary continuous flow microreactors, well-known for their synthetic application, also provide sound physical chemistry data. These data are now used to develop the selective alkylation of multifunctional natural products in our laboratory.

## EXPERIMENTAL SECTION

**Materials.** All chemicals were in the highest purity available and were used as received without further purification. For some experiments (specified in the text), DMF was dried over  $3 \text{ \AA}$  pore freshly activated molecular sieves.

**Methods.** The high pressure syringe pump (pumping force up to  $1926 \text{ N}$ ) was fitted with two  $8 \text{ mL}$  stainless steel syringes which are driven simultaneously. The two syringes, containing the reagents, are connected via  $0.30 \text{ m}$  capillaries with internal diameter smaller (*i.e.*  $50 \text{ }\mu\text{m}$ ) than the one of the capillary reactor to the micromixer. As micromixer, we utilized a commercially available multilaminating distributive micromixer chip. Capillary reactor internal diameter and length were  $75 \text{ }\mu\text{m}$  and  $300 \text{ cm}$  respectively. In order to provide heating (up to  $70 \text{ }^\circ\text{C}$ ) or cooling (down to  $4 \text{ }^\circ\text{C}$ ) the capillary tubular reactor was immersed in a water bath equipped with a thermostat or an ice/water bath.

For different flow rates,  $240 \text{ }\mu\text{L}$  sample of reaction medium was collected at the outlet of the tubular reactor and quenched in a mixture of  $400 \text{ }\mu\text{L}$  of dichloromethane and  $50 \text{ }\mu\text{L}$  of formic acid. For each flow rate, two samples were taken directly and analyzed independently. A volume of  $30 \text{ }\mu\text{L}$  of the taken sample was diluted by  $400 \text{ }\mu\text{L}$  of iodoanisole in dichloromethane solution. This sample, was later derivatized by  $50 \text{ }\mu\text{L}$  of BSTFA and  $20 \text{ }\mu\text{L}$  of pyridine and was kept overnight for GC/MS analysis. To control the system performance, two internal

standards, 1,3,5-trimethoxybenzene (TMB) and 1,4-dimethoxybenzene (DMB), were dissolved in reagents inlet streams. 4-iodoanisole is another internal standard that was added to the samples to control the analysis, just before being analyzed.

Batch kinetics studies were conducted in a  $10 \text{ mL}$  vial containing the required volume solution of acid and base in DMF. To begin the reaction, a stoichiometric volume of alkylating reagent was injected as rapidly as possible. During the experiments samples of  $240 \text{ }\mu\text{L}$  volume, were withdrawn at different times and were quenched. Quenching medium, dilution and derivatization, as well as the analysis method, were exactly those that were applied in continuous method.

All samples were analyzed on an ion trap mass spectrometer using electron ionization (EI,  $70 \text{ eV}$ ) fitted with a gas chromatograph equipped with a split/splitless injector and an autosampler. Separations were accomplished using a  $60 \text{ m} \times 0.25 \text{ mm}$  column coated with a 5% diphenyl/95% dimethyl polysiloxane film of  $0.50 \text{ }\mu\text{m}$  thickness. Liquid injections of  $1 \text{ }\mu\text{L}$  were introduced into the injector heated at  $250 \text{ }^\circ\text{C}$  with a 50:1 split ratio and a mobile phase (helium) flow rate of  $1 \text{ mL}/\text{min}$ . All analyses were carried out using a linear temperature program from  $50 \text{ }^\circ\text{C}$  to  $250 \text{ }^\circ\text{C}$  at  $10 \text{ }^\circ\text{C}/\text{min}$  followed by a plate at  $250 \text{ }^\circ\text{C}$  for  $10 \text{ min}$ . The mass spectrometer was scanned from  $40$  to  $400 (m/z)$ .

## ASSOCIATED CONTENT

### Supporting Information

Flow rates used in kinetics studies and their corresponding residence times, results of a typical GC/MS quantification experiment and statistical analysis, tables of calculated Löwdin charges and relative  $V_{\text{min}}$  values for different substituted benzoic acids, benzoic acid alkylation by iodomethane rate constant logarithm versus  $\sigma^-$  and  $V_{\text{min}}$ , second-order kinetics plot of benzoic acid alkylation by iodomethane at different temperatures, and plot of Kamlet-Taft  $V_s$ ,  $\alpha$ ,  $\beta$ , and  $\pi^*$  parameter substituent incremental values versus Hammett  $\sigma$  constant. This material is available free of charge via the Internet at <http://pubs.acs.org>.

## AUTHOR INFORMATION

### Corresponding Author

\*Christian.Rolando@univ-lille1.fr

### Notes

The authors declare no competing financial interest.

## ACKNOWLEDGMENTS

The Mass Spectrometry facilities used in this study were funded by the European Community (FEDER), Région Nord-Pas de Calais (France), CNRS, and the Université de Lille 1, Sciences et Technologies. A.G. acknowledges the scholarship by The French Ministry of Foreign affairs. The authors thank Anne-Sophie Lacoste and Geoffrey Vauvy for their technical assistance and Dr. Maria van Aghoven for her help with editing this manuscript.

## REFERENCES

- (1) (a) Yoshida, J.-i.; Kim, H.; Nagaki, A. *ChemSusChem* **2011**, *4*, 331. (b) Mak, X. Y.; Laurino, P.; Seeberger, P. H. *Beilstein J. Org. Chem.* **2009**, *5*. (c) Tanaka, K.; Fukase, K. *Org. Process Res. Dev.* **2009**, *13*, 983. (d) Geyer, K.; Gustafsson, T.; Seeberger, P. H. *Synlett* **2009**, 2382. (e) Wiles, C.; Watts, P. *Chem. Commun.* **2011**, *47*, 6512. (f) Watts, P.; Haswell, S. J. *Chem. Soc. Rev.* **2005**, *34*, 235. (g) Haswell, S. J.; Middleton, R. J.; O'Sullivan, B.; Skelton, V.; Watts, P.; Strying, P.



- Chem. Commun.* **2001**, 391. (h) Jas, G.; Kirschning, A. *Chem.—Eur. J.* **2003**, *9*, 5708.
- (2) (a) Struempel, M.; Ondruschka, B.; Daute, R.; Stark, A. *Green Chem.* **2008**, *10*, 41. (b) Irfan, M.; Glasnov, T. N.; Kappe, C. O. *Org. Lett.* **2011**, *13*, 984. (c) Bartrum, H. E.; Blakemore, D. C.; Moody, C. J.; Hayes, C. J. *Chem.—Eur. J.* **2011**, *17*, 9586. (d) Tomida, Y.; Nagaki, A.; Yoshida, J.-i. *J. Am. Chem. Soc.* **2011**, *133*, 3744. (e) Razzaq, T.; Glasnov, T. N.; Kappe, C. O. *Eur. J. Org. Chem.* **2009**, 1321.
- (3) (a) Ahmed-Omer, B.; Brandt, J. C.; Wirth, T. *Org. Biomol. Chem.* **2007**, *5*, 733. (b) Baumann, M.; Baxendale, I. R.; Brasholz, M.; Hayward, J. J.; Ley, S. V.; Nikbin, N. *Synlett* **2011**, 2011, 1375. (c) Li, P.; Buchwald, S. L. *Angew. Chem.* **2011**, *123*, 6520. (d) Riva, E.; Rencurosi, A.; Gagliardi, S.; Passarella, D.; Martinelli, M. *Chem.—Eur. J.* **2011**, *17*, 6221. (e) Hessel, V.; Kralisch, D.; Krtschil, U. *Energy Environ. Sci.* **2008**, *1*, 467. (f) Mason, B. P.; Price, K. E.; Steinbacher, J. L.; Bogdan, A. R.; McQuade, D. T. *Chem. Rev.* **2007**, *107*, 2300. (g) Wirth, T. *ChemSusChem* **2012**, *5*, 215 and all the articles in this special issue for Flow Chemistry.
- (4) (a) Calabrese, G. S.; Pissavini, S. *AIChE J.* **2011**, *57*, 828. (b) Hessel, V. *Chem. Eng. Technol.* **2009**, *32*, 1655.
- (5) (a) Valera, F. E.; Quaranta, M.; Moran, A.; Blacker, J.; Armstrong, A.; Cabral, J. T.; Blackmond, D. G. *Angew. Chem., Int. Ed.* **2010**, *49*, 2478. (b) Baldyga, J.; Bourne, J. R. *Turbulent Mixing and Chemical Reactions*; Wiley: New York, 1999; p 867. (c) Baldyga, J.; Bourne, J. R.; Walker, B. *Can. J. Chem. Eng.* **1998**, *76*, 641. (d) Dolman, S. J.; Nyrop, J. L.; Kuethe, J. T. *J. Org. Chem.* **2011**, *76*, 993. (e) Koelbl, A.; Kraut, M.; Schubert, K. *AIChE J.* **2008**, *54*, 639.
- (6) (a) Daridon, A.; Sequeira, M.; Pennarun-Thomas, G.; Dirac, H.; Krog, J. P.; Gravesen, P.; Lichtenberg, J.; Diamond, D.; Verpoorte, E.; de Rooij, N. F. *Sens. Actuators, B* **2001**, *87*, 235. (b) Mozharov, S.; Nordon, A.; Littlejohn, D.; Wiles, C.; Watts, P.; Dallin, P.; Girkin, J. M. *J. Am. Chem. Soc.* **2011**, *133*, 3601. (c) Baldwin, R. P.; Roussel, T. J., Jr.; Crain, M. M.; Bathlagunda, V.; Jackson, D. J.; Gullapalli, J.; Conklin, J. A.; Pai, R.; Naber, J. F.; Walsh, K. M.; Keynton, R. S. *Anal. Chem.* **2002**, *74*, 3690. (d) Salmon, J.-B.; Dubroccq, C.; Tabeling, P.; Charier, S.; Alcor, D.; Jullien, L.; Ferrage, F. *Anal. Chem.* **2005**, *77*, 3417. (e) Kerby, M. B.; Legge, R. S.; Tripathi, A. *Anal. Chem.* **2006**, *78*, 8273. (f) Keybl, J.; Jensen, K. F. *Ind. Eng. Chem. Res.* **2011**, *50*, 11013.
- (7) (a) Gisin, B. F. *Helv. Chim. Acta* **1973**, *56*, 1476. (b) Wang, S.-S.; Gisin, B. F.; Winter, D. P.; Makofske, R.; Kulesha, I. D.; Tzougraki, C.; Meienhofer, J. *J. Org. Chem.* **1977**, *42*, 1286. (c) Shaw, J. E.; Kunerth, D. C. *J. Org. Chem.* **1974**, *39*, 1968. (d) Kruizinga, W. H.; Kellogg, R. M. *J. Am. Chem. Soc.* **1981**, *103*, 5183. (e) Hencken, C. P.; Genna, D. T.; Siegler, M. A.; Posner, G. H. *J. Org. Chem.* **2011**, *76*, 5149. (f) Eriksson, J.; Antoni, G.; Langstroem, B. *J. Labelled Compd. Radiopharm.* **2006**, *49*, 1105.
- (8) (a) Kondo, Y.; Fujiwara, T.; Hayashi, A.; Kusabayashi, S.; Takagi, T. *J. Chem. Soc., Perkin Trans. 2* **1990**, 741. (b) Kondo, Y.; Sugitani, W.; Tokui, M.; Takagi, T. *J. Chem. Soc., Perkin Trans. 2* **1995**, 1049. (c) Kondo, Y.; Tsukamoto, T.; Kimura, N. *J. Chem. Soc., Perkin Trans. 2* **1997**, 1765. (d) Kondo, Y.; Urade, M.; Yamanishi, Y.; Chen, X. *J. Chem. Soc., Perkin Trans. 2* **2002**, 1449.
- (9) (a) Ono, N.; Yamada, T.; Saito, T.; Tanaka, K.; Kaji, A. *Bull. Chem. Soc. Jpn.* **1978**, *51*, 2401. (b) Mal, D.; Jana, A.; Ray, S.; Bhattacharya, S.; Patra, A.; De, S. R. *Synth. Commun.* **2008**, *38*, 3937.
- (10) (a) Barton, D. H. R.; Elliott, J. D.; Gero, S. D. *J. Chem. Soc., Perkin Trans. 1* **1982**, 2085. (b) Barton, D. H. R.; Elliott, J. D.; Gero, S. D. *J. Chem. Soc., Chem. Commun.* **1981**, 1136. (c) Ishikawa, T.; Kumamoto, T. *Synthesis* **2006**, 737. (d) Kocienski, P. J.; Brown, R. C. D.; Pommier, A.; Procter, M.; Schmidt, B. *J. Chem. Soc., Perkin Trans. 1* **1998**, 9.
- (11) (a) Bouktaib, M.; Atmani, A.; Rolando, C. *Tetrahedron Lett.* **2002**, *43*, 6263. (b) Bouktaib, M.; Lebrun, S.; Atmani, A.; Rolando, C. *Tetrahedron* **2002**, *58*, 10001. (c) Kajjout, M.; Rolando, C. *Tetrahedron* **2011**, *67*, 4731.
- (12) (a) Alexander, R.; Ko, E. C. F.; Parker, A. J.; Broxton, T. J. *J. Am. Chem. Soc.* **1968**, *90*, 5049. (b) Parker, A. J. *Chem. Rev.* **1969**, *69*, 1.
- (13) (a) Raab, V.; Kipke, J.; Gschwind, R. M.; Sundermeyer, J. *Chem.—Eur. J.* **2002**, *8*, 1682. (b) Alder, R. W.; Bowman, P. S.; Steele, W. R. S.; Winterman, D. R. *Chem. Commun.* **1968**, 723. (c) Alder, R. W.; Goode, N. C. *J. Chem. Soc., Chem. Commun.* **1976**, 108.
- (14) (a) Przybylski, P.; Gierczyk, B.; Schroeder, G.; Zundel, G.; Brzezinski, B.; Bartl, F. *J. Mol. Struct.* **2007**, *844–845*, 157. (b) Novak, I.; Wei, X.; Chin, W. S. *J. Phys. Chem. A* **2001**, *105*, 1783. (c) Ishikawa, T.; Ed. *Superbases for Organic Synthesis: Guanidines, Amidines, Phosphazenes and Related Organocatalysts*; 2009; p 326. (d) Daasbjerg, K. *Acta Chem. Scand.* **1995**, *49*, 878. (e) Maran, F.; Celadon, D.; Severin, M. G.; Vianello, E. *J. Am. Chem. Soc.* **1991**, *113*, 9320.
- (15) (a) Hartman, R. L.; Jensen, K. F. *Lab Chip* **2009**, *9*, 2495. (b) Jaehnisch, K.; Hessel, V.; Loewe, H.; Baerns, M. *Angew. Chem., Int. Ed.* **2004**, *43*, 406. (c) McMullen, J. P.; Jensen, K. F. *Annu. Rev. Anal. Chem.* **2010**, *3*, 19.
- (16) Lin, W.-Y.; Wang, Y.; Wang, S.; Tseng, H.-R. *Nano Today* **2009**, *4*, 470.
- (17) (a) Bessoth, F. G.; deMello, A. J.; Manz, A. *Anal. Commun.* **1999**, *36*, 213. (b) Kakuta, M.; Jayawickrama, D. A.; Wolters, A. M.; Manz, A.; Sweedler, J. V. *Anal. Chem.* **2003**, *75*, 956. (c) Honda, T.; Miyazaki, M.; Nakamura, H.; Maeda, H. *Lab Chip* **2005**, *5*, 812. (d) Nguyen, N.-T.; Wu, Z. *J. Micromech. Microeng.* **2005**, *15*, R1.
- (18) Kockmann, N. *Transport Phenomena in Micro Process Engineering*; Springer: New York, 2008.
- (19) Roberts, D. W.; Schultz, T. W.; Wolf, E. M.; Aptula, A. O. *Chem. Res. Toxicol.* **2010**, *23*, 228.
- (20) (a) Jaffe, H. H. *Chem. Rev.* **1953**, *53*, 191. (b) Hansch, C.; Leo, A.; Taft, R. W. *Chem. Rev.* **1991**, *91*, 165. (c) Beteringhe, A. *Cent. Eur. J. Chem.* **2005**, *3*, 585. (d) Verma, M.; Chaudhry, A. F.; Fahmi, C. J. *Org. Biomol. Chem.* **2009**, *7*, 1536. (e) Exner, O.; Fiedler, P.; Budesinsky, M.; Kulhanek, J. *J. Org. Chem.* **1999**, *64*, 3513. (f) Kolthoff, I. M.; Chantooni, M. K., Jr. *J. Am. Chem. Soc.* **1971**, *93*, 3843. (g) Bartnicka, H.; Bojanowska, I.; Kalinowski, M. K. *Aust. J. Chem.* **1992**, *46*, 31. (h) Seaton, C. C.; Chadwick, K.; Sadiq, G.; Guo, K.; Davey, R. J. *Cryst. Growth Des.* **2009**, *10*, 726. (i) Jover, J.; Bosque, R.; Sales, J. *QSAR Comb. Sci.* **2008**, *27*, 563. (j) Ludwig, M.; Baron, V.; Kalfus, K.; Pytela, O.; Vecera, M. *Collect. Czech. Chem. Commun.* **1986**, *51*, 2135.
- (21) (a) Hollingsworth, C. A.; Seybold, P. G.; Hadad, C. M. *Int. J. Quantum Chem.* **2002**, *90*, 1396. (b) Suresh, C. H.; Gadre, S. R. *J. Phys. Chem. A* **2007**, *111*, 710. (c) Sayyed, F. B.; Suresh, C. H. *New J. Chem.* **2009**, *33*, 2465.
- (22) (a) Wiberg, K. B. *J. Org. Chem.* **2002**, *67*, 4787. (b) McMahon, T. B.; Keparle, P. *J. Am. Chem. Soc.* **1977**, *99*, 2222.
- (23) (a) Herbst, R. L., Jr.; Jacox, M. E. *J. Am. Chem. Soc.* **1952**, *74*, 3004. (b) Hammond, G. S.; Reeder, C. E.; Fang, F. T.; Kochi, J. K. *J. Am. Chem. Soc.* **1958**, *80*, 568. (c) Kloosterziel, H.; Backer, H. J. *J. Am. Chem. Soc.* **1952**, *74*, 5806. (d) Miron, R. R.; Hercules, D. M. *Anal. Chem.* **1961**, *33*, 1770. (e) Nagarajan, K.; Lee, T. W. S.; Perkins, R. R.; Stewart, R. *Can. J. Chem.* **1986**, *64*, 1090.
- (24) (a) Kamlet, M. J.; Doherty, R. M.; Abraham, M. H.; Marcus, Y.; Taft, R. W. *J. Phys. Chem.* **1988**, *92*, 5244. (b) Hickey, J. P.; Passino-Reader, D. R. *Environ. Sci. Technol.* **1991**, *25*, 1753.
- (25) Um, L.-H.; Han, H.-J.; Ahn, J.-A.; Kang, S.; Buncel, E. *J. Org. Chem.* **2002**, *67*, 8475.

## COMMUNICATION

Cite this: DOI: 10.1039/c0xx00000x

www.rsc.org/xxxxxx

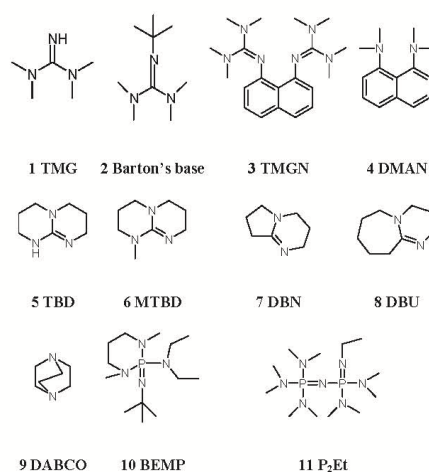
Kinetics screening of the *N*-alkylation of organic superbases using a continuous flow microfluidic device: basicity versus nucleophilicityAzarmidokht Gholamipour-Shirazi<sup>a</sup> and Christian Rolando<sup>a,\*</sup>

Received (in XXX, XXX) Xth XXXXXXXXX 20XX, Accepted Xth XXXXXXXXX 20XX

DOI: 10.1039/b000000x

We describe here the determination of the alkylation rate of a set of organic superbases by iodomethane in DMF using a microfluidic continuous flow reactor. Surprisingly,  $\text{Log } k_{\text{Alkylation}}$  follows the inverse trend of  $\text{p}K_{\text{BH}^+}$  of the base. Mayr's equation allows a more quantitative approach. From a synthetic point of view, TMGN and BEMP are demonstrated to be the best choices.

Organic superbases and proton sponges<sup>1</sup> are playing an increasingly important role in organic chemistry since they lead to soluble ion-pairs that avoid the formation of aggregates commonly generated by lithium bases in apolar solvents.<sup>2,3</sup> New organic superbases are still being developed and they have already found new application fields.<sup>4,5</sup> They are the best choices for reactions conducted in microsystems with micron-scale dimensions since the solution must remain homogeneous.<sup>6</sup> In order to be useful in an alkylating reaction, the product of the equilibrium constant of an organic superbase with the reacting acidic substrate multiplied by the reaction rate with the alkylating reagent must be higher than the superbase's own alkylation rate with the alkylating reagent. Elsewhere, the base is alkylated instead of the substrate. This criterion implies both a high basicity and a low nucleophilicity for the organic superbase. The basicity of organic superbases and proton sponges in an aprotic solvent like acetonitrile has received considerable attention.<sup>7-9</sup> Their  $\text{p}K_{\text{BH}^+}$  can be predicted using DFT theoretical calculation.<sup>8</sup> However, their alkylation rate has received much less attention especially in dipolar aprotic solvents such as *N,N'*-dimethylformamide (DMF) used for the synthesis of polar organic natural compounds like polyphenol metabolites.<sup>10</sup> In this paper, we determine the alkylation rate of some of the most commonly used organic superbases **1-11** (Scheme 1) by iodomethane in DMF. The investigated organic superbases and proton sponges encompass six chemical families: guanidine **1** TMG, **2** Barton's base, cyclic guanidines **5** TBD, **6** MTBD



**Scheme 1** Structure of the studied compounds: **2** Barton's Base: 2-tert-butyl-1,1,3,3-tetramethylguanidine; **10** BEMP: 2-tert-butylimino-2-diethylamino-1,3-dimethylperhydro-1,3,2-diazaphosphorine; **9** DABCO: 1,4-diazabicyclo[2.2.2]octane; **7** DBN: 1,5-diazabicyclo[4.3.0]non-5-ene; **8** DBU: 1,8-diazabicyclo[5.4.0]undec-7-ene; **4** DMAN: 1,8-bis(dimethylamino)naphthalene; **6** MTBD: 7-methyl-1,5,7-triazabicyclo[4.4.0]dec-5-ene, **11** P<sub>2</sub>Et: 1-ethyl-2,2,4,4,4-pentakis(dimethylamino)-2λ<sup>5</sup>,4λ<sup>5</sup>-catenadi(phosphazene); **5** TBD: 1,5,7-triazabicyclo[4.4.0]dec-5-ene; **1** TMG: 1,1,3,3-tetramethylguanidine; **3** TMGN: *N,N''''*-1,8-naphthalenediylbis[*N,N,N',N'*-tetramethyl]guanidine.

amidine **7** DBN, **8** DBU, strained bicyclic diamine **9** DABCO, proton sponge 1,8-bis(dimethylamino)naphthalene **4** DMAN and its combination with guanidine in **3** TMGN, and finally phosphazenes **10** BEMP, **11** P<sub>2</sub>Et. The kinetics studies were carried out in a continuous flow microfluidic device,<sup>11,12</sup> which is shown in Fig. 1 and was made from readily available and commercially items. The set-up is composed of a high pressure syringe pump delivering two streams of liquid at the same rate to

<sup>a</sup> USR CNRS 3290, Miniaturisation pour la Synthèse, l'Analyse et la Protéomique and FR CNRS 2638 Michel-Engène Chevreul, Université de Lille 1, Sciences et Technologies, 59655 Villeneuve d'Ascq, France  
Fax: +33 (0)3 20 33 61 36; Tel: +33 (0)3 20 43 49 77;

<sup>45</sup> E-mail: christian.rolando@univ-lille1.fr

## COMMUNICATION

**Table 1**  $pK_{BH^+}$  in acetonitrile, calculated  $pK_{BH^+}$  in DMF, calculated, measured kinetic rate constant for the alkylation by MeI in DMF, estimated nucleophilicity parameter for bases 1-11.

Base	Acronym	Initial concentration <sup>a</sup> (mM)	$pK_{BH^+}$ in acetonitrile	$pK_{BH^+}$ in DMF, calculated <sup>13</sup>	$k_{Alkylation}$ ( $mol^{-1}.L. s^{-1}$ )	Nucleophilicity parameter
1	TMG	458.3	23.3 <sup>b</sup>	14.7-15.8	$1.7 \pm 1.0 \times 10^{-2}$ <sup>hi</sup>	12.7
2	Barton's base	478.2	23.56 <sup>c</sup>	14.9-16.0	$1.4 \pm 0.4 \times 10^{-2}$	12.5
3	TMGN	155.4	25.10 <sup>d</sup>	16.4-17.5	$1.2 \pm 0.01 \times 10^{-4}$	7.8
4	DMAN	46.1	18.18 <sup>b</sup>	9.9-10.8	No reaction	-
5	TBD	5.5	25.98 <sup>e</sup>	17.2-18.4	$2.5 \pm 1.0$ <sup>hi</sup>	17.6
6	MTBD	470.1	24.70 <sup>c</sup>	16.0-17.1	$4.8 \pm 0.9 \times 10^{-2}$	13.7
7	DBN	46.0	23.79 <sup>he</sup>	15.2-16.3	$5.5 \pm 1.2 \times 10^{-1}$	16.1 <sup>i</sup>
8	DBU	46.8	24.33 <sup>he</sup>	15.7-16.8	$2.5 \pm 0.1 \times 10^{-1}$	15.3 <sup>i</sup>
9	DABCO	46.3	18.29 <sup>f</sup>	10.0-10.9	$8.3 \pm 1.0$	18.8 <sup>j</sup>
10	BEMP	46.3	27.63 <sup>c</sup>	18.8-20.0	$8.0 \pm 1.6 \times 10^{-4}$	9.7
11	P <sub>2</sub> Ft	4.6	32.8 <sup>g</sup>	23.6-25.0	$72 \pm 12$	20.9

<sup>a</sup>Concentration at the exit the nanomixer, half of the concentration in the syringe.  $pK_{BH^+}$  values: <sup>b</sup> from reference<sup>1</sup>; <sup>c</sup> from reference<sup>14</sup>; <sup>d</sup> from reference<sup>15</sup>; <sup>e</sup> from reference<sup>16</sup>; <sup>f</sup> from reference<sup>17</sup>; <sup>g</sup> from reference<sup>18</sup>. <sup>h</sup>Second alkylation rate  $k_{Second\ alkylation}$  (1, TMG) =  $2.2 \times 10^{-2} mol^{-1}.L. s^{-1}$ ,  $k_{Second\ alkylation}$  (5, TBD) =  $1.6 \times 10^{-2} mol^{-1}.L. s^{-1}$ . <sup>i</sup>Base overall consumption rate including protonation:  $k_{Overall}$  (1, TMG) =  $3.3 \pm 1.3 \times 10^{-2}$ ,  $k_{Overall}$  (5, TBD) =  $3.9 \pm 1.9$ . <sup>j</sup>Nucleophilicity parameters from reference<sup>19</sup>.

a micromixer, in order to minimize the mixing time, followed by a fused silica-based capillary tubular reactor.<sup>20</sup>

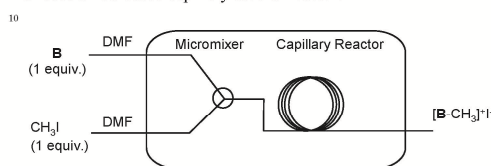


**Fig 1** Experimental set-up. It comprises of a micromixer and a fused silica-based capillary tubular reactor.

For each compound we ran several preliminary experiments in order to optimize the initial and final yield in order to cover the largest possible scale. For reaching this purpose we modified the initial concentration of the base and the residence time range by modifying the capillary length and diameter and choosing the best suited micromixer. The capillary tubular reactor was kept in a water bath at 20°C. The mixing time within the two micromixers was in the order of 1 ms. At this scale, continuous flow and batch processes lead to the same results but using a microfluidic device allows a more precise control of the reaction parameters and especially of the reaction time which may be as low as two seconds.<sup>21</sup> Table S1 in ESI displays the utilized flow rates and their corresponding residence time for bases 1-11.

The reaction rates of organic superbases 1-11 with iodomethane in DMF were determined by monitoring the relative concentrations of the protonated organic base and its methylated product after quenching the reaction by dilution by electrospray

mass spectrometry (ESI-MS) using off-line infusion introduction. During the reaction the sum of the ionic current of the base and the alkylated products remained constant which shows that these species have the same response factor (ESI Table S2 for base 6 MTBD). For each base 8 to 10 residence times were analyzed. The conversion factor  $f$  is defined as the ratio of the alkylated base intensity to the sum of the protonated base and the alkylated base intensities. The values of  $k$  were determined graphically by plotting the function  $1/(1-f)$ , against residence time ( $t$ ) which resulted in a straight line with a slope equal to  $k[B]_0$ , where  $[B]_0$  is the initial concentration of superbase. We observed this straight line relationship in every case, except in the case of the two bases bearing a labile hydrogen on a nitrogen atom 1 TMG and 5 TBD.

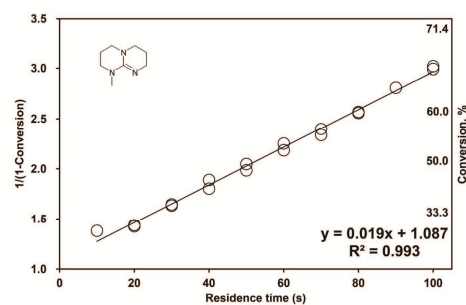


**Fig 2** Plot  $1/(1-f)$  versus residence time for 6 MTBD.



An example of such a plot is given in Fig. 2 for MTBD and for the other bases the plot are presented in Fig. S1 to S8 in the ESI. This plot shows that these reactions follow, as expected, a clean second-order kinetics as shown by the intercept close to 1.0 and the very good linear regression. All the kinetics were studied up to a high conversion ranging from 30% to up to 79% except for **3** TMGN and **10** BEMP (8 and 18% respectively), for which the conversion is limited by the solubility of the base, which demonstrates that the second order law is well obeyed (ESI, Table S3). By varying the residence time from 2.0 to  $7.2 \times 10^3$  s (Table S1) and the concentration from 0.47 to  $4.6 \times 10^{-3}$  mol.L<sup>-1</sup>, we measured rate constants over 5 orders of magnitudes with this set-up (Table 1).

The two bases **1** TMG and **5** TBD in the base set bearing a labile hydrogen on a nitrogen atom deserve a special discussion. The protonated base [TMG + H]<sup>+</sup> and both mono- [TMG + Me]<sup>+</sup>, and di-alkylated [TMG + 2 Me]<sup>+</sup> products of **1**TMG were detected in the mass spectrum at m/z 116.1, m/z 130.1 and m/z 144.2 for their monoisotopic peaks respectively. For bicyclic guanidine **5** TBD both mono- and dialkylated products were also observed at m/z 116.1, m/z 130.1 and m/z 144.2. The observation of the singly charged form of the dimethylated product is due to the loss of a proton in the electrospray Taylor cone.<sup>22</sup> As the protonated alkylated base cannot be alkylated, a supplementary proton transfer step from the alkylated base to the base must take place in order to explain the presence of the dialkylated product which decreases the base availability. Unfortunately mass spectrometry does not give access to the protonated base concentration but to the sum of the base and the protonated base. The pK<sub>BH<sup>+</sup></sub> of pentamethylguanidine in acetonitrile is equal to 25.0 leading to a calculated pK<sub>BH<sup>+</sup></sub> in DMF ranging from 16.3-17.4 (see below for the correlation equations).<sup>8</sup> Pentamethylguanidine **12** is therefore much more basic than the initial base **1** TMG (pK<sub>BH<sup>+</sup></sub> (DMF) = 14.7-15.8) by approximately one order of magnitude. The opposite is true for **5** TBD which is more basic than its methylation product **6** MTBD (pK<sub>BH<sup>+</sup></sub> (DMF) = 17.2-18.4 and 16.0-17.1 respectively). Numerical simulations based on these assumptions gave a very good fit to the experimental values for **5** TBD but for **1** TMG the best fit was obtained with a smaller difference between the basicities between **1** TMG and **12** pentamethylguanidine (ESI Fig. 9 and 10). This difference may be due to the location of the proton on the imine function for **1** TMG and on the amine for **5** TBD. For **1** TMG and **5** TBD the rate constant values given in Table 1 are the monoalkylation rates which are important for the discussions on reactivity. In the footnotes, we give the overall base disappearance rates, which are important for practical purposes, as well as the second alkylation rate leading to the dialkylated product. For **1** TMG the second alkylation rate is higher than the first one and the opposite was found for **5** TBD. The second alkylation rate found for **5** TBD is of the same order of magnitude as the alkylation rate of **6** MTBD which shows the consistency of the data treatment.

Among guanidine bases, **2** Barton's base has a slightly lower methylation rate than the first alkylation rate of **1** TMG due to its steric hindrance.<sup>23</sup> A reaction half-life of less than 5 minutes was reported for the alkylation of a 0.5 mol.L<sup>-1</sup> solution of **2** Barton's base in CDCl<sub>3</sub> by three equivalents of iodomethane at room temperature, using <sup>1</sup>H NMR.<sup>23</sup> From this data we can estimate a

second-order rate constant of  $3.3 \times 10^{-2}$  mol<sup>-1</sup>.L.s<sup>-1</sup>. Using only one equivalent of iodomethane in DMF, we found a slightly slower reaction rate constant of  $1.4 \pm 0.4 \times 10^{-2}$  mol<sup>-1</sup>.L.s<sup>-1</sup>. The previously observed higher reaction rate may be attributed to a warmer temperature inside the NMR probe. The proton sponge **4** DMAN was reported to not react with iodoethane in acetonitrile after four days at reflux.<sup>24</sup> **4** DMAN reacts only with methyl fluorosulphate in carefully controlled conditions.<sup>25</sup> A weak signal corresponding to [DMAN + Me]<sup>+</sup> was observed on the mass spectrum but the alkylation was ruled out using CD<sub>3</sub>I, for which no signal was observed in agreement with previously published results. The guanidine proton sponge **3** TMGN was reported to react with 2.5 equivalents of iodoethane per guanidine function (5 equ. per **3** TMGN molecule) in deuterated dichloromethane (CD<sub>2</sub>Cl<sub>2</sub>), resulting in a mixture of protonated and alkylated products after three days.<sup>15</sup> In the set-up used in this paper, **3** TMGN was alkylated up to 8% at a residence time of 70 min leading to a half-life of eight hours at the concentration of 0.16 M. No dimethylation was observed in our conditions at ambient temperature.<sup>26</sup> The conversion for **3** TMGN was limited by its solubility in DMF and the maximum residence time in the microsystem. We performed batch reaction (ESI Table S4, entry a) up to 11 hours and a conversion of 30%, and a kinetic under first order conditions using 10 equivalents of iodomethane (Table S4, entry d) which both gave the same rate constant. We also check the absence of reaction due to residual water we reported previously for this reaction by adding molecular sieves to the DMF solution and by using a 3 times higher concentration (Table S4 entries b,c). **6** MTBD has a much slower kinetics constant than **5** TBD ( $k = 4.8 \pm 0.9 \times 10^{-2}$  and  $k = 2.5 \times 10^{-1}$  mol<sup>-1</sup>.L. s<sup>-1</sup> respectively). As it is expected that in both cases alkylation takes place on the imine nitrogen, crowding by the methyl group on the amine or by the planarity of the two methyl groups in alkylated **6** MTBD may explain the lower reactivity of MTBD compared to TBD. A reaction half-life of 15 min was reported for MTBD **6** in the same conditions as mentioned just above for TMGN (deuterated dichloromethane, CD<sub>2</sub>Cl<sub>2</sub>). From these data we can estimate the second order constant to be  $1.1 \times 10^{-3}$  mol<sup>-1</sup>.L.s<sup>-1</sup>. Here again the rate constant that we found in DMF ( $k = 4.8 \pm 0.89 \times 10^{-2}$  mol<sup>-1</sup>.L. s<sup>-1</sup>) is, as expected, higher than in deuterated dichloromethane (CD<sub>2</sub>Cl<sub>2</sub>). For **7** DBN a reaction half-life of less than 2 minutes was reported for a 0.5 mol.L<sup>-1</sup> solution containing three equivalents of iodomethane at room temperature in CDCl<sub>3</sub>.<sup>23</sup> From these data we may estimate the second order rate constant to be  $1.5 \times 10^{-2}$  mol<sup>-1</sup>.L.s<sup>-1</sup>. As expected this value is also smaller here than the rate constant we found using DMF as a solvent ( $k = 5.5 \pm 1.2 \times 10^{-1}$ ). In the group of phosphazenes, **10** BEMP is much less nucleophilic than **11** P<sub>2</sub>Et. The reaction rate we observed is not due to the hydrolysis of **11** P<sub>2</sub>Et in our conditions since the formation of [P<sub>2</sub>Et + Me]<sup>+</sup> at m/z 354.3 was observed in the mass spectrum. The steric hindrance shown by **10** BEMP is so significant that it is the second less reactive base just behind **3** TMGN, except for **4** DMAN.

In a second step we tried to correlate alkylation rates with the pK<sub>BH<sup>+</sup></sub> of the base. Since very few pK<sub>BH<sup>+</sup></sub> values in DMF have been reported in the literature, pK<sub>BH<sup>+</sup></sub> values in DMF were obtained from pK<sub>BH<sup>+</sup></sub> data in acetonitrile using the following

equations for benzenesulfonylamides and phenols and carboxylic acids which provide a bracketing for the correlation.<sup>13</sup>

$$pK_a(\text{DMF}) = -6.82 + 0.97pK_a(\text{ACN})$$

$$pK_a(\text{DMF}) = -7.20 + 0.94pK_a(\text{ACN})$$

The interaction of a sterically hindered organic base with a proton is well known to be different than its interaction with an alkylating agent. Due to its small size and its electron deficiency, a proton is able to approach the protonation site of the base, while the alkylating agent attack is blocked.<sup>27</sup> However, a general trend may be observed in Figure 3 between  $\log(k)$  and  $pK_{\text{BH}^+}$  in DMF. Very uncannily, the general trend is that more basic the base the less nucleophilic they are. The cyclic guanidine **5** TBD bearing a labile hydrogen is more reactive than what might be expected from its basicity whereas its structural methylated analogue **6** MTBD has the expected reactivity. On the other hand DMAN **4** (not represented on the figure due to its lack of reactivity) and **3** TMGN are less reactive than expected. The strongest exception to this trend is phosphazene **11** P<sub>2</sub>Et which has by far a too high reactivity according to its basicity for a guanidine base. From a synthetic point of view two bases are particularly interesting for their high  $pK_{\text{BH}^+}$  associated with a low chemical reactivity: **3** TMGN and **10** BEMP. The proton sponge **4** DMAN ( $pK_{\text{BH}^+} = 9.9$ - $10.8$ ) is not basic enough for most applications since it is barely able to deprotonate benzoic acids ( $pK_a(\text{DMF}) = 10.6, 12.3, 12.8$  for *para*-nitro, unsubstituted, and *para*-methoxy respectively) and not at all capable to deprotonate phenols ( $pK_a(\text{DMF}) = 18.0$  for phenol itself).

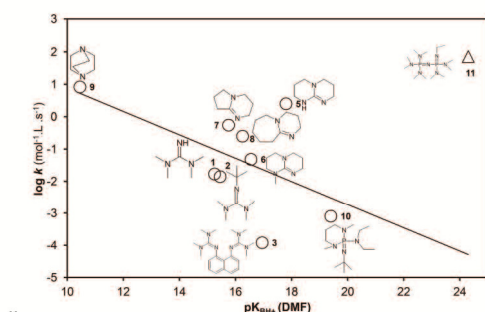


Fig 3 Plot of  $\log k$  and  $pK_a$  for bases 1-11. Correlation line is obtained by least square fitting using all data marked by a circle.

In the last and third step we quantified the nucleophilicity of the investigated bases. Baidya and Mayr have reported the nucleophilicity of **7** DBN, **8** DBU and **9** DABCO using a set of benzhydrylium ions (diarylcarbenium ions) as reference electrophiles.<sup>19</sup> They have found that their reaction rates increase in the series as  $\mathbf{8} < \mathbf{7} < \mathbf{9}$ . We found the same trend in our experiments based on methylation rates. The methylation rates we obtained for bases **7**, **8**, and **9** are very well fitted using the complete Mayr's equation<sup>27,28</sup> as shown in Figure S11:

$$\log k_{20^\circ\text{C}}^{\text{Base 1-11, MeI}} = s_E^{\text{MeI}} s_N^{\text{alkylation}} (N^{\text{Base 1-11}} + E^{\text{MeI}})$$

Using  $s_N^{\text{alkylation 7,8,9}} = 0.67, 0.70$  and  $0.70$  and  $N^{\text{Base 7,8,9}} = 16.28, 15.29$  and  $18.80$  respectively for base alkylation by benzhydrylium from Baidya et al.<sup>19</sup> By adjusting the correlation between experimental data and Mayr's equation we obtained  $s_E^{\text{MeI}} s_N^{\text{alkylation}} = 0.44$  and  $E^{\text{MeI}} = -16.6$  (slope = 1.0,  $R^2 = 0.996$ ). Assuming that  $s_N^{\text{alkylation}}$  is constant for the series of base **1-11** and taking the average value from base **7**, **8**, **9**  $s_N^{\text{alkylation}} = \frac{1}{3} \sum s_N^{\text{alkylation 7,8,9}} = 0.69$  we obtained  $s_E^{\text{MeI}} = 0.64$ . To the best of our knowledge there is no tabulated value for  $s_E$  parameter and this parameter has been the object of a recent debate between Mayr's and Bentley's groups.<sup>29, 30</sup> For strong electrophiles like carbocations, Mayr's assumption is that  $s_E^{\text{Carbocation}} = 1.00$ . However values higher than 1 and up to 1.5 are given by Bentley's group for the Michael addition of carbanion to quinone methide and other strong Michael acceptors.<sup>31</sup> By retreating the data presented in Pearson et al.<sup>32</sup> for the alkylation of various *N* and *O* nucleophiles by MeI in methanol according to the full Mayr's equation we obtained (excluding P(OMe)<sub>3</sub> data)  $s_E^{\text{MeI}} = 0.57$  and  $E^{\text{MeI}} = -22.8$ . The  $s_E^{\text{MeI}}$  is close to our value if we consider the very different system used. The lower  $E^{\text{MeI}}$  value ( $E_{\text{MeOH}}^{\text{MeI}} = -22.8$  compared to  $E_{\text{DMF}}^{\text{MeI}} = -16.6$ ) is easily explained by the higher reactivity in DMF compared to methanol. The  $E_{\text{DMF}}^{\text{MeI}}$  value for MeI is much lower than the corresponding value for benzhydrylium ions (-7 to -10) or Michael acceptors (-10 to -13).<sup>33</sup> From this correlation the nucleophilicity parameters for the bases which are not tabulated in the Mayr's database have been evaluated. The value of  $N^{\text{Base}}$  varies from 7.8 for **3** TMGN to more than 20 for **11** P<sub>2</sub>Et (Table 1).

In summary, a microfluidic set-up based on readily available materials was used to investigate the kinetics of the alkylation of several organic superbases by iodomethane through flow method in synthetic conditions using DMF as a solvent. The alkylation of the base was ascertained and followed by ESI mass spectrometry. These organic bases include a set of the most used organic bases including guanidine, 1,8-diaminonaphthalene and guanidine based proton sponges, bicyclic guanidines, amidines and phosphazenes. The determined rate constants cover six orders of magnitude and are well fitted by the Mayr's equation for the tabulated bases. From our data we found an estimated  $E$  value of -16.6 for MeI and the  $N$  parameters for the studied bases. Unusually when the base strength increases its nucleophilicity decreases expect for the phosphazene **11** P<sub>2</sub>Et. From a synthetic point of view the crowded bis-guanidine **3** TMGN and the phosphazene **10** BEMP are the most interesting bases due to their low alkylation rates associated with their high basicity. This study may be extended easily to other alkylating agents and to other solvents.

## Acknowledgments

The Mass Spectrometry facilities used in this study were funded by the European Community (FEDER), Région Nord-Pas de Calais (France), CNRS, and the Université de Lille 1, Sciences et Technologies. AG acknowledges the scholarship by The French Ministry of Foreign affairs. The Authors thank Anne-Sophie

Lacoste and Geoffrey Vauvy for their technical assistance and Dr. Maria van Aghoven for her help with editing this manuscript. The Authors thank the Referees for their fruitful comments and especially for their helpful remarks on Mayr's equation.

### Notes and references

† Electronic Supplementary Information (ESI) available: experimental protocol, table with capillary reactor diameter and length, residence times in function of flow rates, kinetics curve for each base and correlation with Mayr's equation. See DOI: 10.1039/b000000x/

1. T. Ishikawa, *Superbases for Organic Synthesis: Guanidines, Amidines, Phosphazenes and Related Organocatalysts*, Wiley, 2009.
2. I. Keresztes and P. G. Williard, *J. Am. Chem. Soc.*, 2000, 122, 10228-10229.
3. L. M. Pratt, A. Newman, J. St. Cyr, H. Johnson, B. Miles, A. Lattier, E. Austin, S. Henderson, B. Hershey, M. Lin, Y. Balamraju, L. Sammonds, J. Chermic, J. Karnes, E. Hymel, B. Woodford and C. Carter, *J. Org. Chem.*, 2003, 68, 6387-6391.
4. V. Raab, E. Gauchenova, A. Merkoulov, K. Harms, J. Sundermeyer, B. Kovacevic and Z. B. Maksic, *J. Am. Chem. Soc.*, 2005, 127, 15738-15743.
5. F. Matsumura, N. Oka and T. Wada, *Org. Lett.*, 2008, 10, 5297-5300.
6. S. L. Poe, M. A. Cummings, M. P. Haaf and D. T. McQuade, *Angew. Chem., Int. Ed. Engl.*, 2006, 45, 1544-1548.
7. A. A. Kolomeitsev, I. A. Koppel, T. Rodima, J. Barten, E. Lork, G.-V. Roeschenthaler, I. Kaljurand, A. Kuett, I. Koppel, V. Mäemets and I. Leito, *J. Am. Chem. Soc.*, 2005, 127, 17656-17666.
8. B. Kovacevic and Z. B. Maksic, *Org. Lett.*, 2001, 3, 1523-1526.
9. T. Rodima, I. Kaljurand, A. Pihl, V. Mäemets, I. Leito and I. A. Koppel, *J. Org. Chem.*, 2002, 67, 1873-1881.
10. C. Cren-Olive, S. Lebrun and C. Rolando, *J. Chem. Soc., Perkin Trans. 1*, 2002, 821-830.
11. B. Ahmed-Omer, J. C. Brandt and T. Wirth, *Org. Biomol. Chem.*, 2007, 5, 733-740.
12. K. Geyer, T. Gustafsson and P. H. Seeberger, *Synlett*, 2009, 2382-2391.
13. K. Daasbjerg, *Acta Chem. Scand.*, 1995, 49, 878-887.
14. M. Stanczyk-Dunaj and A. Jarczewski, *Pol. J. Chem.*, 2005, 79, 1025-1032.
15. V. Raab, J. Kipke, R. M. Gschwind and J. Sundermeyer, *Chem. Eur. J.*, 2002, 8, 1682-1693.
16. I. Novak, X. Wei and W. S. Chin, *J. Phys. Chem. A*, 2001, 105, 1783-1788.
17. A. Streitwieser and Y.-J. Kim, *J. Am. Chem. Soc.*, 2000, 122, 11783-11786.
18. G. Schroeder, B. Brzezinski, D. Podebski and E. Grech, *J. Mol. Struct.*, 1997, 416, 11-19.
19. M. Baidya and H. Mayr, *Chem. Commun.*, 2008, 1792-1794.
20. A. Gholamipour-Shirazi and C. Rolando, *Org. Process Res. Dev.*, 2012, 16, 811-818.
21. F. E. Valera, M. Quaranta, A. Moran, J. Blacker, A. Armstrong, J. T. Cabral and D. G. Blackmond, *Angew. Chem., Int. Ed. Engl.*, 2010, 49, 2478-2485.
22. F. Charbonnier, L. Berthelot and C. Rolando, *Anal. Chem.*, 1999, 71, 1585-1591.
23. D. H. R. Barton, J. D. Elliott and S. D. Gero, *J. Chem. Soc., Chem. Commun.*, 1981, 1136-1137.
24. R. W. Alder, P. S. Bowman, W. R. S. Steele and D. R. Winterman, *Chem. Commun.*, 1968, 723-724.
25. R. W. Alder and N. C. Goode, *Chem. Commun.*, 1976, 108-109.
26. M. A. Povalyakhina, A. S. Antonov, O. V. Dyablo, V. A. Ozeryanskii and A. F. Pozharskii, *J. Org. Chem.*, 2011, 76, 7157-7166.
27. H. Mayr and A. R. Ofial, *Angew. Chem., Int. Ed. Engl.*, 2006, 45, 1844-1854.
28. T. B. Phan, M. Breugst and H. Mayr, *Angew. Chem., Int. Ed. Engl.*, 2006, 45, 3869-3874.
29. H. Mayr, *Angew. Chem., Int. Ed. Engl.*, 2011, 50, 3612-3618.
30. T. W. Bentley, *Angew. Chem., Int. Ed. Engl.*, 2011, 50, 3608-3611.
31. T. W. Bentley, *J. Phys. Org. Chem.*, 2011, 24, 282-291.
32. R. G. Pearson, H. R. Sobel and J. Songstad, *J. Amer. Chem. Soc.*, 1968, 90, 319-326.
33. M. Baidya, S. Kobayashi, F. Brotzel, U. Schmidhammer, E. Riedle and H. Mayr, *Angew. Chem., Int. Ed. Engl.*, 2007, 46, 6176-6179.



## Identification of the Methylation Site of 1,8-Bis(Tetramethylguanidino)Naphthalene (TMGN) by Multinuclear $^1\text{H}$ , $^{13}\text{C}$ , $^{15}\text{N}$ Magnetic Resonance Spectroscopy

Azarmidokht Gholamipour-shirazi,<sup>[a,c]</sup> Xavier Trivelli,<sup>[b,d]</sup> and Christian Rolando<sup>\*[a,c,d]</sup>

**Keywords:** TMGN / *N*-Alkylation / Superbase / Multinuclear Magnetic Resonance Spectroscopy

1,8-Bis(tetramethylguanidino)naphthalene (TMGN) is an organic superbase conceived by combining the skeleton of 1,8-dimethylaminonaphthalene (DMAN) proton sponge and the highly basic *N,N,N',N',N''*-pentamethylguanidine motif. TMGN exhibits the best compromise between basicity and non nucleophilicity and has found several uses in organic, inorganic and analytical chemistry. We recently show that TMGN is slowly alkylated by methyl iodide in DMF. Whereas guanidines are well known to be

alkylated on their imine site, it is no easy to predict the alkylation site in TMGN as the two imine sites are conjugated leading to a lower reactivity and furthermore very crowded due to the 1,8-diaminonaphthalene skeleton. This paper described the identification of the alkylation site of TMGN using  $^1\text{H}$ ,  $^{13}\text{C}$ ,  $^{15}\text{N}$  magnetic resonance spectroscopy which was found to occur on the imine nitrogens of TMGN.

- [a] USR CNRS 3290, Miniaturisation pour la Synthèse, l'Analyse et la Protéomique, Université de Lille 1, Sciences et Technologies, 59655 Villeneuve d'Ascq, France  
Fax: +33 (0)3 20 33 61 36  
E-mail: Christian.Rolando@univ-lille1.fr
- [b] UMR 8576, Unité de Glycobiologie Structurale et Fonctionnelle, Université de Lille 1, Sciences et Technologies, 59655 Villeneuve d'Ascq, France
- [c] FR CNRS 2638, Institut Michel Chevreul, Université de Lille 1, Sciences et Technologies, 59655 Villeneuve d'Ascq, France
- [d] IFR 147, Protéomique, Modifications Post-Traductionnelles et Glycobiologie, Université de Lille 1, Sciences et Technologies, 59655 Villeneuve d'Ascq, France  
Supporting information for this article is available on the WWW under <http://www.eurjoc.org/> or from the author.

Cao et al. employed TMGN as the matrix for the quantitative detection of acidic perfluorinated compounds in environmental water samples by MALDI-TOF-MS.<sup>[6]</sup> Besides achieving high sensitivity, they have obtained clear spectra without any matrix ions interference. Our interest in TMGN and its alkylation arose during the kinetic studies of the alkylation by iodomethane of substituted benzoic acids deprotonated by TMGN in DMF. We used TMGN as it allows studying the three possible reagents combination: (i) benzoic acid and TMGN, MeI; (ii) benzoic acid and MeI, TMGN; but also (iii) b TMGN and MeI, benzoic acid. We observed that in this last condition TMGN is slowly alkylated.<sup>[7]</sup> We extended this study to ten strong organic bases and we found that TMGN has the best compromise between basicity and alkylation rate.<sup>[8]</sup>

### Introduction

1,8-Bis(tetramethylguanidino)naphthalene (*N,N,N',N',N''*-1,8-naphthalenediylbis[*N,N,N',N'*-tetramethyl]-guanidine), abbreviated as TMGN, was conceived by Raab and co-workers by combining the proton sponge skeleton of 1,8-dimethylaminonaphthalene (DMAN), with the highly basic *N,N,N',N',N''*-pentamethylguanidine (PMG).<sup>[1]</sup> It represents one of the most basic guanidine with a  $\text{pK}_a$  of 25.1 in acetonitrile.<sup>[2]</sup> By comparison the  $\text{pK}$  value for 2,8-dimethylaminonaphthalene (DMAN) is only 18.2 but reaches 25.0 for pentamethylguanidine also in acetonitrile.<sup>[2]</sup> The high basicity of TMGN is explained by the unfavourable nonbonded repulsions in the initial base, the large proton affinity of guanidine group and the strong intramolecular hydrogen bond present in the protonated species.<sup>[3]</sup>

TMGN has already been used for several purposes in organic, inorganic and analytical chemistry. Schilf, W. et al reported that TMGN can remove the proton from the intramolecular hydrogen bond in case of 5-nitrosalicylaldehyde and isopropyl amine derivative.<sup>[4]</sup> However DMAN appeared to be not strong enough to remove this proton. Lemaire et al have developed a new method to synthesize [ $^{18}\text{F}$ ]-fluorodeoxyglucose (FDG) using a variety of different organic bases.<sup>[5]</sup> Using these bases make their method suitable to be implemented in microreactors and microfluidics chips. They reported a yield of 87% while using TMGN as base.

The structure of TMGN as well as the structure of its mono-protonated and di-protonated derivatives has been studied and reported by  $^1\text{H}$  NMR.<sup>[1]</sup> Its proton accepting properties has also been studied extensively by  $^{13}\text{C}$  NMR, FT-IR and ESI MS spectroscopy.<sup>[9]</sup> Also, its transition metal complex has already been synthesized and its structure has comprehensively been investigated by  $^1\text{H}$ NMR.<sup>[10]</sup> Whereas guanidines are well known to be alkylated on their imine site, it is no easy to predict the alkylation site in TMGN as the two imine sites are conjugated leading to a lower reactivity and furthermore very crowded due to the 1,8-diaminonaphthalene skeleton. In the present work we report a multinuclear  $^1\text{H}$ ,  $^{13}\text{C}$ ,  $^{15}\text{N}$  magnetic resonance investigation for the alkylation product obtained by reacting TMGN with  $\text{CH}_3\text{I}$  in 1:1 ratio in  $[\text{D}_6]\text{DMSO}$  at room temperature.

### Results and Discussion

Preliminary studies by MS-MS spectroscopy demonstrated that TMGN is alkylated by iodomethane and its protonated base  $[\text{TMGN} + \text{H}]^+$  and its mono-alkylated  $[\text{TMGN} + \text{Me}]$  were detected in the mass spectrum at  $m/z$  355.4 and  $m/z$  369.4 for their monoisotopic peaks respectively. No di-alkylated product was observed.

## 12 BIBLIOGRAPHY

1. Geyer, K., T. Gustafsson, and P.H. Seeberger, *Developing continuous-flow microreactors as tools for synthetic chemists*. *Synlett* 2009(15): p. 2382-2391.
2. Yoshida, J.-i., H. Kim, and A. Nagaki, *Green and Sustainable Chemical Synthesis Using Flow Microreactors*. *ChemSusChem*. **4**(3): p. 331-340.
3. Mak, X.Y., P. Laurino, and P.H. Seeberger, *Asymmetric reactions in continuous flow*. *Beilstein J. Org. Chem.*, 2009. **5**: p. No 19, No pp given.
4. Tanaka, K. and K. Fukase, *Renaissance of Traditional Organic Reactions under Microfluidic Conditions: A New Paradigm for Natural Products Synthesis*. *Org. Process Res. Dev.*, 2009. **13**(5): p. 983-990.
5. Wiles, C. and P. Watts, *Recent advances in micro reaction technology*. *Chem. Commun. (Cambridge, U. K.)*. **47**(23): p. 6512-6535.
6. Watts, P. and S.J. Haswell, *The application of micro reactors for organic synthesis*. *Chem. Soc. Rev.*, 2005. **34**(3): p. 235-246.
7. Haswell, S.J., et al., *The application of micro reactors to synthetic chemistry*. *Chem. Commun. (Cambridge, U. K.)*, 2001(5): p. 391-398.
8. Jas, G. and A. Kirschning, *Continuous flow techniques in organic synthesis*. *Chem.--Eur. J.*, 2003. **9**(23): p. 5708-5723.
9. Struempel, M., et al., *Making diazomethane accessible for R&D and industry: generation and direct conversion in a continuous micro-reactor set-up*. *Green Chem.*, 2008. **10**(1): p. 41-43.
10. Irfan, M., T.N. Glasnov, and C.O. Kappe, *Continuous Flow Ozonolysis in a Laboratory Scale Reactor*. *Org. Lett.* **13**(5): p. 984-987.
11. Bartrum, H.E., et al., *Rapid Access to alpha-Alkoxy and alpha-Amino Acid Derivatives through Safe Continuous-Flow Generation of Diazoesters*. *Chem.--Eur. J.* **17**(35): p. 9586-9589.
12. Tomida, Y., A. Nagaki, and J.-i. Yoshida, *Asymmetric carbolithiation of conjugated enynes: a flow microreactor enables the use of configurationally unstable intermediates before they epimerize*. *J. Am. Chem. Soc.* **133**(11): p. 3744-3747.
13. Razzaq, T., T.N. Glasnov, and C.O. Kappe, *Continuous-flow microreactor chemistry under high-temperature/pressure conditions*. *Eur. J. Org. Chem.*, 2009(9): p. 1321-1325.
14. Ahmed-Omer, B., J.C. Brandt, and T. Wirth, *Advanced organic synthesis using microreactor technology*. *Org. Biomol. Chem.*, 2007. **5**(5): p. 733-740.
15. Whitesides, G.M. and A.D. Stroock, *Flexible methods for microfluidics*. *Phys. Today*, 2001. **54**(6): p. 42-48.
16. Kaneda, S. and T. Fujii, *Integrated microfluidic systems*. *Adv. Biochem. Eng./Biotechnol.* **119**(Nano/Micro Biotechnology): p. 179-194.
17. Hartman, R.L. and K.F. Jensen, *Microchemical systems for continuous-flow synthesis*. *Lab Chip*, 2009. **9**(17): p. 2495-2507.
18. Zimmerman, W.B., *Electrochemical microfluidics*. *Chem. Eng. Sci.* **66**(7): p. 1412-1425.
19. Lion, N., et al., *Microfluidic systems in proteomics*. *Electrophoresis*, 2003. **24**(21): p. 3533-3562.
20. Nguyen, N.-T., *Micromixers - Fundamentals, Design and Fabrication*. 2008: William Andrew Publishing.

21. Roberge, D.M., et al., *Microreactor technology: a revolution for the fine chemical and pharmaceutical industries?* Chem. Eng. Technol., 2005. **28**(3): p. 318-323.
22. Pennemann, H., et al., *Benchmarking of Microreactor Applications*. Org. Process Res. Dev., 2004. **8**(3): p. 422-439.
23. Mason, B.P., et al., *Greener Approaches to Organic Synthesis Using Microreactor Technology*. Chem. Rev. (Washington, DC, U. S.), 2007. **107**(6): p. 2300-2318.
24. Kiwi-Minsker, L. and A. Renken, *Microstructured reactors for catalytic reactions*. Catal. Today, 2005. **110**(1-2): p. 2-14.
25. Valera, F.E., et al., *The Flow's the Thing...Or Is It? Assessing the Merits of Homogeneous Reactions in Flask and Flow*. Angew. Chem., Int. Ed. **49**(14): p. 2478-2485, S2478/1-S2478/5.
26. Calabrese, G.S. and S. Pissavini, *From batch to continuous flow processing in chemicals manufacturing*. AIChE J. **57**(4): p. 828-834.
27. Hessel, V., D. Kralisch, and U. Krtischil, *Sustainability through green processing - novel process windows intensify micro and milli process technologies*. Energy Environ. Sci., 2008. **1**(4): p. 467-478.
28. Hessel, V., *Novel Process Windows - Gate to Maximizing Process Intensification via Flow Chemistry*. Chem. Eng. Technol., 2009. **32**(11): p. 1655-1681.
29. Mills, P.L., D.J. Quiram, and J.F. Ryley, *Microreactor technology and process miniaturization for catalytic reactions-A perspective on recent developments and emerging technologies*. Chem. Eng. Sci., 2007. **62**(24): p. 6992-7010.
30. Sun, P., et al., *Continuous production of biodiesel from high acid value oils in microstructured reactor by acid-catalyzed reactions*. Chem. Eng. J. (Amsterdam, Neth.), 2010. **162**(1): p. 364-370.
31. Struempel, M., B. Ondruschka, and A. Stark, *Continuous Production of the Diazomethane Precursor N-Methyl-N-nitroso-p-toluenesulfonamide: Batch Optimization and Transfer into a Microreactor Setup*. Org. Process Res. Dev., 2009. **13**(5): p. 1014-1021.
32. Kulkarni, A.A., et al., *Miniaturized Systems for Homogeneously and Heterogeneously Catalyzed Liquid-Phase Esterification Reaction*. Ind. Eng. Chem. Res., 2007. **46**(16): p. 5271-5277.
33. Yao, X., et al., *Fast Esterification of Acetic Acid with Short Chain Alcohols in Microchannel Reactor*. Catal. Lett., 2009. **132**(1-2): p. 147-152.
34. Brivio, M., et al., *Surface effects in the esterification of 1-pyrenebutyric acid within a glass micro reactor*. Chem. Commun. (Cambridge, U. K.), 2003(15): p. 1924-1925.
35. Wiles, C., et al., *Solution phase synthesis of esters within a micro reactor*. Tetrahedron, 2003. **59**(51): p. 10173-10179.
36. Cummings, E.B., et al., *Conditions for Similitude between the Fluid Velocity and Electric Field in Electroosmotic Flow*. Anal. Chem., 2000. **72**(11): p. 2526-2532.
37. McMullen, J.P. and K.F. Jensen, *Integrated microreactors for reaction automation: new approaches to reaction development*. Annu. Rev. Anal. Chem. **3**: p. 19-42.
38. Arnaut, L., S. Formosinho, and H. Burrows, *Chemical Kinetics: From Molecular Structure to Chemical Reactivity* 2007: Elsevier.
39. Connors, K.A., *Chemical Kinetics. The Study of Reaction Rates in Solution*. 1990. 480 pp.
40. McMullen, J.P. and K.F. Jensen, *Rapid Determination of Reaction Kinetics with an Automated Microfluidic System*. Org. Process Res. Dev. **15**(2): p. 398-407.
41. Tirronen, E. and T. Salmi, *Process development in the fine chemical industry*. Chem. Eng. J. (Amsterdam, Neth.), 2003. **91**(2-3): p. 103-114.

42. Helfferich, F.G., *Kinetics of Homogeneous Multistep Reactions*. 2001. 426 pp.
43. Wojciechowski, B.W. and N.M. Rice, *Experimental Methods in Kinetic Studies, Revised Edition*. 2003. No pp given.
44. Bringer, M.R., et al., *Microfluidic systems for chemical kinetics that rely on chaotic mixing in droplets*. Philos. Trans. R. Soc. London, Ser. A, 2004. **362**(1818): p. 1087-1104.
45. Daridon, A., et al., *Chemical sensing using an integrated microfluidic system based on the Berthelot reaction*. Sens. Actuators, B, 2001. **B76**(1-3): p. 235-243.
46. Song, H. and R.F. Ismagilov, *Millisecond kinetics on a microfluidic chip using nanoliters of reagents*. J. Am. Chem. Soc., 2003. **125**(47): p. 14613-14619.
47. Wensink, H., et al., *Measuring reaction kinetics in a lab-on-a-chip by microcoil NMR*. Lab Chip, 2005. **5**(3): p. 280-284.
48. Kerby, M.B., R.S. Legge, and A. Tripathi, *Measurements of Kinetic Parameters in a Microfluidic Reactor*. Anal. Chem., 2006. **78**(24): p. 8273-8280.
49. Kang, L., et al., *Microfluidics for drug discovery and development: From target selection to product lifecycle management*. Drug Discovery Today, 2008. **13**(1/2): p. 1-13.
50. Wells, P.R., *Linear Free Energy Relationships*. Chemical Reviews, 1963. **63**(2): p. 171-219.
51. Williams, A., *Free Energy Relationships in Organic and Bio-Organic Chemistry*. 2003. 297 pp.
52. Haslam, E., *Recent developments in methods for the esterification and protection of the carboxyl group*. Tetrahedron, 1980. **36**(17): p. 2409-33.
53. Gisin, B.F., *Preparation of Merrifield resins through total esterification with cesium salts*. Helv. Chim. Acta, 1973. **56**(5): p. 1476-82.
54. Wang, S.-S., et al., *Facile synthesis of amino acid and peptide esters under mild conditions via cesium salts*. J. Org. Chem., 1977. **42**(8): p. 1286-90.
55. Shaw, J.E. and D.C. Kunerth, *Quantitative conversion of carboxylic acids and phenols to esters and ethers by reaction of their salts with alkyl halides*. J. Org. Chem., 1974. **39**(13): p. 1968-70.
56. Kruizinga, W.H. and R.M. Kellogg, *Preparation of macrocyclic lactones by ring closure of cesium carboxylates*. J. Am. Chem. Soc., 1981. **103**(17): p. 5183-9.
57. Hencken, C.P., et al., *Highly stereocontrolled and regiocontrolled syntheses of 2,3,4-trisubstituted alkanoates and lactones*. J. Org. Chem. **76**(12): p. 5149-5155.
58. Eriksson, J., G. Antoni, and B. Langstroem, *Synthesis of [1-11C]propyl and [1-11C]butyl iodide from [11C]carbon monoxide and their use in alkylation reactions*. J. Labelled Compd. Radiopharm., 2006. **49**(12): p. 1105-1116.
59. Kondo, Y., et al., *Relative reactivity of methyl iodide to ethyl iodide in nucleophilic substitution reactions in acetonitrile and partial desolvation accompanying activation*. J. Chem. Soc., Perkin Trans. 2, 2002(8): p. 1449-1454.
60. Kondo, Y., et al., *Solvation of carboxylate ions and of transition-state anions for the reaction of carboxylate ion with ethyl iodide in acetonitrile-methanol mixtures. Thermodynamic and quantum mechanical approaches*. J. Chem. Soc., Perkin Trans. 2, 1995(6): p. 1049-54.
61. Kondo, Y., et al., *Nucleophilic substitution reactions of aliphatic and aromatic carboxylate ions with ethyl iodide. Specific interactions and isokinetic relationships in acetonitrile-methanol mixtures*. J. Chem. Soc., Perkin Trans. 2, 1990(5): p. 741-6.
62. Ishikawa, T. and T. Kumamoto, *Guanidines in organic synthesis*. Synthesis, 2006(5): p. 737-752.

63. Loupy, A., M. Pedoussaut, and J. Sansoulet, *Solid-liquid phase-transfer catalysis without solvent: mild and efficient conditions for saponifications and preparations of hindered esters*. J. Org. Chem., 1986. **51**(5): p. 740-2.
64. Ono, N., et al., *A convenient procedure for esterification of carboxylic acids*. Bull. Chem. Soc. Jpn., 1978. **51**(8): p. 2401-4.
65. Mal, D., et al., *DBU-CH<sub>3</sub>I, a potential substitute for CH<sub>2</sub>N<sub>2</sub> in the preparation of methyl esters and methyl aryl ethers. Studies with assorted acids*. Synth. Commun., 2008. **38**(22): p. 3937-3946.
66. Barton, D.H.R., J.D. Elliott, and S.D. Gero, *Synthesis and properties of a series of sterically hindered guanidine bases*. J. Chem. Soc., Perkin Trans. 1, 1982(9): p. 2085-90.
67. Barton, D.H.R., J.D. Elliott, and S.D. Gero, *The synthesis and properties of a series of strong but hindered organic bases*. J. Chem. Soc., Chem. Commun., 1981(21): p. 1136-7.
68. Kocienski, P.J., et al., *Synthesis of salinomycin*. J. Chem. Soc., Perkin Trans. 1, 1998(1): p. 9-40.
69. Alexander, R., et al., *Solvation of ions. XIV. Protic-dipolar aprotic solvent effects on rates of bimolecular reactions. Solvent activity coefficients of reactants and transition states at 25.deg*. J. Amer. Chem. Soc., 1968. **90**(19): p. 5049-69.
70. Parker, A.J., *Protic-dipolar aprotic solvent effects on rates of bimolecular reactions*. Chem. Rev., 1969. **69**(1): p. 1-32.
71. Maran, F., et al., *Electrochemical determination of the pK<sub>a</sub> of weak acids in N,N-dimethylformamide*. J. Am. Chem. Soc., 1991. **113**(24): p. 9320-9.
72. Raab, V., et al., *1,8-bis(tetramethylguanidino)naphthalene (TMGN): a new, superbasic and kinetically active "proton sponge"*. Chem.-Eur. J., 2002. **8**(7): p. 1682-1693.
73. Daasbjerg, K., *Estimation of the pK<sub>a</sub> for some hydrocarbons and aldehydes and solvation energies of the corresponding anions*. Acta Chem. Scand., 1995. **49**(12): p. 878-87.
74. Kockmann, N., *Transport Phenomena in Micro Process Engineering Heat and Mass Transfer 2008*: Springer.
75. Jarczewski, A. and C.D. Hubbard, *A review of proton transfer reactions between various carbon-acids and amine bases in aprotic solvents*. J. Mol. Struct., 2003. **649**(3): p. 287-307.
76. Ogg, R.A., Jr., *Hydrolysis of methyl iodide*. J. Am. Chem. Soc., 1938. **60**: p. 2000-1.
77. Cau Dit Coumes, C., J. Chopin-Dumas, and F. Devisme, *Kinetics of the Reaction of Methyl Iodide with Hydroxylamine in an Aqueous Solution within the Framework of Nuclear Spent Fuel Reprocessing*. Ind. Eng. Chem. Res., 2001. **40**(17): p. 3721-3731.
78. Kondo, Y., T. Tsukamoto, and N. Kimura, *Reaction enthalpy of nucleophilic substitution of ethyl iodide in acetonitrile and its mechanistic significance*. J. Chem. Soc., Perkin Trans. 2, 1997(9): p. 1765-1769.
79. Roberts, D.W., et al., *Experimental Reactivity Parameters for Toxicity Modeling: Application to the Acute Aquatic Toxicity of SN<sub>2</sub> Electrophiles to Tetrahymena pyriformis*. Chemical Research in Toxicology, 2009. **23**(1): p. 228-234.
80. Ogg, R.A., *The Mechanism of the Decomposition of Ethylene Iodide*. J. Am. Chem. Soc., 1936. **58**(4): p. 607-609.
81. Iredale, T. and L.W.O. Martin, *The Thermal Decomposition of Gaseous Ethylene Iodide*. The Journal of Physical Chemistry, 1934. **38**(3): p. 365-376.

82. Hanessian, S., D. Delorme, and Y. Dufresne, *Mild cleavage of methoxymethyl (MOM) ethers with trimethylsilyl bromide*. Tetrahedron Letters, 1984. **25**(24): p. 2515-2518.
83. Jaffe, H.H., *A re-overdot.examination of the Hammett equation*. Chem. Rev. (Washington, DC, U. S.), 1953. **53**: p. 191-261.
84. Jover, J., R. Bosque, and J. Sales, *QSPR prediction of pKa for benzoic acids in different solvents*. QSAR Comb. Sci., 2008. **27**(5): p. 563-581.
85. Bartnicka, H., I. Bojanowska, and M.K. Kalinowski, *Solvent effect on the Hammett reaction constant of substituted benzoic acids*. Aust. J. Chem., 1992. **46**(1): p. 31-6.
86. Seaton, C.C., et al., *Designing Acid/Acid Co-Crystals through the Application of Hammett Substituent Constants*. Cryst. Growth Des. **10**(2): p. 726-733.
87. Ludwig, M., et al., *Solvent effects of dissociation of weak acids. IV. Dissociation constants of substituted benzoic acids in water and in organic solvents*. Collect. Czech. Chem. Commun., 1986. **51**(10): p. 2135-42.
88. Exner, O., et al., *Conformation and Steric Effects in Mono- and Dimethoxybenzoic Acids*. J. Org. Chem., 1999. **64**(10): p. 3513-3518.
89. Verma, M., A.F. Chaudhry, and C.J. Fahrni, *Predicting the photoinduced electron transfer thermodynamics in polyfluorinated 1,3,5-triarylpyrazolines based on multiple linear free energy relationships*. Org. Biomol. Chem., 2009. **7**(8): p. 1536-1546.
90. Beteringhe, A., *QSPR study on pKa values of N-methoxy-polynitroaniline derivatives*. Cent. Eur. J. Chem., 2005. **3**(4): p. 585-591.
91. Hansch, C., A. Leo, and R.W. Taft, *A survey of Hammett substituent constants and resonance and field parameters*. Chem. Rev., 1991. **91**(2): p. 165-95.
92. Hollingsworth, C.A., P.G. Seybold, and C.M. Hadad, *Substituent effects on the electronic structure and pKa of benzoic acid*. Int. J. Quantum Chem., 2002. **90**(4/5): p. 1396-1403.
93. Suresh, C.H. and S.R. Gadre, *Electrostatic Potential Minimum of the Aromatic Ring as a Measure of Substituent Constant*. J. Phys. Chem. A, 2007. **111**(4): p. 710-714.
94. Sayyed, F.B. and C.H. Suresh, *Quantification of substituent effects using molecular electrostatic potentials: Additive nature and proximity effects*. New J. Chem., 2009. **33**(12): p. 2465-2471.
95. Naray-Szabo, G. and G.G. Ferenczy, *Molecular Electrostatics*. Chem. Rev. (Washington, D. C.), 1995. **95**(4): p. 829-47.
96. Miron, R.R. and D.M. Hercules, *Behavior of substituted aromatic acids in selected non-aqueous solvents*. Anal. Chem., 1961. **33**: p. 1770-4.
97. Nagarajan, K., et al., *Steric activation in prototropic reactions of pyrazine derivatives. II. The Broensted relation*. Can. J. Chem., 1986. **64**(6): p. 1090-2.
98. Kamlet, M.J., et al., *Linear solvation energy relationship. 46. An improved equation for correlation and prediction of octanol/water partition coefficients of organic nonelectrolytes (including strong hydrogen bond donor solutes)*. The Journal of Physical Chemistry, 1988. **92**(18): p. 5244-5255.
99. Wiberg, K.B., *Substituent Effects on the Acidity of Weak Acids. 2. Calculated Gas-Phase Acidities of Substituted Benzoic Acids*. J. Org. Chem., 2002. **67**(14): p. 4787-4794.
100. McMahan, T.B. and P. Kebarle, *Intrinsic acidities of substituted phenols and benzoic acids determined by gas-phase proton-transfer equilibria*. J. Am. Chem. Soc., 1977. **99**(7): p. 2222-30.

101. Kolthoff, I.M. and M.K. Chantooni, Jr., *Substituent effects on dissociation of benzoic acids and heteroconjugation of benzoates with p-bromophenol in acetonitrile, N,N-dimethylformamide, and dimethyl sulfoxide. Intramolecular hydrogen bonding in o-hydroxybenzoic acids and their anions.* J. Amer. Chem. Soc., 1971. **93**(16): p. 3843-9.
102. Uggerud, E., *Nucleophilicity-periodic trends and connection to basicity.* Chem.--Eur. J., 2006. **12**(4): p. 1127-1136.
103. Jaramillo, P., P. Perez, and P. Fuentealba, *Relationship between basicity and nucleophilicity.* J. Phys. Org. Chem., 2007. **20**(12): p. 1050-1057.
104. Bordwell, F.G. and D.L. Hughes, *Direct relationship between nucleophilicity and basicity in SN2 reactions of fluorenyl anions with benzyl chloride in dimethyl sulfoxide solution.* J. Org. Chem., 1980. **45**(16): p. 3314-20.
105. Cieplak, A.S., *Parabolic Relationship between the Basicity of the Nucleophile and  $\tilde{\epsilon}$ -Face Selection in Addition of the Substituted Acetylide Ions to Cyclohexanone and Cyclohexanethione.* J. Org. Chem., 1998. **63**(3): p. 521-530.
106. Edwards, J.O. and R.G. Pearson, *The factors determining nucleophilic reactivities.* J. Am. Chem. Soc., 1962. **84**(1): p. 16-24.
107. Novak, I., X. Wei, and W.S. Chin, *Electronic Structures of Very Strong, Neutral Bases.* J. Phys. Chem. A, 2001. **105**(10): p. 1783-1788.
108. Schroeder, G., et al., *Proton transfer reactions from dimethyl (4-nitrophenyl)malonate to N-bases in acetonitrile.* J. Mol. Struct., 1996. **384**(2-3): p. 127-133.
109. Otera, J., *Esterification: Methods, Reactions and Applications.* 2003. 450 pp.
110. Vlasov, V.M. and I.A. Os'kina, *Basicity and Nucleophilicity of Aryl-Containing N-Anions.* Russ. J. Org. Chem., 2002. **38**(12): p. 1705-1718.
111. Chopra, A.B. and A.P. Murray, *Nucleophilicity vs Basicity in the Reaction of Sodium tert-Butoxide with  $\hat{I}^2$ -Stannyl Ketones.* Organometallics, 2001. **20**(7): p. 1476-1478.
112. Gierczyk, B., G. Schroeder, and B. Brzezinski, *Reaction of Some Strong N-Bases with Chloropentafluorobenzene in the Presence of Water Molecules.* J. Org. Chem., 2003. **68**(8): p. 3139-3144.
113. Ishikawa, T. and Editor, *Superbases for Organic Synthesis: Guanidines, Amidines, Phosphazenes and Related Organocatalysts.* 2009. 326 pp.
114. Stanczyk-Dunaj, M. and A. Jarczewski, *Homoconjugation of some organic bases in acetonitrile.* Pol. J. Chem., 2005. **79**(6): p. 1025-1032.
115. Streitwieser, A. and Y.-J. Kim, *Ion Pair Basicity of Some Amines in THF: Implications for Ion Pair Acidity Scales.* J. Am. Chem. Soc., 2000. **122**(48): p. 11783-11786.
116. Schroeder, G., et al., *Proton transfer reactions from N-H acid [5,10,15,20-tetrakis(pentafluorophenyl)-21-H, 23-H-porphyrin] to strong bases in acetonitrile.* J. Mol. Struct., 1997. **416**(1-3): p. 11-19.
117. Sommer, H.Z., H.I. Lipp, and L.L. Jackson, *Alkylation of amines. General exhaustive alkylation method for the synthesis of quaternary ammonium compounds.* J. Org. Chem., 1971. **36**(6): p. 824-8.
118. Schuchardt, U., R.M. Vargas, and G. Gelbard, *Alkylguanidines as catalysts for the transesterification of rapeseed oil.* J. Mol. Catal. A: Chem., 1995. **99**(2): p. 65-70.
119. Whitney, R.A., et al., *Cross-Linking of Brominated Poly(isobutylene-co-isoprene) by N-Alkylation of the Amidine Bases DBU and DBN.* Macromolecules, 2005. **38**(11): p. 4625-4629.



120. Baidya, M. and H. Mayr, *Nucleophilicities and carbon basicities of DBU and DBN*. Chem. Commun. (Cambridge, U. K.), 2008(15): p. 1792-1794.
121. Wiberg, K.B., R.F.W. Bader, and C.D.H. Lau, *Theoretical analysis of hydrocarbon properties. 2. Additivity of group properties and the origin of strain energy*. J. Am. Chem. Soc., 1987. **109**(4): p. 1001-12.
122. Ferguson, L.N., *Ring strain and reactivity of alicycles*. Journal of Chemical Education, 1970. **47**(1): p. 46-null.
123. Schuchardt, U., R. Sercheli, and R.M. Vargas, *Transesterification of vegetable oils: a review*. J. Braz. Chem. Soc., 1998. **9**(3): p. 199-210.
124. Przybylski, P., et al., *Spectroscopic and PM5 semiempirical studies of the proton accepting properties of 1,8-bis(tetramethylguanidino)naphthalene*. J. Mol. Struct., 2007. **844-845**: p. 157-165.
125. Wild, U., et al., *The first metal complexes of the proton sponge 1,8-bis(N,N,N',N'-tetramethylguanidino)naphthalene: syntheses and properties*. Eur. J. Inorg. Chem., 2008(28): p. 4440-4447.
126. Wishart, D.S., et al., *<sup>1</sup>H, <sup>13</sup>C and <sup>15</sup>N chemical shift referencing in biomolecular NMR*. J. Biomol. NMR, 1995. **6**(2): p. 135-40.
127. Kovacevic, B. and Z.B. Maksic, *The proton affinity of the superbase 1,8-bis(tetramethylguanidino)naphthalene (TMGN) and some related compounds: a theoretical study*. Chem.--Eur. J., 2002. **8**(7): p. 1694-1702.
128. Wiench, J.W., et al., *Two amidine derivatives studied by <sup>1</sup>H, <sup>13</sup>C, <sup>14</sup>N, <sup>15</sup>N NMR and GIAO-CHF calculations*. J. Chem. Soc., Perkin Trans. 2, 1999(4): p. 885-890.
129. Webb, G.A. and Editor, *Nuclear Magnetic Resonance. [In: Nucl. Magn. Reson., 2008; 37]*. 2008. 356 pp.
130. Sibi, M.P. and R.L. Lichter, *Nitrogen-15 nuclear magnetic resonance spectroscopy. Natural-abundance nitrogen-15 chemical shifts of ring-methylated N,N-dimethylanilines. Effect of inhibition of conjugation*. J. Org. Chem., 1977. **42**(18): p. 2999-3004.
131. Witanowski, M., et al., *Nitrogen NMR Spectroscopy*, in *Annual Reports on NMR Spectroscopy*. 1982, Academic Press. p. 1-486.
132. Cohen, Y., L. Avram, and L. Frish, *Diffusion NMR spectroscopy in supramolecular and combinatorial chemistry: An old parameter - new insights*. Angew. Chem., Int. Ed., 2005. **44**(4): p. 520-554.
133. Stejskal, E.O. and J.E. Tanner, *Spin diffusion measurements: spin echoes in the presence of a time-dependent field gradient*. J. Chem. Phys., 1965. **42**(1): p. 288-92.
134. Fournial, A.-G., *Contributions des techniques de RMN avancées à la déformulation de systèmes fluides complexes*, in *Ecole Doctorale Biologie Santé*. 2008, Université de Lille 2: Lille.
135. Wu, D., A. Chen, and C.S. Johnson, Jr., *An improved diffusion-ordered spectroscopy experiment incorporating bipolar-gradient pulses*. J. Magn. Reson., Ser. A, 1995. **115**(2): p. 260-4.
136. Kavakka, J.S., et al., *Enhanced chromatographic NMR with polyethyleneglycol. A novel resolving agent for diffusion ordered spectroscopy*. Magn. Reson. Chem. **48**(10): p. 777-781.
137. Delgado, J.M.P.Q., *Molecular diffusion coefficients of organic compounds in water at different temperatures*. J. Phase Equilib. Diffus., 2007. **28**(5): p. 427-432.
138. Oda, H., M. Kishida, and C. Yokokawa, *Adsorption of benzoic acid and phenol from aqueous solution by activated carbons--effect of surface acidity*. Carbon, 1981. **19**(4): p. 243-248.



139. Sanecki, P.T. and P.M. Skital, *The electroreduction of alkyl iodides and polyiodides: The kinetic model of EC(C)E and ECE-EC(C)E mechanisms with included transfer coefficient variability*. *Electrochimica Acta*, 2007. **52**(14): p. 4675-4684.
140. Pandey, J.D., R. Dey, and B. Datt Bhatt, *Estimation of molecular radius of liquids and liquid mixtures from sound velocity*. *J. Mol. Liq.*, 2004. **111**(1-3): p. 67-71.
141. Kramer, T., R. Schweins, and K. Huber, *Coil Dimensions of Polystyrene Chains in Colloid-Polymer Mixtures at the Protein Limit: A SANS Study*. *Macromolecules*, 2005. **38**(23): p. 9783-9793.
142. Bazito, F.F.C., Y. Kawano, and R.M. Torresi, *Synthesis and characterization of two ionic liquids with emphasis on their chemical stability towards metallic lithium*. *Electrochimica Acta*, 2007. **52**(23): p. 6427-6437.
143. McMullen, J.P. and K.F. Jensen, *An Automated Microfluidic System for Online Optimization in Chemical Synthesis*. *Org. Process Res. Dev.* **14**(5): p. 1169-1176.
144. Lin, W.-Y., et al., *Integrated microfluidic reactors*. *Nano Today*, 2009. **4**(6): p. 470-481.
145. Palmieri, A., et al., *A microfluidic flow chemistry platform for organic synthesis: the Hofmann rearrangement*. *Tetrahedron Lett.*, 2009. **50**(26): p. 3287-3289.
146. Geyer, K., J.D.C. Codee, and P.H. Seeberger, *Microreactors as tools for synthetic chemists - the chemists' round-bottomed flask of the 21st century?* *Chem.--Eur. J.*, 2006. **12**(33): p. 8434-8442.
147. Mattila, P., J. Hellstroem, and R. Toerroenen, *Phenolic Acids in Berries, Fruits, and Beverages*. *J. Agric. Food Chem.*, 2006. **54**(19): p. 7193-7199.
148. Robbins, R.J., *Phenolic Acids in Foods: An Overview of Analytical Methodology*. *J. Agric. Food Chem.*, 2003. **51**(10): p. 2866-2887.
149. Dykes, L. and L.W. Rooney, *Phenolic compounds in cereal grains and their health benefits*. *Cereal Foods World*, 2007. **52**(3): p. 105-111.
150. Kong, W.-J., et al., *Investigation of the effect of 4 organic acids in Radix isatidis on E. coli growth by in. Chin. J. Chem.*, 2008. **26**(1): p. 113-115.
151. Chong, K.P., S. Rossall, and M. Atong, *HPC Fingerprints and In vitro Antimicrobial Activity of Syringic Acid, Caffeic Acid and 4-hydroxybenzoic Acid against Ganoderma boninense*. *Journal of Applied Sciences*, 2011. **11**(13): p. 2284-2291.
152. Stalikas, C.D., *Extraction, separation, and detection methods for phenolic acids and flavonoids*. *J. Sep. Sci.*, 2007. **30**(18): p. 3268-3295.
153. Dai, J. and R.J. Mumper, *Plant phenolics: extraction, analysis and their antioxidant and anticancer properties*. *Molecules*. **15**: p. 7313-7352.
154. Tsao, R., *Chemistry and biochemistry of dietary polyphenols*. *Nutrients*. **2**: p. 1231-1246.
155. Catel, Y., F. Aladedunye, and R. Przybylski, *Synthesis, Radical Scavenging Activity, Protection during Storage, and Frying by Novel Antioxidants*. *J. Agric. Food Chem.* **58**(20): p. 11081-11089.
156. Hristea, E.N., et al., *Reactions of 2,2-diphenyl-1-picrylhydrazyl (DPPH) with two syringylic phenols or one aroxide derivative*. *Eur. J. Org. Chem.*, 2009(5): p. 626-634.
157. Zhang, Y.-C., et al., *Synthesis and pharmacological evaluation of novel conjugates of indomethacin with antioxidant activity*. *Chin. J. Chem.*, 2005. **23**(11): p. 1523-1529.
158. Buisman, G.J.H., et al., *Enzymic esterifications of functionalized phenols for the synthesis of lipophilic antioxidants*. *Biotechnol. Lett.*, 1998. **20**(2): p. 131-136.

159. Liu, C., X. Gu, and Y.Z. Zhu, *Synthesis and biological evaluation of novel leonurine-SPRC conjugate as cardioprotective agents*. *Bioorg. Med. Chem. Lett.* **20**(23): p. 6942-6946.
160. Buser, H.-R., M.D. Mueller, and N. Theobald, *Occurrence of the Pharmaceutical Drug Clofibrilic Acid and the Herbicide Mecoprop in Various Swiss Lakes and in the North Sea*. *Environ. Sci. Technol.*, 1998. **32**(1): p. 188-192.
161. Kimura, K., H. Hara, and Y. Watanabe, *Removal of pharmaceutical compounds by submerged membrane bioreactors (MBRs)*. *Desalination*, 2005. **178**(1-3): p. 135-140.
162. Ok Jang, D., D.H. Cho, and J.-G. Kim, *One-pot preparation of esters from carboxylic acids using the PPh<sub>3</sub>-CCl<sub>3</sub>CN system*. *Synth. Commun.*, 2003. **33**(16): p. 2885-2890.
163. Xiang, J., A. Orita, and J. Otera, *Fluorous biphasic esterification directed towards ultimate atom efficiency*. *Angew. Chem., Int. Ed.*, 2002. **41**(21): p. 4117-4119.
164. Baizer, M.M., M. Karnowsky, and W.G. Bywater, *7-Isopropylpodocarpinol*. *J. Am. Chem. Soc.*, 1950. **72**: p. 3800-1.
165. Robertson, J.D., *synthetic studies with podocarpic acid*, in *Department of Chemistry*. 1980, University of Auckland. p. 196.
166. Staschke, K.A., et al., *Inhibition of influenza virus hemagglutinin-mediated membrane fusion by a compound related to podocarpic acid*. *Virology*, 1998. **248**(2): p. 264-274.
167. Liu, W., et al., *Design, synthesis, and structure-activity relationship of podocarpic acid amides as liver X receptor agonists for potential treatment of atherosclerosis*. *Bioorg. Med. Chem. Lett.*, 2005. **15**(20): p. 4574-4578.
168. Antosiewicz, J., et al., *Influence of structure on the antioxidant activity of indolinic nitroxide radicals*. *Free Radical Biology and Medicine*, 1997. **22**(1-2): p. 249-255.
169. Llorba, E., et al., *A comprehensive study of oxidative stress and antioxidant status in preeclampsia and normal pregnancy*. *Free Radical Biology and Medicine*, 2004. **37**(4): p. 557-570.
170. Tranchimand, S., et al., *First Chemical Synthesis of Three Natural Depsides Involved in Flavonol Catabolism and Related to Quercetinase Catalysis*. *Synth. Commun.*, 2006. **36**(5): p. 587-597.
171. Muller, T., et al., *Improved synthesis of tocopherol fatty alcohols and analogs: microglial activation modulators*. *Tetrahedron*, 2006. **62**(51): p. 12025-12040.
172. Quideau, S., et al., *Plant polyphenols: Chemical properties, biological activities, and synthesis*. *Angew. Chem., Int. Ed.* **50**(3): p. 586-621.
173. Santos, A.C., et al., *Effect of Naturally Occurring Flavonoids on Lipid Peroxidation and Membrane Permeability Transition in Mitochondria*. *Free Radical Biology and Medicine*, 1998. **24**(9): p. 1455-1461.
174. Kroon, P.A., et al., *How should we assess the effects of exposure to dietary polyphenols in vitro?* *Am. J. Clin. Nutr.*, 2004. **80**(1): p. 15-21.
175. Materska, M., *Quercetin and its derivatives: chemical structure and bioactivity-a review*. *Pol. J. Food Nutr. Sci.*, 2008. **58**(4): p. 407-413.
176. O'Leary, K.A., et al., *Effect of flavonoids and Vitamin E on cyclooxygenase-2 (COX-2) transcription*. *Mutation Research/Fundamental and Molecular Mechanisms of Mutagenesis*, 2004. **551**(1-2): p. 245-254.
177. van der Woude, H., et al., *Consequences of quercetin methylation for its covalent glutathione and DNA adduct formation*. *Chem.-Biol. Interact.*, 2006. **160**(3): p. 193-203.

178. Surco-Laos, F., et al., *Effects of O-methylated metabolites of quercetin on oxidative stress, thermotolerance, lifespan and bioavailability on Caenorhabditis elegans*. Food Funct. **2**(8): p. 445-456.
179. Crawford, D.L., R.O. Sinnhuber, and H. Aft, *Effect of methylation on the antioxidant and chelation capacity of quercetin and dihydroquercetin in a lard substrate*. J. Food Sci., 1961. **26**: p. 139-45.
180. Schwingel, L., et al., *Association of 3-O-methylquercetin with  $\beta$ -cyclodextrin: complex preparation, characterization and ex vivo skin permeation studies*. J. Inclusion Phenom. Macrocyclic Chem., 2008. **62**(1-2): p. 149-159.
181. Lee, J., et al., *Isorhamnetin Represses Adipogenesis in 3T3-L1 Cells*. Obesity, 2008. **17**(2): p. 226-232.
182. Igarashi, K. and M. Ohmumam, *Effects of isorhamnetin, rhamnetin, and quercetin on the concentrations of cholesterol and lipoperoxide in the serum and liver and on the blood and liver antioxidative enzyme activities of rats*. Biosci., Biotechnol., Biochem., 1995. **59**(4): p. 595-601.
183. Yesilada, E., et al., *Isolation and characterization of free radical scavenging flavonoid glycosides from the flowers of Spartium junceum by activity-guided fractionation*. J. Ethnopharmacol., 2000. **73**(3): p. 471-478.
184. Zhou, Z.-h., et al., *Selective monomethylation of quercetin*. Synthesis, (23): p. 3980-3986.
185. McCormick, J.M., et al., *Microbially Mediated O-Methylation of Bisphenol a Results in Metabolites with Increased Toxicity to the Developing Zebrafish (Danio rerio) Embryo*. Environmental Science & Technology. **45**(15): p. 6567-6574.
186. Kim, B.-G., et al., *Regiospecific Flavonoid 7-O-Methylation with Streptomyces avermitilis O-Methyltransferase Expressed in Escherichia coli*. J. Agric. Food Chem., 2006. **54**(3): p. 823-828.
187. Matsuda, H., et al., *Structural requirements of flavonoids and related compounds for aldose reductase inhibitory activity*. Chem. Pharm. Bull., 2002. **50**(6): p. 788-795.
188. Al Arni, S., et al., *Study of Aromatic Compounds Derived from Sugarcane Bagasse. Part I: effect of pH*. Chem. Eng. Technol. **33**(6): p. 895-901.
189. Gonzalez, A.G. and M.A. Herrador, *Ionization constants of water insoluble arylpropionic acids in aqueous N,N'-dimethylformamide mixtures from potentiometric pH-titrations*. Anal. Chim. Acta, 1997. **356**(2-3): p. 253-258.
190. Kadjout, M., C. Rolando, and S. Le Gac, *Microreactors for selective organic reactions*. Spec. Publ. - R. Soc. Chem., 2004. **297**(Micro Total Analysis Systems 2004, Volume 2): p. 267-269.
191. Toppet, S., K. Platteborze, and T. Zeegers-Huyskens, *<sup>1</sup>H and <sup>13</sup>C NMR and FT-IR studies of the interaction between 1,8-bis(dimethylamino)naphthalene and 3,5-dichlorophenol*. Journal of the Chemical Society, Perkin Transactions 2, 1995(4): p. 831-834.
192. Pozharskii, A.F., *Naphthalene "proton sponges"*. Usp. Khim., 1998. **67**(1): p. 3-27.
193. Alder, R.W., *Strain effects on amine basicities*. Chemical Reviews, 1989. **89**(5): p. 1215-1223.
194. Brzezinski, B., et al., *Protonation of 1,8-bis(dimethylamino)naphthalene by various acids in acetonitrile*. J. Chem. Soc., Perkin Trans. 2, 1991(6): p. 857-9.
195. Goethals, M., T. Zeegers-Huyskens, and B. Czarnik-Matuszewicz, *Infrared study of hydrogen bonds involving N-heterocyclic bases and phenols*. Journal of Heterocyclic Chemistry, 1999. **36**(1): p. 49-55.

196. Brzezinski, B. and G. Zundel, *Formation of hydrogen-bonded chains between a strong base with guanidine-like character and phenols with various pKa values â€” an FT-IR study*. J. Mol. Struct., 1996. **380**(3): p. 195-204.
197. Scifinder, RN 591-35-5. Calculated using Advanced Chemistry Development (ACD/Labs) Software V11.02 (© 1994-2011 ACD/Labs).
198. Huyskens, P.L., T. Zeegers-Huyskens, and Z. Pawelka, *Influence of proton transfer on the formation of hydrogen-bonded complexes of higher stoichiometry and on their dissociation into free ions*. J. Solution Chem., 1999. **28**(7): p. 915-932.
199. Scifinder, RN 884-35-5. Calculated using Advanced Chemistry Development (ACD/Labs) Software V11.02 (© 1994-2011 ACD/Labs).
200. Liu, P.-Y., et al., *Who Is the King? The alpha-Hydroxy-beta-oxo-alpha, beta-enone Moiety or the Catechol B Ring: Relationship between the Structure of Quercetin Derivatives and Their Pro-Oxidative Abilities*. Chem. Biodiversity. **7**(1): p. 236-244.
201. Trouillas, P., et al., *A DFT study of the reactivity of OH groups in quercetin and taxifolin antioxidants: The specificity of the 3-OH site*. Food Chemistry, 2006. **97**(4): p. 679-688.
202. Jurd, L., *Selective Alkylation of Polyphenols. I. The Use of Diphenylmethylene as a Protective Grouping for o-Dihydroxyflavones*. The Journal of Organic Chemistry, 1962. **27**(3): p. 872-875.
203. Herrero-Martinez, J.M., et al., *Determination of dissociation constants of flavonoids by capillary electrophoresis*. Electrophoresis, 2005. **26**(10): p. 1886-1895.
204. Canbay, H.S., et al., *Chromatographic Determination of pKa Values of Some Water-Insoluble Arylpropionic Acids and Arylacetic Acids in Acetonitrile + Water Media*. J. Chem. Eng. Data. **56**(5): p. 2071-2076.
205. Evangelista, S., D.G. Cooper, and V. Yargeau, *The effect of structure and a secondary carbon source on the microbial degradation of chlorophenoxy acids*. Chemosphere. **79**(11): p. 1084-1088.
206. Zhang, J. and H.K. Lee, *Application of dynamic liquid-phase microextraction and injection port derivatization combined with gas chromatography-mass spectrometry to the determination of acidic pharmaceutically active compounds in water samples*. J. Chromatogr., A, 2009. **1216**(44): p. 7527-7532.
207. Amorati, R., et al., *Solvent and pH Effects on the Antioxidant Activity of Caffeic and Other Phenolic Acids*. J. Agric. Food Chem., 2006. **54**(8): p. 2932-2937.
208. Chmurzynski, L., *Studies on correlations of acid-base properties of substituted pyridine N-oxides in solutions. Part I. Correlations of the pKa values in non-aqueous solvents and water*. Anal. Chim. Acta, 1996. **321**(2-3): p. 237-44.
209. Liptak, M.D. and G.C. Shields, *Accurate pKa Calculations for Carboxylic Acids Using Complete Basis Set and Gaussian-n Models Combined with CPCM Continuum Solvation Methods*. Journal of the American Chemical Society, 2001. **123**(30): p. 7314-7319.
210. Zhang, S., J. Baker, and P. Pulay, *A Reliable and Efficient First Principles-Based Method for Predicting pKa Values. 2. Organic Acids*. The Journal of Physical Chemistry A, 2009. **114**(1): p. 432-442.
211. Chang, P.C., C.Y. Mou, and D.J. Lee, *Micromixing and Macromixing Effects in Unsteady Chemical Reaction System*. J. Phys. Chem. A, 1999. **103**(28): p. 5485-5489.
212. Jones, A.G., *Crystallization Process Systems*. 2002. 384 pp.
213. Bird, R.B., W.E. Stewart, and E.N. Lightfoot, *Transport Phenomena*. 1960. 780 pp.

214. Campbell Christopher, J. and A. Grzybowski Bartosz, *Microfluidic mixers: from microfabricated to self-assembling devices*. Philos Transact A Math Phys Eng Sci, 2004. **362**(1818): p. 1069-86.
215. Hessel, V., H. Loewe, and F. Schoenfeld, *Micromixers - a review on passive and active mixing principles*. Chem. Eng. Sci., 2005. **60**(8-9): p. 2479-2501.
216. Yoshida, J.-i., H. Kim, and A. Nagaki, *Green and Sustainable Chemical Synthesis Using Flow Microreactors*. ChemSusChem, 2011. **4**(3): p. 331-340.
217. Wiles, C. and P. Watts, *Recent advances in micro reaction technology*. Chem. Commun., 2011. **47**(23): p. 6512-6535.
218. Haswell, S.J., et al., *The application of micro reactors to synthetic chemistry*. Chem. Commun., 2001(5): p. 391-398.
219. Jas, G. and A. Kirschning, *Continuous flow techniques in organic synthesis*. Chem.-Eur. J., 2003. **9**(23): p. 5708-5723.
220. Irfan, M., T.N. Glasnov, and C.O. Kappe, *Continuous Flow Ozonolysis in a Laboratory Scale Reactor*. Org. Lett., 2011. **13**(5): p. 984-987.
221. Bartrum, H.E., et al., *Rapid Access to alpha-Alkoxy and alpha-Amino Acid Derivatives through Safe Continuous-Flow Generation of Diazoesters*. Chem.-Eur. J., 2011. **17**(35): p. 9586-9589.
222. Tomida, Y., A. Nagaki, and J.-i. Yoshida, *Asymmetric carbolithiation of conjugated enynes: a flow microreactor enables the use of configurationally unstable intermediates before they epimerize*. J. Am. Chem. Soc., 2011. **133**(11): p. 3744-3747.
223. Calabrese, G.S. and S. Pissavini, *From batch to continuous flow processing in chemicals manufacturing*. AIChE J., 2011. **57**(4): p. 828-834.
224. Mason, B.P., et al., *Greener Approaches to Organic Synthesis Using Microreactor Technology*. Chem. Rev., 2007. **107**(6): p. 2300-2318.
225. Baldyga, J. and J.R. Bourne *Turbulent Mixing and Chemical Reactions*. 1999, New York.: Wiley. 867
226. Baldyga, J., J.R. Bourne, and B. Walker, *Non-isothermal micromixing in turbulent liquids: theory and experiment*. Can. J. Chem. Eng., 1998. **76**(3): p. 641-649.
227. Dolman, S.J., J.L. Nyrop, and J.T. Kuethe, *Magnetically Driven Agitation in a Tube Mixer Affords Clog-Resistant Fast Mixing Independent of Linear Velocity*. J. Org. Chem., 2011. **76**(3): p. 993-996.
228. Koelbl, A., M. Kraut, and K. Schubert, *The iodide iodate method to characterize microstructured mixing devices*. AIChE J., 2008. **54**(3): p. 639-645.
229. Mozharov, S., et al., *Improved Method for Kinetic Studies in Microreactors Using Flow Manipulation and Noninvasive Raman Spectrometry*. J. Am. Chem. Soc., 2011. **133**(10): p. 3601-3608.
230. Baldwin, R.P., et al., *Fully integrated on-chip electrochemical detection for capillary electrophoresis in a microfabricated device*. Anal. Chem., 2002. **74**(15): p. 3690-3697.
231. Salmon, J.-B., et al., *An Approach To Extract Rate Constants from Reaction-Diffusion Dynamics in a Microchannel*. Anal. Chem., 2005. **77**(11): p. 3417-3424.
232. Hencken, C.P., et al., *Highly stereocontrolled and regiocontrolled syntheses of 2,3,4-trisubstituted alkanoates and lactones*. J. Org. Chem., 2011. **76**(12): p. 5149-5155.
233. Jaehnisch, K., et al., *Chemistry in microstructured reactors*. Angew. Chem., Int. Ed., 2004. **43**(4): p. 406-446.

234. McMullen, J.P. and K.F. Jensen, *Integrated microreactors for reaction automation: new approaches to reaction development*. *Annu. Rev. Anal. Chem.*, 2010. **3**: p. 19-42.
235. Bessoth, F.G., A.J. deMello, and A. Manz, *Microstructure for efficient continuous flow mixing*. *Anal. Commun.*, 1999. **36**(6): p. 213-215.
236. Jaffe, H.H., *A re.ovrddot.examination of the Hammett equation*. *Chem. Rev.*, 1953. **53**: p. 191-261.
237. Seaton, C.C., et al., *Designing Acid/Acid Co-Crystals through the Application of Hammett Substituent Constants*. *Cryst. Growth Des.*, 2009. **10**(2): p. 726-733.
238. Herbst, R.L., Jr. and M.E. Jacox, *Effects of alkyl groups linked to conjugated systems. I. Alkaline hydrolysis of some ethyl p-alkylbenzoates*. *J. Am. Chem. Soc.*, 1952. **74**: p. 3004-6.
239. Hammond, G.S., et al., *Benzyl tosylates. V. Some solvent effects*. *J. Am. Chem. Soc.*, 1958. **80**: p. 568-73.
240. Kloosterziel, H. and H.J. Backer, *The effect of the medium upon Hammett's sigma values of p-alkyl groups and hyperconjugation*. *J. Am. Chem. Soc.*, 1952. **74**: p. 5806.
241. Kamlet, M.J., et al., *Linear solvation energy relationship. 46. An improved equation for correlation and prediction of octanol/water partition coefficients of organic nonelectrolytes (including strong hydrogen bond donor solutes)*. *J. Phys Chem.*, 1988. **92**(18): p. 5244-5255.